Contents

Chapter 1

Introduction

1.1 Multicarrier Systems

During the last decade, we have witnessed a widespread deployment of digital communication services requiring an exchange of digital information at constantly increasing data rates (e.g., audio and video conferencing, internet applications, digital television, ...). To satisfy this increasing demand for higher data rates, the data rates over the existing transmission media must be enhanced. For example, for internet connections over twisted pair cables, ISDN (integrated services digital network), that provides only bit rates of 128 kilobits per second (kbps), is becoming superseded by ADSL (asymmetric digital subscriber line), that provides bit rates up to 7 megabits per second (Mbps) in the downlink (from the network to the subscriber) and bit rates up to 800 kbps in the uplink (from the subscriber to the network) [Bah99], [Chw91a], [Chw91b], [Sal98]. The capacity that can be obtained with ADSL decreases with the length of the twisted pair cable. In ADSL, the maximum cable length equals 5.5 km. In the future, the telephone companies will provide fibre to the curb. In this case, the distance that must be bridged by the twisted pair cable reduces to 200 m - 1.5 km. The technology that is developed for these short cable lengths is VDSL (very high-bit-rate digital subscriber line) [Chw91b], that reaches higher capacities than ADSL (up to 55 Mbps in the downlink and up to 2.3 Mbps in the uplink). Another example is cellular telephony. The second generation of cellular telephones (GSM (global system for mobile communications) in Europe and IS-95 (interim standard-95) in North America), that provides digital voice and data services up to rates of 9.6 kbps, will be replaced in the near future by the third generation of cellular telephones (UMTS (universal mobile telephone system) in Europe and IMT-2000 (international mobile telecommunications-2000) in North America) [Oja98], [Kni98], [Ada98], [Dah98], [Nan00]. This third generation of mobile telephones is now being standardised and the products are expected to be available in the coarse of 2000-2001. The third generation of

mobile telephones will support voice and data services up to rates of 2 Mbps. Further, fixed local area networks (LAN) are being extended or replaced by wireless LAN's (WLAN), to allow the subscribers a low mobility (< 36 km/h). Standards for WLAN are IEEE 802.11 and HIPERLAN (European high performance radio LAN), that provide the capability to transmit bit rates up to 11 Mbps and 23.5 Mbps, respectively [Bah99], [IEEE97], [ETSI96], [ETSI99], [vNe00]. In the future, one will provide full mobility for broadband applications up to 155 Mbps with MBS (mobile broadband system). The goal of MBS, which still is in the development stage, is to provide a mobile and wireless extension or replacement of the fixed broadband ISDN (B-ISDN) connections [vNe00].

In conventional single carrier communication, the data symbols, generated at a symbol rate R_s, are transmitted sequentially [Pro95], [Mey98], [Kur00], [Sim95]. Each data symbol of the data stream at the transmitter is represented by a pulse, of which the duration is inversely proportional to R_s. The pulses are modulated on a fixed sinusoidal carrier, and one by one transmitted over the channel at a rate R_s. The channel is dispersive, and is characterised by its impulse response. When the duration of the transmitted pulses is large as compared to the duration of the impulse response, the pulses are only slightly disturbed by the channel. However, when the duration of the transmitted pulses is small as compared to the duration of the impulse response, the pulses at the input of the receiver are widely spread in time. In this case, the received pulses overlap considerably, resulting in intersymbol interference (ISI). For a given channel, the amount of ISI increases for increasing symbol rate R_s.

To reduce the ISI, the receiver can make use of an equaliser. The required number of equaliser coefficients increases with the amount of ISI. For an equaliser with M coefficients, operating at the symbol rate R_s, M complex multiplications per symbol interval are necessary. As the channel impulse response is not a priori known to the receiver, and may even be time varying (e.g., radio transmission subject to fading), the equalisation is performed adaptively; based on the signal at the output of the equaliser, the equaliser coefficients are adjusted continuously. An adaptive equaliser with a large number of coefficients is not only computationally intensive, the convergence rate is also low; this is especially disadvantageous in time-varying channels. Hence, equalisation for conventional single carrier communication is complex at high data rates.

To solve the equalisation problems occurring in conventional single carrier communication (where only one carrier is modulated), multicarrier modulation can be used [Cha66], [Sal67], [Hir80], [Wei71], [Hir81]. It is assumed that the channel transfer function in the case of multicarrier modulation is the same as for conventional single carrier communication. In multicarrier modulation, the data stream at rate R_s is split into N parallel data streams, each having a rate R_s/N. In figure 1.1, the signals for the conventional single carrier communication system and the multicarrier communication system are shown. Each of the N data streams is modulated on a different sinusoidal carrier. By selecting the number of carriers N sufficiently large, the resulting symbol duration per carrier (N/R_s) is much larger than the duration of the channel impulse response.

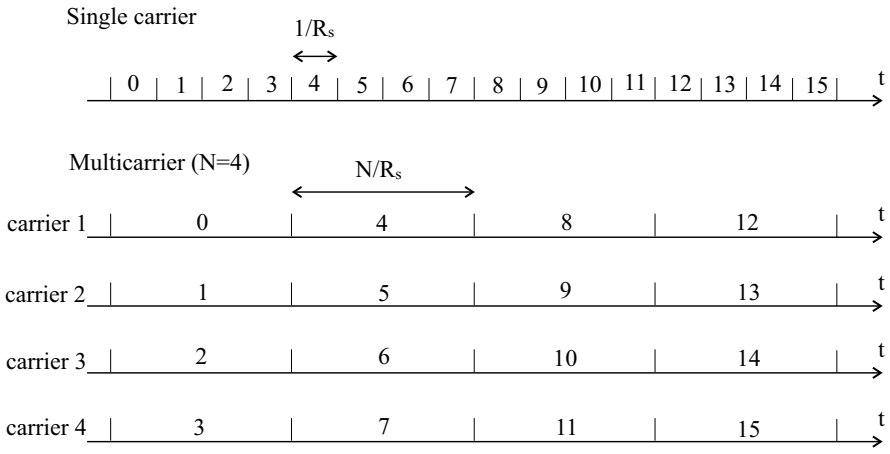

Figure 1.1: Single carrier and multicarrier signal

Hence, the received pulses on the different carriers are only slightly disturbed by the dispersive channel, such that the pulses only overlap at the boundaries of the pulses, as shown in figure 1.2. The receiver uses only the central part of these pulses, which is not affected by interference from other symbols on the considered carrier [Pel80]. Furthermore, the spacing of the carrier frequencies is chosen carefully such that in the central part of the pulse, no interference occurs between symbols on different carriers. In this case, the channel introduces an attenuation and rotation of each individual carrier. At the receiver, this effect is compensated by N equalisers, each operating on a different carrier. Each equaliser consists of a one-tap equaliser, that scales and rotates the corresponding carrier to compensate for the attenuation and rotation introduced by the channel. This equalisation requires only one complex multiplication per symbol interval ($1/R_s$), which is significantly lower than for conventional single carrier communication. The equalisers are implemented as adaptive equalisers; as they consist of only one equaliser coefficient, the rate of convergence is much higher than for conventional single carrier communication. To generate (at the transmitter) and to demodulate (at the receiver) the multicarrier signal, the computationally efficient (inverse) fast Fourier transform (FFT) can be used. This allows to use a large number of carriers (typically the number of carriers is of the order of 100 to 1000).

When different users want to make use of the same transmission medium, their signals must be generated following a specific multiple access scheme, such that the signals of the different users can be separated at the receiver. In this work, we pay a lot of attention to the code-division multiple access (CDMA) technique. In CDMA, the data stream to be transmitted at a rate R_s is at the transmitter multiplied with a user-dependent spreading sequence, having a rate NR_s. Hence, each data symbol is converted into a sequence of N chips, that have to be transmitted over the channel. The signals of the different users

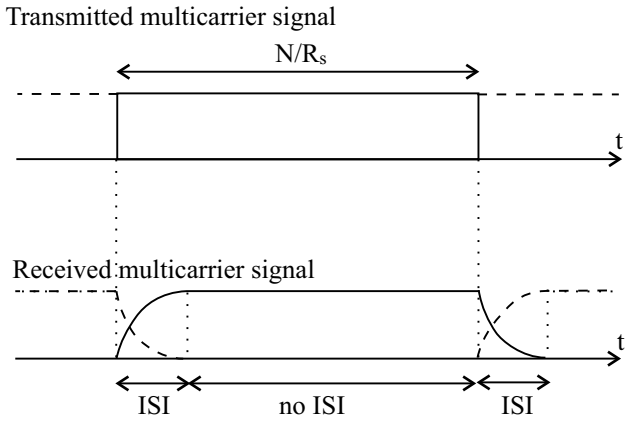

Figure 1.2: Transmitted and received multicarrier signal in the presence of a dispersive channel

can be separated at the receiver, as each user is assigned a unique spreading sequence. In direct sequence CDMA (DS-CDMA), the spread data symbols are modulated on a fixed carrier, and transmitted sequentially over the channel at a rate NR_s. In multicarrier CDMA (MC-CDMA), the N chips that are multiplied with the same data symbol are transmitted on N different carriers; the rate of chips per carrier equals R_s.

Multicarrier modulation is proposed or accepted for various applications. Orthogonal frequency division multiplexing (OFDM) has been exploited for broadband xDSL (digital subscriber line) applications for transmission over twisted pair cables [Chw91a], [Chw91b], [Bah99], [Sal98]. In the form of DMT (discrete multitone), the OFDM technique has been accepted as a world wide standard for ADSL (asymmetric digital subscriber line) [Chw91b], [Bah99]. It is also a candidate for a VDSL (very high-bit-rate digital subscriber line) standard [Chw91b]. In addition, the OFDM technique has been studied and implemented for broadcasting of digital audio (DAB - digital audio broadcasting) [LeF89], [ETSI97] and digital television (DVB - digital video broadcasting, DTTB - digital terrestrial television broadcasting) [Sar95], [Rei98]. Furthermore, the IEEE 802.11 standardisation group has selected OFDM as a basis for the new IEEE 802.11 5GHz standard for wireless LAN [Bah99], [vNe00], [Tak98], [IEEE99], [vNe97]. Moreover, the OFDM system has been studied in the context of data communication over mobile radio channels [San95], [Chi95], [Cas91], [Ali97]. Orthogonal frequency division multiple access (OFDMA) has been proposed for the return path of the CATV (cable area television) network [Sar96]. Another multicarrier technique, multicarrier CDMA has been proposed for mobile radio communication [Faz93], [Yee93], [Cho93].

The transmitter of a digital communication system contains a clock, that indicates the timing instants at which the data symbols must be transmitted.

Furthermore, the transmitter contains a carrier oscillator, necessary for the upconversion of the data carrying baseband signal to the bandpass signal to be transmitted [Pro95], [Mey98]. At the receiver, the received bandpass signal is downconverted using a local carrier oscillator. The resulting baseband signal is sampled at timing instants determined by the receiver clock. Based on the resulting samples, a decision is taken about the transmitted data symbols. The maximum reliability of this decision is obtained when the frequencies and the phases of the carrier oscillator and the clock at the transmitter are related with those of the receiver. The receiver contains a synchroniser structure to estimate the ideal frequencies and phases of the carrier oscillator and the clock at the receiver, based on the received signal. Because the presence of interference, noise and other disturbances, these estimations are not perfect, such that the reliability of the resulting decisions is lower than in the case of perfect synchronisation.

1.2 Overview of this Work

In this work, we study the effect of synchronisation errors (carrier phase errors and timing errors) on the performance of a number of multicarrier systems. To this aim, we compute the signal-to-noise ratio (SNR) at the input of the decision device. The multicarrier systems that will be considered in this work are the OFDM system, the OFDMA system and the MC-CDMA system. Furthermore, we compare these multicarrier systems with single carrier systems, with respect to their sensitivity to synchronisation errors. With the results obtained in this work, we are able to derive requirements on the accuracy of carrier and timing synchronisation algorithms and on the stability of the carrier and clock oscillators, when an acceptable amount of performance degradation is given.

This work is organised as follows. In chapter 2, we derive an equivalent time-varying model for a generic system for digital bandpass communication. This equivalent time-varying model takes into account the synchronisation errors. With this model, we are able to investigate the influence of various types of synchronisation errors on different systems with one or more carriers, using a single analysis method. Furthermore, we consider a mathematical model for the different types of synchronisation errors, and we derive an expression for the equaliser coefficients. Finally, we define a performance measure, the signal-to-noise ratio, that is defined in terms of the samples at the input of the decision device. In many cases of practical interest, this SNR is directly related to the bit error rate (BER). The former equivalent model will be used in the next chapters to determine, based upon analytical computations, the SNR in the presence of various types of synchronisation errors, for the different types of single carrier and multicarrier systems that are considered in this work. The analytical results will be verified with computer simulations.

In chapters 3 and 4, we study the systems with a single carrier. In chapter 3, we describe the conventional single carrier communication system, where the

data symbols are transmitted sequentially. Chapter 4 presents a single carrier direct sequence CDMA system, where the data symbols are first spread before transmission. We investigate the influence of various types of synchronisation errors on these single carrier systems in the case of an ideal channel.

In chapters 5 and 6, we extensively study the multicarrier systems. The OFDM system and the OFDMA system are described in chapter 5. The MC-CDMA system is presented in chapter 6. The effect of various types of synchronisation errors on these multicarrier systems is investigated in the case of an ideal channel, for both the uplink and the downlink. Further, we study the influence of the synchronisation errors in the presence of a dispersive channel.

Chapter 7 contains a comparison of the different considered communication systems with respect to their sensitivity to synchronisation errors, assuming each system accommodates N users, operating at the same data rate R_s. Finally, the conclusions of this work are presented in chapter 8, and we give some suggestions for future work.

Chapter 2

A Generic Model for Linear Digital Communication

2.1 Introduction

In the past decades, communication has moved from analogue to digital. In many cases of practical interest, digital communication systems make use of linear bandpass modulation. The linear digital bandpass communication system adequately describes a large number of systems for communication over telephone lines, coaxial cables or radio and satellite channels.

In section 2.2, we give a generic description of a point-to-point linear bandpass communication system. This description contains the timing clocks and the carrier oscillators at the transmitter and the receiver. In order to obtain a reliable communication, the phases of the timing clock and the carrier oscillator at the receiver should be related to the corresponding quantities at the transmitter. However, because of various disturbances, carrier phase errors and timing errors occur. In section 2.3.1, these synchronisation errors are incorporated into the channel transfer function. This unified approach allows us to present a single analysis method which is valid for various linear modulation formats and various types of synchronisation errors. A model for the synchronisation errors to be considered in this work is presented in section 2.3.2.

Many practical communication systems consist of a base station communicating with a number of users at different locations. Depending on the direction of communication, we use the terms 'downlink communication', to indicate the communication from the base station to the users, and 'uplink communication', to indicate the communication from the users to the base station. Section 2.4.1 extends the point-to-point system model of section 2.2 for point-to-multipoint communication (downlink) and multipoint-to-point communication

(uplink). Furthermore, the equivalent channel model that includes the synchronisation errors is extended for the cases of downlink and uplink communication. To allow for many users to communicate simultaneously over a common physical medium, the signals of the different users must be separable to avoid excessive interference between the users. Section 2.4.2 presents a number of multiplexing and multiple access techniques that have been developed to separate the user signals. In section 2.4.3, we focus on spreading sequences, which are used in the code-division multiple-access (CDMA) from section 2.4.2. We describe a number of possible sets of spreading sequences that can be used to separate the user signals.

In a practical implementation, the receiver is often designed to (adaptively) minimise the mean-square error (MSE) between the input and the output of the decision device. In section 2.5, we present a receiver structure that contains a number of one-tap equalisers to mitigate the effect of the channel and the synchronisation errors. We derive an expression for the equaliser that minimises the MSE, i.e., for the minimum mean-square error (MMSE) equaliser. To measure the quality of communication, we present in section 2.6 a signal-to-noise ratio (SNR) that is defined in terms of the samples at the input of the decision device. When these samples are essentially Gaussian, the SNR is directly related to the bit error rate (BER).

2.2 Point-to-Point Communication

The conceptual block diagram of a point-to-point digital communication system [Pro95], [Mey98], [Lee88], [Van99], [Moe99a], [Moe99b] is shown in figure 2.1. This system consists of the modulator at the transmitter side, the channel and the demodulator at the receiver side. The sequence of data symbols $\mathbf{a}$, which are values belonging to a finite complex-valued constellation alphabet, is applied to the digital modulator, which converts the sequence of data symbols into a continuous-time signal $s(t)$. The communication channel is the physical medium that is used to send the signal $s(t)$ from the transmitter to the receiver. The effect of the channel on the transmitted signal will be described by means of a mathematical model. The continuous-time signal $r(t)$ at the output of the channel is applied to the demodulator, which converts the signal $r(t)$ into a sequence of decisions about the transmitted data symbols. The estimated data symbols $\hat{\mathbf{a}}$ at the output of the receiver belong to the same constellation alphabet as the transmitted data symbols $\mathbf{a}$.

In the case of a linear digital bandpass communication system, the transmitter structure is shown in figure 2.2. The data symbols, which are generated at the symbol rate R_s, are grouped into blocks of N_s symbols $\mathbf{a}_i = [a_{i,0}a_{i,1}\ldots a_{i,N_s-1}]^T$, where $a_{i,n}$ denotes the nth data symbol transmitted during the ith block. The block $\mathbf{a}_i$ is applied to a linear transformation $\mathbf{T}_{tr,i}$ that converts the block of N_s data symbols into a block of M_s samples

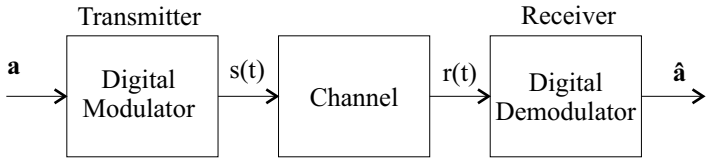

Figure 2.1: Conceptual block diagram of the digital communication system

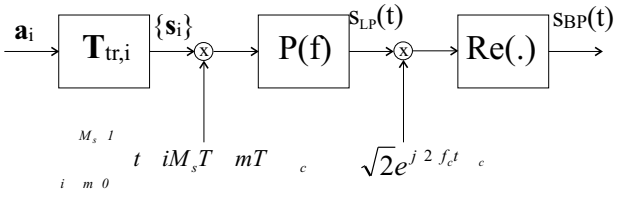

Figure 2.2: Block diagram of the transmitter of a linear bandpass digital communication system

$\mathbf{s}_i = [s_{i,0} s_{i,1} \dots s_{i,M_s-1}]^T$, which are transmitted at a rate $1/T = (M_s/N_s)R_s$:

$$\mathbf{s}_i = \mathbf{T}_{tr,i}\mathbf{a}_i \tag{2.1}$$

where $\mathbf{T}_{tr,i}$ is a matrix of dimension $M_s \times N_s$, that can depend on the block index i. The discrete-time sequence of samples $\{s_{i,m}\}$ is applied to a lowpass filter with transfer function $P(f)$ and impulse response $p(t)$, yielding a continuous-time lowpass signal $s_{LP}(t)$. In figure 2.2, this transition from the discrete-time to the continuous-time domain is modelled by applying to the filter a sequence of Dirac impulses at a rate $1/T$, with weights equal to the samples $\{s_{i,m}\}$. This weighted sequence of Dirac impulses results from multiplying the samples $\{s_{i,m}\}$ with the transmit clock signal, consisting of a periodic sequence of Dirac impulses. This yields

$$s_{LP}(t) = \sum_{i=-\infty}^{+\infty} \sum_{m=0}^{M_s-1} s_{i,m} p(t - iM_sT - mT - \tau_c) \tag{2.2}$$

where τ_c is a time delay which represents the transmit clock phase. The transmit filter is assumed to be a unit-energy square-root Nyquist filter with respect to the time interval T, i.e.,

$$\int_{-\infty}^{+\infty} p(t)p^*(t - kT)dt = \delta_k \tag{2.3}$$

In many cases of practical interest, the communication system is assigned a bandpass channel, so the lowpass signal $s_{LP}(t)$ must be frequency-translated by means of carrier modulation. In figure 2.2 the resulting bandpass signal $s_{BP}(t)$

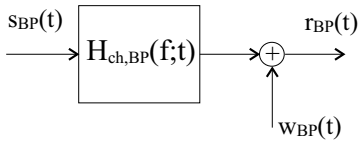

Figure 2.3: Bandpass channel

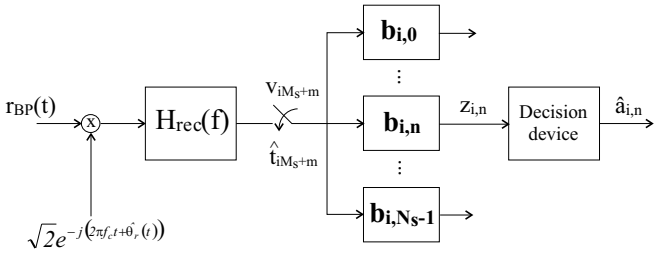

Figure 2.4: Block diagram of the receiver of a linear digital communication system

is modelled as the real part of the product of $s_{LP}(t)$ and a complex exponential with carrier frequency f_c and a carrier phase θ_c :

$$s_{BP}(t) = \sqrt{2}Re\left(s_{LP}(t)e^{j(2\pi f_c t+\theta_c)}\right) \tag{2.4}$$

The frequency content of $s_{BP}(t)$ is concentrated near the carrier frequency f_c. The bandpass signal $s_{BP}(t)$ is applied to the possibly time-varying bandpass channel with transfer function $H_{ch,BP}(f;t)$, and is disturbed by zero-mean additive white Gaussian bandpass noise $w_{BP}(t)$, with independent real and imaginary parts, each having a power spectral density (psd) of $N_0/2$ (figure 2.3). In wired communication (e.g., over the telephone line or the coaxial cable), the channel can be considered as time-invariant; in this case, the channel transfer function does not depend on t, and is represented by $H_{ch,BP}(f)$. In wireless communication, fading may occur, indicating that the channel is time-varying; in this case, the channel $H_{ch,BP}(f;t)$ is modelled as a random process that is stationary with respect to the variable t [Stl92].

At the receiver, the bandpass signal $r_{BP}(t)$ is downconverted to baseband [Fra80]. As indicated in figure 2.4, this downconversion is accomplished by multiplying $r_{BP}(t)$ with a local oscillator signal with a 'total' phase equal to $-(2\pi f_c t + \hat{\theta}_r(t))$. This time-varying phase $\hat{\theta}_r(t)$ will be discussed in section 2.3. The resulting signal is applied to a receiver filter with transfer function $H_{rec}(f)$, which shapes the useful component of the received signal and suppresses the out-of-band signals. In this work, the receiver filter is assumed to be matched to the transmit filter: $H_{rec}(f) = P^*(f)$. The signal at the output of the receiver filter is sampled at the instants $\hat{t}_{iM_s+m} = (iM_s+m)T+\hat{\tau}_{r,iM_s+m}$, yielding the samples v_{iM_s+m}. This time-varying delay $\hat{\tau}_{r,iM_s+m}$ will be discussed in section 2.3. The

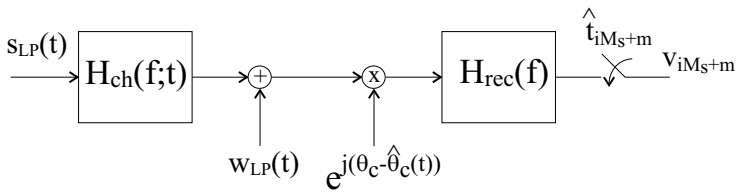

Figure 2.5: Lowpass equivalent of the bandpass system

sequence of samples $\{v_{iM_s+m}\}$ is applied to N_s parallel linear transformations $\{\mathbf{b}_{i,n}\}$ where $\mathbf{b}_{i,n} = [b_{iM_s,n} b_{iM_s+1,n} \dots b_{iM_s+M_s-1,n}]^T$ can depend on the block index i. The resulting outputs $\{z_{i,n}\}$, given by

$$z_{i,n} = \sum_{m=0}^{M-1} b_{iM_s+m,n} v_{iM_s+m} \tag{2.5}$$

are used to make decisions about the transmitted data symbols $\{a_{i,n}\}$. The decision device selects the constellation point $\hat{a}_{i,n}$ that is the closest to $z_{i,n}$. In general, intersymbol interference (ISI), which is interference caused by other transmitted data symbols, affects the detection of the considered symbol.

In the receiver structure of figure 2.4, the received signal is sampled at a rate $1/T$. This sampling rate is optimum when the channel is ideal ($H_{ch,BP}(f;t) = 1$), as the resulting samples provide sufficient statistics. When the channel is not ideal ($H_{ch,BP}(f;t) \neq 1$), the optimum receiver contains a receiver filter that is matched to the channel and the transmit filter (i.e., $H_{rec}(f) = H^*_{ch,BP}(f - f_c;t)P^*(f)$). The receiver filter output is sampled at a rate $1/T$. However, this receiver filter may be complex to realise, as we do not a priori know the channel and the channel may vary in time. To avoid the high complexity of the receiver filter, an alternative optimum receiver can be used. In this alternative structure, the receiver filter is matched to the transmit filter only ($H_{rec}(f) = P^*(f)$). The receiver filter output is sampled at a rate K/T ($K \geq 1$) to avoid aliasing. The matching of the receiver to the channel (i.e., to $H_{ch,BP}(f - f_c;t)$) is done digitally, which can easily be implemented adaptively. Usually, the sampling rate is twice the sample rate ($K = 2$).

In the multicarrier systems that will be considered in this work, there is virtually no aliasing, even for $K = 1$, because of the structure of the multicarrier signal. Hence, the receiver structure of figure 2.4 is optimum for the considered multicarrier systems.

Without loss of generality, the bandpass signals can be represented by an equivalent lowpass signal [Pro95], [Mey98], [Lee88], [Van99], [Moe99a], [Moe99b], i.e., the complex envelope of the signal. The equivalent lowpass block diagram of the linear digital communication system is shown in figure 2.5. The transmitted lowpass signal $s_{LP}(t)$ is applied to the lowpass equivalent $H_{ch}(f;t)$ of the channel is disturbed by the equivalent lowpass additive white Gaussian

noise (AWGN) disturbance $w_{LP}(t)$ and affected by the carrier phase difference $\theta_c - \hat{\theta}_r(t)$. The AWGN disturbance has independent real and imaginary parts, each having a power spectral density $N_0/2$. The resulting signal is applied to the receiver filter and sampled at the timing instants $\hat{t}_{iM_s+m}$. In this work, the complex envelope of the signals will be used to describe the considered bandpass systems.

Example: Let us consider a simple example, consisting of transmission over an ideal channel ($H_{ch}(f;t) = 1$). Further, we assume that the receiver knows the transmitter's carrier phase θ_c and clock phase τ_c, and selects $\hat{\theta}_r(t) = \theta_c$ and $\hat{\tau}_{r,iM+m} = \tau_c$: the receiver is perfectly synchronised to the transmitter. Taking into account the square-root Nyquist property (2.3) of the transmit and the receiver filter, it follows that

$$v_{iM_s+m} = s_{i,m} + w_{iM_s+m} \tag{2.6}$$

where w_{iM_s+m} denotes the contribution from the noise $w_{LP}(t)$, and $s_{i,m}$ is related to the data symbols by (2.1). Hence, v_{iM_s+m} is a noisy version of the sample $s_{i,m}$ that was generated by the transmitter.

Now let us assume that the N_s columns of the $M_s \times N_s$ matrix $\mathbf{T}_{tr,i}$ (2.1) are orthogonal (this requires $M_s \geq N_s$):

$$\sum_{m=0}^{M_s-1} (\mathbf{T}_{tr,i})^*_{m,n_1} (\mathbf{T}_{tr,i})_{m,n_2} = \delta_{n_1-n_2} \tag{2.7}$$

where $(\mathbf{T}_{tr,i})^*$ is the complex conjugate of the matrix $\mathbf{T}_{tr,i}$. Selecting $\mathbf{b}_{i,n}$ (2.5) as the nth column of $(\mathbf{T}_{tr,i})^*$ yields

$$z_{i,n} = a_{i,n} + W_{i,n} \tag{2.8}$$

where $a_{i,n}$ is the nth data symbol from the ith block, and $W_{i,n}$ denotes the contribution from the noise. This simple example indicates that $z_{i,n}$ is not affected by intersymbol interference (ISI) when the channel is ideal, the receiver is perfectly synchronised to the transmitter, the rows of the matrix $\mathbf{T}_{tr,i}$ are orthogonal and $\mathbf{b}_{i,n}$ is selected as the nth column of $(\mathbf{T}_{tr,i})^*$. In practical systems, ISI occurs because of non-ideal channel conditions and imperfect synchronisation.

2.3 Synchronisation Errors (Point-to-Point)

2.3.1 Equivalent Channel Transfer Function

In this section, we derive the discrete-time transfer function of an equivalent channel, that describes the transfer from the samples $\mathbf{s}_i$ (2.1) at the input of the

transmit filter (as shown in figure 2.2) to the samples $\mathbf{v}_i$ at the output of the receiver filter (see figure 2.4). Hence, this transfer function contains the cascade of the transmit filter $P(f)$, the original channel $H_{ch}(f;t)$ and the receiver filter $P^*(f)$, and includes the effects of the timing clocks and the carrier oscillators at the transmitter and the receiver.

The reliability of the detected data symbols strongly depends on the frequency and phase of the carrier oscillator and the sampling clock at the receiver. In the case of a time-invariant channel, the total phases of the local oscillator and of the sampling clock yielding optimum performance are denoted $2\pi f_c t + \theta_r$ and $t_{iM_s+m} = (iM_s + m)T + \tau_r$, respectively: the carrier oscillators and the clocks at the receiver and the transmitter should have the same frequencies f_c and $1/T$, respectively. When the channel is non-ideal, the optimum carrier oscillator phase θ_r and sampling clock phase τ_r are not the same as the corresponding phases at the transmitter, and can be represented as

$$\begin{aligned} \theta_r &= \theta_c + \Delta\theta \\ \tau_r &= \tau_c + \Delta\tau \end{aligned} \tag{2.9}$$

where the phase shift $\Delta\theta$ and the time delay $\Delta\tau$ depend on the channel characteristics.

In the case of a time-varying channel, the optimum phase shift (between the carrier oscillators at receiver and transmitter) and time delay (between the clocks at receiver and transmitter) become time-varying as well. This yields for the optimum carrier and clock phases

$$\begin{aligned} \theta_r(t) &= \theta_c + \Delta\theta(t) \\ \tau_{r,iM_s+m} &= \tau_c + \Delta\tau_{iM_s+m} \end{aligned} \tag{2.10}$$

Assuming that the channel varies slowly with respect to the sampling interval T, the quantities $\Delta\theta(t)$ and $\Delta\tau_{iM_s+m}$ are slowly varying as well. In figure 2.6, the different time delays are depicted, where $p(t)$ is the transmit pulse and $h(t;t_{iM_s+m})$ is the impulse response of the cascade of the transmit filter, the time-varying channel and the receiver filter. The optimum time delay corresponds to the maximum of the pulse $h(t;t_{iM_s+m})$.

The receiver has no a priori knowledge about $\theta_r(t)$ and τ_{r,iM_s+m}. Therefore, part of the receiver consists of a carrier synchroniser and a clock synchroniser, which produce estimates $\hat{\theta}_r(t)$ and $\hat{\tau}_{r,iM_s+m}$ of $\theta_r(t)$ and τ_{r,iM_s+m}. The corresponding carrier phase and timing errors are denoted $\phi(t)$ and $\epsilon_{iM_s+m}T$:

$$\begin{aligned} \phi(t) &= \theta_r(t) - \hat{\theta}_r(t) \\ \epsilon_{iM_s+m}T &= \hat{\tau}_{r,iM_s+m} - \tau_{r,iM_s+m} \end{aligned} \tag{2.11}$$

In most cases of practical interest, the carrier phase and timing errors are slowly varying with respect to the sampling interval T.

In this section, the carrier phase errors and the timing errors are included in the end-to-end transfer function, which results in a time-varying filter. This

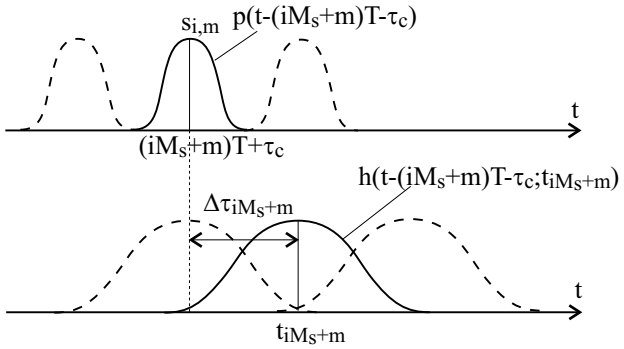

Figure 2.6: The different time delays

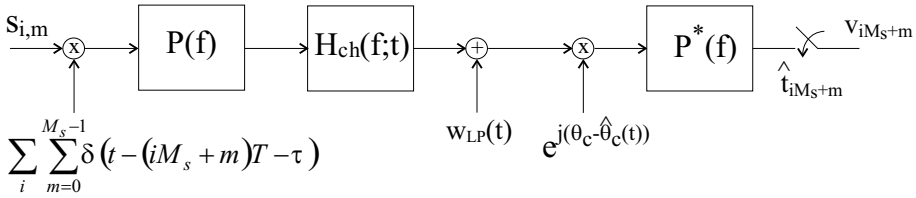

Figure 2.7: Block diagram of a point-to-point communication system in the presence of synchronization errors

unified approach allows us to present a single analysis valid for both carrier phase errors and timing errors. The block diagram of a point-to-point linear digital communication system in the presence of synchronisation errors is shown in figure 2.7. The transmitted signal, consisting of a periodic sequence of Dirac impulses modulated with the discrete-time sequence $\{s_{i,m}\}$ is applied to the transmit filter, which is a unit-energy square-root Nyquist filter with transfer function $P(f)$, and transmitted over the dispersive channel with transfer function $H_{ch}(f;t)$. The output of the dispersive channel is affected by AWGN $w_{LP}(t)$, which has independent real and imaginary parts, each having a power spectral density of $N_0/2$. At the receiver, the signal disturbed by the carrier phase difference $\theta_c - \hat{\theta}_r(t)$ is applied to the receiver filter, which is matched to the transmit filter. The resulting signal is sampled at the instants $\hat{t}_{iM_s+m} = t_{iM_s+m} + \epsilon_{iM_s+m}T$, where $t_{iM_s+m} = (iM_s + m)T + \tau_{r,iM_s+m}$ are the optimum sampling instants and ϵ_{iM_s+m} is the normalised timing error of the mth sample during the ith transmitted block. Assuming the channel slowly varies as compared to the sampling interval T, the phase shift $\Delta\theta(t)$ and the time delay $\Delta\tau_{iM_s+m}$, related to the cascade of the transmit filter, the channel and the receiver filter, are slowly varying as well. The resulting time-domain

samples v_{iM_s+m} are given by

$$\begin{aligned} v_{iM_s+m} &= \int_{-\infty}^{+\infty}\int_{-\infty}^{+\infty} dtdup^*(t-\hat{t}_{iM_s+m})h_{ch}(u;t)e^{j(\theta_c-\hat{\theta}_r(t))} \\ &\quad \sum_{i'=-\infty}^{+\infty}\sum_{m'=0}^{M_s-1} s_{i',m'}p(t-u-(i'M_s+m')T-\tau_c) \\ &+ \int_{-\infty}^{+\infty} p^*(t-\hat{t}_{iM_s+m})w_{LP}(t)dt \end{aligned} \tag{2.12}$$

We assume that the dispersive channel and the carrier phase error are slowly varying as compared to the duration of the receiver filter impulse response $p^*(-t)$. Furthermore, we assume that the timing error is small, i.e., the estimated optimum timing instants $\hat{t}_{iM_s+m}$ are close to the optimum timing instants t_{iM_s+m}. In this case, the samples v_{iM_s+m} yield

$$\begin{aligned} v_{iM_s+m} &\approx \int_{-\infty}^{+\infty}\int_{-\infty}^{+\infty} dtdup^*(t-\hat{t}_{iM_s+m})h_{ch}(u;t_{iM_s+m})e^{j(\theta_c-\hat{\theta}_r(t_{iM_s+m}))} \\ &\quad \sum_{i'=-\infty}^{+\infty}\sum_{m'=0}^{M_s-1} s_{i',m'}p(t-u-(i'M_s+m')T-\tau_c) \\ &+ \int_{-\infty}^{+\infty} p^*(t-\hat{t}_{iM_s+m})w_{LP}(t)dt \\ &= \sum_{i'=-\infty}^{+\infty}\sum_{m'=0}^{M_s-1} s_{i',m'}h_{eq}((iM_s+m)T-(i'M_s+m')T;t_{iM_s+m}) \\ &+ w_{iM_s+m} \end{aligned} \tag{2.13}$$

where w_{iM_s+m} is the matched filter output noise value at the instant $\hat{t}_{iM_s+m}$ and $h_{eq}(t;t_{iM_s+m})$ is the equivalent time-varying end-to-end impulse response; its Fourier transform with respect to the variable t is $H_{eq}(f;t_{iM_s+m})$, given by

$$H_{eq}(f;t_{iM_s+m}) = H(f;t_{iM_s+m})e^{j(\phi(t_{iM_s+m})-\Delta\theta(t_{iM_s+m}))}e^{j2\pi f(\epsilon_{iM_s+m}T+\Delta\tau_{iM_s+m})} \tag{2.14}$$

where $H(f;t_{iM_s+m})$ is the transfer function of the cascade of the transmit filter, the channel and the receiver filter: $H(f;t_{iM_s+m}) = |P(f)|^2 H_{ch}(f;t_{iM_s+m})$ [Lin99], [Fre98]. The effect of the synchronisation parameters on the equivalent time-varying end-to-end impulse response $H_{eq}(f;t_{iM_s+m})$ (2.14) can be explained as follows. The transmitted baseband signal $s_{LP}(t)$ (see figure 2.2) is upconverted using a carrier oscillator with a total phase of $2\pi f_c t + \theta_c$ and the received bandpass signal $r_{BP}(t)$ (see figure 2.4) is downconverted using a carrier oscillator with total phase $-(2\pi f_c t + \hat{\theta}_r(t))$. The cascade of the upconversion and downconversion yields a phase rotation over $(2\pi f_c t + \theta_c) - (2\pi f_c t + \hat{\theta}_r(t))$. The cascade of the upconversion and downconversion operation can be viewed as if the carriers at the transmitter and the receiver are perfectly synchronised, and the phase rotation over $(2\pi f_c t + \theta_c) - (2\pi f_c t + \hat{\theta}_r(t))$ is intro-

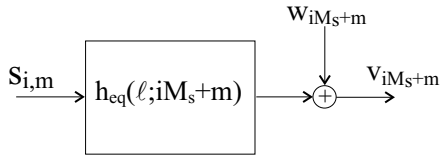

Figure 2.8: Equivalent discrete-time domain channel model

duced by the channel. Considering the definition of the carrier phase error $\phi(t)$ (2.11) and the optimum phase shift $\theta_r(t)$ (2.10), this phase rotation can be written as $(2\pi f_c t + \theta_c) - (2\pi f_c t + \hat{\theta}_r(t)) = \phi(t) - \Delta\theta(t)$. Hence, the equivalent time-varying end-to-end impulse response includes a phase rotation $\phi(t_{iM_s+m}) - \Delta\theta(t_{iM_s+m})$ introduced by the carrier phase difference at the instant t_{iM_s+m}. Further, the samples $\mathbf{s}_i$ (figure 2.2) are transmitted at the instants $(iM_s + m)T + \tau_c$. The signal at the output of the receiver filter (figure 2.4) is sampled at the instants $\hat{t}_{iM_s+m} = (iM_s + m)T + \hat{\tau}_{r,iM_s+m}$. The difference between the timing instants at the transmitter and the receiver can be viewed as if the transmitter and receiver clock are perfectly synchronised and produce samples at the same timing instants t_{iM_s+m}, and the time delay $((iM_s + m)T + \tau_c) - ((iM_s + m)T + \hat{\tau}_{r,iM_s+m})$ is introduced by the channel. Considering the definition of the timing error $\epsilon_{iM_s+m}T$ (2.11) and the optimum time delay τ_{r,iM_s+m} (2.10), this time delay can be written as $((iM_s+m)T+\tau_c)-((iM_s+m)T+\hat{\tau}_{r,iM_s+m}) = -(\epsilon_{iM_s+m}T+\Delta\tau_{iM_s+m})$. Hence, the equivalent time-varying end-to-end impulse response includes a time delay $-(\epsilon_{iM_s+m}T + \Delta\tau_{iM_s+m})$, caused by the difference between the timing instants between the transmitter and the receiver. Considering (2.13), the continuous-time structure from figure 2.7 is equivalent to the discrete-time structure from figure 2.8, consisting of an equivalent linear time-varying discrete-time impulse response $h_{eq}(k; iM_s + m)$ that includes the synchronisation errors, followed by an additive Gaussian noise disturbance w_{iM_s+m}. The Fourier transform of $h_{eq}(k; iM_s + m)$ equals the folded Fourier transform $H_{eq}(f; t_{iM_s+m})$

$$FT[h_{eq}(k; iM_s + m)](f) = \frac{1}{T} \sum_{n=-\infty}^{+\infty} H_{eq}\left(f - \frac{n}{T}; t_{iM_s+m}\right) \tag{2.15}$$

and the autocorrelation function of the noise disturbance w_{iM_s+m} is given by

$$\begin{aligned} E[w_{iM_s+m} w^*_{i'M_s+m'}] &= N_0 \int_{-\infty}^{+\infty} |P(f)|^2 e^{j2\pi f(\hat{t}_{iM_s+m} - \hat{t}_{i'M_s+m'})} df \\ &= N_0 g(\hat{t}_{iM_s+m} - \hat{t}_{i'M_s+m'}) \end{aligned} \tag{2.16}$$

where $g(t)$ is the inverse Fourier transform of $|P(f)|^2$. From (2.3) it follows that $g(kT) = \delta_k$. Assuming that the timing instants $\hat{t}_{iM_s+m}$ are essentially equidistant with spacing T over the duration of $g(t)$ (this implies that $H_{ch}(f; t)$ and the timing error are slowly varying as compared to the duration of $g(t)$),

we obtain

$$E[w_{iM_s+m}w^*_{i'M_s+m'}] \approx N_0\delta_{i-i'}\delta_{m-m'} \tag{2.17}$$

which indicates that the noise contributions are essentially statistically independent.

2.3.2 Model of Synchronisation Errors

In the previous section we have derived a channel model that includes the synchronisation errors. In this section, we present a model for these synchronisation errors.

First, a model is presented for the carrier phase errors. In this work two types of carrier phase error are considered [Ste97a], [Ste97b], [Ste99c], [Ste99f], [Pol95a].

- When the receiver uses a free-running oscillator for the RF to baseband conversion with a frequency close to the frequency of the carrier at the transmitter, a small carrier frequency offset ΔF occurs [Ste97a], [Ste99f]. In this case, the carrier phase error linearly increases in time: $\phi(t) = 2\pi\Delta Ft+\phi(0)$. As a result of the carrier frequency offset, the receiver filter output samples v_{iM_s+m} rotate at a speed of $2\pi\Delta F$ rad/s. Another effect is shown in figure 2.9: the carrier frequency offset gives rise to a frequency shift of the downconverted signal. Because of this frequency shift, a part of the received power falls outside the bandwidth of the receiver filter, resulting in signal distortion and power loss. Hence, a communication system will suffer from a carrier frequency offset if no countermeasures are taken.
- When the phase $\hat{\theta}_r(t)$ of the local oscillator is derived from the received signal by means of a feedback carrier synchronisation mechanism, the local oscillator has an average frequency exactly equal to that of the RF carrier [Mey98]. The resulting carrier phase error $\phi(t)$ can be decomposed as the sum of a constant phase offset and a zero-mean random jitter. When a second-order loop is used to derive the phase $\hat{\theta}_r(t)$ of the local oscillator, a constant phase offset can be eliminated. The jitter power spectral density $S_\phi(f)$ has a bandwidth f_B that is much smaller than the signal bandwidth, and consists of two contributions [Mey98], [Ste97a], [Ste97b], [Ste99c], [Ste99f], [Pol95a]. The first contribution originates from the loop noise within the synchroniser bandwidth, which represents the statistical fluctuations caused e.g., by the additive noise and the random nature of the data symbols. The second contribution originates from the oscillator phase noise outside the synchroniser bandwidth. This yields

  $$S_\phi(f) = |H_c(f)|^2 S_L(f) + |1 - H_c(f)|^2 S_{PN}(f) \tag{2.18}$$

  In (2.18), $H_c(f)$ is the closed-loop transfer function of the synchroniser, and $S_L(f)$ and $S_{PN}(f)$ are the power spectra of the loop noise and the

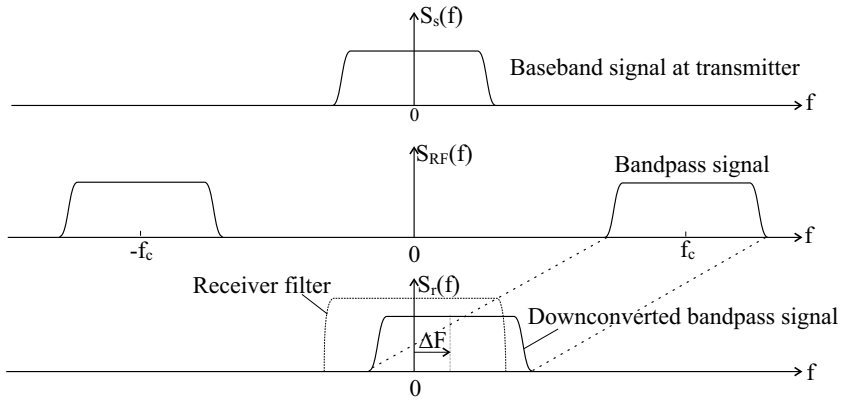

Figure 2.9: Influence of a carrier frequency offset on the power spectrum

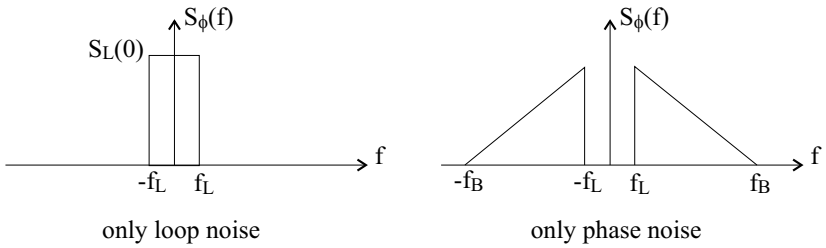

Figure 2.10: Typical spectrum of the carrier phase error resulting from a PLL

oscillator phase noise, respectively. The closed-loop transfer function can be approximated by an ideal lowpass filter with $H_c(0) = 1$ and bandwidth f_L. Hence, the carrier phase error $\phi(t)$ contains the lowpass ($|f| < f_L$) components of the loop noise and the highpass ($|f| > f_L$) components of the oscillator phase noise (figure 2.10). Within the bandwidth of the closed-loop transfer function, the loop noise is approximately white, i.e., $S_L(f) \approx S_L(0)$ for $|f| < f_L$. A similar jitter model applies when a feed-forward carrier synchroniser is used.

Next, a model is presented for the timing errors. In this work, the following types of timing error will be considered [Ste97a], [Ste97b], [Ste99c], [Ste99f], [Pol95a].

- When the sampling at the receiver is performed by means of a free-running clock whose frequency is close to the frequency of the clock at the transmitter, a small clock frequency offset occurs. In this case, the normalised timing error linearly increases in time, as shown in figure 2.11: $\epsilon_{iM_s+m} = (iM_s + m)\Delta T/T + \epsilon_0$, where $\Delta T/T$ is the normalised clock frequency offset. Due to the clock frequency offset, the duration of a block

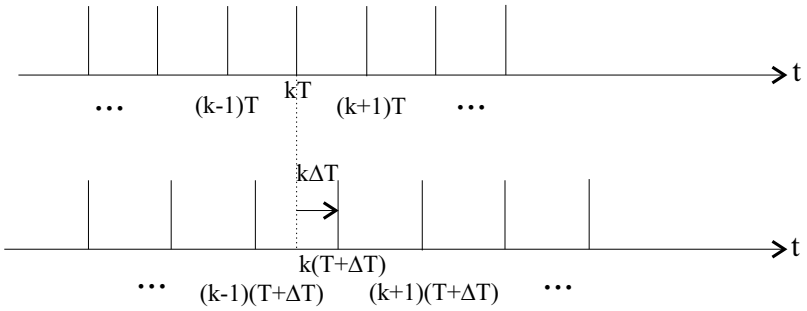

Figure 2.11: A clock frequency offset

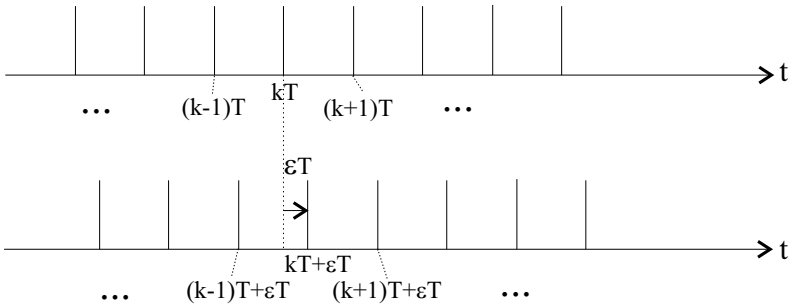

Figure 2.12: A constant timing offset

of M_s samples at the receiver differs from the one at the transmitter. This yields an increasing misalignment between the samples $s_{i,m}$ at the transmitter and the samples v_{iM_s+m} at the receiver.

- When the timing instants at the receiver are derived from the signal by means of a feedback or feedforward clock synchronisation mechanism, the receiver is able to extract a timing signal with an average frequency exactly equal to the frequency of the transmitter clock. The resulting timing error $\epsilon_{iM_s+m}T$ can be decomposed as the sum of a constant timing offset and a zero-mean random jitter, caused by the disturbances in the channel and the clock synchroniser. A constant mismatch between the optimum time delay τ_{r,iM_s+m} and the estimated time delay $\hat{\tau}_{r,iM_s+m}$ results in a constant timing offset $\epsilon_{iM_s+m} = \epsilon$, as shown in figure 2.12. The jitter power spectral density $S_\epsilon(\exp(j2\pi fT))$ has a bandwidth that is much smaller than the signal bandwidth, and a shape similar to the phase jitter spectrum from figure 2.10.

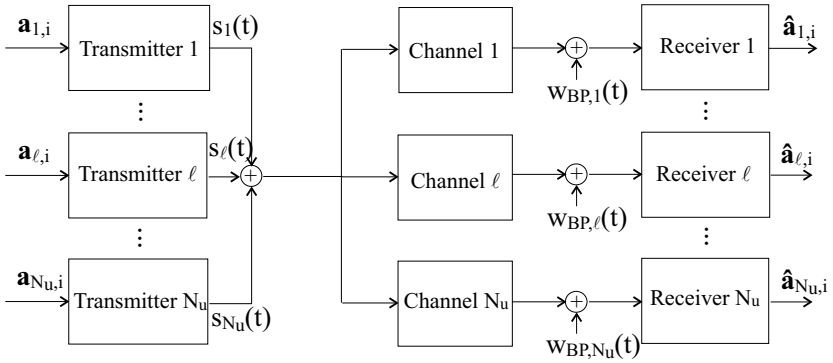

Figure 2.13: Downlink communication

2.4 Multiple Access and Multiplexing

2.4.1 Multiple Users

In mobile radio communication [Stl92], [Lin99], [Fre98], [Red95], the network consists of a base station communicating with N_u mobile users. Depending on the direction of communication, the terms downlink communication (from the base station to the users) and uplink communication (from the users to the base station) are used. To allow many users to communicate simultaneously over a common physical medium without introducing severe interference between the signals transmitted by (uplink) or transmitted to (downlink) the different users, multiple access and multiplexing techniques are used. Multiplexing and multiple access define how downlink and uplink signals should be transmitted, respectively. In the following, we separately consider the cases of downlink and uplink communication and we present a single equivalent channel model for both downlink and uplink communication that includes the synchronisation errors. In both cases, the base station provides a network synchronisation reference signal, containing the timing instants and the carrier frequency and phase used by the base station, from which the different mobile users can extract the frequencies and phases for their local clock signal and local carrier oscillator.

In downlink communication, also called downstream communication or the forward link, the transmitter is located at the base station. The base station broadcasts the signals to the different users. At the base station, the sequence of data symbols $\mathbf{a}_{i,\ell}$ transmitted to user ℓ ($\ell = 1, \ldots, N_u$) during the ith block is converted into a continuous-time bandpass signal $s_\ell(t)$ (see figure 2.13). A common clock signal and carrier oscillator are provided by the base station and the signals are synchronised, such that the time delay τ_c, the clock frequency $1/T$, the carrier frequency f_c and the carrier phase θ_c are equal for all signals $s_\ell(t)$. The base station multiplexes the signals $s_\ell(t)$ and broadcasts the multiplexed signal to all users. As the users generally are on different locations,

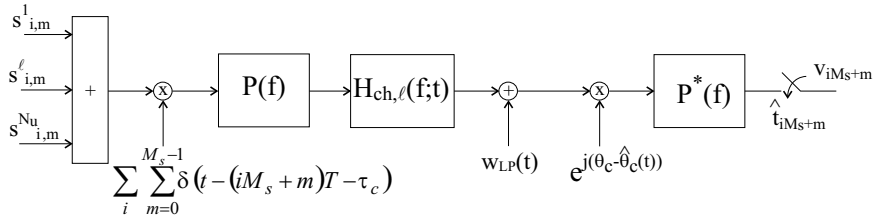

Figure 2.14: Block diagram of a downlink linear digital communication system

the transfer function from the base station to the receiver of user ℓ depends of the user index ℓ. The receiver of user ℓ makes use of a local clock and a local carrier oscillator to extract a discrete-time sequence $v_{iM_s+m,\ell}$ at the receiver filter output. This discrete-time sequence at receiver ℓ consists of contributions of data symbols transmitted to all users. All these contributions are affected by the same carrier phase error and timing error, as they are synchronised at the base station and are upconverted and downconverted by the same carrier oscillators. Furthermore, all contributions have experienced the same channel transfer function $H_{ch,\ell}(f;t)$ as all signals were transmitted over the same channel ℓ. From this discrete-time sequence, the receiver has to extract the data symbols that were transmitted to user ℓ. Note that downlink communication is very similar to point-to-point communication, but in downlink communication, all quantities that are related to the transmitter and the channel have an additional user index ℓ.

The block diagram of a downlink linear digital communication system in the presence of synchronisation errors is shown in figure 2.14. The transmitted discrete-time sequence $\{s_{i,m}\}$ consists of the superposition of the discrete-time sequences $\{s^{\ell}_{i,m}\}$, where $s^{\ell}_{i,m}$ is the mth sample transmitted to user ℓ during the ith block.

$$s_{i,m} = \sum_{\ell=1}^{N_u} s^{\ell}_{i,m} \tag{2.19}$$

where the time sequence transmitted to user ℓ is given by $\mathbf{s}^{\ell}_i = \mathbf{T}_{tr,i,\ell}\mathbf{a}_{\mathbf{i},\ell}$, where $\mathbf{T}_{tr,i,\ell}$ is the transmitter matrix of user ℓ during the ith block. In the following, we consider the communication between the base station and user ℓ. The transfer function from the base station to the receiver of user ℓ is given by $H_{ch,\ell}(f;t)$. The output of the dispersive channel is disturbed by AWGN $w_{LP}(t)$. At the receiver of user ℓ, the signal affected by the carrier phase difference $\theta_c - \hat{\theta}_{r,\ell}(t)$, where θ_c is the carrier phase of the transmitter carrier oscillator and $\hat{\theta}_{r,\ell}(t)$ is the estimated optimum phase of the receiver carrier oscillator. The carrier phase yielding the optimum performance is $\theta_{r,\ell}(t) = \theta_c + \Delta\theta_\ell(t)$, where the carrier phase $\Delta\theta_\ell(t)$ depends on the characteristics of the channel $H_{ch,\ell}(f;t)$. The carrier phase error $\phi_\ell(t)$ is defined as the difference between the optimum carrier phase $\theta_{r,\ell}(t)$ and the estimated optimum carrier phase $\hat{\theta}_{r,\ell}(t)$: $\phi_\ell(t) = \theta_{r,\ell}(t) - \hat{\theta}_{r,\ell}(t)$. The resulting signal is applied to the receiver

filter and sampled at the instants $\hat{t}_{iM_s+m,\ell} = t_{iM_s+m,\ell} + \epsilon_{iMs+m,\ell}T$, where $t_{iM_s+m,\ell} = (iM_s + m)T + \tau^{\ell}_{r,iM_s+m}$ are the optimum sampling instants and $\epsilon_{iM_s+m,\ell}$ is the normalised timing error at receiver ℓ of the mth sample during the ith transmitted block. The time delay τ^{ℓ}_{r,iM_s+m} yielding the optimum performance is given by $\tau^{\ell}_{r,iM_s+m} = \tau_c + \Delta\tau_{iM_s+m,\ell}$, where τ_c is the time delay representing the transmit clock phase and $\Delta\tau_{iM_s+m,\ell}$ depends on the characteristics of the channel $H_{ch,\ell}(f;t)$. Following a similar analysis as in section 2.3.1 for point-to-point communication, the synchronisation errors can be included into an equivalent time-varying impulse response, yielding

$$\begin{aligned} v_{iM_s+m,\ell} &\approx \sum_{i'=-\infty}^{+\infty} \sum_{m'=0}^{M_s-1} \sum_{\ell'=1}^{N_u} s^{\ell'}_{i',m'} h_{eq,\ell}((iM_s+m)T - (i'M_s+m')T; t_{iM_s+m,\ell}) \\ &+ \quad w_{iM_s+m,\ell} \end{aligned} \tag{2.20}$$

where $w_{iM_s+m,\ell}$ is the matched filter output noise value at the instant $\hat{t}_{iM_s+m,\ell}$ and $h_{eq,\ell}(t; t_{iM_s+m,\ell})$ is the equivalent time-varying end-to-end impulse response; its Fourier transform with respect to the variable t is $H_{eq,\ell}(f; t_{iM_s+m,\ell})$, given by

$$\begin{aligned} H_{eq}(f; t_{iM_s+m,\ell}) &= H_{\ell}(f; t_{iM_s+m,\ell}) e^{j(\phi_{\ell}(t_{iM_s+m,\ell}) - \Delta\theta_{\ell}(t_{iM_s+m,\ell}))} \cdot \\ &\qquad e^{j2\pi f(\epsilon_{iM_s+m,\ell}T + \Delta\tau_{iM_s+m,\ell})} \end{aligned} \tag{2.21}$$

where $H_{\ell}(f; t_{iM_s+m,\ell})$ is the transfer function of the cascade of the transmit filter, the channel and the receiver filter: $H_{\ell}(f; t_{iM_s+m,\ell}) = |P(f)|^2 H_{ch,\ell}(f; t_{iM_s+m,\ell})$ [Lin99], [Fre98]. We can define, similarly as for the case of point-to-point communication, an equivalent linear discrete-time channel with impulse response $h_{eq,\ell}(k; iM_s+m)$, whose Fourier transform equals the folded Fourier transform $H_{eq,\ell}(f; t_{iM_s+m,\ell})$

$$FT[h_{eq,\ell}(k; iM_s+m)](f) = \frac{1}{T} \sum_{n=-\infty}^{+\infty} H_{eq,\ell}\left(f - \frac{n}{T}; t_{iM_s+m,\ell}\right) \tag{2.22}$$

The autocorrelation function of the noise disturbance $w_{iM_s+m,\ell}$ is given by

$$E[w_{iM_s+m,\ell} w^*_{i'M_s+m',\ell}] = N_0 \int_{-\infty}^{+\infty} |P(f)|^2 e^{j2\pi f(\hat{t}_{iM_s+m,\ell} - \hat{t}_{i'M_s+m',\ell})} df \tag{2.23}$$

Similarly as for point-to-point communication, when we assume that the timing error and the channel transfer function are slowly varying as compared to the impulse response duration of the filter with transfer function $|P(f)|^2$, the autocorrelation function of the noise disturbance can be approximated by

$$E[w_{iM_s+m,\ell} w^*_{i'M_s+m',\ell}] \approx N_0 \delta_{i-i'} \delta_{m-m'} \tag{2.24}$$

In uplink communication, also called upstream communication or the reverse link, multiple access is used to transmit the signals generated by the different

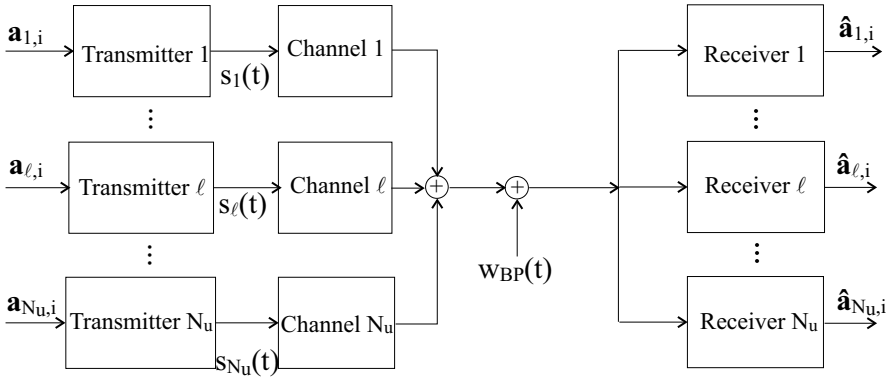

Figure 2.15: Uplink communication

mobile users to the base station. The sequence of data symbols $\mathbf{a}_{i,\ell}$ transmitted by user ℓ ($\ell = 1, \ldots, N_u$) during the ith block is converted into a continuous-time bandpass signal $s_\ell(t)$ (see figure 2.15). At the base station, the sum of the received signals is downconverted and sampled using one carrier oscillator and one sampling clock, respectively. From the resulting sequence, the base station detects the symbols from each individual user. In order to limit the interference between user signals, the mobile transmitters should be synchronised. To this aim, the base station broadcasts a pilot tone from which the mobile users derive their transmit carrier oscillator and transmit clock. Because of the disturbances in the system, it is clear that all transmitters will have slightly different clock and carrier frequencies and phases. Furthermore, the transfer function from the transmitter of user ℓ to the base station depends on the user index ℓ, as the users are at different locations. The base station receives the superposition of the signals transmitted by the different users and extracts after the receiver filter a discrete-time sequence consisting of contributions of data symbols transmitted by all users. The contribution from each user is affected by a different carrier phase error and timing error, and has been transmitted over a different channel.

The block diagram of an uplink linear digital communication system in the presence of synchronisation errors is shown in figure 2.16. The transmitter of user ℓ derives a clock signal and a carrier oscillator signal from the network synchronisation reference signal, resulting in a transmit clock with frequency $1/T$ and time-varying phase $\tau_{iM_s+m,\ell}$ and a transmit carrier oscillator with frequency f_c and time-varying phase $\theta_{c,\ell}(t)$. The time sequence transmitted by user ℓ is given by $\mathbf{s}_i^\ell = \mathbf{T}_{tr,i,\ell}\mathbf{a}_{i,\ell}$, where $\mathbf{T}_{tr,i,\ell}$ is the transmitter matrix of user ℓ during the ith block. The discrete-time sequence $\mathbf{s}_i^\ell$ is converted into a continuous-time signal by multiplying the samples $\mathbf{s}_i^\ell$ with the transmit clock signal. The resulting sequence of weighted Dirac impulses is applied to the transmit filter. The transmitted lowpass signal is upconverted using the transmit carrier oscillator, which can be represented in the lowpass equivalent block diagram of figure 2.16 as a rotation over the phase $\theta_{c,\ell}(t)$. The lowpass equivalent channel

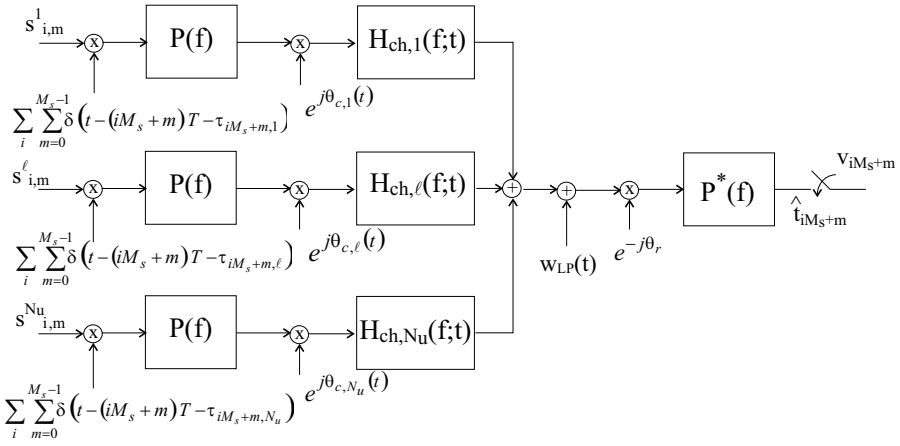

Figure 2.16: Block diagram of an uplink linear digital communication system

transfer function from the transmitter of user ℓ to the base station is given by $H_{ch,\ell}(f;t)$. At the base station, the received bandpass signal consists of the superposition of the passband signals transmitted by the different users, disturbed by additive white Gaussian bandpass noise with lowpass equivalent $w_{LP}(t)$. The optimum total phases of the base station carrier oscillator and sampling clock for user ℓ are denoted $2\pi f_c t + \theta_{r,\ell}(t)$ and $(iM_s+m)T + \tau^{\ell}_{r,iM_s+m}$, respectively. The optimum carrier phase $\theta_{r,\ell}(t)$ and time delay τ^{ℓ}_{r,iM_s+m} to be applied at the receiving base station are given by

$$\begin{aligned} \theta_{r,\ell}(t) &= \theta_{c,\ell}(t) + \Delta\theta_{\ell}(t) \\ \tau^{\ell}_{r,iM_s+m} &= \tau_{iM_s+m,\ell} + \Delta\tau_{iM_s+m,\ell} \end{aligned} \tag{2.25}$$

where the phase shift $\Delta\theta_{\ell}(t)$ and the time delay $\Delta\tau_{iM_s+m,\ell}$ depend on the channel characteristics of user ℓ. However, the base station uses one oscillator with phase θ_r and one sampling clock with time delay τ_r for all users. Hence, the contributions from the different users to the receiver output samples are affected by a different carrier phase error and timing error, given by

$$\begin{aligned} \phi_{\ell}(t) &= \theta_{r,\ell}(t) - \theta_r \\ \epsilon_{iM_s+m,\ell}T &= \tau_r - \tau^{\ell}_{r,iM_s+m} \end{aligned} \tag{2.26}$$

The base station downconverts the received bandpass signal by multiplying the signal with the oscillator signal with 'total' phase $-(2\pi f_c t + \theta_r)$. In the lowpass equivalent block diagram of figure 2.16 this downconversion is represented by a rotation over the phase $-\theta_r$. The resulting lowpass signal is applied to the receiver filter and sampled at the instants $t_{iM_s+m} = (iM_s+m)T + \tau_r$. The

resulting time-domain samples v_{iM_s+m} are given by

$$\begin{aligned} v_{iM_s+m} &= \int_{-\infty}^{+\infty}\int_{-\infty}^{+\infty} dtdup^*(t-t_{iM_s+m})\sum_{\ell=1}^{N_u} h_{ch,\ell}(u;t)e^{j(\theta_{c,\ell}(t)-\theta_r)} \\ &\quad \sum_{i'=-\infty}^{+\infty}\sum_{m'=0}^{M_s-1} s^{\ell}_{i',m'}p(t-u-(i'M_s+m')T-\tau_{i'M_s+m',\ell}) \\ &+ \int_{-\infty}^{+\infty} p^*(t-t_{iM_s+m})w_{LP}(t)dt \end{aligned} \tag{2.27}$$

Assuming the dispersive channels and the carrier phase errors are slowly varying as compared to the duration of the receiver filter impulse response $p^*(-t)$, the samples v_{iM_s+m} yield

$$\begin{aligned} v_{iM_s+m} &\approx \int_{-\infty}^{+\infty}\int_{-\infty}^{+\infty} dtdup^*(t-t_{iM_s+m})\sum_{\ell=1}^{N_u} h_{ch,\ell}(u;t_{iM_s+m})e^{j(\theta_{c,\ell}(t_{iM_s+m})-\theta_r)} \\ &\quad \sum_{i'=-\infty}^{+\infty}\sum_{m'=0}^{M_s-1} s^{\ell}_{i',m'}p(t-u-(i'M_s+m')T-\tau_{i'M_s+m',\ell}) \\ &+ w_{iM_s+m} \end{aligned} \tag{2.28}$$

where w_{iM_s+m} is the matched filter output noise value at the instant t_{iM_s+m}. Similar as for the downlink, we define $H_\ell(f;t_{iM_s+m})$ as the transfer function of the cascade of the transmit filter, the channel and the receiver filter: $H_\ell(f;t_{iM_s+m}) = |P(f)|^2 H_{ch,\ell}(f;t_{iM_s+m})$. Assuming the timing error slowly varies as compared to the duration of the composite channel impulse response with transfer function $H_\ell(f;t_{iM_s+m})$, the samples v_{iM_s+m} yield

$$v_{iM_s+m} \approx \sum_{i'=-\infty}^{+\infty}\sum_{m'=0}^{M_s-1}\sum_{\ell=1}^{N_u} s^{\ell}_{i',m'}h_{eq}(t_{iM_s+m}-t_{i'M_s+m'};t_{iM_s+m}) + w_{iM_s+m} \tag{2.29}$$

where the equivalent time-varying impulse response $h_{eq,\ell}(t;t_{iM_s+m})$ is the same as for downlink communication, with Fourier transform (2.21). The autocorrelation function of the noise disturbance w_{iM_s+m} is given by

$$\begin{aligned} E[w_{iM_s+m}w^*_{i'M_s+m'}] &= N_0 g(t_{iM_s+m}-t_{i'M_s+m'}) \\ &= N_0\delta_{i-i'}\delta_{m-m'} \end{aligned} \tag{2.30}$$

because the spacing of the samples at the receiver filter output equals T. Similarly as for downlink communication, an equivalent linear time-varying discrete-time impulse response $h_{eq,\ell}(k;iM_s+m)$ with Fourier transform (2.22) can be defined.

As the equivalent time-varying discrete-time transfer function $h_{eq,\ell}(k;iM_s+m)$ (2.22) and the noise disturbance $w_{iM_s+m,\ell}$ (see (2.24) and (2.30)) are defined in a similar way for downlink and uplink communication, an equivalent

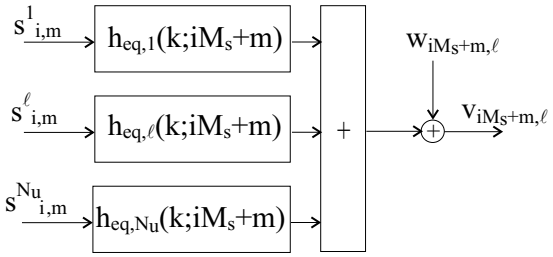

Figure 2.17: Equivalent channel model for multiuser communication

time-varying discrete-time channel model for multiuser communication can be defined as shown in figure 2.17. This model describes the communication between the basestation and the users for both the downlink and the uplink. In downlink communication, the sequences $\mathbf{s}_i^\ell$ $(\ell = 1, \ldots, N_u)$ are broadcasted by the base station to the different users. At the receiver of user ℓ, all contributions have experienced the same equivalent time-varying discrete-time channel, i.e., $h_{eq,\ell'}(k; iM_s + m) = h_{eq,\ell}(k; iM_s + m)$ $(\ell' = 1, \ldots, N_u)$. The channel is followed by an additive noise disturbance $w_{iM_s+m,\ell}$ with autocorrelation function (2.24), resulting in the samples $v_{iM_s+m,\ell}$. The noise disturbance $w_{iM_s+m,\ell}$ and the samples $v_{iM_s+m,\ell}$ depend on the user index ℓ as the receiver of user ℓ uses a local sampling clock to extract the transmitted data. In uplink communication, the sequences $\mathbf{s}_i^\ell$ $(\ell = 1, \ldots, N_u)$ are transmitted to the base station. The equivalent time-varying discrete-time channel $h_{eq,\ell}(k; iM_s + m)$ depends on the user index ℓ as the users are on different locations. The sum of the channel output signals is disturbed by additive noise w_{iM_s+m} with autocorrelation function (2.30), resulting in the samples v_{iM_s+m}. The noise disturbance w_{iM_s+m} and the samples v_{iM_s+m} are independent of the user index ℓ as the basestation uses one clock to extract the data of all users.

Example: Let us consider a simple example, consisting of a mobile communication system where two mobile users transmit data to the base station. We assume the channels are non-dispersive, but only introduce a time delay: the transfer function from the transmitter of user ℓ $(\ell = 1, 2)$ to the base station is given by

$$H_{ch,\ell}(f) = e^{-j2\pi f t_\ell} \tag{2.31}$$

Furthermore, we assume that the transmitters of both users know the clock frequency $1/T$ and the carrier frequency f_c. Assuming the transmitter of user ℓ $(\ell = 1, 2)$ knows the time delay t_ℓ introduced by the channel ℓ, the transmitter of user ℓ selects the clock phase $\tau_{iM_s+m,\ell} = -t_\ell$, i.e., the blocks of M_s samples originating from the two users are aligned at the base station. Furthermore, the carrier used for upconverting the lowpass signal transmitted by user ℓ has a carrier phase $\theta_{c,\ell}$, as shown in figure 2.18.

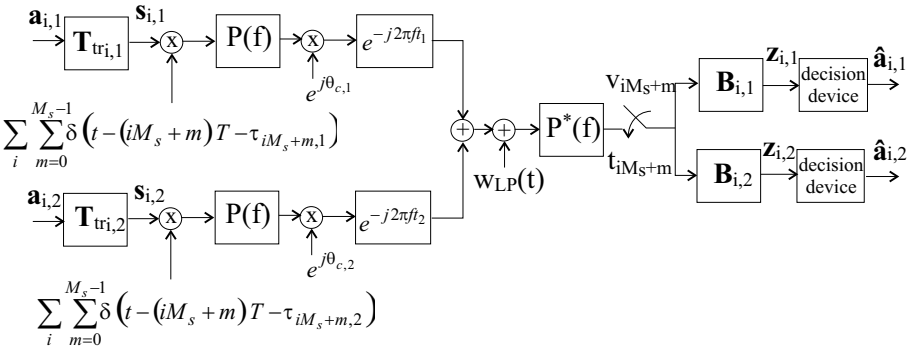

Figure 2.18: Block diagram of two mobile users transmitting data to the base station

At the base station, the received signal consists of the sum of the signals transmitted by the two users disturbed by noise. Further, we assume that the carrier phase of the carrier at the base station θ_r=0 and that the clock phase of the base station clock $\tau_r = 0$. Taking into account the square-root Nyquist property (2.3) of the transmit and the receiver filter, it follows that

$$v_{iM_s+m} = s^1_{i,m} e^{j\theta_{c,1}} + s^2_{i,m} e^{j\theta_{c,2}} + w_{iM_s+m} \tag{2.32}$$

where w_{iM_s+m} denotes the contribution from the noise $w_{LP}(t)$ and $\mathbf{s}_{i,\ell} = [s^\ell_{i,1} \dots s^\ell_{i,M_s-1}]^T$ is related to the data symbols $\mathbf{a}_{i,\ell}$, transmitted by user ℓ, by

$$\mathbf{s}_{i,\ell} = \mathbf{T}_{tr,i,\ell} \mathbf{a}_{i,\ell} \tag{2.33}$$

where $\mathbf{T}_{tr,i,\ell}$ is the linear transformation matrix of user ℓ. The samples v_{iM_s+m} are applied to a linear transformation $\mathbf{B}_{i,\ell} = [\mathbf{b}_{0,i,\ell} \dots \mathbf{b}_{N_s-1,i,\ell}]^T$ in order to detect the data symbols transmitted by user ℓ.

Now let us assume that the N_s columns of the $M_s \times N_s$ matrices $\mathbf{T}_{tr,i,\ell}$ ($\ell = 1, 2$) are orthogonal and the matrices $\mathbf{T}_{tr,i,1}$ and $\mathbf{T}_{tr,i,2}$ are mutually orthogonal (this requires $M_s \geq 2N_s$):

$$\mathbf{T}^\dagger_{tr,i,\ell_1} \mathbf{T}_{tr,i,\ell_2} = \mathbf{T}^\dagger_{tr,i,\ell_2} \mathbf{T}_{tr,i,\ell_1} = I_{N_s} \delta_{\ell_1 - \ell_2} \tag{2.34}$$

(2.4-16) where I_{N_s} is the identity matrix of order $N_s \times N_s$. Selecting $\mathbf{B}_\ell = exp(-j\theta_{c,\ell}) \mathbf{T}^\dagger_{tr,i,\ell}$ ($\ell = 1, 2$), the samples at the input of the decision device of user ℓ yield

$$z^\ell_{i,n} = a^\ell_{i,n} + W^\ell_{i,n} \tag{2.35}$$

where $a^\ell_{i,n}$ is the nth data symbol of user ℓ transmitted during the ith block, and $W^\ell_{i,n}$ denotes the noise contribution. This simple example indicates that the sample $z^\ell_{i,n}$ is not affected by intersymbol

interference (ISI) or multiuser interference (MUI) when the channel is non-dispersive, the blocks of M_s samples transmitted by the two users are aligned at the base station, the carrier frequency is known at the transmitters and the matrices $\mathbf{T}_{tr,i,\ell}$ are orthogonal. Furthermore, it follows that a constant carrier phase offset does not affect the orthogonality of the signals of the different users. In general, when there are N_u mobile users, the orthogonality conditions of the matrices $\mathbf{T}_{tr,i,\ell}$ require that $M_s \geq N_u N_s$. In practical systems, ISI and MUI will occur because of non-ideal channel conditions and imperfect synchronisation. Furthermore, when the matrices $\mathbf{T}_{tr,i,\ell}$ are not mutually orthogonal, MUI will be introduced.

2.4.2 Multiple Access and Multiplexing Techniques

To avoid multiuser interference (MUI), which is interference between signals sent to (downlink) or received from (uplink) different users, the receiver should be able to separate the user signals. This separation is achieved by making the signals orthogonal, e.g., by making the matrices $\mathbf{T}_{tr,\ell}$ mutually orthogonal. Different multiple access and multiplexing techniques have been developed to separate the user signals.

- In TDM(A) (time division multiplexing/ multiple access), the time axis is divided into a number of time non-overlapping time slots. Each user signal is assigned a different set of time slots during which he can occupy the whole system bandwidth. The signals of the different users can be separated provided they occupy non-overlapping time intervals.

  Example: Let us consider two perfectly synchronised mobile users, transmitting data to the base station using the TDMA technique. The linear transformation matrices $\mathbf{T}_{tr,i,\ell}$ $(\ell = 1, 2)$ at the transmitters are given by:

  $$\mathbf{T}_{tr,i,1} = \begin{pmatrix} \hat{\mathbf{T}}_{tr,i,1} \\ \mathbf{0} \end{pmatrix} \qquad \mathbf{T}_{tr,i,2} = \begin{pmatrix} \mathbf{0} \\ \hat{\mathbf{T}}_{tr,i,2} \end{pmatrix} \tag{2.36}$$

  where $\mathbf{T}_{tr,i,\ell}$ $(\ell = 1, 2)$ is a matrix of dimension $M_s \times N_s$ and $\hat{\mathbf{T}}_{tr,i,\ell}$ $(\ell = 1, 2)$ is a matrix of dimension $(M_s/2) \times N_s$. The N_s columns of the matrices $\hat{\mathbf{T}}_{tr,i,\ell}$ $(\ell = 1, 2)$ are orthogonal. Note that the matrices $\mathbf{T}_{tr,i,1}$ and $\mathbf{T}_{tr,i,2}$ (2.36) are mutually orthogonal by construction. This example corresponds to the case where the first user and the second user occupy the odd-numbered and the even-numbered time slots, respectively.

- In FDM(A) (frequency division multiplexing/ multiple access), the available bandwidth is divided into a number of non-overlapping frequency

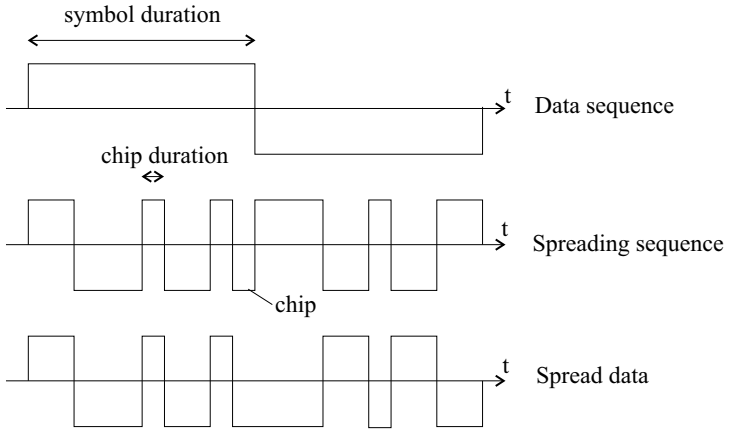

Figure 2.19: Spreading of the data symbols

bands. Each user is assigned a different frequency band, which is occupied as long as the corresponding user signal is active. The signals of the different users are separated in the frequency-domain. FDM(A) with non-overlapping frequency bands is equivalent to a set of non-interacting single user systems.

- In CDM(A) (code division multiplexing/ multiple access), each user signal occupies the whole system bandwidth during the time the user is active. The data symbols are spread by multiplying the data symbols with a higher rate spreading sequence, as shown in figure 2.19. The number of chips per data symbol is called the spreading factor. Each user is assigned a unique spreading sequence. The signals of the different users can be separated by making the spreading sequences orthogonal.

  Example: Let us consider two perfectly synchronised mobile users, transmitting data to the base station using the CDMA technique. The sequence of samples $\mathbf{s}_i^\ell$ transmitted by user ℓ is given by $\mathbf{s}_i^\ell = \mathbf{T}_{tr,i,\ell} a_{i,\ell}$ $(\ell = 1, 2)$, where $a_{i,\ell}$ is the data symbol transmitted by user ℓ during the ith symbol interval (i.e., N_s=1) and $\mathbf{T}_{tr,i,\ell}$ is a vector that converts the data symbol $a_{i,\ell}$ into a block of M_s samples. In many cases of practical interest, the vector $\mathbf{T}_{tr,i,\ell}$ can be written as

  $$\mathbf{T}_{tr,i,\ell} = \mathbf{T}\mathbf{c}_{i,\ell} \tag{2.37}$$

  where $\mathbf{T}$ is a $(M_s \times N_c)$ matrix that is independent of the user index ℓ. The N_c columns of the matrix $\mathbf{T}$ are orthogonal, i.e., $\mathbf{T}^\dagger\mathbf{T} = I_{N_c}$, where $\mathbf{T}^\dagger$ is the Hermitian of the matrix $\mathbf{T}$ and I_{N_c} is the identity matrix of order $(N_c \times N_c)$. The vector

$\mathbf{c}_{i,\ell} = [c_{iN_c,\ell} \ldots c_{iN_c+N_c-1,\ell}]^T$ contains the chips of the spreading sequence assigned to user ℓ. The number N_c of chips per symbol is the spreading factor.

We assume the case of an ideal channel ($H_{ch,\ell}(f;t) = 1$). As the two users are perfectly synchronised and taking into account the square-root Nyquist property (2.3 of the transmit and the receiver filter, the samples $\mathbf{v}_i$ at the output of the receiver filter are given by

$$\mathbf{v}_i = \mathbf{s}_i^1 + \mathbf{s}_i^2 + \mathbf{w}_i \tag{2.38}$$

where $\mathbf{w}_i$ denotes the contribution of the noise $w_{LP}(t)$. To extract the data symbols transmitted by user ℓ, the samples $\mathbf{v}_i$ are applied to the linear transformation $\mathbf{T}_{tr,i,\ell}^{\dagger}$. The sample $z_{i,\ell}$ at the input of the decision device yields

$$\begin{aligned} z_{i,\ell} &= \mathbf{c}_{i,\ell}^{\dagger}\mathbf{T}^{\dagger}\mathbf{v}_i \\ &= \mathbf{c}_{i,\ell}^{\dagger}\mathbf{c}_{i,1}a_{i,1} + \mathbf{c}_{i,\ell}^{\dagger}\mathbf{c}_{i,2}a_{i,2} + W_{i,\ell} \end{aligned} \tag{2.39}$$

where $W_{i,\ell}$ is the noise contribution.

Now, let us assume that the spreading sequences are mutually orthogonal

$$\mathbf{c}_{i,\ell_1}^{\dagger}\mathbf{c}_{i,\ell_2} = \delta_{\ell_1-\ell_2} \tag{2.40}$$

In this case, the sample at the input of the decision device of user ℓ yields

$$z_{i,\ell} = a_{i,\ell} + W_{i,\ell} \tag{2.41}$$

This example indicates that the sample $z_{i,\ell}$ at the input of the decision device is not affected by multiuser interference (MUI) or intersymbol interference (ISI) when the channel is non-dispersive, the users are perfectly synchronised and the spreading sequences assigned to the different users are orthogonal.

In several existing systems, combinations of the above multiplexing and multiple access techniques are used to separate the user signals.

When the system has to support a large number of users that are spread over a large area, such as in a mobile radio communication system a cellular structure is used to reduce the system complexity. The covered area typically is partitioned into a number of hexagonal cells, resulting in a cellular structure as shown in figure 2.20. Each cell is covered by one base station, communicating with the users present in the cell. Within each cell, the former multiplexing and multiple access techniques can be used for the communication between the base station and the users in the cell. Communication between base stations of different cells is in generally provided by a high-capacity optical fibre. As the distance between the transmitter and receiver within a cell is small, the power levels can be reduced. Furthermore, as a base station only has to communicate

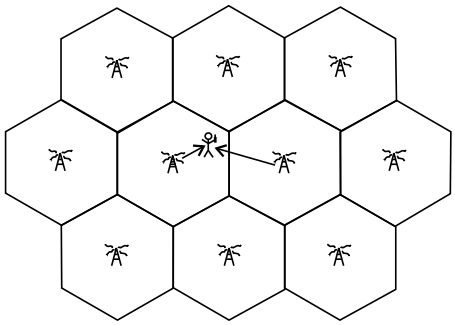

Figure 2.20: Cellular structure

with a small number of users, the implementation complexity of the base station can be reduced. The size of a cell depends on the user density of the covered area. For a high user density, the cell size has to decrease to limit the number of users in each cell. Depending on the user density, one distinguishes between macro cells with a size of 1km-30km (in rural areas), micro cells with a size of 100m-1km (in dense areas such as urban areas) and pico cells with a size of 10m-100m (in very dense areas such as office buildings).

To ensure that the intercell interference, which is the mutual interference between cells, remains below a harmful level, the signals in the different cells have to be separated. This means that neighbouring cells have to be assigned different system resources (e.g., different frequency bands or different spreading sequences). However, it is preferable to reuse the available system resources, as the spectral resources are limited. Because of the path loss, the received power in a mobile radio communication system is inversely proportional to d^x, where d is the distance between the transmitter and the receiver and x is a coefficient that depends on the topology of the covered area. Typically, this coefficient x is larger than two ($x = 2$ for the free space, while $x \approx 4$ for an urban area). This indicates that the same system resources can be reused if the distance between the different cells that use the same system resources is sufficiently large.

2.4.3 Spreading Sequences

As mentioned in the previous section, spreading sequences are a means to separate different users [Moe99b], [Red95], [Has98]. In this section, some types of spreading sequences are considered.

Orthogonal Sequences

One possible set of orthogonal sequences are Walsh-Hadamard (WH) sequences [Moe99a], [Lin99]. These sequences are real-valued sequences that are built of

chips that belong to the set $\{-1, +1\}$. The sequences are easily constructed using a recursive matrix operation

$$\mathbf{H}_\gamma = \begin{pmatrix} \mathbf{H}_{\gamma-1} & \mathbf{H}_{\gamma-1} \\ \mathbf{H}_{\gamma-1} & -\mathbf{H}_{\gamma-1} \end{pmatrix} \tag{2.42}$$

where $\mathbf{H}_\gamma$ is the $2^\gamma \times 2^\gamma$ Hadamard matrix that is formed using the Hadamard matrix $\mathbf{H}_{\gamma-1}$ of size $2^{\gamma-1} \times 2^{\gamma-1}$, and $\mathbf{H}_2$ is given by

$$\mathbf{H}_2 = \begin{pmatrix} 1 & 1 \\ 1 & -1 \end{pmatrix} \tag{2.43}$$

Each row in the matrix $\mathbf{H}_\gamma$ (2.42) provides a sequence of $N_c = 2^\gamma$ chips that spread the data of one user: denoting by $WH_{n,\ell}$ the nth chip of the ℓth WH sequence, we obtain $WH_{n,\ell} = (\mathbf{H}_\gamma)_{\ell,n}$. From (2.42) it follows that the length N_c of a WH sequence always is a power of two. As the maximum number of WH sequences of length N_c equals N_c, the maximum number N_u of active users equals N_c. In general, the assignment of the WH sequences to the different users does not change from one symbol interval to the next, i.e., all symbols of a user are spread with the same WH sequence. In this case, the chips are independent of the time index i

$$c_{iN_c+n,\ell} = WH_{n,\ell} \tag{2.44}$$

As the users are assigned different WH sequences that repeat from one symbol to the next, the performance in the case of a dispersive channel and/or synchronisation errors is user-dependent. This dependence could be avoided by changing the assignment from one symbol to the next, such that on the long run each user has been assigned all WH sequences evenly. However, because of the co-ordination required, this changing assignment is not carried out in practice.

Random Sequences

The performance of the different users becomes independent of the user index when the spreading sequences are random [Moe99a], [Lin99]. In this case, the different users are assigned statistically independent spreading sequences. Furthermore, the chips belonging to a spreading sequence are modelled as zero-mean statistically independent complex-valued random variables. This yields

$$E[c^*_{iN_c+n,\ell} c_{i'N_c+n',\ell'}] = \delta_{i,i'}\delta_{n,n'}\delta_{\ell,\ell'} \tag{2.45}$$

However, as the receiver must correlate the received signal with the spreading sequence, that sequence must be available at the receiver, either by storing the sequence or by generating it at the receiver. In practice, pseudo-noise (PN) sequences with some period L are used, i.e., $c_{iN_c+n,\ell} = c_{iN_c+n+L,\ell}$. A popular class of real-valued binary PN sequences is generated by means of shift-registers [Moe99a], [Lin99]. Assuming the period L is much larger than the spreading factor N_c, the L chips of the constructed sequence can be considered as statistically independent. Complex-valued spreading sequences are constructed from

two real-valued PN sequences. As the random sequences are not orthogonal, multiuser interference occurs as soon as two users are active, even in the case of an ideal channel. In order to avoid excessive MUI, the number of active users N_u has to be much less than the spreading factor N_c.

Overlay Sequences

To overcome the problems encountered with the orthogonal sequences and the random sequences, random sequences and orthogonal sequences can be combined. In this section, we consider overlay sequences [Moe99a] that consist of an orthogonal sequence multiplied with a random sequence. To construct the overlay sequences, we make use of the set of real-valued Walsh-Hadamard sequences $\{WH_{n,\ell}\}$, with chips belonging to the set $\{-1,+1\}$, of length N_c and one complex-valued random sequence (e.g., a complex-valued pseudo-noise sequence of length $L \gg N_c$) $\{PN_{iN_c+n}\}$, with chips belonging to the set $\{\exp(j\pi/2), \exp(j3\pi/2), \exp(-j3\pi/2), \exp(-j\pi/2)\}$, that has the same chip rate as the WH sequence. The complex-valued chips $c_{iN_c+n,\ell}$ of the sequence assigned to user ℓ, consists of the product of the real-valued WH sequence, corresponding to user ℓ, and the complex-valued random sequence, which is the same for all users:

$$c_{iN_c+n,\ell} = WH_{n,\ell} PN_{iN_c+n} \tag{2.46}$$

Similarly as for the WH sequences, the spreading factor N_c is equal to the length of the WH sequence, i.e., a power of two. As the maximum number of orthogonal overlay sequences equals the number of possible WH sequences N_c, the maximum number Nu of active users equals N_c. The overlay sequences belonging to different users are still orthogonal. However, they do not repeat from one symbol to the next, so that the performance is essentially the same for all users.

2.5 The Minimum Mean-Square Error Equaliser

As shown earlier in this chapter, the sequence of samples $\{v_{iM_s+m,\ell}\}$ at the output of the receiver filter is applied to a number N_s of parallel linear transformations $\{\mathbf{b}_{i,n}^{\ell}\}$ (figure 2.4), in order to make decisions about the data symbols $a_{i,n}^{\ell}$, the nth data symbol belonging to user ℓ during the ith transmitted block. In order to obtain reliable decisions, the transformation $\mathbf{b}_{i,n}^{\ell}$ should be a function of a number of (possibly time-varying) parameters, such as the channel transfer function and the phase or frequency offset of the carrier oscillator or sampling clock at the receiver. The adaptation of $\mathbf{b}_{i,n}^{\ell}$ to these parameters is often called 'equalisation'; $\mathbf{b}_{i,n}^{\ell}$ is said to 'track' these parameters. Usually, minimum mean-square error (MMSE) equalisation is performed, i.e., equalisation is such that

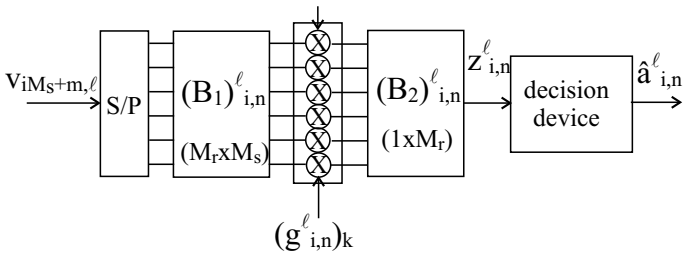

Figure 2.21: Block diagram of the linear transformation at the receiver

the mean-square error (MSE) between the input and the output of the decision device is minimised [Pro95], [Van99]. In this work, we will consider transformations $\mathbf{b}_{i,n}^{\ell}$ that can be decomposed as shown in figure 2.21. The sequence of samples $\{v_{iMs+m,\ell}\}$ is applied to a linear transformation $\mathbf{B}_{1,i,n}^{\ell}$ $(M_r \times M_s)$ that converts the block of M_s samples $\{v_{iM_s+m,\ell}\}$ into a block of M_r samples. The linear transformation $\mathbf{B}_{1,i,n}^{\ell}$ is followed by one-tap equalisers with coefficients $(g_{i,n}^{\ell})_k$ $(k = 0, \ldots, M_r - 1)$ that scale and rotate the M_r outputs of the linear transformation $\mathbf{B}_{1,i,n}^{\ell}$. The outputs of the one-tap equalisers are applied to a second linear transformation $\mathbf{B}_{2,i,n}^{\ell}$ that converts the M_r equaliser outputs into a scalar $z_{i,n}^{\ell}$, which is used to make a decision about the data symbol $a_{i,n}^{\ell}$. The mean-square error between the sample $z_{i,n}^{\ell}$ and the data symbol $a_{i,n}^{\ell}$, given by

$$MSE_{i,n}^{\ell} = E[|z_{i,n}^{\ell} - a_{i,n}^{\ell}|^2] \tag{2.47}$$

should be minimised by proper selection of the equaliser coefficients. The operator $E[.]$ in (2.47) denotes the expectation, conditioned on the parameters to be tracked, so that the resulting MMSE is indeed a function of these parameters.

The sample $z_{i,n}^{\ell}$ at the input of the decision device is related to the received discrete-time sequence $\mathbf{v}_{i,\ell} = [v_{iM_s,\ell} \ldots v_{iM_s+M_s-1,\ell}]^T$ as follows

$$z_{i,n}^{\ell} = \mathbf{B}_{2,i,n}^{\ell} \mathbf{G}_{i,n}^{\ell} \mathbf{B}_{1,i,n}^{\ell} \mathbf{v}_{i,\ell} \triangleq (\mathbf{b}_{i,n}^{\ell})^T \mathbf{v}_{i,\ell} \tag{2.48}$$

where $\mathbf{B}_{1,i,n}^{\ell}$ and $\mathbf{B}_{2,i,n}^{\ell}$ are matrices of the order $(M_r \times M_s)$ and $(1 \times M_r)$, respectively, and $\mathbf{G}_{i,n}^{\ell}$ is the diagonal matrix of the order $(M_r \times M_r)$ with as diagonal elements the equaliser coefficients: $(\mathbf{G}_{i,n}^{\ell})_{k,k'} = \delta_{k,k'}(g_{i,n}^{\ell})_k$. Considering the data symbols $\{a_{i,n}^{\ell}\}$ of user ℓ are converted at the transmitter into a discrete-time sequence $\mathbf{s}_{i,\ell}$ using the linear transformation $\mathbf{T}_{tr,i,\ell}$ (see figure 2.2), i.e., $\mathbf{s}_{i,\ell} = \mathbf{T}_{tr,i,\ell}\mathbf{a}_{i,\ell}$, and the resulting discrete-time sequence $\mathbf{s}_{i,\ell}$ is transmitted over the channel with the equivalent channel transfer function (2.22) (see figure 2.17), the received discrete-time sequence $\mathbf{v}_{i,\ell}$ yields

$$\mathbf{v}_{i,\ell} = \sum_{\ell'=1}^{N_u} \sum_{i'=-\infty}^{+\infty} (\mathbf{H}_{eq})_{i,i'}^{\ell'} \mathbf{T}_{tr,i',\ell'} \mathbf{a}_{i',\ell'} + \mathbf{w}_{i,\ell} \tag{2.49}$$

where N_u is the number of active users, $((\mathbf{H}_{eq})^{\ell'}_{i,i'})_{m,m'} = h_{eq,\ell'}((iM_s+m)-(i'M_s+m');iM_s+m)$ is the $(M_s \times M_s)$ matrix consisting of the impulse response of the equivalent channel including the synchronisation errors, and $\mathbf{w}_{i,\ell}$ is the additive noise disturbance. Defining $\mathbf{A}^{\ell,\ell'}_{i,i'} \triangleq \mathbf{B}^{\ell}_{1,i,n}(\mathbf{H}_{eq})^{\ell'}_{i,i'}\mathbf{T}_{tr,i',\ell'}$ and $\mathbf{W}^{\ell}_{i,n} \triangleq \mathbf{B}^{\ell}_{1,i,n}\mathbf{w}_{i,\ell}$, the samples $z^{\ell}_{i,n}$ at the input of the decision device can be written as

$$z^{\ell}_{i,n} = \mathbf{B}^{\ell}_{2,i,n}\mathbf{G}^{\ell}_{i,n}\left(\sum_{\ell'=1}^{N_u}\sum_{i'=-\infty}^{+\infty}\mathbf{A}^{\ell,\ell'}_{i,i'}\mathbf{a}_{i',\ell'} + \mathbf{W}^{\ell}_{i,n}\right) \tag{2.50}$$

Hence, the samples $z^{\ell}_{i,n}$ at the input of the decision device consist of a linear combination of all data symbols of the considered user, a linear combination of all data symbols from other users, and additive noise. Substituting (2.50) in (2.47) and minimising the MSE with respect to the equaliser coefficients, it is easily verified that the resulting equaliser coefficients $\mathbf{g}^{\ell}_{i,n} = [(g^{\ell}_{i,n})_0 \ldots (g^{\ell}_{i,n})_{M_r-1}]^T$ are given by

$$\mathbf{g}^{\ell}_{i,n} = \left((\mathbf{D}^{\ell}_{i,n})^{-1}\mathbf{C}^{\ell}_{i,n}\right)^* \tag{2.51}$$

where $\mathbf{D}^{\ell}_{i,n}$ is a matrix of order $(M_r \times M_r)$ and $\mathbf{C}^{\ell}_{i,n}$ is a vector of order $(M_r \times 1)$, given by

$$\begin{aligned}
(\mathbf{D}^{\ell}_{i,n})_{k,k'} &= \sum_{\ell'=1}^{N_u}\sum_{i'=-\infty}^{+\infty} E\left[(\mathbf{B}^{\ell}_{2,i,n})_k(\mathbf{A}^{\ell,\ell'}_{i,i'}\mathbf{R}_{\mathbf{a}\ell'}(\mathbf{A}^{\ell,\ell'}_{i,i'})^{\dagger})_{k,k'}(\mathbf{B}^{\ell}_{2,i,n})^{\dagger}_{k'}\right] \\
&+ E\left[(\mathbf{B}^{\ell}_{2,i,n})_k(\mathbf{R}_{\mathbf{W}})_{k,k'}(\mathbf{B}^{\ell}_{2,i,n})^{\dagger}_{k'}\right] \\
(\mathbf{C}^{\ell}_{i,n})_k &= E_{s,\ell,n}E\left[(\mathbf{B}^{\ell}_{2,i,n})_k(\mathbf{A}^{\ell,\ell'}_{i,i'})_{k,n}\right]
\end{aligned} \tag{2.52}$$

In (2.52), the matrices $(\mathbf{R}_{\mathbf{a}\ell})_{n,n'} = E[a^{\ell}_{i,n}(a^{\ell}_{i,n'})^*] = E_{s,\ell,n}\delta_{n,n'}$ and $\mathbf{R}_{\mathbf{W}} = E[\mathbf{W}^{\ell}_{i,n}(\mathbf{W}^{\ell}_{i,n})^{\dagger}]$ are the autocorrelation matrices of the data symbols $a^{\ell}_{i,n}$ of user ℓ and the noise disturbance $\mathbf{W}^{\ell}_{i,n}$, respectively. Note that $\mathbf{D}^{\ell}_{i,n}$ is a Hermitian matrix, i.e., $(\mathbf{D}^{\ell}_{i,n})^{\dagger} = \mathbf{D}^{\ell}_{i,n}$. The MMSE equaliser coefficients (2.51) depend on the user index ℓ, the block index i and the symbol index n. In many cases of practical interest, the dependency of (2.51) on one or more indices disappears, because the random variables in (2.52) are stationary with respect to the block index i and/or the symbol index n. In the following chapters, the coefficients of the MMSE equaliser will be computed using the equation (2.51).

In a practical receiver, the equaliser coefficients (2.51) can not be implemented, because the expectations contained in (2.52) are not a priori known. Fortunately, there exist various practical algorithms (least mean-square (LMS), recursive least-square (RLS), ...) [Pro95], [Van99] that yield equaliser coefficients that approximate the MMSE equaliser coefficients (2.51). Basically, in these practical algorithms the expectation in (2.52) are replaced by time-averages. Because of this time-averaging, the equaliser is able to track only those parameters that are slowly varying within the time interval over which the averaging is performed. Hence, the expectations in (2.52) are with respect

to the parameters that vary rapidly within the averaging interval. Taking into account that the average is taken over many blocks, the equaliser is able to track the channel transfer function (unless it is rapidly varying), and a phase and frequency offset of the carrier oscillator and the sampling clock at the receiver; the average in (2.52) is with respect to the noise, spreading sequences, carrier phase jitter and timing jitter.

2.6 The Signal-to-Noise Ratio

We consider a performance measure that is defined in terms of the samples zi,m at the input of the decision device, i.e., the signal-to-noise ratio (SNR). We show that a suitably defined SNR is directly related to the bit error rate (BER).

The quality of a digital communication system is often measured by the bit error rate (BER), which is defined as the ratio of the average number of erroneous detected bits to the total number of transmitted bits:

$$BER = \frac{\text{average number of incorrectly detected bits}}{\text{total number of transmitted bits}} \tag{2.53}$$

When the constellation contains M different points, each data symbol represents $\log_2 M$ bits. Furthermore, the probability of a bit error depends on the decision rule. In this work, the memoryless minimum-distance detector is used, i.e., the detector selects the symbol in the alphabet that is closest in Euclidean distance to the sample $z_{i,n}^{\ell}$ (2.50) at the input of the decision device, i.e.,

$$\hat{a}_{i,n}^{\ell} = \arg\min_{\hat{a}} |z_{i,n}^{\ell} - \hat{a}|^2 \tag{2.54}$$

Because of the presence of additive noise and interference, an incorrect decision can be made by the receiver, resulting in one or more incorrect bits.

Regardless of the type of linear digital modulation, each sample $z_{i,n}^{\ell}$ (2.50) at the input of the decision device can be viewed as the sum of the following contributions.

- A linear combination of all data symbols $\mathbf{a}_{i,\ell}$ from the considered user. It can be further decomposed into the sum of a useful component $a_{i,n}^{\ell} s_{i,n}^{\ell}$ (that contains the data symbol to be detected) and an ISI term $ISI_{i,n}^{\ell}$ (that contains all other data symbols from the considered user).

- A linear combination of all data symbols from all other users. This MUI contribution to $z_{i,n}^{\ell}$ is denoted $MUI_{i,n}^{\ell}$. In (2.50) we observe that this term has a similar structure as the contribution from the symbols $\mathbf{a}_{i,\ell}$.

- A linear transformation of the AWGN $w_{LP}(t)$. This noise contribution to $z_{i,n}^{\ell}$ is denoted as $n_{i,n}^{\ell} = (\mathbf{b}_{i,n}^{\ell})^T \mathbf{w}_{i,\ell}$ (see (2.48) and (2.49)).

Combining the contributions $ISI_{i,n}^{\ell}$ and $MUI_{i,n}^{\ell}$ into the interference term $Int_{i,n}^{\ell}$, $z_{i,n}^{\ell}$ can be represented as

$$z_{i,n}^{\ell} = a_{i,n}^{\ell} s_{i,n}^{\ell} + Int_{i,n}^{\ell} + n_{i,n}^{\ell} \tag{2.55}$$

The coefficients of the linear combinations of all data symbols and the noise involved in $z_{i,n}^{\ell}$ must in general be considered as random, because of the presence of random synchronisation errors and random components (e.g., random spreading sequences) of the matrices $\mathbf{T}_{tr,i,\ell}$ (at the transmitter, figure 2.1) and the vector $\mathbf{b}_{i,n}^{\ell}$ (2.48) (at the receiver, figure 2.21). These random quantities are independent of the data symbols and the noise $w_{LP}(t)$.

When conditioning on $\mathbf{b}_{i,n}^{\ell}$, it follows from (2.49) that $n_{i,n}^{\ell}$ is a zero-mean complex-valued Gaussian random variable with statistically independent real and imaginary parts, with

$$\begin{aligned} E\left[\left(Re[n_{i,n}^{\ell}]\right)^2 \left|\mathbf{b}_{i,n}^{\ell}\right.\right] &= E\left[\left(Im[n_{i,n}^{\ell}]\right)^2 \left|\mathbf{b}_{i,n}^{\ell}\right.\right] \\ &= \frac{N_0}{2}(\sigma_{i,n}^{\ell})^2 \end{aligned} \tag{2.56}$$

where

$$(\sigma_{i,n}^{\ell})^2 = (\mathbf{b}_{i,n}^{\ell})^{\dagger}\mathbf{b}_{i,n}^{\ell} \tag{2.57}$$

In (2.56) the averaging is done over the random contributions from the noise $w_{LP}(t)$ (see figure 2.5). In the following, we will replace $n_{i,n}^{\ell}$ by the statistically equivalent random variable $W_{i,n}^{\ell}\sigma_{i,n}^{\ell}$, where $W_{i,n}^{\ell}$ is a zero-mean complex-valued Gaussian random variable with statistically independent real and imaginary parts, each having a variance equal to $N_0/2$. In this way, the effects of the noise $w_{LP}(t)$ and of the additional random variables are contained in $W_{i,n}^{\ell}$ and $\sigma_{i,n}^{\ell}$, respectively. Furthermore, we decompose the contribution of the considered data symbol $s_{i,n}^{\ell}$ (2.55) into an average useful component $E[s_{i,n}^{\ell}]$ and a zero-mean fluctuation $\Delta s_{i,n}^{\ell} = s_{i,n}^{\ell} - E[s_{i,n}^{\ell}]$, the self-interference. This yields

$$z_{i,n}^{\ell} = a_{i,n}^{\ell} E[s_{i,n}^{\ell}] + a_{i,n}^{\ell}\Delta s_{i,n}^{\ell} + Int_{i,n}^{\ell} + W_{i,n}^{\ell}\sigma_{i,n}^{\ell} \tag{2.58}$$

We define the instantaneous signal-to-noise ratio (SNR) as the ratio of the power of the average useful component to the sum of the powers of the additive noise, the self-interference, the multiuser interference and the intersymbol interference. This yields

$$SNR_{i,n}^{\ell} = \frac{E_{s,n,\ell}|E[s_{i,n}^{\ell}]|^2}{N_0 E[(\sigma_{i,n}^{\ell})^2] + E_{s,n,\ell}E[|\Delta s_{i,n}^{\ell}|^2] + E[|Int_{i,n}^{\ell}|^2]} \tag{2.59}$$

where $E_{s,n,\ell} = E[|a_{i,n}^{\ell}|^2]$. In the case of a non-ideal channel or in the presence of synchronisation errors, the SNR will be degraded as compared to the case of an ideal channel and in the absence of synchronisation errors. To compare the

quality of the different systems that will be considered in this work, the SNR (2.59) and its degradation are used.

In appendix A, we show that when the sample $z_{i,n}^{\ell}$ conditioned on $a_{i,n}^{\ell}$ can be modelled as a Gaussian variable, the SNR (2.59) is directly related to the bit error rate (BER) for QPSK (i.e., the constellation alphabet is $\{\exp(j\pi/2), \exp(j3\pi/2), \exp(-j3\pi/2), \exp(-j\pi/2)\}$):

$$BER_{i,n}^{\ell} = Q\left(\sqrt{SNR_{i,n}^{\ell}}\right) \tag{2.60}$$

where $Q(x)$ denotes the complementary error function:

$$Q(x) = \int_{x}^{+\infty} \frac{1}{\sqrt{2\pi}} e^{-\frac{z^2}{2}} dz \tag{2.61}$$

The assumption that the sample $z_{i,n}^{\ell}$ conditioned on $a_{i,n}^{\ell}$ can be modelled as a Gaussian variable holds within a good approximation when

- the quantity $\sigma_{i,n}^{\ell}$ is non-random
- the interference contribution $Int_{i,n}^{\ell}$ and the self-interference contribution $\Delta s_{i,n}^{\ell}$ are small as compared to the noise contribution $n_{i,n}^{\ell}$

For the communication systems to be considered in this work, the quantity $\sigma_{i,n}^{\ell}$ turns out to be non-random when the channel is not time-varying. Furthermore, as only small degradations of the system performance can be tolerated, the contributions of the interference and the self-interference must be small as compared to the noise contribution. Therefore, the disturbance of the average useful component is dominated by the noise contribution, which can be modelled as a Gaussian variable. In this case, the relation between the BER and the SNR (2.60) holds within a good approximation. Note that, when the samples $z_{i,n}^{\ell}$ conditioned on $a_{i,n}^{\ell}$ can not be modelled as a Gaussian variable, e.g., for a fading channel (where the quantity $\sigma_{i,n}^{\ell}$ is a random variable) or when the interference is large as compared to the noise, the SNR (2.59) still can be defined as a performance measure. However, in this case, the relation (2.60) between the SNR and the BER does not hold.

The BER (2.60) and the SNR (2.59) still contain the indices i, n and ℓ, which indicates that the performance in principle depends on the block index i, the symbol index n within a block and the user index ℓ. However, in many cases of practical interest, the dependency on one or more indices disappears, because the random variables contained in $s_{i,n}^{\ell}$, $Int_{i,n}^{\ell}$ and $\sigma_{i,n}^{\ell}$ are stationary with respect to i and/or n, and their distribution does not depend on the user index ℓ. If this stationarity with respect to i and/or n does not hold, a meaningful SNR which does not longer depend on i and n is obtained by averaging the denominator and the numerator in (2.59) over i and n. For the communication systems to be considered in this work, $SNR_{i,n}^{\ell}$ turns out to be independent of i when the channel is not time-varying.

Chapter 3

Conventional Single Carrier Communication

3.1 Introduction

In this work, we investigate the effect of synchronisation errors on multicarrier systems. These synchronisation errors, in general, introduce a performance degradation. For the sake of comparison, we introduce two single carrier reference systems whose performance degradation caused by the synchronisation errors are used as a reference in the comparison with the considered multicarrier systems. The single carrier reference systems we consider are a conventional single carrier communication system and a single carrier direct-sequence CDMA system. In these reference systems, the data is transmitted over an additive white Gaussian noise (AWGN) channel [Mey98], [Fra80]. In this chapter, we present the conventional single carrier communication system. The single carrier DS-CDMA system is discussed in the next chapter.

In the conventional single carrier communication system, the data symbols, originating from a single user, are transmitted sequentially. During each symbol interval, the frequency spectrum of each data symbol may occupy the whole available system bandwidth. Furthermore, we consider the case of the transmit and receiver filter being square-root Nyquist filters with respect to the symbol interval. This implies that no intersymbol interference (ISI), i.e., interference between data symbols transmitted during other symbol intervals, occurs in the absence of synchronisation errors. The presence of synchronisation errors in generally introduces ISI and/or an attenuation of the useful component, which results in a reduction of the system performance.

In this chapter, the sensitivity of the conventional single carrier communication system to synchronisation errors is investigated. In section 3.2, the conventional single carrier communication system is defined. We separately consider

the effect of the carrier phase errors and the timing errors on the conventional single carrier communication system in section 3.3. The conclusions are drawn in section 3.4.

3.2 The Conventional Single Carrier Communication System

The conceptual block diagram of the conventional single carrier communication system is shown in figure 3.1. The sequence of data symbols $\{a_k\}$, where a_k is the kth transmitted data symbol, is transmitted at a rate $R_s = 1/T$. Hence, the transmitter matrix $\mathbf{T}_{tr}$ (2.1) is a scalar and equals $T_{tr,k} = 1$. To convert the sequence of data symbols into a continuous-time signal, the sequence is multiplied with the transmit clock signal and applied to the transmit filter $p(t)$ with transfer function $P(f)$, which is a square-root Nyquist filter with respect to the symbol interval T, resulting in the continuous-time signal $s(t)$

$$s(t) = \sum_{k=-\infty}^{+\infty} a_k p(t - kT - \tau_c) \tag{3.1}$$

where τ_c represents the transmit clock phase. The signal $s(t)$ is transmitted over an AWGN channel, i.e., the signal is transmitted over an ideal channel ($H_{ch}(f;t) = 1$) and is disturbed by AWGN $w_{LP}(t)$, whose independent real and imaginary parts have the same power spectral density (psd) $N_0/2$. Furthermore, the signal is disturbed by the carrier phase difference $\theta_c - \hat{\theta}_r(t)$, where θ_c is the carrier phase at the transmitter and $\hat{\theta}_r(t)$ (2.10) is the estimated optimum carrier phase of the receiver carrier oscillator. In the case of the ideal channel, the optimum carrier phase $\theta_r(t)$ at the receiver equals the carrier phase θ_c at the transmitter. Hence, the carrier phase error $\phi(t)$ (2.11) equals the carrier phase difference: $\phi(t) = \theta_c - \hat{\theta}_r(t)$. The resulting signal $r(t)$ enters the receiver filter, which is matched to the transmit filter and is sampled at the instants $\hat{t}_k = t_k + \epsilon_k T$, where $t_k = kT + \tau_c$ are the optimum sampling instants and ϵ_k is the normalised timing error at the instant t_k. Assuming the carrier phase error slowly varies as compared to the duration of the receiver filter impulse response, the received discrete-time samples v_k yield

$$v_k = \sum_{k=-\infty}^{+\infty} a_{k'} h_{eq}(t_k - t_{k'}; t_k) + w_k \tag{3.2}$$

where w_k is the matched filter output noise value at the instant $\hat{t}_k$ and $h_{eq}(t;t_k)$ is the equivalent time-varying filter that includes the synchronisation errors, as defined in section 2.3.1. The Fourier transform of $h_{eq}(t;t_k)$ with respect to the variable t is given by

$$H_{eq}(f;t_k) = |P(f)|^2 e^{j\phi(t_k)} e^{j2\pi f \epsilon_k T} \tag{3.3}$$

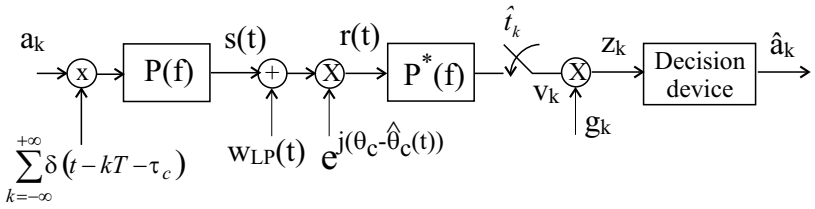

Figure 3.1: Conceptual block diagram of the conventional single carrier communication system

The time-domain sample v_k is fed to a one-tap equaliser with coefficient g_k, that scales and rotates the sample v_k, and applied to the decision device in order to detect the data symbol a_k. Hence, the linear transformation $\mathbf{b}_k$ (2.5) at the receiver is a scalar: $b_k = g_k$. The equaliser is implemented as an MMSE equaliser and is computed using (2.51). The samples at the input of the decision device can be decomposed as follows:

$$z_k = a_k I_{k,k} + \sum_{k'=-\infty; k' \neq k}^{+\infty} a_{k'} I_{k,k'} + W_k \tag{3.4}$$

where W_k is a zero-mean complex-valued additive Gaussian noise term and

$$I_{k,k'} = g_k h_{eq}(t_k - t_{k'}; t_k) \tag{3.5}$$

The decision device selects the data symbol in the alphabet that is the closest in Euclidean distance to the sample z_k. In (3.4), the first contribution is the useful component. When the synchronisation errors can be modelled as random processes, the useful component can be further decomposed into an average useful component $E[I_{k,k}]$ and a zero-mean fluctuation $I_{k,k} - E[I_{k,k}]$, the self-interference (SI). The second contribution in (3.4) ($k' \neq k$) is the intersymbol interference (ISI), originating from data symbols transmitted during other instants. The last contribution is the additive noise. The variance of the additive noise is given by

$$E[|W_k|^2] = N_0 |g_k|^2 \triangleq N_0 \sigma_k^2 \tag{3.6}$$

To express the performance of the conventional single carrier communication system, we consider the signal-to-noise ratio (SNR) (2.59), which is the ratio of the power of the average useful component $P_{U,k}$ to the sum of the powers of the self-interference $P_{SI,k}$, the intersymbol interference $P_{ISI,k}$ and the noise. This yields

$$SNR_k = \frac{E_s P_{U,k}}{N_0 \sigma_k^2 + E_s (P_{SI,k} + P_{ISI,k})} \tag{3.7}$$

where $E_s = E[|a_k|^2]$ is the energy per symbol and

$$\begin{aligned} P_{U,k} &= |E[I_{k,k}]|^2 \\ P_{SI,k} &= E[|I_{k,k} - E[I_{k,k}]|^2] \qquad (3.8) \\ P_{ISI_k} &= \sum_{k'=-\infty; k' \neq k}^{+\infty} E[|I_{k,k'}|^2] \qquad (3.9) \end{aligned}$$

As we observe from (3.7), the SNR depends on the symbol index k.

In the absence of synchronisation errors, the receiver filter output samples are given by (see (2.6))

$$v_k = a_k + w_k \qquad (3.10)$$

where the noise contribution w_k is Gaussian with $E[w_k w_{k'}^*] = N_0 \delta_{k,k'}$, and a_k is the transmitted data symbol. Note that v_k contains the data symbol a_k, but no other data symbols: because of the non-dispersive channel, no ISI occurs. The one-tap equaliser operating on v_k has coefficient g_k given by $g_k = E_s/(E_s + N_0)$; note that g_k does not depend on the symbol index. Taking into account that $E_s = E[|a_k|^2]$, the resulting SNR (3.7) is independent of the symbol index k and yields

$$SNR(0) = \frac{E_s}{N_0} \qquad (3.11)$$

The presence of synchronisation errors, in general, causes a reduction of the SNR as compared to the case of no synchronisation errors. The degradation of the SNR as compared to $SNR(0)$ (expressed in dB), caused by the synchronisation errors, is given by

$$Deg_k = -10 \log \left(\frac{P_{U,k}}{\sigma_k^2 + \frac{E_s}{N_0}(P_{SI,k} + P_{ISI,k})} \right) \qquad (3.12)$$

3.3 Effect of Synchronisation Errors

In this section, we investigate the influence of synchronisation errors on the performance of the conventional single carrier communication system. In section 2.2, the synchronisation errors are classified in two categories: the carrier phase errors and the timing errors. In the literature, the effect of the following synchronisation errors on the conventional single carrier communication system have been studied. The influence of a carrier frequency offset has been studied in [Pol96]. In [Pol98] and [Pol95], the sensitivity of the conventional single carrier communication system to carrier phase jitter is investigated. The influence of random carrier phase and timing errors is studied in [Buc95]. In [Moe99a], the effect of a constant timing offset is presented. The sensitivity of a conventional single carrier communication system to timing jitter is investigated in [Buc93]. In the following, we separately consider the effect of the carrier phase errors and the timing errors.

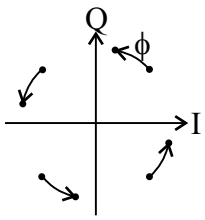

Figure 3.2: Influence of a constant phase rotation on the samples at the input of the decision device, $g_k = 1$

3.3.1 Carrier Phase Errors

In this section, the effect of the carrier phase errors on the performance of the conventional single carrier communication system is investigated in the absence of timing errors ($\epsilon_k = 0$). In this case, the quantities $I_{k,k'}$ (3.5) reduce to

$$I_{k,k'} = g_k e^{j\phi(t_k)} \delta_{k,k'} \tag{3.13}$$

As we observe in (3.13), the carrier phase errors do not cause intersymbol interference, but only introduce a phase rotation of the useful component. In the following, we separately consider the cases of a constant phase offset, a carrier frequency offset and carrier phase jitter.

Constant Phase Offset

In the case of a constant phase mismatch between the carrier oscillators at the transmitter and the receiver, a constant phase offset $\phi(t) = \phi$ is introduced. This constant phase offset gives rise to a rotation over an angle ϕ of the discrete-time samples v_k (3.2) at the receiver, but introduces no intersymbol interference. Hence, in the absence of an equaliser ($g_k = 1$), the constant phase offset yields a rotation of the samples at the input of the decision device, as shown in figure 3.2. To compensate for the reduction of the noise margins caused by the constant phase offset, the equaliser introduces a rotation over (an estimate of) the angle $-\phi$. Hence, the MMSE equaliser has equaliser coefficients $(g_{MMSE})_k = C \exp(-j\phi)$, where

$$C = \frac{\sqrt{E_s}}{N_0 + E_s} \tag{3.14}$$

is the MMSE equaliser coefficient in the case of a zero phase offset. The MMSE equaliser coefficients in the case of the constant phase offset are independent of the symbol index k. Taking into account that a phase rotation of the samples at the input of the decision device has no influence on the noise power level, the constant phase offset is compensated by the equaliser without loss of performance.

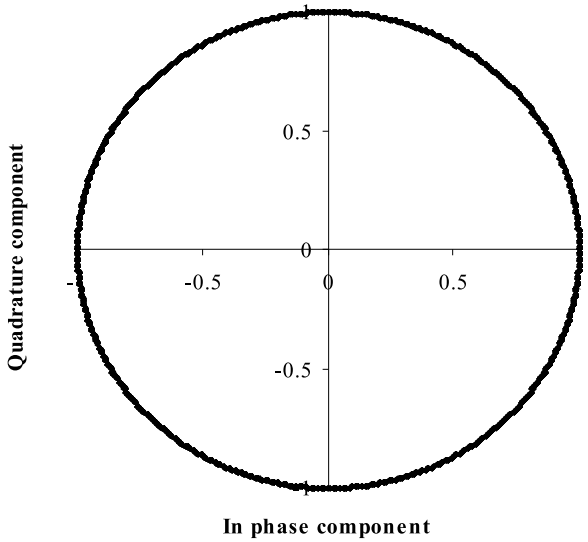

Figure 3.3: Carrier frequency offset, $g_k = 1, \Delta FT = 2.10^{-3}$

Carrier Frequency Offset

In the case of a carrier frequency offset ΔF between the carrier oscillators at the transmitter and the receiver, the carrier phase error linearly increases in time: $\phi(t) = 2\pi\Delta Ft + \phi(0)$. In section 2.3.2, it is mentioned that the effect of the carrier frequency offset is twofold. First it causes a rotation at a constant speed of $2\pi\Delta F$ rad/s of the receiver filter output samples v_k. Further, the frequency shift of the downconverted signal causes signal distortion and power loss, resulting in an attenuation of the useful component and intersymbol interference.

Following the analysis described in section 2.3.1, where we have neglected the attenuation of the useful component and the ISI caused by the frequency shift, it is clear that the carrier frequency offset introduces no ISI but only gives rise to a pure phase rotation at a speed of $2\pi\Delta FT$ rad/symbol of the samples at the input of the decision device, as shown in the scatter diagram in figure 3.3. Assuming the receiver can estimate the carrier frequency offset, the equaliser is able to compensate for the systematic phase rotation of the useful component, i.e., $(g_{MMSE})_k = C\exp(-j(2\pi\Delta FT + \phi(0)))$, where C is defined in (3.14). Hence, if we neglect the effect of the frequency shift, the performance of the conventional single carrier communication system is not degraded in the presence of a carrier frequency offset, as a pure phase rotation of the samples at the input of the decision device has no influence on the noise variance.

In the following, we take into account the effect of the frequency shift of

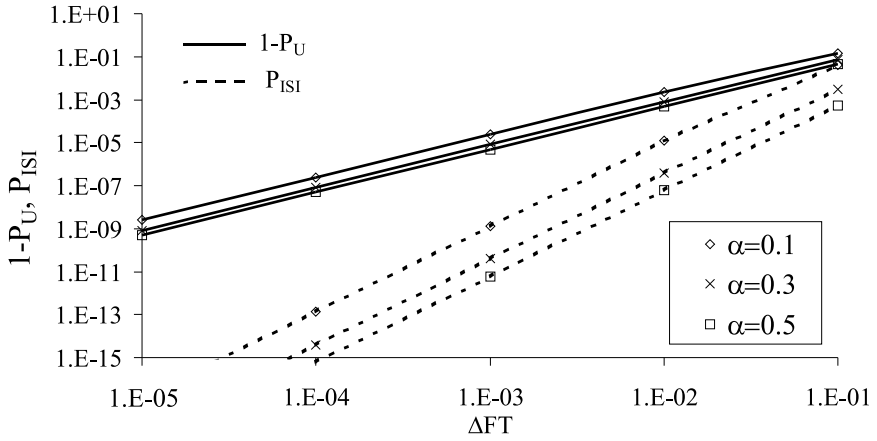

Figure 3.4: Influence of the carrier frequency offset on the reduction of the power of the average useful component $(1 - P_U)$ and the ISI power P_{ISI}

the downconverted signal. We assume that the equaliser compensates for the systematic phase rotation of the samples at the input of the decision device. In this case, the quantities $I_{k,k'}$ (3.5) yield

$$I_{k,k'} = \int_{-\infty}^{+\infty} P(f)P^*(f + \Delta F)e^{j2\pi(k-k')fT}df \tag{3.15}$$

In the case of the transmit and the receiver filter being square-root raised-cosine filters with rolloff α (see appendix B), it can be verified that the useful component $I_{k,k}$ reduces for $|\Delta F|T \leq \alpha \leq 0.5$ to

$$I_{k,k} = (1 - \alpha - |\Delta F|T) + \frac{4\alpha}{\pi} \sin \frac{\pi|\Delta F|T}{2\alpha} + (\alpha - |\Delta F|T) \cos \frac{\pi|\Delta F|T}{2\alpha} \tag{3.16}$$

For small ΔFT, this reduces to

$$I_{k,k} \approx 1 - \frac{(\pi|\Delta F|T)^2}{8\alpha} \tag{3.17}$$

Hence, the useful component is attenuated by the factor $|I_{k,k}| < 1$. This yields a reduction of the power of the average useful component P_U (3.8), i.e.,

$$1 - P_U \approx \frac{(\pi|\Delta F|T)^2}{4\alpha} \tag{3.18}$$

The power of the ISI (3.8) becomes

$$P_{ISI} = \sum_{n=-\infty;n\neq 0}^{+\infty} \left| \int_{-\infty}^{+\infty} P(f)P^*(f + \Delta F)e^{j2\pi nfT}df \right|^2 \tag{3.19}$$

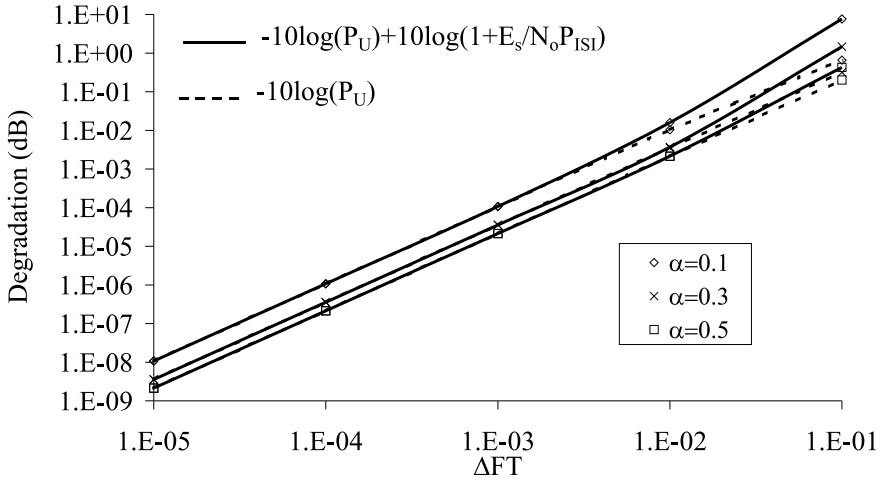

Figure 3.5: Degradation caused by the reduction of the power of the average useful component only and the degradation caused by the reduction of the average useful component and the ISI, $SNR(0) = 20$ dB

Considering the reduction of the useful component and the presence of ISI, the conventional single carrier communication system is degraded in the presence of a carrier frequency error as compared to the case of a zero carrier frequency offset. As the useful component $I_{k,k}$ (3.17), the intersymbol interference power (3.18) and the magnitude of $(g_{MMSE})_k$, hence the noise power (3.6), are independent of the symbol index k, the performance degradation (3.12) is independent of the symbol index.

In figure 3.4, the reduction of the power of the average useful component $(1 - P_U)$ (3.18) and the ISI power (3.19) are shown as function of the carrier frequency offset. As we observe, the reduction of the power of the average useful component $(1 - P_U)$ is proportional to $(\Delta FT)^2$, while the ISI power is proportional to $(\Delta FT)^4$. The degradation caused by the reduction of the power of the average useful component only and the degradation caused by both the reduction of the power of the average useful component and the ISI are shown in figure 3.5, for SNR(0)=20 dB. As we observe in figures 3.4 and 3.5, the influence of the ISI is negligible for carrier frequency offsets of practical interest, i.e., $\Delta FT \ll 1$. Hence, the degradation of the conventional single carrier communication system performance is essentially caused by the attenuation of the useful component. Furthermore, we observe in figure 3.5 that, when the carrier frequency offset is small as compared to the system bandwidth, i.e., for $\Delta FT \ll 1$, this performance degradation is very small.

Carrier Phase Jitter

When a carrier synchronisation mechanism is used to estimate the optimum carrier phase $\theta_r(t)$ at the receiver, we can get rid of a constant phase offset and a carrier frequency offset. The resulting phase jitter can be modelled as a zero-mean stationary random process with jitter power spectral density $S_\phi(f)$ and jitter variance σ_ϕ^2. Assuming the carrier phase jitter is slowly varying as compared to T, the bandwidth f_B of the jitter spectrum satisfies $f_B T \ll 1$. Considering (3.13), the carrier phase jitter does not introduce intersymbol interference, but only gives rise to a random phase rotation of the useful component. Hence, the carrier phase jitter introduces self-interference. For small jitter variances $\sigma_\phi^2 \ll 1$, the approximation $\exp(j\phi(t)) \approx 1 + j\phi(t)$ can be used. In this case, the quantities $I_{k,k'}$ (3.13) can be approximated by

$$I_{k,k'} = g_k(1 + j\phi(t_k))\delta_{k,k'} \tag{3.20}$$

When the carrier phase jitter rapidly varies as compared to the averaging time of the MMSE equaliser, the equaliser is not able to track the variations caused by the carrier phase jitter. The equaliser averages in the time over the variations caused by the carrier phase jitter. As for small jitter variances, the time average of $\exp(j\phi(t))$ can be approximated by $E[\exp(j\phi(t))] \approx E[1 + j\phi(t)] = 1$, the MMSE equaliser is essentially the same as in the absence of carrier phase errors, i.e., $(g_{MMSE})_k = C$, where C is defined in (3.14). In this case, the powers of the average useful component, the self-interference (3.8) and the noise (3.6) yield

$$\begin{aligned} P_U &= |C|^2 \\ P_{SI} &= |C|^2\sigma_\phi^2 \\ E[|W_k|^2] &= N_0|C|^2 \end{aligned} \tag{3.21}$$

where the jitter variance σ_ϕ^2 is given by

$$\sigma_\phi^2 = \int_{-\infty}^{+\infty} S_\phi(f)df \tag{3.22}$$

From (3.21) it follows that the self-interference power is independent of the spectral contents of the jitter but only depends on the jitter variance. The degradation (3.12) of the SNR as compared to $SNR(0)$ (3.11), caused by the carrier phase jitter, does not depend on the symbol index k, but only depends on the jitter variance and is given by

$$Deg = 10\log\left(1 + \frac{E_s}{N_0}\sigma_\phi^2\right) \tag{3.23}$$

In figure 3.6, the degradation (3.23) is shown as a function of the jitter variance. As we observe, the degradation is small for small jitter variances. We have simulated the conventional single carrier communication system in the

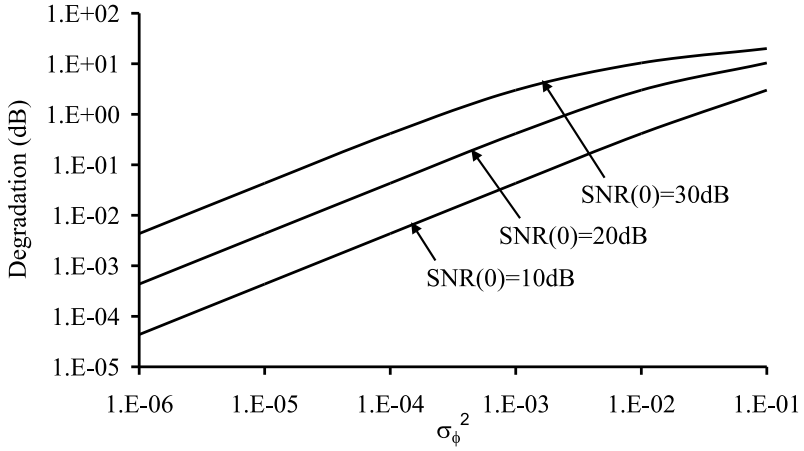

Figure 3.6: Carrier phase jitter

Table 3.1: Mean square deviation of the samples at the input of the decision device

Theoretical	Simulations
5E-3	5.094E-3

absence of additive noise ($N_0 = 0$), for QPSK modulation and a jitter variance of $\sigma_\phi^2 = 5.10^{-3}$ rad^2. The resulting scatter diagram is shown in figure 3.7. As expected, the scatter diagram shows an angular displacement of the samples at the input of the decision device. In table 3.1, the mean square deviation of the samples at the input device is shown for the simulations of the scatter diagram of figure 3.7. As we observe, the simulation result and the theoretical result well correspond.

3.3.2 Timing Errors

In this section, the sensitivity of the conventional single carrier communication system to timing errors is investigated in the absence of carrier phase errors ($\phi(t) = 0$). In this case, the quantities $I_{k,k'}$ (3.5) are given by

$$I_{k,k'} = g_k h((k - k' + \epsilon_k)T) \tag{3.24}$$

where $h(t)$ is the impulse response of the cascade of the transmit filter and the receiver filter. Its Fourier transform is $H(f) = |P(f)|^2$. From (3.24) it follows that a timing error introduces intersymbol interference ($I_{k,k'} \neq 0$ for $k' \neq k$). Let us consider the effect of the ISI on the continuous-time signal $v(t)$ at the

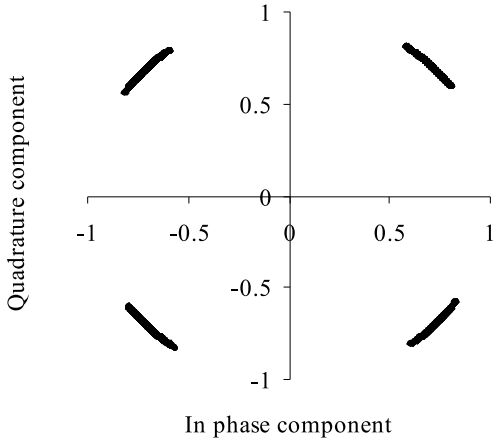

Figure 3.7: Carrier phase jitter, $f_B = 0.01/T, \sigma_\phi^2 = 5.10^{-3}$ rad^2

output of the receiver filter in the absence of additive noise:

$$v(t) = \sum_{k=-\infty}^{+\infty} a_k h(t - kT - \tau_c) \tag{3.25}$$

The eye diagram [Moe99a] displays $v(t)$ for all possible data sequences $\{a_k\}$ during the time interval $t - \tau_c \in [-T, T]$. Figure 3.8 shows the eye diagram in the case of BPSK modulation and the transmit filter being a square-root raised-cosine filter with rolloff $\alpha = 0.3$. As the transmit filter and the receiver filter are square-root Nyquist filters, no intersymbol interference occurs when the signal $v(t)$ is sampled at the ideal sampling instants, i.e., $\epsilon_k = 0$. Note that this also can be observed in the eye diagram. For $\epsilon_k \neq 0$, intersymbol interference is introduced. Let us define the noise margin $M(\epsilon_k)$ as the vertical eye opening in the eye diagram:

$$M(\epsilon_k) = |h(\epsilon_k T)| - \max_{\{a_k\}} \left| \sum_{m=-\infty; m\neq 0}^{+\infty} a_{k-m} h((m + \epsilon_k)T) \right| \tag{3.26}$$

To avoid decision errors in the absence of noise, the maximum amplitude of the ISI should be smaller than the amplitude of the useful component, i.e., $M(\epsilon_k) > 0$. As we observe in the eye diagram, the noise margin $M(\epsilon_k)$ is reduced as compared to the noise margin in the absence of timing errors $M(0)$. When $M(\epsilon_k) < 0$, a decision error surely occurs for the sequence $\{a_k\}$ yielding the maximum amplitude of the ISI: the eye is closed at the considered instant. Hence, timing errors corresponding with $M(\epsilon_k) < 0$ must be avoided. For

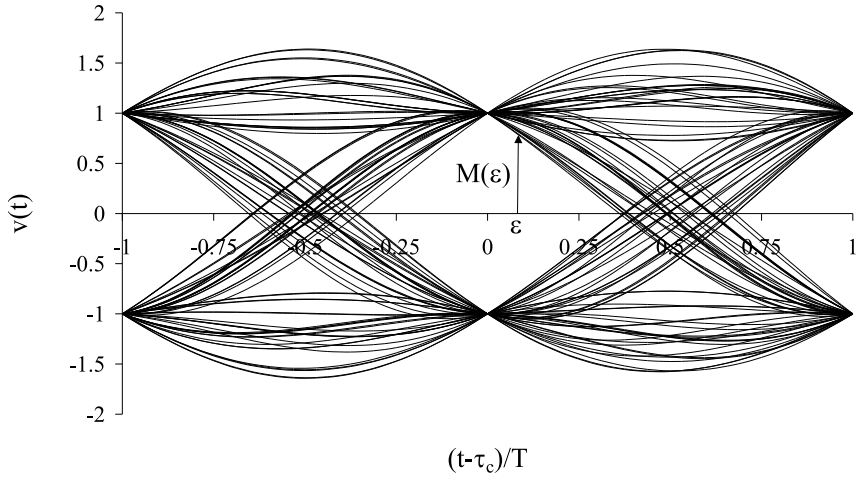

Figure 3.8: Eye diagram for a raised-cosine filter, $\alpha = 0.3$

$M(\epsilon_k) > 0$, i.e., when the eye is open, no decision error occurs if the magnitude of the noise is smaller than the noise margin. Hence, as a timing error introduces ISI, which results in a reduction of the noise margin, the performance of the conventional single carrier communication system is degraded. In the following, we consider the effect of a constant timing offset, a clock frequency offset and timing jitter.

Constant Timing Offset

In the case of a constant mismatch between the estimated and the ideal timing instants, a constant timing offset $\epsilon_k = \epsilon$ occurs. The quantities $I_{k,k'}$ (3.24) reduce to

$$I_{k,k'} = g_k h((k - k' + \epsilon)T) \tag{3.27}$$

The equaliser that minimises the MSE does not depend on the symbol index k, but depends on the constant timing error ϵ

$$(g_{MMSE})_k = \frac{\sqrt{E_s} h^*(\epsilon T)}{N_0 + E_s \sum_{n=-\infty}^{+\infty} |h((n+\epsilon)T)|^2} \triangleq C_\epsilon \tag{3.28}$$

As the timing error is non-random, no self-interference is introduced. The powers of the average useful component, the intersymbol interference (3.8) and the

noise (3.6) yield

$$\begin{aligned} P_U &= |C_\epsilon|^2 |h(\epsilon T)|^2 \\ P_{ISI} &= |C_\epsilon|^2 \sum_{n=-\infty; n\neq 0}^{+\infty} |h((n+\epsilon)T)|^2 \\ &= |C_\epsilon|^2 \left(\frac{1}{T} \sum_{n=-\infty}^{+\infty} e^{j2\pi\epsilon n} \int_{-\infty}^{+\infty} H(f) H\left(f + \frac{n}{T}\right) df - |h(\epsilon T)|^2 \right) \\ E[|W_k|^2] &= N_0 |C_\epsilon|^2 \end{aligned} \tag{3.29}$$

We observe in (3.29) that the power of the average useful component, the intersymbol interference and the noise are independent of the symbol index k. Considering the case of the transmit filter and the receiver filter being square-root raised-cosine filters with rolloff α (see appendix B), the power of the intersymbol interference yields

$$P_{ISI} = |C_\epsilon|^2 \left(1 - \frac{\alpha}{4}(1 - \cos 2\pi\epsilon) - |h(\epsilon T)|^2\right) \tag{3.30}$$

The degradation (3.12) of the SNR as compared to the case of a zero timing offset is given by

$$Deg = -10 \log |h(\epsilon T)|^2 + 10 \log \left(1 + \frac{E_s}{N_0} \left(1 - \frac{\alpha}{4}(1 - \cos 2\pi\epsilon) - |h(\epsilon T)|^2\right)\right) \tag{3.31}$$

The degradation (3.31) is independent of the symbol index k. When the timing error is small ($\epsilon \ll 1$), we can approximate $h(\epsilon T)$ and $\cos 2\pi\epsilon$ by a truncated Taylor series expansion about $\epsilon = 0$:

$$\begin{aligned} h(\epsilon T) &\approx h(0) + \epsilon T h'(0) + \frac{(\epsilon T)^2}{2} h''(0) \\ \cos 2\pi\epsilon &\approx 1 - \frac{(2\pi\epsilon)^2}{2} \end{aligned} \tag{3.32}$$

where $h'(0)$ and $h''(0)$ are the first order and second order derivative of $h(t)$ at the instant $t = 0$, respectively. Considering the results of appendix B, we can approximate the degradation (3.31) of the SNR by

$$Deg \approx -10 \log(1 - \epsilon^2 A(\alpha)) + 10 \log \left(1 + \frac{E_s}{N_0} \epsilon^2 B(\alpha)\right) \tag{3.33}$$

where

$$\begin{aligned} A(\alpha) &= \frac{\pi^2}{3} + \alpha^2(\pi^2 - 8) \\ B(\alpha) &= A(\alpha) - \frac{\alpha\pi^2}{2} \end{aligned} \tag{3.34}$$

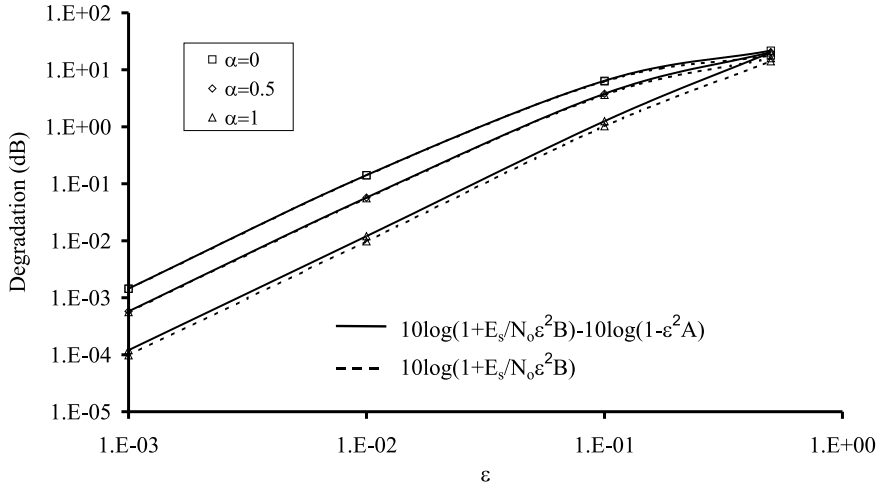

Figure 3.9: Constant timing offset, $SNR(0) = 20$ dB

In figure 3.9, the degradation (3.33) is shown as function of the timing error. Furthermore, the degradation caused by the ISI only is also shown in figure 3.9. As we observe, the effect of the reduction of the useful component can be neglected as compared to the effect of the ISI. Hence, the degradation can be approximated by

$$Deg \approx 10 \log \left(1 + \frac{E_s}{N_0} \epsilon^2 B(\alpha) \right) \tag{3.35}$$

The quantity $B(\alpha)$ (3.33) monotonically decreases for increasing α ($0 \leq \alpha \leq 1$), thus the degradation decreases for increasing rolloff, as we observe in the figure. As expected, the degradation is essentially proportional to ϵ^2 for small ϵ.

Clock Frequency Offset

In the case of a clock frequency offset $\Delta T/T$, the timing error linearly increases with time: $\epsilon_k = k\Delta T/T + \epsilon_0$. Hence, an increasing misalignment between the transmitted data symbols a_k and the received samples v_k is introduced. This increasing misalignment can not be tolerated. To compensate for this increasing misalignment, the following coarse synchronisation algorithm could be used. The detection of the symbol a_k is based upon the sample $v_{k'}$, for which the sampling instant $\hat{t}_{k'}$ is closest to the ideal sampling instant t_k. This coarse synchronisation requires that at regular intervals, samples are duplicated ($\Delta T > 0$) or removed ($\Delta T < 0$), as shown in figure 3.10. The average rate of samples used for detection is equal to the symbol rate $1/T$. The resulting relative timing error $\tilde{\epsilon}_k = (\hat{t}_{k'} - t_k)/T$ varies over an interval $[-0.5, 0.5]$. For small clock frequency offsets, i.e., when the resulting timing error slowly varies

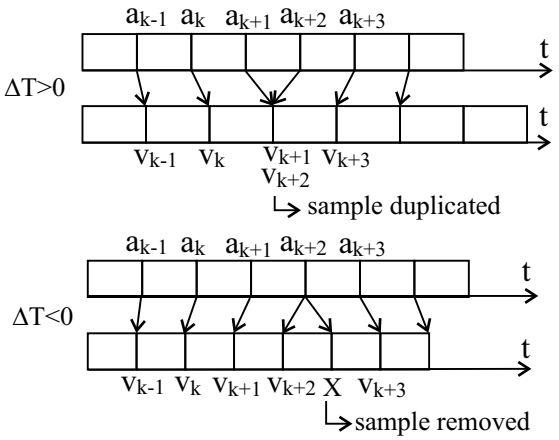

Figure 3.10: Coarse synchronisation algorithm

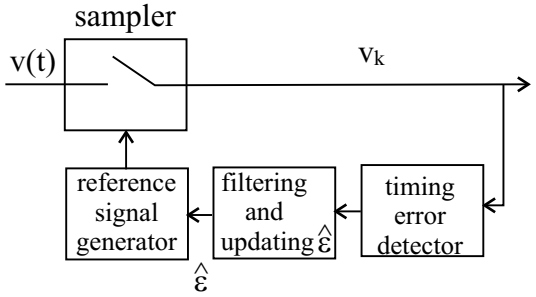

Figure 3.11: Feedback synchroniser structure

as compared to the averaging time of the equaliser, the equaliser is able to track the variation of the timing error. In this case, a similar analysis can be made as for the constant timing offset. The degradation of the SNR caused by the residual timing error slowly varies with the symbol index k. The instantaneous degradation can be defined as (3.34), where ϵ is replaced by the residual timing error $\tilde{\epsilon}_k$. As we observe in figure 3.9, the degradation is maximum for $|\tilde{\epsilon}_k| = 0.5$. In this worst case, the degradation is of the order of 20 dB. This implies that, even when a coarse synchronisation algorithm is used to compensate for the increasing misalignment, the conventional single carrier communication system is strongly degraded by a clock frequency offset.

To get rid of a clock frequency offset, two methods can be used [Mey98], [Fra80], [Gar93], [Eru93]. In the first method, the synchronisation structure adjusts the timing phase of the receiver clock such that the resulting average sampling rate at the receiver exactly equals the clock frequency at the transmitter [Mey98], [Fra80]. Figure 3.11 shows the structure of a feedback synchroniser. The timing error detector, that estimates the timing error from the received sig-

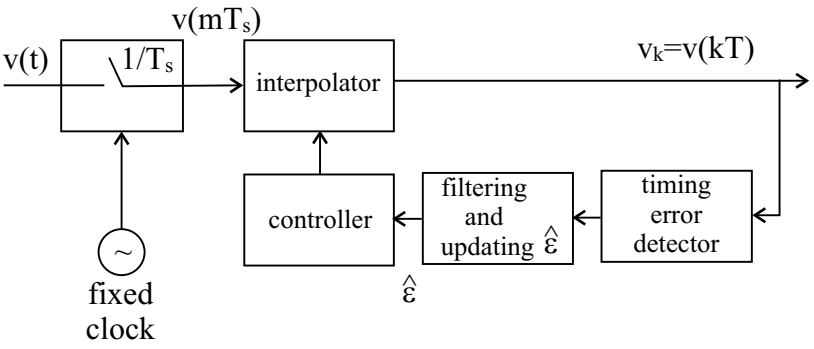

Figure 3.12: Feedback interpolation structure

nal, consists of a non-linear operation whose output yields an indication of the amplitude and the sign of the timing error. A filtered version of the timing error detector output is used to adjust the timing estimate $\hat{\epsilon}$. The timing estimate $\hat{\epsilon}$ is applied to a reference signal generator, whose output $r(t;\hat{\epsilon})$ controls the sampling operation of $v(t)$. The synchroniser can also make use of a feedforward structure to extract the timing information.

In the second method, interpolation is used (see figure 3.12) [Mey98], [Gar93], [Eru93]. The receiver samples the incoming signal $v(t)$ by means of a free-running clock at a fixed rate $1/T_s$. This sampling rate has to be selected such that no aliasing of the signal occurs. Typically, the sampling rate $1/T_s$ is at least twice the symbol rate $1/T$. As in general the receiver clock is not synchronised to the transmitter clock, the two rates are incommensurate. The samples $v(mT_s)$ at a rate $1/T_s$ are fed to the interpolator, which computes the interpolants $v(kT)$. In a feedback structure, the timing error is measured by the timing error detector, of which the output is filtered and applied to the controller that controls the computations in the interpolator. The interpolator can also be implemented using a feedforward structure to extract the timing information.

Timing Jitter

When a timing synchronisation algorithm, that eliminates a constant timing offset and a clock frequency offset (based on the adjustment of the timing phase of the sampling clock or interpolation, as mentioned in the previous section) is used to extract the samples v_k, the resulting timing error can be modelled as a zero-mean stationary random process with power spectral density $S_\epsilon(\exp(j2\pi fT))$ and jitter variance σ_ϵ^2. When the timing jitter rapidly varies as compared to the averaging time of the MMSE equaliser, the equaliser is not able to track the variations caused by the timing jitter. The equaliser averages in the time over the variations caused by the timing jitter. For small jitter variances, $\sigma_\epsilon^2 \ll 1$, the time average of $h((n+\epsilon_k)T)$ can be approximated by

$E[h((n+\epsilon_k)T)] \approx E[h(nT)+\epsilon_k T h'(nT)] = h(nT)$, where $h'(t)$ is the first order derivative of $h(t)$. Hence, the MMSE equaliser is essentially the same as in the absence of timing errors, i.e., $g_k \approx C$ where C is defined in (3.14). As the jitter is a random process, the jitter introduces, in addition to intersymbol interference, self-interference. The powers of the average useful component, the self-interference, the intersymbol interference (3.8) and the noise (3.6) are given by

$$\begin{aligned} P_U &= |C|^2 |E[h(\epsilon_k T)]|^2 \\ P_{SI} &= |C|^2 E[h(\epsilon_k T) - |E[h(\epsilon_k T)]|^2] \\ P_{ISI} &= |C|^2 \sum_{n=-\infty; n\neq 0}^{+\infty} E[h((n+\epsilon_k)T)|^2] \\ &= |C|^2 \left(\frac{1}{T} \sum_{n=-\infty}^{+\infty} E[e^{j2\pi\epsilon_k n}] \int_{-\infty}^{+\infty} H(f) H\left(f+\frac{n}{T}\right) df \right. \\ &\quad \left. - E[|h(\epsilon_k T)|^2] \right) \\ E[|W_k|^2] &= N_0 |C|^2 \end{aligned} \tag{3.36}$$

For small jitter variances, we can approximate $h((n+\epsilon_k)T)$ and $\exp(j2\pi n\epsilon_k)$ by a truncated Taylor series expansion

$$\begin{aligned} h((n+\epsilon_k)T) &\approx h(nT) + T h'(nT) + \frac{(\epsilon_k T)^2}{2} h''(nT) \\ e^{j2\pi n\epsilon_k} &\approx 1 + j2\pi n\epsilon_k - \frac{1}{2}(2\pi n\epsilon_k)^2 \end{aligned} \tag{3.37}$$

For the case of square-root raised-cosine filters, the powers of the average useful component, the self-interference and the intersymbol interference (3.36) can be approximated by

$$\begin{aligned} P_U &\approx |C|^2 (1 - \sigma_\epsilon^2 A(\alpha)) \\ P_{SI} &\approx 0 \\ P_{ISI} &\approx |C|^2 \sigma_\epsilon^2 B(\alpha) \end{aligned} \tag{3.38}$$

where $A(\alpha)$ and $B(\alpha)$ are defined in (3.34) and the jitter variance is given by

$$\sigma_\epsilon^2 = \int_{-1/2T}^{+1/2T} S_\epsilon(e^{j2\pi fT}) df \tag{3.39}$$

The power of the self-interference is negligible as compared to the ISI power and the reduction of the average useful component, as this term is proportional to σ_ϵ^4. Hence, the degradation (3.12) as compared to $SNR(0)$ (3.11) caused by the timing jitter yields

$$Deg \approx -10\log(1 - \sigma_\epsilon^2 A(\alpha)) + 10\log\left(1 + \frac{E_s}{N_0}\sigma_\epsilon^2 B(\alpha)\right) \tag{3.40}$$

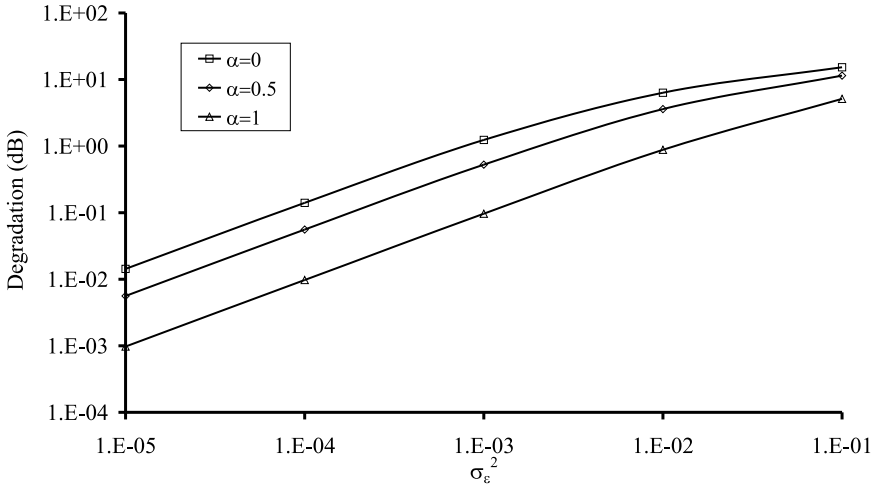

Figure 3.13: Timing jitter, $SNR(0) = 20$ dB

The degradation (3.40) is independent of the symbol index k. As we observe in (3.33) and (3.40), the sensitivity of the conventional single carrier communication system to a constant timing offset ϵ and timing jitter is essentially the same, when the jitter variance equals ϵ^2. Similarly as for a constant timing offset, it can be verified that the effect of reduction of the useful component can be neglected as compared to the effect of the ISI. Hence, the degradation can be approximated by

$$Deg \approx 10 \log \left(1 + \frac{E_s}{N_0} \sigma_\epsilon^2 B(\alpha) \right) \tag{3.41}$$

In figure 3.13, the degradation (3.41) is shown as function of the jitter variance. The degradation decreases for increasing rolloff, as $B(\alpha)$ decreases for increasing α ($0 \leq \alpha \leq 1$). Furthermore, for small jitter variances, the degradation is essentially proportional to the jitter variance σ_ϵ^2.

3.4 Conclusions and Remarks

In this chapter, we have defined a reference system, consisting of a single carrier system where a single user transmits data symbols sequentially. The conventional single carrier communication system is used in this work as a reference in the comparison of the different considered multicarrier systems. We have investigated the sensitivity of the conventional single carrier communication system to synchronisation errors.

A constant carrier phase offset can be compensated without loss of performance. The sensitivity of the conventional single carrier communication system to a carrier frequency offset is entirely caused by the effect of the frequency shift of the transmitted signal, as the systematic phase rotation of the samples at the input of the decision device can be compensated without loss of performance. This frequency shift causes mainly a reduction of the useful component and the degradation depends on the product ΔFT. The degradation is small when the frequency offset is small as compared to the system bandwidth. The carrier phase jitter causes a degradation that is independent of the spectral contents of the jitter, but only depends on the jitter variance.

Timing errors degrade the system performance of the conventional single carrier communication system. A constant timing offset introduces ISI and a reduction of the useful component. For small timing offsets, the effect of the reduction of the useful component is negligible as compared to the effect of the ISI, and the resulting degradation is proportional to the square of the timing offset. A clock frequency offset introduces an increasing misalignment between the transmitted data symbols and the received samples. As this increasing misalignment can not be tolerated, a coarse synchronisation algorithm can be used to compensate for the increasing misalignment. The residual timing error introduces, however, a strong degradation of the performance. To avoid this strong degradation, a clock frequency offset must be eliminated by adjusting the sampling clock or by interpolating between the available samples. The timing jitter introduces a degradation that only depends on the jitter variance, but not on the spectral contents of the jitter. Furthermore, the degradations caused by the constant timing offset and the timing jitter are essentially the same when the square of the timing offset equals the jitter variance.

The results for the conventional single carrier communication system can also be used for other systems, e.g., for FDM(A) systems or for TDM(A) systems. In FDM(A), where the system bandwidth is divided into a number of non-overlapping frequency bands, the signals are separated in the frequency domain. When in each frequency band the data symbols, originating from a single user, are transmitted sequentially, the performance of the FDM(A) system is the same as for the conventional single carrier communication system. In TDM(A), where the time axis is divided into a number of non-overlapping time slots, the signals of the different users are separated in the time domain. Each user is assigned one time slot during which he can transmit a number of symbols sequentially, as shown in figure 3.14. In order to avoid that bursts transmitted by the different users partially overlap because of transmit clock synchronisation errors, a guard interval (during which no signal is allowed) is inserted between time slots. Hence, when the number of data symbols transmitted during a time slot is sufficiently large, the performance of the TDM(A) system is essentially the same as for the conventional single carrier communication system.

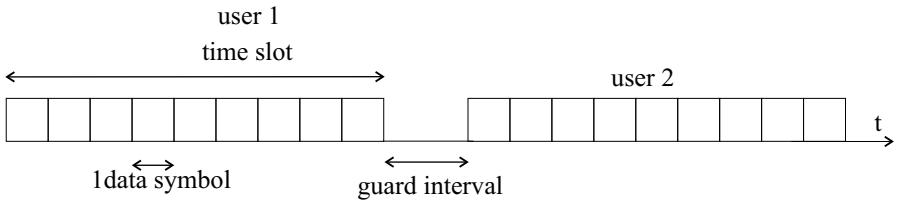

Figure 3.14: The TDMA signal

Chapter 4

Single Carrier Direct Sequence CDMA

4.1 Introduction

In a conventional single carrier transmission technique, such as described in chapter 3, an efficient use of the system resources requires that the system bandwidth is strictly limited, i.e. $R_s/2 \leq$ one-sided bandwidth $\leq R_s$, where R_s is the symbol rate. Hence, all power is concentrated in a small frequency band, which implies that the conventional single carrier signal is very sensitive to deep fades or jamming at the considered frequency. In a direct-sequence spread-spectrum (DS/SS) system [Has95], [Pah95], [Lin99], [Mos96], [Koh95], [Moe99a], [Sar99a], [Sar99b], the data symbols originating from a single user are multiplied with a higher rate chip sequence before transmission. Considering N_c as the number of chips per symbol, the bandwidth of the resulting DS/SS signal is expanded with a factor N_c as compared to the case of the conventional single carrier signal. Hence, the factor N_c is also called the spreading factor. By spreading the signal power over a large bandwidth, the signal is more robust to deep fades and jamming. Furthermore, when the DS/SS signal has the same power as the conventional single carrier signal, the power spectral density of the DS/SS signal is N_c times lower than for the conventional single carrier signal. This means that, when the spreading factor is sufficiently high, the DS/SS signal is buried in the background noise. Hence, the DS/SS system can coexist with other systems without introducing severe interference and the probability of intercepting the DS/SS signal is low.

The single carrier direct-sequence CDMA (DS-CDMA) system we consider in this chapter, makes use of the DS/SS technique: the signal transmitted to/by each user is a DS/SS signal. To separate the signals of the different users, each user is assigned a unique spreading sequence. This chapter illustrates the basic

principles of a reference DS-CDMA system and serves as an introduction to the combination of CDMA with a multicarrier system, which will be discussed in chapter 6. We investigate the influence of the spreading of the signal on the performance degradation caused by the synchronisation errors. To clearly isolate the effect of the synchronisation errors, we consider a reference DS-CDMA in the case of an ideal channel. Furthermore, the signals transmitted to/by the different users are mutually synchronised, i.e. we consider the case of synchronous DS-CDMA. In this case, the boundaries of the symbols transmitted to/by the different users coincide. In addition, the signals transmitted to/by the different users are assumed to be orthogonal, i.e. we only consider the cases of Walsh-Hadamard sequences and overlay sequences, such that in the absence of synchronisation errors no multiuser interference (MUI) occurs. The case of random sequences is not considered, as in this case even in the absence of synchronisation errors, MUI is introduced.

In this chapter, we investigate the sensitivity of the reference DS-CDMA system to synchronisation errors. The chapter is organised as follows: section 4.2 presents the reference DS-CDMA system. The effect of synchronisation errors is considered in section 4.3. We separately investigate the effect of carrier phase errors and timing errors. The conclusions are drawn in section 4.4.

4.2 The Reference DS-CDMA System

The conceptual block diagram of the DS-CDMA transmitter [Mos96] for a single user is shown in figure 4.1. Without loss of generality, the terminology for the downlink is used. The data symbols $\{a_{i,\ell}\}$ transmitted at a rate R_s, are multiplied with a higher rate chip sequence $\mathbf{c}_{i,\ell} = (1/\sqrt{N_c})[c_{iN_c,\ell} \ldots c_{iN_c+N_c-1,\ell}]^T$. The data symbol $a_{i,\ell}$ denotes the ith symbol transmitted to the user ℓ, and the chip $c_{iN_c+n,\ell}$ is the nth chip of the spreading sequence assigned to the user ℓ during the ith symbol interval. The number of chips per symbol N_c is called the spreading factor. The resulting time-domain sequence $\mathbf{s}_{i,\ell} = [s_{iN_c,\ell} \ldots s_{iN_c+N_c-1,\ell}]^T$ after spreading the data symbols yields

$$\mathbf{s}_{i,\ell} = \mathbf{c}_{i,\ell} a_{i,\ell} \tag{4.1}$$

Hence, the transmitter converts each data symbol in a block of N_c samples. The corresponding transmitter matrix $\mathbf{T}_{tr,i,\ell}$ (2.1) is a vector of length N_c: $\mathbf{T}_{tr,i,\ell} = \mathbf{c}_{i,\ell}$. The time-domain sequence is converted into a continuous-time signal by multiplying the sequence with the transmit clock signal, which has a clock frequency $1/T = N_c R_s$. In the literature, often the notation T_c is used for the duration of the chip interval and T for the duration of the symbol interval. However, in this work, we use a single notation for the sampling rate at the receiver for the different systems (i.e., $1/T$, see chapter 2). Hence, the quantity T in this chapter corresponds to the chip interval and not to the symbol interval. The continuous-time signal is applied to the transmit filter $p(t)$ with transfer

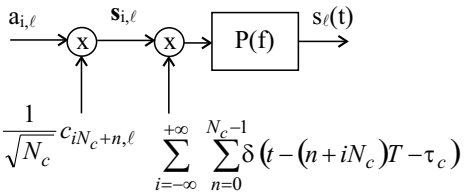

Figure 4.1: The DS-CDMA transmitter for a single user

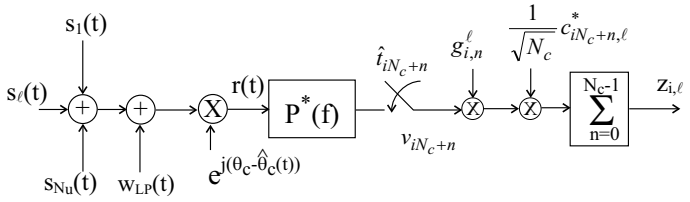

Figure 4.2: The DS-CDMA receiver for a single user

function $P(f)$, a square-root Nyquist filter with respect to the chip interval T (2.3), resulting in the signal $s_\ell(t)$

$$s_\ell(t) = \sum_{i=-\infty}^{+\infty} \sum_{n=0}^{N_c-1} s_{iN_c+n,\ell} p(t-(iN_c+n)T-\tau_c) \tag{4.2}$$

where τ_c represents the transmit clock phase.

In the following, we consider the case of synchronous DS-CDMA transmitted over an AWGN channel. In synchronous DS-CDMA, the signals of the different users are synchronised, i.e. the symbol boundaries of the different users coincide. This implies that the different users exhibit the same timing errors and transmit clock phase τ_c. Furthermore, it is assumed that the carrier oscillators of the different users are synchronised, i.e. the transmit carrier oscillators exhibit the same carrier frequency and phase. Hence, the different users are affected by the same carrier phase error. Under these conditions, the analysis for the uplink and the downlink is the same.

The receiver structure of the DS-CDMA system is shown in figure 4.2 for a single user. The superposition of the signals $s_\ell(t)$ sent to the different users is transmitted over an ideal channel, i.e. $H_{ch}(f;t) = 1$. The sum of the signals is disturbed by additive white Gaussian noise (AWGN) $w_{LP}(t)$, whose independent real and imaginary parts have the same power spectral density $N_0/2$. All signals are affected by the same carrier phase difference $\theta_c - \hat{\theta}_r(t)$, where θ_c is the carrier phase at the transmitter and $\hat{\theta}_r(t)$ is the estimated optimum carrier phase at the receiver. In the case of the ideal channel, the optimum carrier phase $\theta_r(t)$ at the receiver equals the carrier phase θ_c at the transmitter. Hence, the carrier phase error $\phi(t)$ (2.11) equals the carrier phase difference: $\phi(t) = \theta_c - \hat{\theta}_r(t)$.

The resulting signal $r(t)$ is applied to the receiver filter, which is matched to the transmit filter, and sampled at the instants $\hat{t}_{iN_c+n} = t_{iN_c+n} + \epsilon_{iN_c+n}T$, where $t_{iN_c+n} = (n + iN_c)T + \tau_c$ are the optimum sampling instants (see (2.10)) and ϵ_{iN_c+n} is the normalised timing error of the nth sample of the ith transmitted symbol. The resulting samples $\mathbf{v}_i = (v_{iN_c} \dots v_{iN_c+N_c-1})^T$ can be written as

$$v_{iN_c+n} = \sum_{i'=-\infty}^{+\infty} \sum_{n'=0}^{N_c-1} \sum_{\ell=1}^{N_u} s_{i'N_c+n',\ell} h_{eq}(t_{iN_c+n} - t_{i'N_c+n'}; t_{iN_c+n}) + w_{iN_c+n} \quad (4.3)$$

where N_u is the number of active users, w_{iN_c+n} is the value of the matched filter output noise at the instant $\hat{t}_{iN_c+n}$, originating from the noise contribution $w_{LP}(t)$ and $h_{eq}(t; t_{iN_c+n})$ is the impulse response of the equivalent time-varying filter including the synchronisation errors, as defined in section 2.3.1. The Fourier transform of $h_{eq}(t; t_{iN_c+n})$ with respect to t equals (see (2.21))

$$H_{eq}(f; t_{iN_c+n}) = |P(f)|^2 e^{j\phi(t_{iN_c+n})} e^{j2\pi f \epsilon_{iN_c+n}T} \quad (4.4)$$

The receiver scales and rotates the sample v_{iN_c+n} with an equaliser coefficient $g_{i,n}^{\ell}$. The equaliser is implemented as an MMSE equaliser and is computed using (2.51). The resulting sequence is multiplied with the complex conjugate of the corresponding chip of the considered user and summed to obtain the samples $z_{i,\ell}$ at the input of the decision device

$$z_{i,\ell} = a_{i,\ell} I_{i,i,\ell,\ell} + \sum_{i'=-\infty; i' \neq i}^{+\infty} a_{i',\ell} I_{i,i',\ell,\ell} + \sum_{i'=-\infty; i' \neq i}^{+\infty} \sum_{\ell'=1; \ell' \neq \ell}^{N_u} a_{i',\ell'} I_{i,i',\ell,\ell'} + W_{i,\ell} \quad (4.5)$$

where $W_{i,\ell}$ is a zero-mean complex-valued additive Gaussian noise term and

$$I_{i,i',\ell,\ell'} = \frac{1}{N_c} \sum_{n,n'=1}^{N_c-1} c_{iN_c+n,\ell} c^*_{i'N_c+n',\ell'} g_{i,n}^{\ell} h_{eq}(t_{iN_c+n} - t_{i'N_c+n'}; t_{iN_c+n}) \quad (4.6)$$

Considering (2.24), the variance of the additive Gaussian noise term yields

$$E[|W_{i,\ell}|^2] = N_0 \frac{1}{N_c} \sum_{n=1}^{N_c-1} |g_{i,n}^{\ell}|^2 \triangleq N_0 \sigma_{i,\ell}^2 \quad (4.7)$$

Hence, the receiver demodulates the data with a linear transformation $\mathbf{b}_{i,\ell}$ of length N_c: $\mathbf{b}_{i,\ell} = \mathbf{c}_{i,\ell}\mathbf{G}_{i,\ell}$, where $\mathbf{G}_{i,\ell}$ is a diagonal matrix of the order $N_c \times N_c$ with diagonal elements the equaliser coefficients, i.e. $(\mathbf{G}_{i,\ell})_{n,n'} = g_{i,n}^{\ell}\delta_{n,n'}$. In (4.5), the sample $z_{i,\ell}$ is decomposed into four contributions. The first term $I_{i,i,\ell,\ell}$ is the useful component. This contribution can be further decomposed into an average useful component $E[I_{i,i,\ell,\ell}]$, and a zero-mean fluctuation $I_{i,i,\ell,\ell} - E[I_{i,i,\ell,\ell}]$, i.e. the self-interference (SI). The second contribution ($I_{i,i',\ell,\ell}$ for $i' \neq i$) is the intersymbol interference (ISI), caused by the other data symbols

transmitted to the considered user. The third contribution ($I_{i,i',\ell,\ell'}$ for $\ell' \neq \ell$) is the multiuser interference (MUI), caused by data symbols transmitted to other users and the last contribution is the additive noise term.

The performance of the DS-CDMA system is expressed by the signal-to-noise ratio (SNR), as defined in section 2.6. The SNR is the ratio of the power of the average useful component P_U to the sum of the powers of the self-interference P_{SI}, the intersymbol interference P_{ISI}, the multiuser interference P_{MUI} and the noise. This yields

$$SNR_{i,\ell} = \frac{E_s P_{U,i,\ell}}{N_0\sigma^2_{i,\ell} + E_s(P_{SI,i,\ell} + P_{ISI,i,\ell} + P_{MUI,i,\ell})} \tag{4.8}$$

where $E_s = E[|a_{i,\ell}|^2]$ is the energy per symbol and

$$\begin{aligned} P_{U,i,\ell} &= |E[I_{i,i,\ell,\ell}]|^2 \\ P_{SI,i,\ell} &= E[|I_{i,i,\ell,\ell} - E[I_{i,i,\ell,\ell}]|^2] \\ P_{ISI,i,\ell} &= \sum_{i'=-\infty;i'\neq i}^{+\infty} E[|I_{i,i',\ell,\ell}|^2] \\ P_{MUI,i,\ell} &= \sum_{i'=-\infty}^{+\infty} \sum_{\ell'=1;\ell'\neq\ell}^{N_u} E[|I_{i,i',\ell,\ell'}|^2] \end{aligned} \tag{4.9}$$

The SNR (4.8) depends on the user index ℓ and the symbol index i.

In the absence of synchronisation errors, the receiver filter output samples v_{iN_c+n} are given by (see (2.6))

$$v_{iN_c+n} = \sum_{\ell=1}^{N_u} s_{iN_c+n,\ell} + w_{iN_c+n} \tag{4.10}$$

where the noise contributions w_{iN_c+n} are Gaussian with $E[w_{iN_c+n}w^*_{i'N_c+n'}] = N_0\delta_{i,i'}\delta_{n,n'}$ and $s_{iN_c+n,\ell}$ is given by (4.1). The one-tap equaliser operating on v_{iN_c+n} has coefficient $g^\ell_{i,n}$ given by $g^\ell_{i,n} = E_s/(E_s + N_0)$; note that $g^\ell_{i,n}$ is independent of the symbol index i, the chip index n and the user index ℓ. After despreading, the samples at the input of the decision device yield (see (2.41))

$$z_{i,\ell} = a_{i,\ell} + W_{i,\ell} \tag{4.11}$$

where

$$W_{i,\ell} = \frac{1}{\sqrt{N_c}} \sum_{n=1}^{N_c-1} w_{iN_c+n}c^*_{iN_c+n,\ell} \tag{4.12}$$

yielding $E[|W_{i,\ell}|^2] = N_0$. Note that $z_{i,\ell}$ contains the data symbol $a_{i,\ell}$ but no other symbols: because of the orthogonality of the sequences $\mathbf{c}_{i,\ell}$, no MUI occurs, and because of the non-dispersive channel, no ISI occurs. Taking into

account that $E_s = E[|a_{i,\ell}|^2]$, the resulting SNR (4.8) is independent of the indices i and ℓ and yields

$$SNR(0) = \frac{E_s}{N_0} \tag{4.13}$$

The presence of synchronisation errors generally causes interference. Hence, the DS-CDMA system performance is degraded as compared to the case of no synchronisation errors. The degradation of the SNR (4.8) as compared to $SNR(0)$ (4.13) (expressed in dB) is given by

$$Deg_{i,\ell} = -10 \log \left(\frac{P_{U,i,\ell}}{\sigma^2_{i,\ell} + \frac{E_s}{N_0}(P_{SI,i,\ell} + P_{ISI,i,\ell} + P_{MUI,i,\ell})} \right) \tag{4.14}$$

The computation complexity of the expressions (4.9) strongly increases for an increasing spreading factor N_c. To reduce this computation complexity, we present accurate approximations for (4.9). In the following, we make use of the simplified expressions of appendix C for (4.9).

4.3 Effect of Synchronisation Errors

In this section, we investigate the effect of synchronisation errors on the performance of the considered DS-CDMA system. In [Ste99e], we have studied the effect of the carrier phase errors on a downlink orthogonal DS-CDMA system. In the literature, the effect of the following synchronisation errors on the DS-CDMA system have been studied: the effect of a carrier frequency offset and clock frequency offset on the DS-CDMA system has been investigated in [Sou90]. The sensitivity of DS-CDMA to random carrier phase and timing errors has been studied in [Buc95]. In [Par96], the impact of timing errors on a DS-CDMA system is investigated. The sensitivity to timing jitter is studied in [Buc93]. As in section 2.2, we separately consider the effect of the carrier phase errors and the timing errors.

4.3.1 Carrier Phase Errors

The sensitivity of the DS-CDMA system to carrier phase errors is investigated in this section, in the case no timing errors are present ($\epsilon_{iN_c+n} = 0$). In this case, the quantities $I_{i,i',\ell,\ell'}$ (4.6) are given by

$$I_{i,i',\ell,\ell'} = \delta_{i,i'} \frac{1}{N_c} \sum_{n,n'=1}^{N_c-1} c_{iN_c+n,\ell} c^*_{i'N_c+n',\ell'} g^{\ell}_{i,n} e^{j\phi(t_{iN_c+n})} \tag{4.15}$$

In (4.15), we observe that the carrier phase errors do not introduce intersymbol interference, but only cause self-interference and multiuser interference. In the following, we consider the cases of a constant phase offset, a carrier frequency offset and carrier phase jitter.

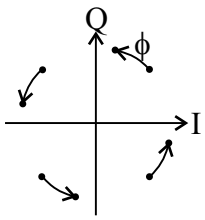

Figure 4.3: Effect of a constant phase offset on the samples $z_{i,\ell}$, $g_{i,n}^{\ell} = 1$

Constant Phase Offset

A constant mismatch of the phase between the carrier oscillators at the transmitter and the receiver introduces a constant phase offset $\phi(t_{iN_c+n}) = \phi$. The constant phase offset causes a phase rotation over an angle ϕ of the received samples v_{iN_c+n}, but no interference is introduced. Hence, in the absence of an equaliser ($g_{i,n}^{\ell} = 1$), a constant phase offset gives rise to a constant phase rotation of the samples at the input of the decision device, as shown in figure 4.3, resulting in a reduction of the noise margins. To compensate for the reduction of the noise margins, the equaliser rotates the samples v_{iN_c+n} over (an estimate of) the angle $-\phi$, i.e. the MMSE equaliser is given by $(g_{MMSE})_{i,n}^{\ell} = Ce^{-j\phi}$, where

$$C = \frac{\sqrt{E_s}}{N_0 + E_s} \tag{4.16}$$

are the equaliser coefficients in the absence of synchronisation errors. The MMSE equaliser in the case of the constant phase offset is independent of the symbol index i, the user index ℓ and the chip index n. As the phase rotation of the samples v_{iN_c+n} does not introduce an enhancement of the noise power level, the constant phase offset is compensated without loss of performance.

Carrier Frequency Offset

When a constant mismatch of the frequency between the carrier oscillators at the transmitter and the receiver occurs, the carrier phase error linearly increases in time: $\phi(t_{iN_c+n}) = 2\pi(n+iN_c)\Delta FT+\phi(0)$, where ΔF is the carrier frequency offset. A carrier frequency offset introduces a rotation at a constant speed of $2\pi\Delta F$ rad/s of the receiver filter output samples v_{iN_c+n}, and a frequency shift of the transmitted signal, resulting in a reduction of the useful component and interference, as shown in the previous chapter.

First, we concentrate on the effect of the phase rotation on the system performance. When no correction of the systematic phase rotation of the samples v_{iN_c+n} is present, i.e. $g_{i,n}^{\ell} = 1$, the useful component of the sample $z_{i,\ell}$ at the input of the decision device is subjected to a rotation at a constant speed of

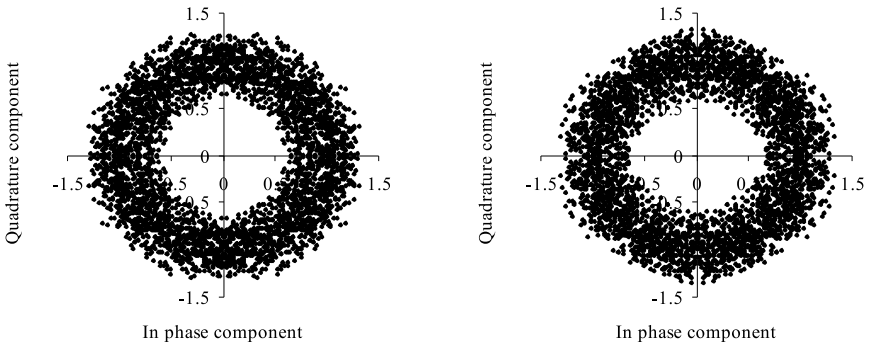

Figure 4.4: Carrier frequency offset, $N_u = N_c, g_{i,n}^{\ell} = 1, N_c = 64, \Delta FT = 2.10^{-3}$, (a) Walsh Hadamard sequences (b) overlay sequences

$2\pi N_c \Delta FT$ rad/symbol and a reduction of the amplitude (4.6):

$$I_{i,i,\ell,\ell} = e^{j\phi(0)} e^{j2\pi i N_c \Delta FT} D(\Delta FT) \tag{4.17}$$

where

$$D(x) = \frac{1}{N_c} \sum_{n=1}^{N_c-1} e^{j2\pi nx} = e^{j\pi(N_c-1)x} \frac{\sin \pi N_c x}{N_c \sin \pi x} \tag{4.18}$$

This amplitude reduction of the useful component is introduced as the contributions of the different chips that have to be summed to obtain the sample $z_{i,\ell}$ are not in phase. Furthermore, this sample dependent rotation of v_{iN_c+n} gives rise to a large amount of MUI. Hence, a carrier frequency offset reduces the performance when no equalisation is performed. Figures 4.4 (a)-(b) show the scatter diagrams of the samples at the input of the decision device in the absence of additive noise, for the cases of the Walsh-Hadamard sequences and the overlay sequences. Furthermore, it is assumed that the carrier frequency offset equals $\Delta FT = 2.10^{-3}$, the spreading factor $N_c = 64$, and the number of active users equals $N_u = N_c$, i.e. for the maximal load. In these figures, we observe that the scatter diagrams are the same for the Walsh-Hadamard sequences and the overlay sequences. As expected, the samples at the input of the decision device are rotated and disturbed by a large amount of MUI.

To avoid the systematic rotation of the samples $z_{i,\ell}$ at a constant speed of $2\pi N_c \Delta FT$ rad/symbol, a one-tap equaliser can be applied after despreading. However, in this case, the sampling dependent rotation of the receiver output samples still causes a reduction of the useful component and introduces a large amount of MUI. To avoid this reduction of the useful component and the MUI, a one-tap equaliser is applied to the output of the receiver filter. Assuming the

receiver is able to estimate the carrier frequency offset, the equaliser rotates the sample v_{iN_c+n} over the angle $-(2\pi(n+iN_c)\Delta FT + \phi(0))$:

$$(g_{MMSE})_{i,n}^{\ell} = Ce^{-j2\pi(n+iN_c)\Delta FT}e^{-j\phi(0)} \tag{4.19}$$

where C is defined in (4.16). In this case, the quantities $I_{i,i',\ell,\ell'}$ (4.15) reduce to

$$I_{i,i',\ell,\ell'} = C\delta_{i,i'}\delta_{\ell,\ell'} \tag{4.20}$$

Hence, when the systematic phase rotation is compensated, no interference or a reduction of the useful component is introduced. Furthermore, as the phase rotation of the receiver samples v_{iN_c+n} does not enhance the noise power level, no degradation is introduced.

In the preceding analysis, we have shown that the effect of the phase rotation of the receiver filter output samples v_{iN_c+n} can be compensated without loss of performance by the equaliser. However, in this analysis, we have neglected the effect of the frequency shift of the transmitted signal. Because of the frequency shift, a part of the transmitted signal falls outside the bandwidth of the receiver filter, resulting in signal distortion and power loss. In chapter 3, it is shown that this frequency shift results in a reduction of the useful component in the samples v_{iN_c+n} and the introduction of interference. Assuming the equaliser compensates for the systematic phase rotation of the samples v_{iN_c+n}, the quantities $I_{i,i',\ell,\ell'}$ (4.6) yield

$$\begin{aligned} I_{i,i',\ell,\ell'} &= \frac{C}{N_c}\sum_{n,n'=0}^{N_c-1} c^*_{iN_c+n,\ell}c_{i'N_c+n',\ell'} \cdot \\ &\quad \int_{-\infty}^{+\infty} P(f)P^*(f+\Delta F)e^{j2\pi(n-n'+(i-i')N_c)fT}df \end{aligned} \tag{4.21}$$

In the case of the maximum load ($N_u = N_c$), which corresponds with the worst case as the multiuser interference power is maximal, the power of the average useful component P_U, the total interference power P_I (which is the sum of the powers of the self-interference, the intersymbol interference and the multiuser interference) (4.9) and the noise (4.7), for both the Walsh-Hadamard sequences and the overlay sequences, are independent of the block index i and the user index ℓ and yield

$$\begin{aligned} P_U &= |C|^2\left|\int_{-\infty}^{+\infty} P(f)P^*(f+\Delta F)df\right|^2 \\ P_I &= |C|^2\sum_{n=-\infty;n\neq 0}^{+\infty}\left|\int_{-\infty}^{+\infty} P(f)P^*(f+\Delta F)e^{j2\pi nfT}df\right|^2 \\ E[|W_{i,\ell}|^2] &= N_0|C|^2 \end{aligned} \tag{4.22}$$

As we observe from (4.22), the power of the average useful component, the total interference power and the noise power are independent from the spreading

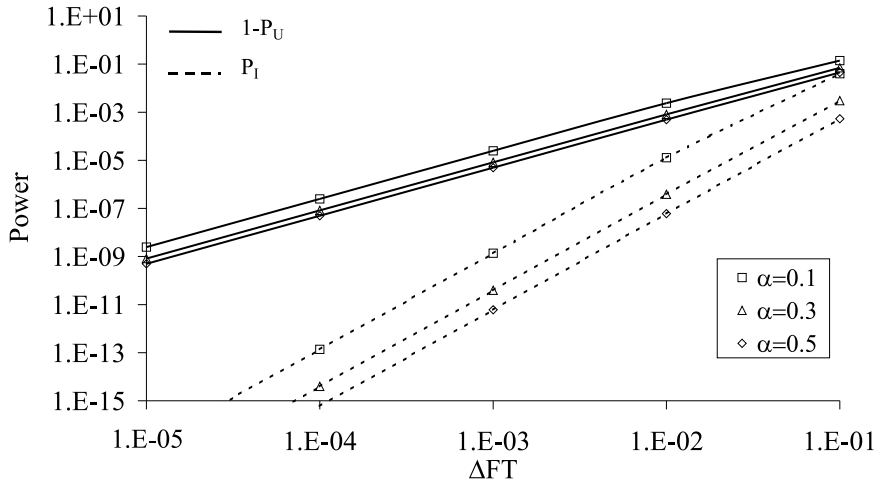

Figure 4.5: Influence of the carrier frequency offset on the reduction of the power of the average useful component $(1-P_U)$ and the total interference power $(P_I = P_{SI} + P_{ISI} + P_{MUI})$, $N_c = 64, N_u = N_c$

factor N_c. In the case of the transmit and the receiver filter being square-root raised-cosine filters with rolloff α (see appendix B), and when the carrier frequency offset is small, i.e. $\Delta FT \ll 1$, the power of the average useful component (4.22) can be approximated by

$$P_U \approx 1 - \frac{(\pi|\Delta F|T)^2}{4\alpha} \tag{4.23}$$

Hence, the power of the average useful component is reduced as compared to the case of a zero carrier frequency offset. The power of the average useful component and the total interference power are a function of the product ΔFT. In figure 4.5, the reduction of the power of the average useful component $(1 - P_U)$ and the total interference power P_I (4.22) are shown as function of the product ΔFT, a spreading factor $N_c = 64$ and the maximum load $(N_u = N_c)$. Similarly as for the conventional single carrier communication system, the total interference power, which is proportional to $(\Delta FT)^4$ can be neglected as compared to the reduction of the power of the useful component, which is proportional to $(\Delta FT)^2$, for small frequency offsets $(\Delta FT \ll 1)$. The degradation as compared to the case of a zero carrier frequency offset, caused by the reduction of the useful component only and the degradation caused by both the reduction of the useful component and the interference are shown in figure 4.6. We observe that the degradation is mainly caused by the reduction of the useful component. This degradation is independent of the spreading factor N_c. The degradation is small when the frequency offset is small as compared to the system bandwidth:

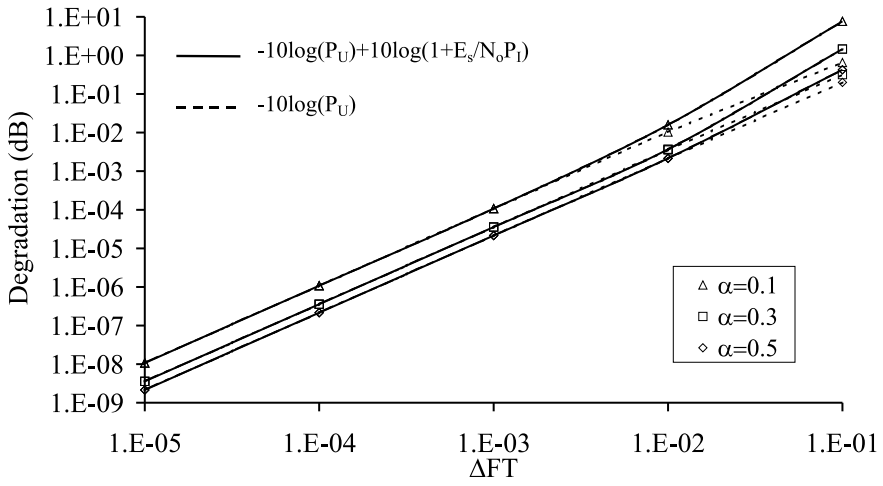

Figure 4.6: Degradation caused by the reduction of the power of the average useful component only and the reduction of the power of the average useful component and the interference power, $SNR(0) = 20\text{dB}, N_c = 64, N_u = N_c$

$\Delta F \ll 1/T = N_c R_s$. The sensitivity of the DS-CDMA system to a carrier frequency offset is the same as for the conventional single carrier communication system.

Carrier Phase Jitter

To get rid of a carrier frequency offset and a constant phase offset, a carrier synchronisation mechanism can be used to estimate the optimum phase $\theta_r(t)$. The phase jitter resulting from such a synchroniser structure can be modelled as a zero-mean stationary random process with jitter power spectral density $S_\phi(f)$ and jitter variance σ_ϕ^2. When the phase jitter slowly varies as compared to the duration of the impulse response of the transmit filter, and for small jitter variances $\sigma_\phi^2 \ll 1$, the quantities $I_{i,i',\ell,\ell'}$ (4.15) can be approximated by

$$I_{i,i',\ell,\ell'} = \frac{1}{N_c} \sum_{n,n'=0}^{N_c-1} c^*_{iN_c+n,\ell} c_{i'N_c+n',\ell'} g^\ell_{i,n} (1 + j\phi(t_{iN_c+n})) \tag{4.24}$$

When the carrier phase jitter rapidly varies as compared to the averaging time of the MMSE equaliser, the equaliser is not able to track the variations caused by the carrier phase jitter. The equaliser averages in the time over the variations caused by the carrier phase jitter. As for small jitter variances, the time average of $\exp(j\phi(t))$ can be approximated by $E[\exp(j\phi(t))] \approx E[1 + j\phi(t)] = 1$, the MMSE equaliser is essentially the same as in the absence of synchronisation

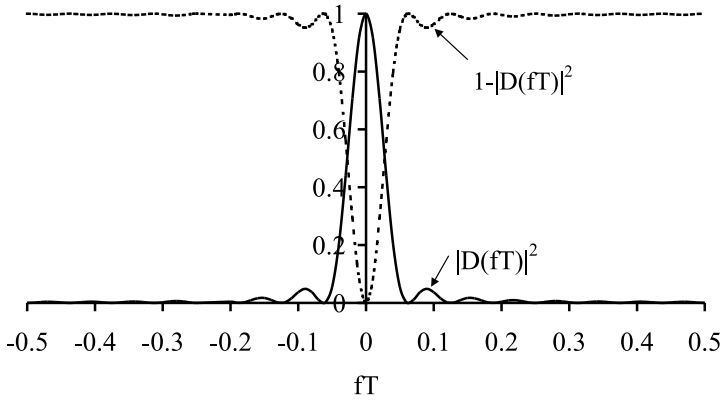

Figure 4.7: The weight functions $|D(fT)|^2$ and $(1-|D(fT)|^2)$, $N_c = 16$

errors, i.e. $(g_{MMSE})_{i,n}^{\ell} = C$, where C is defined in (4.16). The MMSE filter is independent of the symbol index i, the chip index n and the user index ℓ. From (4.24) it follows that the carrier phase jitter introduces self-interference and multiuser interference. However, the average useful component is not attenuated, nor intersymbol interference is introduced. Considering the approximations for the moments of the spreading sequences (appendix C), the powers of the average useful component, the self-interference, the multiuser interference (4.9) and the noise (4.7) are given by

$$\begin{aligned} P_U &= |C|^2 \\ P_{SI} &= |C|^2 \int_{-\infty}^{+\infty} S_\phi(f)|D(fT)|^2 df \\ P_{MUI} &= |C|^2 \frac{N_u - 1}{N_c - 1} \int_{-\infty}^{+\infty} S_\phi(f)(1-|D(fT)|^2) df \\ E[|W_{i,\ell}|^2] &= N_0|C|^2 \end{aligned} \tag{4.25}$$

From (4.25) it follows that the powers of the average useful component, the self-interference, the multiuser interference and the noise are independent of the user index ℓ and the symbol index i. As we observe in (4.25) and in figure 4.7, the self-interference and the multiuser interference mainly consist of the low frequency components ($|f| < 1/(N_cT) = R_s$) and the high frequency components ($|f| > 1/(N_cT) = R_s$) of the jitter spectrum $S_\phi(f)$, respectively. For the highest load ($N_u = N_c$), the sum of the powers of the self-interference and the multiuser interference becomes independent of the spectral contents of the jitter and of the spreading factor N_c, and only depends on the jitter variance σ_ϕ^2, given by

$$\sigma_\phi^2 = \int_{-\infty}^{+\infty} S_\phi(f) df \tag{4.26}$$

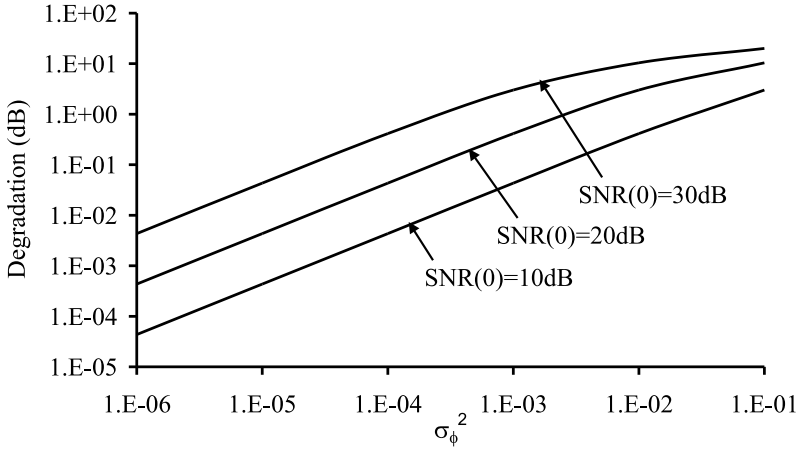

Figure 4.8: Carrier phase jitter, $N_u = N_c$

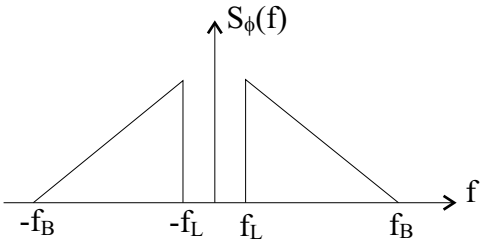

Figure 4.9: Jitter spectrum

In this case, the degradation (4.14) of the SNR, caused by the carrier phase jitter, is independent of the spreading factor N_c and of the spectral contents of the jitter, but only depends on the jitter variance:

$$Deg = 10 \log \left(1 + \frac{E_s}{N_0} \sigma_\phi^2 \right) \tag{4.27}$$

The performance degradation (4.25) is the same for all users and is independent of the symbol index i.

In figure 4.8, the degradation (4.27) is shown as function of the jitter variance. The degradation of figure 4.8 yields an upper bound for the degradation for $N_u < N_c$.

The DS-CDMA system is simulated in the absence of additive noise ($N_0 = 0$), in the case of QPSK modulation, for a spreading factor $N_c = 64$, the maximum load and a jitter variance of $\sigma_\phi^2 = 5.10^{-3}$ rad^2. The jitter spectrum is of the shape of figure 4.9. Figures 4.10 (a)-(b) and 4.11 (a)-(b) show the scatter diagrams for $f_L = 0, f_B = 1/(N_c T) = R_s$ and $f_L = 2/(N_c T) = 2R_s, f_B =$

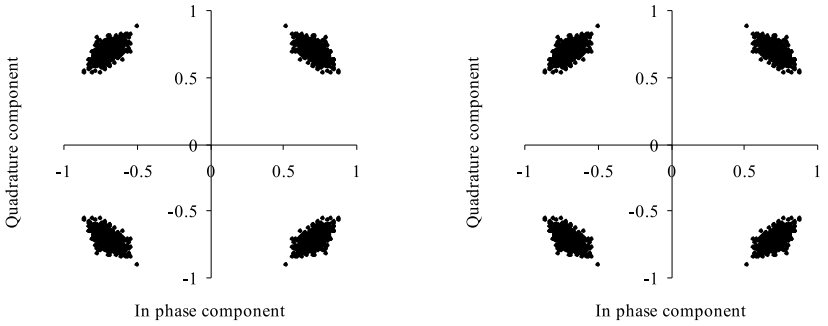

(a) (b)

Figure 4.10: Carrier phase jitter, $N_u = N_c, f_L = 0, f_B = 1/(N_cT) = R_s, N_c = 64, \sigma_\phi^2 = 5.10^{-3}$ rad^2, (a) Walsh-Hadamard sequences (b) overlay sequences

Table 4.1: Mean square deviation of the samples at the input of the decision device

		Theoretical	Simulations
$f_L = 0,$	Walsh-Hadamard	$5E-3$	$5.064E-3$
$f_B = 1/(N_cT) = R_s$	overlay	$5E-3$	$5.064E-3$
$fL = 2/(N_cT) = 2R_s,$	Walsh-Hadamard	$5E-3$	$5.052E-3$
$fB = 4/(N_cT) = 4R_s$	overlay	$5E-3$	$5.052E-3$

$4/(N_cT) = 4R_s$, respectively, in the cases of the Walsh-Hadamard sequences and the overlay sequences. We observe that the scatter diagrams for the Walsh-Hadamard sequences and the overlay sequences are the same. Although the mean-square deviation of the samples at the input of the decision device are equal for all scatter diagrams and equals σ_ϕ^2, the scatter diagrams differ considerably. When $f_L = 0, f_B = 1/(N_cT) = R_s$, the main interference contribution is the self-interference, as the jitter contains only low frequency components ($|f| < 1/(N_cT) = R_s$). Hence, the jitter gives rise to a random phase rotation of the useful component and the scatter diagram shows mainly an angular displacement of the samples at the input of the decision device. When $f_L = 2/(N_cT) = 2R_s, f_B = 4/(N_cT) = 4R_s$, the jitter contains only high frequency components ($|f| > 1/(N_cT) = R_s$) and therefore introduces mainly MUI. Hence, the jitter causes both an angular and a radial displacement of the samples at the input of the decision device, resulting in a circular cloud in the scatter diagram, as the term of the MUI has uncorrelated real and imaginary parts, each having the same variance. In table 4.1, the mean square deviation of the samples at the input device is shown for the simulations of the scatter diagrams of figures 4.10 and 4.11. As we observe, the simulation results agree well with the theoretical results.

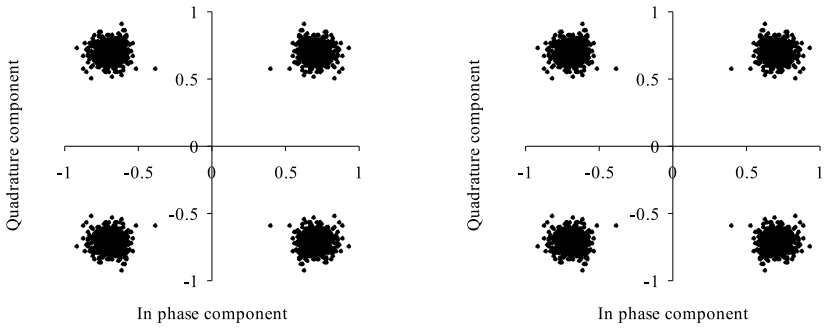

Figure 4.11: Carrier phase jitter, $N_u = N_c, f_L = 2/(N_cT) = 2R_s, f_B = 4/(N_cT) = 4R_s, N_c = 64, \sigma_\phi^2 = 5.10^{-3}$ rad^2, (a) Walsh-Hadamard sequences (b) overlay sequences

4.3.2 Timing Errors

In this section, we investigate the sensitivity of the DS-CDMA system to timing errors in the absence of carrier phase errors ($\phi(t) = 0$). In this case, the quantities $I_{i,i',\ell,\ell'}$ (4.6) are given by

$$I_{i,i',\ell,\ell'} = \frac{1}{N_c} \sum_{n,n'=1}^{N_c-1} c^*_{iN_c+n,\ell} c_{i'N_c+n',\ell'} g^\ell_{i,n} h((n-n'+(i-i')N_c+\epsilon_{iN_c+n})T) \tag{4.28}$$

where $h(t)$ is the impulse response of the cascade of the transmit filter and the receiver filter. Its Fourier transform equals $H(f) = |P(f)|^2$. From (4.26) it follows that a timing error introduces interference. In the following, we consider the effect of a constant timing offset, a clock frequency offset and timing jitter.

Constant Timing Offset

In the case of a constant mismatch between the estimated and the ideal timing instants, a constant timing offset $\epsilon_{iN_c+n} = \epsilon$ occurs. In the case of the maximum load, which corresponds to the worst case as the multiuser interference power is maximal, the MMSE equaliser coefficients are the same for the Walsh-Hadamard sequences and the overlay sequences. Furthermore, the equaliser coefficients are independent of the symbol index i, the chip index n and the user index ℓ and equal

$$(g_{MMSE})^\ell_{i,n} = \frac{\sqrt{E_s} h^*(\epsilon T)}{N_0 + E_s \sum_{n=-\infty}^{+\infty} |h((n+\epsilon)T)|^2} \triangleq C_\epsilon \tag{4.29}$$

In the case of the maximum load, the power of the average useful component, the total interference power P_I (which is the sum of the powers of the self-interference, the intersymbol interference and the multiuser interference) (4.9) and the noise power (4.7) are the same for the Walsh-Hadamard sequences and the overlay sequences, and are given by

$$\begin{aligned} P_U &= |C_\epsilon|^2 |h(\epsilon T)|^2 \\ P_{ISI} &= |C_\epsilon|^2 \sum_{n=-\infty; n\neq 0}^{+\infty} |h((n+\epsilon)T)|^2 \\ &= |C_\epsilon|^2 \left(\frac{1}{T} \sum_{n=-\infty}^{+\infty} e^{j2\pi\epsilon n} \int_{-\infty}^{+\infty} H(f) H\left(f + \frac{n}{T}\right) df - |h(\epsilon T)|^2 \right) \\ E[|W_{i,\ell}|^2] &= N_0 |C_\epsilon|^2 \end{aligned} \tag{4.30}$$

As we observe in (4.30), the powers of the average useful component, the total interference power and the noise are independent of the spreading factor N_c, the user index ℓ and the symbol index i. When the transmit filter and receiver filter are square-root raised-cosine filters with rolloff a (see appendix B), the total interference power (4.30) is given by

$$P_I = |C_\epsilon|^2 \left(1 - \frac{\alpha}{4}(1 - \cos 2\pi\epsilon) - |h(\epsilon T)|^2\right) \tag{4.31}$$

Hence, the degradation (4.14) of the SNR as compared to the case of a zero timing offset yields

$$Deg = -10 \log |h(\epsilon T)|^2 + 10 \log \left(1 + \frac{E_s}{N_0} \left(1 - \frac{\alpha}{4}(1 - \cos 2\pi\epsilon) - |h(\epsilon T)|^2\right)\right) \tag{4.32}$$

The degradation is independent of the spreading factor N_c and is equal for all users. For a small timing error ($\epsilon \ll 1$), we can use the approximations (3.32). In this case, the degradation (4.32) can be approximated by

$$Deg \approx -10 \log(1 - \epsilon^2 A(\alpha)) + 10 \log \left(1 + \frac{E_s}{N_0} \epsilon^2 B(\alpha)\right) \tag{4.33}$$

where $A(\alpha)$ and $B(\alpha)$ are defined in (3.34).

In figure 4.12, the degradation (4.33) and the degradation caused by the interference only are shown as function of the constant timing offset. As we observe, the effect of the reduction of the useful component can be neglected as compared to the effect of the interference. In figure 4.13, the total interference power and the powers of the self-interference, the intersymbol interference and the multiuser interference are shown as function of the constant timing offset for the maximum load. As expected, the interference power is proportional to ϵ^2 for small ϵ. It can easily be verified that the SI power is inversely proportional to N_c and that the ISI power is about N_c times smaller than the SI power.

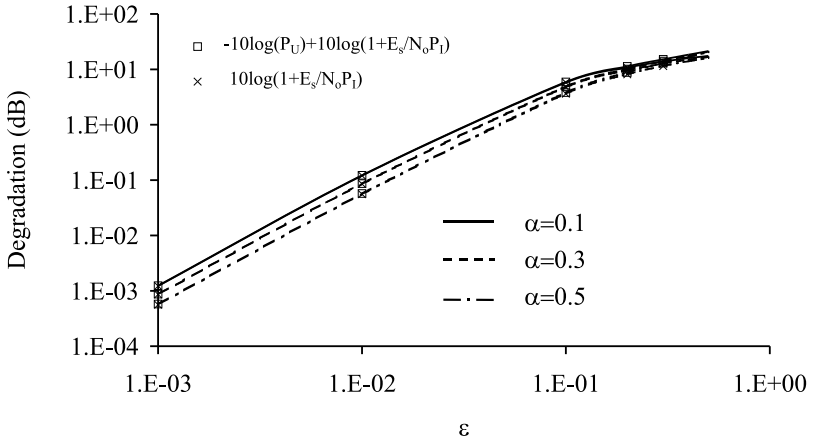

Figure 4.12: Constant timing offset, $N_c = 64, N_u = N_c, SNR(0) = 20$ dB

Furthermore, the MUI power per disturbing user is of the same order of the SI power and also inversely proportional to N_c. The MUI power is proportional to the number of disturbing users. When no disturbing users are present, the MUI power is zero. For the maximum load, the MUI power is maximum and is shown in the figure. We observe in figure 4.13 that for the maximum load and for a large spreading factor, the dominating interference term is the MUI. Although the self-interference power, the intersymbol interference power and the multiuser interference power depend on the spreading factor, the sum of the powers, i.e. the total interference power, is independent of the spreading factor N_c when all users are active ($N_u = N_c$).

Clock Frequency Offset

In the case of a clock frequency offset $\Delta T/T$ between the transmitter and receiver clock, the timing error linearly increases with time: $\epsilon_{iN_c+n} = (iN_c + n)\Delta T/T + \epsilon_0$. Hence, an increasing misalignment between the transmitted chips $c_{iN_c+n,\ell}$ and the received samples v_{iN_c+n} occurs. This increasing misalignment can not be tolerated. To compensate for this increasing misalignment, a coarse synchronisation algorithm could be used, as described in section 3.3.2. At the receiver, the chip $c^*_{iN_c+n,\ell}$ is multiplied with the sample $v_{i'N_c+n'}$, for which the sampling instant $\hat{t}_{i'N_c+n'}$ is closest to the ideal sampling instant t_{iN_c+n}. This involves duplicating ($\Delta T > 0$) or removing ($\Delta T < 0$) samples at regular intervals, so that the average rate of samples used by the receiver equals the chip rate $1/T$. The resulting relative timing error $\tilde{\epsilon}_{iN_c+n} = (\hat{t}_{i'N_c+n'} - t_{iN_c+n})/T$ is limited to the interval $[-0.5, 0.5]$. When $\Delta T/T$ is so small that $\tilde{\epsilon}_{iN_c+n}$ is slowly varying over the averaging time of the equaliser, the timing error is tracked by

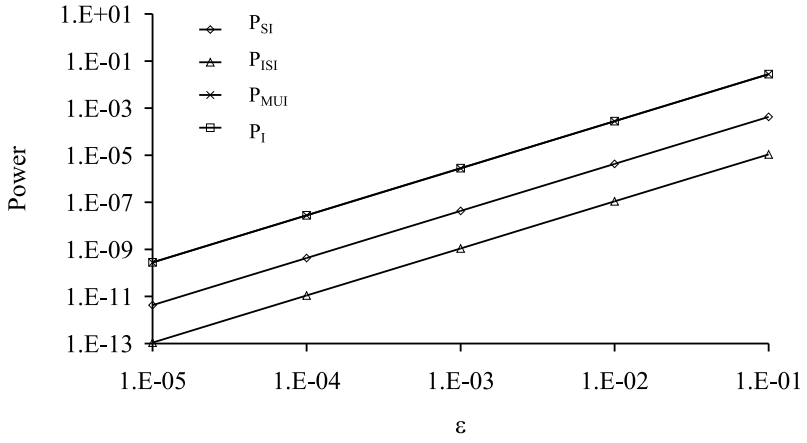

Figure 4.13: Constant timing offset, $N_c = 64, N_u = N_c, \alpha = 0.1$

the equaliser, and is essentially constant over a symbol interval. The resulting degradation of the SNR depends on the symbol index i, and is given by (4.32), with ϵ replaced by the average over $\tilde{\epsilon}_{iN_c+n}$ over the considered symbol interval. For $\tilde{\epsilon}_{iN_c+n}$ $(n = 0, \ldots, N_c - 1)$ close to 0.5 or -0.5, this degradation is in the order of 20 dB. Hence, even when a coarse synchronisation algorithm is used to compensate for the increasing misalignment, the DS-CDMA system is severely degraded. To avoid this strong degradation, a clock frequency offset must be eliminated, by using a synchroniser structure that adjusts the timing phase of the receiver clock or interpolates between the available samples, as described in section 3.3.2.

Timing Jitter

When sampling is performed by means of a timing synchronisation algorithm that eliminates a constant timing offset and a clock frequency offset, the resulting timing jitter can be modelled as a zero-mean stationary random process with jitter power spectral density $S_\epsilon(\exp(j2\pi fT))$ and jitter variance σ_ϵ^2. When the timing jitter rapidly varies as compared to the averaging time of the MMSE equaliser, the equaliser is not able to track the variations caused by the timing jitter. The equaliser averages in the time over the variations caused by the timing jitter. For small jitter variances $\sigma_\epsilon^2 \ll 1$, the time average of $h((n + \epsilon_{iN_c+n})T)$ can be approximated by $E[h((n + \epsilon_{iN_c+n}T)] \approx E[h(nT) + \epsilon_{iN_c+n}Th'(nT)] = h(nT)$, where $h'(t)$ is the first order derivative of $h(t)$. Hence, the MMSE equaliser is essentially the same as in the absence of timing errors, i.e. $(g_{MMSE})_{i,n}^{\ell} \approx C$ where C is defined in (4.16). It can easily be verified that in the case of the maximum load ($N_u = N_c$), the power of the average useful component, the total interference power P_I (which is the

sum of the powers of the self-interference, the intersymbol interference and the multiuser interference) (4.9) and the noise power (4.7) are the same for the Walsh-Hadamard sequences and the overlay sequences, and are given by

$$\begin{aligned} P_{U,i} &= |C|^2 |E[h(\epsilon_{iN_c+n}T)]|^2 \\ P_{I,i} &= |C|^2 \sum_{k=-\infty;k\neq 0}^{+\infty} E[h((k+\epsilon_{iN_c+n})T)|^2] \\ &= |C|^2 \left(\frac{1}{T} \sum_{k=-\infty}^{+\infty} E[e^{j2\pi\epsilon_{iN_c+n}k}] \int_{-\infty}^{+\infty} H(f)H\left(f+\frac{k}{T}\right) df \right. \\ &\quad \left. -E[|h(\epsilon_{iN_c+n}T)|^2] \right) \\ E[|W_{i,\ell}|^2] &= N_0|C|^2 \end{aligned} \tag{4.34}$$

We observe in (4.34) that the powers of average useful component, the total interference and the noise are independent of the spreading factor N_c and the user index ℓ. For small jitter variances, the approximations (3.37) can be used. When the transmit and receiver filter are square-root raised-cosine filters with rolloff α, the power of the average useful component and the total interference power (4.34) can be approximated by

$$\begin{aligned} P_U &\approx |C|^2(1-\sigma_\epsilon^2 A(\alpha)) \\ P_I &\approx |C|^2 \sigma_\epsilon^2 B(\alpha) \end{aligned} \tag{4.35}$$

where $A(\alpha)$ and $B(\alpha)$ are defined in (3.33) and the jitter variance is given by

$$\sigma_\epsilon^2 = \int_{-1/2T}^{+1/2T} S_\epsilon(e^{j2\pi fT}) df \tag{4.36}$$

The powers of the average useful component and the total interference (4.33) are independent of the symbol index i. The degradation (4.14) of the SNR of the DS-CDMA system caused by the timing jitter is independent of the spreading factor and the spectral contents of the jitter, but only depends on the jitter variance

$$Deg = -10\log(1-\sigma_\epsilon^2 A(\alpha)) + 10\log\left(1+\frac{E_s}{N_0}\sigma_\epsilon^2 B(\alpha)\right) \tag{4.37}$$

The degradation is the same for all users and is independent of the symbol index i. Observing (4.33) and (4.37), it is clear that the sensitivity of the DS-CDMA system to a constant timing offset and timing jitter is essentially the same, when the jitter variance is equal to ϵ^2.

In figure 4.14, the total interference power and the powers of the self-interference, the intersymbol interference and the multiuser interference are

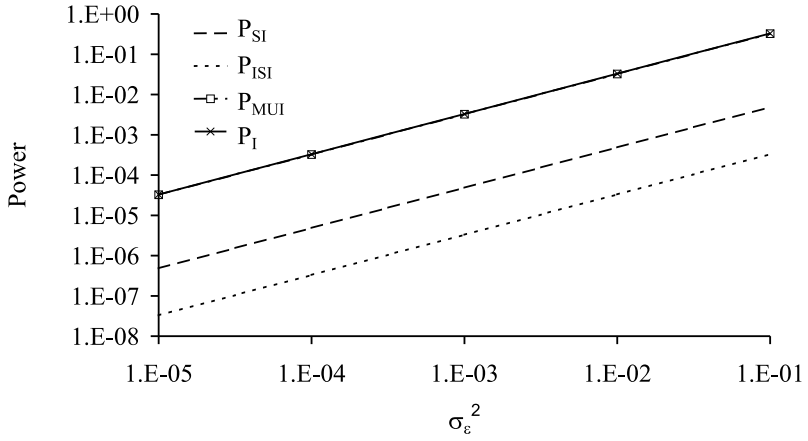

Figure 4.14: Effect of the timing jitter on the interference powers, $N_c = 64$, $N_u = N_c, \alpha = 0$

shown as function of the jitter variance, in the case of the Walsh-Hadamard sequences and of the maximum load ($N_u = N_c$). The power of the self-interference is inversely proportional to N_c. As we observe, the power of the intersymbol interference is small as compared to the self-interference power: the ISI power is about N_c times smaller than the SI power. Furthermore, it can be verified that the MUI power per disturbing user is of the same order of the SI power and is also inversely proportional to N_c. The MUI power is proportional to the number of disturbing users. Hence, for the lowest load ($N_u = 1$), the MUI power is zero and for the highest load ($N_u = N_c$) the MUI power is maximum. The maximum MUI power (for $N_u = N_c$) is shown in figure 4.14. We observe that for the maximum load and for a large spreading factor, the dominating interference term is the MUI. Although the self-interference power, the intersymbol interference power and the multiuser interference power depend on the spreading factor, the total interference power, i.e. the sum of these powers, is independent of the spreading factor N_c when all users are active ($N_u = N_c$). Similar results can be found for the case of the overlay sequences. In figure 4.15, the degradation (4.35) and the degradation caused by the interference only is shown as function of the jitter variance. Similarly as in the case of the constant timing offset, the effect of the reduction of the useful component can be neglected as compared to the effect of the interference. Hence, the degradation can be well approximated by

$$Deg \approx 10 \log \left(1 + \frac{E_s}{N_0} \sigma_\epsilon^2 B(\alpha) \right) \tag{4.38}$$

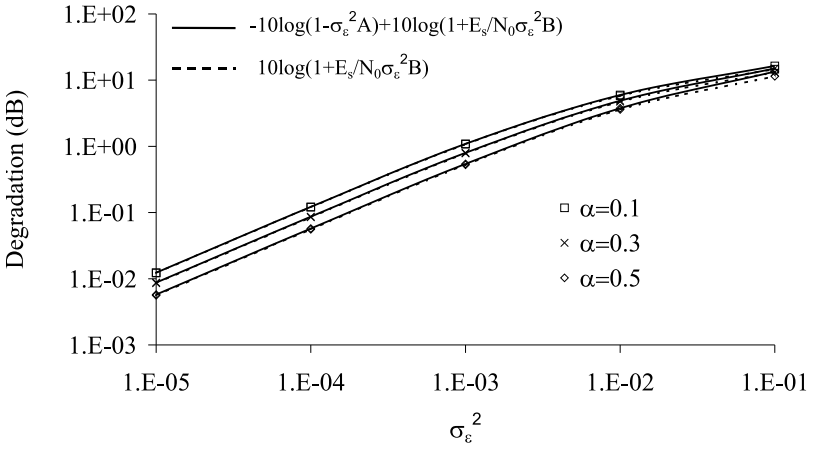

Figure 4.15: Timing jitter on the interference powers, $N_c = 64, N_u = N_c, SNR(0) = 20$ dB

4.4 Conclusions and Remarks

In this chapter, we have considered a reference DS-CDMA system as an introduction to the combination of CDMA with a multicarrier system that will be presented in chapter 6. For the reference DS-CDMA system, we considered the case of synchronous DS-CDMA transmission over an AWGN channel. We have investigated the sensitivity of this reference DS-CDMA system to synchronisation errors. The performance of the DS-CDMA system is essentially independent of the user index ℓ, as the effect of the distortions is mitigated by spreading the data.

The DS-CDMA system is not degraded by a constant phase offset as the effect of the constant phase offset can be compensated without loss of performance by the equaliser. A carrier frequency offset introduces severe performance degradation, when the time-dependent phase rotation of the receiver filter output samples is not compensated. An equaliser can compensate for this time-dependent phase rotation without loss of performance. However, the frequency shift of the transmitted signal introduces a performance degradation that can not be corrected by the equaliser without enhancing the noise power level. Similarly as for the conventional single carrier communication system, the degradation is mainly caused by the reduction of the useful component. This performance degradation depends on the product ΔFT and is independent of the spreading factor. When the carrier frequency offset is small as compared to the system bandwidth $\Delta F \ll 1/T = N_c R_s$, the degradation caused by this frequency shift is small. In the case of the maximum load, the carrier phase jitter introduces a degradation that is independent of the spreading fac-

tor and of the spectral contents of the jitter, but only depends on the jitter variance. The scatter diagrams in this case, however, depend considerably on the spectral contents of the jitter. Jitter with mainly low frequency components ($|f| < 1/(N_cT) = R_s$) causes mainly an angular displacement of the samples at the input of the decision device. Jitter with mainly high frequency components ($|f| > 1/(N_cT) = R_s$) causes a combination of an angular and a radial displacement of the samples at the input of the decision device, resulting in a circular cloud in the scatter diagram.

A constant timing offset gives rise to a reduction of the useful component and interference. The interference term mainly consists of multiuser interference. The degradation caused by the constant timing offset is independent of the spreading factor and for small timing offsets, it is proportional to the square of the timing offset. Furthermore, the effect of the reduction of the useful component is negligible as compared to the effect of the interference when the timing offset is small. A clock frequency offset introduces an increasing misalignment between the chips and the received samples. To compensate for the increasing misalignment, a coarse synchronisation algorithm that duplicates or removes samples at regular instants can be used. However, the residual timing error introduces a strong degradation of the DS-CDMA system. To avoid this degradation, a clock frequency offset must be eliminated by adjusting the sampling clock phase or by interpolating between the available samples. The timing jitter introduces a degradation that is independent of the spreading factor and of the spectral contents of the jitter, when the number of active users is maximal. In this case, the degradation only depends on the jitter variance. The degradations caused by the constant timing offset and the timing jitter are essentially the same when the jitter variance equals the square of the timing offset.

Chapter 5

Orthogonal Frequency Division Multiplexing and Multiple Access

5.1 Introduction

In a single carrier system where the data symbols are transmitted sequentially, strong intersymbol interference (ISI) is introduced when the duration of the impulse response of the dispersive channel exceeds the symbol interval length. The influence of the intersymbol interference caused by the dispersive channel can be reduced by increasing the duration of a transmitted data symbol. This can be achieved by means of a multicarrier technique, consisting of frequency-division multiplexing (FDM) [Cha66], [Bin90], [Zou95], [vdB99], [Kal89], [Wei71], [Moe99b], [Bah99], [vNe00], [Lin99]: the available bandwidth is divided into a number of narrow subchannels, each corresponding with a carrier of the multicarrier signal. The symbol sequence to be transmitted is split into a large number of lower speed symbol streams, which each modulate in parallel a carrier from a different subchannel. As the available bandwidth is divided in many narrow subchannels, the frequency response over each subchannel is relatively flat. Hence, equalisation is potentially simpler than in a single carrier system.

In the conventional FDM technique, the system bandwidth is divided into non-overlapping subchannels. However, as each subchannel requires its own carrier oscillator and narrowband filter with sharp cut-off (both at transmitter and receiver), the number of subchannels is limited by the implementation complexity. In the orthogonal frequency-division multiplexing (OFDM) technique, a discrete Fourier transform (DFT) [Bin90], [Zou95], [vdB99], [Kal89], [Wei71], [Moe99b], [Bah99], [vNe00], [Lin99] is used to modulate and demodulate the

parallel data streams. In this technique, the subchannels are not band-limited and spectrally overlap, so a high spectral efficiency can be achieved. The center frequency of a subchannel is called the carrier frequency. In this multicarrier technique, interference between carriers is eliminated by selecting the carrier spacing equal to the reciprocal of the per carrier symbol period. The transmitter and receiver of OFDM can be implemented efficiently by using fast Fourier transform (FFT) techniques.

A problem encountered in the OFDM technique is that channel dispersion destroys the orthogonality between the carriers, causing interference between symbols. This problem is solved by inserting a cyclic extension of the OFDM signal. When the duration of the cyclic prefix exceeds the duration of the impulse response of the dispersive channel, the orthogonality between the carriers is maintained and interference between symbols is avoided [Pel80], [Bin90], [Zou95], [vdB99], [Kal89], [Wei71], [Bah99], [vNe00]. In this case, equalisation is very simple and can be implemented as one-tap equalisers after demodulation. However, as inserting a cyclic prefix reduces the power efficiency and the data throughput, the cyclic prefix must be a small fraction of the per carrier symbol duration [vdB99], [Pol97], [Ste99i], [Ste96], [Ste98c].

The OFDM technique is not a multiple access technique as all carriers of the OFDM system are modulated with data symbols from a single user. To support multiple users, OFDM must be combined with a multiple access scheme.

- OFDM in combination with TDMA: The time axis is divided in non-overlapping time slots. A user is assigned a set of time slots. During each of these time slots, the user transmits a number of data symbols by means of the OFDM technique, occupying the whole system bandwidth.
- OFDM in combination with FDMA: The available bandwidth is divided in non-overlapping frequency bands. A user is assigned a frequency band, in which he transmits an OFDM signal as long as he is active.
- OFDM in combination with CDMA: Each user occupies the whole system bandwidth (which is equal to the bandwidth of the OFDM signal) during the whole time the user is active. Each user is assigned a unique spreading sequence, which allows to separate the different users.

In the cases of OFDM combined with TDMA or FDMA, the signals of the different users are physically separated in time or in frequency, respectively. Hence, the signals belonging to the different users do not interfere and the system can be interpreted as a number of point-to-point communication systems. In the case of OFDM combined with CDMA, all users simultaneously occupy the entire system bandwidth; this case will be discussed in chapter 6. The OFDM technique has been proposed and/or accepted for various applications, such as broadcasting of digital audio and digital television [Sar95], mobile radio [Pol97], [Ste96], [Ste98c], [San95], [Chi95], [Tuf98], [Rus95] and transmission over twisted pair cables [Chw91a], [Chw91b].

Orthogonal frequency-division multiple access (OFDMA) is closely related to OFDM. In the case of OFDMA, the sum of the different user signals can be viewed as an OFDM signal, but with each carrier generated by a different user instead of all carriers generated by the same user. The OFDMA technique, where the carriers are spaced as densely as possible while maintaining the orthogonality between the carriers, is spectrally more efficient than traditional FDMA, where the carriers occupy non-overlapping frequency bands. Furthermore, OFDMA is more advantageous as traditional FDMA, as an FFT is less complex to implement than a bank of filters and oscillators. The OFDMA technique has been proposed as an access technique for the return path in a CATV (community area television) network [Sar96], i.e., for the communication from the users to the head-end.

In this chapter, we investigate the sensitivity of OFDM and OFDMA to synchronisation errors for both the uplink and the downlink. The chapter is organised as follows: in section 5.2, the OFDM system is considered. The downlink and uplink OFDMA system is investigated in section 5.3. In section 5.4, we separately consider the influence of carrier phase errors and timing errors on both OFDM and OFDMA in the case of an ideal channel. The effect of the synchronisation errors on the OFDM and OFDMA system in the presence of a dispersive channel is discussed in section 5.5, and in section 5.6 conclusions are drawn.

5.2 Orthogonal Frequency Division Multiplexing

When TDMA or FDMA is used as an access technique in combination with the OFDM modulation technique, the OFDM signals transmitted to (downlink) or transmitted by (uplink) the different users do not interfere as they are physically separated in time or in frequency, respectively. In these cases, the system can be interpreted as N_u independent point-to-point OFDM systems, where N_u denotes the number of active users. Furthermore, as the signals of the different users do not interfere, it is clear that the difference in analysis between the downlink and the uplink disappears and that we can focus on the OFDM system for a single user. Without loss of generality, we use the terminology for the downlink.

The conceptual block diagram of the OFDM transmitter for a single user is shown in figure 5.1. The complex-valued data symbols to be transmitted at a rate R_s by the basestation to the considered user, are organised into blocks of NFFT data symbols; $a_{i,n}$ denotes the nth data symbol of the ith block. In OFDM, the available bandwidth is partitioned into N_{FFT} subchannels, that are made orthogonal be using a carrier spacing equal to the per carrier symbol rate. The nth carrier is modulated by the symbols $\{a_{i,n}|i = -\infty, \ldots, +\infty\}$ and the modulated carriers are summed before transmission. In a practical implementation, the N_{FFT} samples of the transmitted sequence during the ith

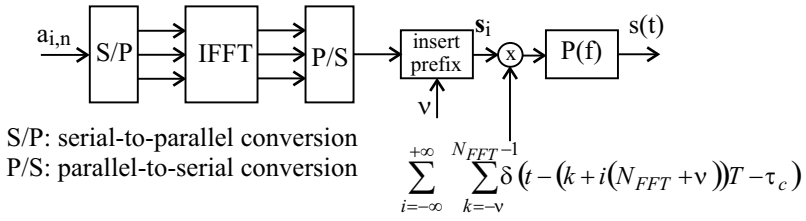

Figure 5.1: Conceptual block diagram of the OFDM transmitter

block are generated by feeding the data symbols $\mathbf{a}_i = [a_{i,0} \dots a_{i,N_{FFT}-1}]^T$ to an inverse fast Fourier transform (IFFT). The resulting time-domain samples $\mathbf{s}_i = [s_{i,0} \dots s_{i,N_{FFT}-1}]^T$ are given by

$$s_{i,k} = \frac{1}{\sqrt{N_{FFT}}} \sum_{n=0}^{N_{FFT}-1} a_{i,n} e^{j2\pi \frac{kn}{N_{FFT}}}, \qquad k = 0, \dots, N_{FFT}-1 \tag{5.1}$$

This can also be written as

$$\mathbf{s}_i = \mathbf{F}\mathbf{a}_i \tag{5.2}$$

where $\mathbf{F}_{k,n} = (1/\sqrt{N_{FFT}}) \exp(j2\pi kn/N_{FFT})$ denotes the matrix corresponding to the inverse FFT. Note that $\mathbf{F}$ is an orthogonal matrix, i.e., $\mathbf{F}\mathbf{F}^\dagger = \mathbf{F}^\dagger\mathbf{F} = \mathbf{I}_{N_{FFT}}$, where $\mathbf{I}_{N_{FFT}}$ is the identity matrix of order $N_{FFT} \times N_{FFT}$. In the presence of a dispersive channel, the orthogonality between the carriers is lost and intercarrier interference (ICI) is introduced. Furthermore, interference between adjacent transmitted OFDM blocks occurs, resulting in intersymbol interference (ISI). To combat the interference introduced by the dispersive channel, each OFDM block is preceded by a prefix of ν samples, containing a cyclic extension of the time-domain samples $\mathbf{s}_i$. The resulting $N_{FFT} + \nu$ time-domain samples of the ith block are $\mathbf{s}_i = [s_{i,-\nu} \dots s_{i,N_{FFT}-1}]^T$, where the first ν samples are a duplication of the last ν samples: $\{s_{i,k} | k = -\nu, \dots, -1\} = \{s_{i,k} | k = N_{FFT} - \nu, \dots, N_{FFT} - 1\}$. After a normalisation such that the energy per symbol transmitted by carrier n equals $E_{s,n}$, where $E_{s,n} = E[|a_{i,n}|^2]$, the resulting time-domain sequence $\mathbf{s}_i$ yields

$$\mathbf{s}_i = \sqrt{\frac{N_{FFT}}{N_{FFT}+\nu}} \mathbf{\Omega}\mathbf{F}\mathbf{a}_i \tag{5.3}$$

where $\mathbf{\Omega}$ is an $(N_{FFT} + \nu) \times N_{FFT}$ matrix

$$\mathbf{\Omega} = \begin{pmatrix} \mathbf{0} & \mathbf{I}_\nu \\ & \mathbf{I}_{N_{FFT}} \end{pmatrix} \tag{5.4}$$

and $\mathbf{I}_M$ is the identity matrix of dimension $M \times M$ and $\mathbf{0}$ is a matrix containing only zeroes. Hence, the transmitter converts N_{FFT} data symbols into a block of $N_{FFT} + \nu$ samples using the linear transformation $\mathbf{T}_{tr,i}$ (2.1):

$$\mathbf{T}_{tr,i} = \sqrt{\frac{N_{FFT}}{N_{FFT}+\nu}} \mathbf{\Omega}\mathbf{F} \tag{5.5}$$

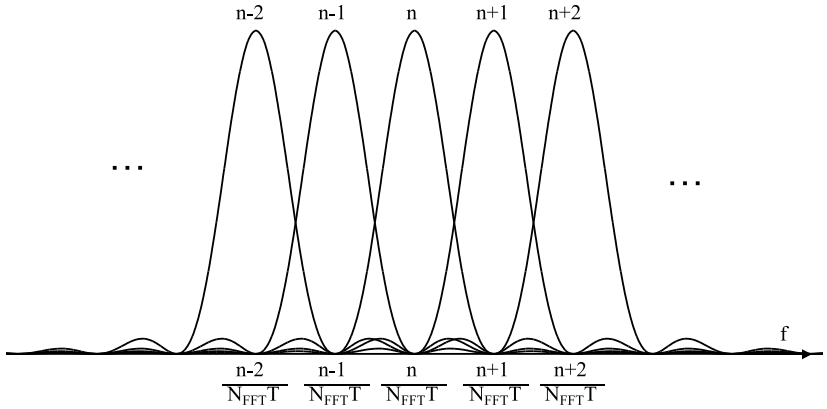

Figure 5.2: Spectrum of the carriers

The time-domain sequence $\mathbf{s}_i$ (5.3) is multiplied with the transmit clock signal, consisting of a periodic sequence of Dirac impulses, and is fed to the transmit filter $P(f)$, which is a square-root Nyquist filter with respect to the time interval $T = N_{FFT}/((N_{FFT} + \nu)R_s)$. The resulting multicarrier signal $s(t)$ (complex baseband representation) is given by

$$s(t) = \sum_{i=-\infty}^{+\infty} s_i(t - i(N_{FFT} + \nu)T) \tag{5.6}$$

where

$$s_i(t) = \sum_{k=-\nu}^{N_{FFT}-1} s_{i,k} p(t - kT - \tau_c) \tag{5.7}$$

and τ_c is a time delay that represents the transmit clock phase. Hence, $s(t)$ can be viewed as a sequence of signals $s_i(t)$, with $s_i(t)$ containing the samples $s_{i,k}$ $(k = -\nu, \ldots, N_{FFT} - 1)$ that are a function of the data symbols $a_{i,n}$ $(n = 0, \ldots, N_{FFT} - 1)$. The samples $s_{i,k}$ $(k = -\nu, \ldots, N_{FFT} - 1)$ are referred to as the ith OFDM block. Taking into account (5.3), $s_{i,k}$ can be written as

$$s_{i,k} = \frac{1}{\sqrt{N_{FFT} + \nu}} \sum_{k=0}^{N_{FFT}-1} a_{i,n} e^{j2\pi \frac{kn}{N_{FFT}}}, \qquad k = -\nu, \ldots, N_{FFT} - 1 \tag{5.8}$$

As the spacing between the samples $s_{i,k}$ equals T, the carriers of the multicarrier signal $s(t)$ are located at the frequencies $n/(N_{FFT}T)$, $n = 0, \ldots, N_{FFT} - 1$. Figure 5.2 shows the spectrum of some of the carriers. Note that the carriers spectrally overlap.

The multicarrier signal $s(t)$ (5.6) is transmitted by the basestation to the considered user. The transfer function from the basestation to the receiver of the considered user is given by $H_{ch}(f;\tau)$. The output of the dispersive channel is disturbed by additive white Gaussian noise (AWGN) $w_{LP}(t)$, with uncorrelated real and imaginary parts, each having a power spectral density (psd) of $N_0/2$. Furthermore, the signal is affected by the carrier phase difference between the carrier oscillator (for upconversion from baseband to bandpass) at the basestation and the carrier oscillator (for downconversion from bandpass to baseband) at the receiver of the considered user. As all OFDM carriers are upconverted and downconverted using the same carrier oscillators, all carriers exhibit the same carrier phase difference $\theta_c - \hat{\theta}_r(t)$, where θ_c is the carrier phase at the basestation and $\hat{\theta}_r(t)$ is the estimated optimum carrier phase at the receiver of the considered user. The received complex baseband signal $r(t)$ is applied to the receiver filter and sampled at the instants $\hat{t}_{i(N_{FFT}+\nu)+k} = t_{i(N_{FFT}+\nu)+k} + \epsilon_{i(N_{FFT}+\nu)+k}T$. The timing instants $t_{i(N_{FFT}+\nu)+k} = (k + i(N_{FFT}+\nu))T + \tau_{r,i(N_{FFT}+\nu)+k}$ are the optimum sampling instants, defined in (2.10), and $\epsilon_{i(N_{FFT}+\nu)+k}$ is the normalised timing error at the instant $t_{i(N_{FFT}+\nu)+k}$. Considering the case where the channel and the carrier phase difference are slowly varying as compared to the duration of the impulse response of the receiver filter, the received discrete time-domain sequence $\mathbf{v}_i = [v_{i,-\nu} \dots v_{i,N_{FFT}-1}]^T$ at the output of the receiver filter yields

$$v_{i,k} = \sum_{i'=-\infty}^{+\infty} \sum_{k'=-\nu}^{N_{FFT}-1} s_{i',k'} h_{eq}(t_{i(N_{FFT}+\nu)+k} - t_{i'(N_{FFT}+\nu)+k'}; t_{i(N_{FFT}+\nu)+k}) + w_{i,k} \tag{5.9}$$

The impulse response $h_{eq}(t; t_{i(N_{FFT}+\nu)+k})$ of the equivalent time-varying channel, defined in section 2.3.1, includes the synchronisation errors; its Fourier transform with respect to the variable t is given by (2.15):

$$\begin{aligned} H_{eq}(f; t_{i(N_{FFT}+\nu)+k}) &= H(f; t_{i(N_{FFT}+\nu)+k}) \\ & \quad e^{j\phi(t_{i(N_{FFT}+\nu)+k}) - \Delta\theta(t_{i(N_{FFT}+\nu)+k})} \\ & \quad e^{j2\pi f(\epsilon_{i(N_{FFT}+\nu)+k}T + \Delta\tau_{i(N_{FFT}+\nu)+k})} \end{aligned} \tag{5.10}$$

In (5.10), the phase shift $\Delta\theta(t)$ and the time delay $\Delta\tau_{i(N_{FFT}+\nu)+k}$ depend on the channel characteristics, $\phi(t)$ is the carrier phase error and $H(f; t_{i(N_{FFT}+\nu)+k})$ is the transfer function of the cascade of the transmit filter, the dispersive channel and the receiver filter, i.e., $H(f;\tau) = H_{ch}(f;\tau)|P(f)|^2$. The additive noise component $w_{i,k}$ is the value of the matched filter output noise at the instant $\hat{t}_{i(N_{FFT}+\nu)+k}$, originating from the noise contribution $w_{LP}(t)$.

For each transmitted OFDM block of $N_{FFT}+\nu$ samples, the receiver removes the ν samples corresponding to the cyclic prefix, and keeps the remaining N_{FFT} samples for further processing. In appendix D it is shown that the MMSE receiver structure operating on these samples consists of an FFT of length N_{FFT}, followed by N_{FFT} one-tap equalisers. The equaliser coefficient $g_{i,n}$ scales and rotates the nth FFT output during the ith block. The equaliser is implemented

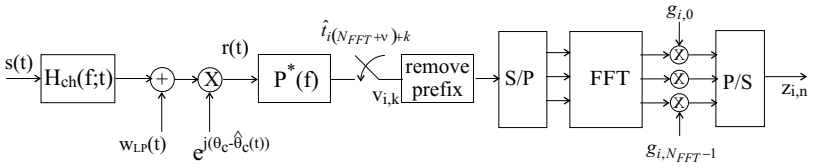

Figure 5.3: Channel and receiver structure for OFDM

as an MMSE equaliser and is computed using (2.51). The corresponding receiver structure is shown in figure 5.3. The samples $z_{i,n}$ at the input of the decision device are given by

$$z_{i,n} = (\mathbf{D}_i \mathbf{F}^\dagger \mathbf{\Xi} \mathbf{v}_i)_n \tag{5.11}$$

where $(\mathbf{D}_i)_{n,n'} = \delta_{n,n'} g_{i,n}$ is the diagonal matrix of the equaliser coefficients, $\mathbf{F}^\dagger$ is the Hermitian of the matrix $\mathbf{F}$ ($\mathbf{F}^\dagger$ denotes the FFT operation) and the matrix $\mathbf{\Xi} = (\mathbf{0} \quad \mathbf{I}_{N_{FFT}})$ is an $N_{FFT} \times (N_{FFT} + \nu)$ matrix. Note that $\mathbf{\Xi\Omega} = \mathbf{I}_{N_{FFT}}$ and $\mathbf{F}^\dagger \mathbf{\Xi\Omega F} = \mathbf{F}^\dagger \mathbf{F} = \mathbf{I}_{N_{FFT}}$. Hence, the receiver demodulates the received samples $\mathbf{v}_i$ by using N_{FFT} linear transformations $\mathbf{b}_{i,n}$ (2.5), where $\mathbf{b}_{i,n}$ is the nth row of the $N_{FFT} \times (N_{FFT} + \nu)$ matrix $\mathbf{D}_i \mathbf{F} \mathbf{\Xi}$. The sample $z_{i,n}$ at the input of the decision device is decomposed into four contributions:

$$\begin{aligned} z_{i,n} &= \sqrt{\frac{N_{FFT}}{N_{FFT}+\nu}} a_{i,n} I_{i,i,n,n} + \sqrt{\frac{N_{FFT}}{N_{FFT}+\nu}} \sum_{i'=-\infty; i' \neq i}^{+\infty} a_{i',n} I_{i,i',n,n} \\ &+ \sqrt{\frac{N_{FFT}}{N_{FFT}+\nu}} \sum_{i'=-\infty; i' \neq i}^{+\infty} \sum_{n'=0; n' \neq n}^{N_{FFT}-1} a_{i',n'} I_{i,i',n,n'} + W_{i,n} \end{aligned} \tag{5.12}$$

where

$$I_{i,i',n,n'} = g_{i,n} A_{i,i',n,n'} \tag{5.13}$$

$$\begin{aligned} A_{i,i',n,n'} &= \frac{1}{N_{FFT}} \sum_{k=0}^{N_{FFT}-1} \sum_{k'=-\nu}^{N_{FFT}-1} e^{-j2\pi \frac{kn-k'n'}{N_{FFT}}} \cdot \\ &\quad h_{eq}(t_{i(N_{FFT}+\nu)+k} - t_{i'(N_{FFT}+\nu)+k'}; t_{i(N_{FFT}+\nu)+k}) \end{aligned} \tag{5.14}$$

The quantity $A_{i,i',n,n'}$ denotes the contribution of the symbol $a_{i',n'}$ on the nth FFT output during the ith OFDM block, while $I_{i,i',n,n'}$ denotes the contribution from the same symbol $a_{i',n'}$ to the input of the decision device. In (5.12), the first contribution is the useful component. This contribution can be decomposed further into an average useful component $E[I_{i,i,n,n}]$ and a zero-mean fluctuation $I_{i,i,n,n} - E[I_{i,i,n,n}]$ about its average, i.e., the self-interference (SI). The second contribution ($i' \neq i, n' = n$) is the intersymbol interference (ISI), caused by the symbols transmitted on the considered carrier in other OFDM blocks. The third contribution ($n' \neq n$) denotes the intercarrier interference (ICI) at the nth

output of the FFT, caused by the symbols transmitted on the other carriers. The last contribution is the additive Gaussian noise term with variance

$$E[|W_{i,n}|^2] = N_0|g_{i,n}|^2 \triangleq N_0\sigma_{i,n}^2 \tag{5.15}$$

To measure the performance of the OFDM system, we use the signal-to-noise ratio (SNR) (2.59), which is the ratio of the power of the average useful component P_U to the sum of the powers of the self-interference P_{SI}, the intersymbol interference P_{ISI}, the intercarrier interference P_{ICI} and the noise. This yields

$$SNR_{i,n} = \frac{\sqrt{\frac{N_{FFT}}{N_{FFT}+\nu}}E_{s,n}P_{U,i,n}}{N_0\sigma_{i,n}^2 + \frac{N_{FFT}}{N_{FFT}+\nu}E_{s,n}(P_{SI,i,n} + P_{ISI,i,n} + P_{ICI,i,n})} \tag{5.16}$$

where $E_{s,n} = E[|a_{i,n}|^2]$ is the energy per symbol on the nth carrier, and

$$\begin{aligned} P_{U,i,n} &= |E[I_{i,i,n,n}]|^2 \\ P_{SI,i,n} &= E[|I_{i,i,n,n} - E[I_{i,i,n,n}]|^2] \\ P_{ISI,i,n} &= \sum_{i'=-\infty;i'\neq i}^{+\infty} E[|I_{i,i',n,n}|^2] \\ P_{ICI,i,n} &= \sum_{i'=-\infty}^{+\infty}\sum_{n'=0;n'\neq n}^{N_{FFT}-1} \frac{E_{s,n'}}{E_{s,n}} E[|I_{i,i',n,n'}|^2] \end{aligned} \tag{5.17}$$

The instantaneous SNR (5.16) in general depends on the block index i and the carrier index n. In many cases of practical interest, however, $SNR_{i,n}$ turns out to be independent of the block index i.

In the case of an ideal channel ($H_{ch}(f;\tau) = 1$) and in the absence of synchronisation errors, the matched filter output samples are given by (see (2.6))

$$v_{i,k} = s_{i,k} + w_{i,k} \qquad k = -\nu \ldots N_{FFT} - 1 \tag{5.18}$$

where the noise contributions $w_{i,k}$ are Gaussian with $E[w_{i,k}^* w_{i',k'}] = N_0\delta_{i-i'}\delta_{k-k'}$, and $s_{i,k}$ is given by (5.3). Removing the cyclic prefix and applying the remaining samples to the FFT yields the following expression for the nth FFT output $y_{i,n}$

$$y_{i,n} = \sqrt{\frac{N_{FFT}}{N_{FFT}+\nu}}a_{i,n} + W_{i,n} \tag{5.19}$$

where

$$W_{i,n} = \frac{1}{\sqrt{N_{FFT}}} \sum_{k=0}^{N_{FFT}-1} w_{i,k}e^{j2\pi\frac{kn}{N_{FFT}}} \tag{5.20}$$

yielding $E[|W_{i,n}|^2] = N_0$. Note that $y_{i,n}$ contains the symbol $a_{i,n}$, but no other symbols: because of the orthogonality of the IFFT-matrix $\mathbf{F}$, no ICI

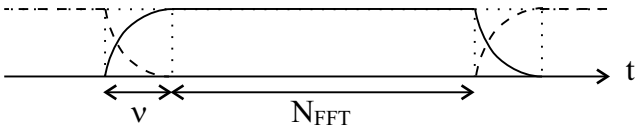

Figure 5.4: The OFDM signal

occurs (this implies that the transmitted carriers are orthogonal over the selected interval of duration $N_{FFT}T$), and because of the non-dispersive channel, no ISI occurs. The one-tap equaliser operating on $y_{i,n}$ has coefficients $g_{i,n}$ given by $g_{i,n} = E_{s,n}\sqrt{\frac{N_{FFT}}{(N_{FFT}+\nu)}}/(N_0 + E_{s,n}\frac{N_{FFT}}{(N_{FFT}+\nu)})$; note that $g_{i,n}$ does not depend on the block index i. Taking into account that $E[|a_{i,n}|^2] = E_{s,n}$, the SNR resulting from (5.16) is independent of the block index i, and yields

$$SNR_n(0) = \frac{N_{FFT}}{N_{FFT}+\nu}\frac{E_{s,n}}{N_0} \tag{5.21}$$

The factor $N_{FFT}/(N_{FFT}+\nu)$ in (5.21) accounts for the loss of power efficiency, that results from not using the ν samples that are contained in the cyclic prefix.

When a dispersive channel or/and synchronisation errors are present, the SNR is reduced, as compared to the case of an ideal channel and in the absence of synchronisation errors. The degradation of the SNR as compared to $SNR_n(0)$ (expressed in dB), caused by the dispersive channel and the synchronisation errors, depends on the block index i and the carrier index n and is given by

$$Deg_{i,n} = -10\log\left(\frac{P_{U,i,n}}{\sigma^2_{i,n} + SNR_n(0)(P_{SI,i,n} + P_{ISI,i,n} + P_{ICI,i,n})}\right) \tag{5.22}$$

Let us consider the case of a sufficient cyclic prefix length, i.e., the duration of the impulse response $h_{eq}(t; t_{i(N_{FFT}+\nu)+k})$ does not exceed the duration of the cyclic prefix ($h_{eq}(t; t_{i(N_{FFT}+\nu)+k}) = 0$ for $t < 0$ or $t > \nu T$). In this case, the transients at the boundaries of an OFDM block disturb the adjacent blocks only during the cyclic prefix, as shown in figure 5.4. As the receiver selects the samples outside the cyclic prefix, no intersymbol interference is introduced ($I_{i,i',n,n'} = 0$, for $i' \neq i$, i.e., $P_{ISI,n} = 0$). In appendix D it is shown that in this case, the quantities $A_{i,i',n,n'}$ (5.14) reduce to

$$A_{i,i',n,n'} = \delta_{i,i'}\frac{1}{\sqrt{N_{FFT}}}\sum_{k=0}^{N_{FFT}-1} e^{-j2\pi\frac{k(n-n')}{N_{FFT}}} G_{n'}(t_{i(N_{FFT}+\nu)+k}) \tag{5.23}$$

where

$$G_n(t_{i(N_{FFT}+\nu)+k}) = \frac{1}{T}\sum_{m=-\infty}^{+\infty} H_{eq}\left(\frac{n}{N_{FFT}T} + \frac{m}{T}; t_{i(N_{FFT}+\nu)+k}\right) \tag{5.24}$$

is the folded transfer function of the equivalent time-varying filter defined in (5.10), evaluated at the carrier frequencies $n/(N_{FFT}T)$.

5.3 Orthogonal Frequency Division Multiple Access

In orthogonal frequency division multiple access (OFDMA), the data streams that are transmitted on the different carriers belong to different users. Hence, the signals of the different users are partially overlapping in frequency. In this case, when the orthogonality between the different carriers is lost, interference between the different users occurs. Hence, the analysis for downlink and uplink OFDMA differs. In the following, we separately consider the cases of downlink and uplink OFDMA.

5.3.1 Downlink OFDMA

In downlink OFDMA, the signals transmitted to the different users are synchronised at the basestation. Hence, the timing errors of the different signals are the same. Furthermore, as all transmitted carriers are upconverted with the same carrier oscillator, the carrier phase errors are the same for the contributions of all users. In addition, the contributions of the different users at the receiver of user n have experienced the same channel transfer function. Hence, the analysis for downlink OFDMA is identical as for the OFDM system, described in the previous section. However, in downlink OFDMA, terminology is different from that in OFDM. The conceptual block diagram of the downlink OFDMA transceiver is shown in figure 5.5. In downlink OFDMA, the data symbol $a_{i,n}$ denotes the ith data symbol transmitted to user n and $E_{s,n} = E[|a_{i,n}|^2]$ is the energy per symbol transmitted to user n. A similar analysis as for OFDM yields the samples $z_{i,n}$ (5.12), which are used to take decisions about the data symbols $a_{i,n}$. The samples $z_{i,n}$ (5.12) can be decomposed into a useful component ($i' = i, n' = n$), intersymbol interference ($n = n', i' \neq i$), multiuser interference ($n' \neq n$) and noise. The multiuser interference term in the case of downlink OFDMA has the same structure as the intercarrier interference term in the case of OFDM. In the following, we use the term intercarrier interference instead of multiuser interference for the convenience of a single notation for both OFDM and OFDMA. Similarly as for OFDM, the signal-to-noise ratio (5.16) is defined for downlink OFDMA.

5.3.2 Uplink OFDMA

In the case of uplink OFDMA, the transmitters of the different users are on different locations. The transmitter of each user generates a clock signal and a carrier oscillator signal, of which the frequencies and phases are estimated from a network synchronisation signal that is broadcast by the base station. At the base station, the sum of the received user signals is downconverted and sampled by means of a carrier oscillator and a sampling clock, that have phases corresponding to the network synchronisation signal. This implies that the

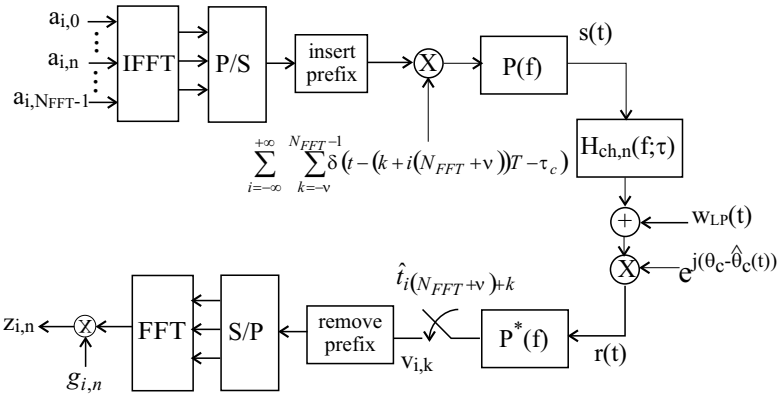

Figure 5.5: Downlink OFDMA transceiver structure

signals transmitted by the different users exhibit different synchronisation errors. The uplink OFDMA communication system is shown in figure 5.6. The time-varying carrier phase $\theta_{c,n}(t)$ and the clock phase, represented by the time delay $\tau_{i(N_{FFT}+\nu)+k,n}$, include the time-varying carrier phase errors and timing errors, made by the transmitter in the estimation of the frequencies and phases from the network reference synchronisation signal, as shown in section 2.4. The time-domain sequence $\mathbf{s}_{i,n} = [s^n_{i,-\nu} \dots s^n_{i,N_{FFT}-1}]^T$ transmitted by user n is given by

$$s^n_{i,k} = \frac{1}{\sqrt{N_{FFT}+\nu}} a_{i,n} e^{j2\pi \frac{kn}{N_{FFT}}} \tag{5.25}$$

Hence, in the case of uplink OFDMA, the linear transformation $\mathbf{T}_{tr,i,n}$ (2.1) converts one data symbol into a block of $N_{FFT}+\nu$ samples. The $(N_{FFT}+\nu)\times 1$ transmitter matrix $\mathbf{T}_{tr,i,n}$ of user n consists of the nth row of the matrix defined in (5.5). The transmitted sequence $\mathbf{s}_{i,n}$ is multiplied with the transmit clock signal and applied to the transmit filter, yielding the continuous-time signal $s_n(t)$

$$s_n(t) = \sum_{i=-\infty}^{+\infty} \sum_{k=-\nu}^{N_{FFT}-1} s^n_{i,k} p(t-(k+i(N_{FFT}+\nu))T - \tau_{i(N_{FFT}+\nu)+k,n}) \tag{5.26}$$

The transfer function from the transmitter of user n to the basestation is given by $H_{ch,n}(f;\tau)$. The output of the dispersive channel is affected by the carrier phase difference $\theta_{c,n}(t) - \theta_r$, where θ_r is the phase of the basestation carrier oscillator. The basestation receives the sum of the signals transmitted by the different users, disturbed by additive white Gaussian noise $w_{LP}(t)$. The resulting signal $r(t)$ is applied to the receiver filter and sampled at the instants $t_{i(N_{FFT}+\nu)+k} = (k+i(N_{FFT}+\nu))T + \tau_r$, where τ_r represents the time-delay corresponding to the phase of the basestation clock. Assuming the dispersive channels and the carrier phase differences are slowly varying as compared to

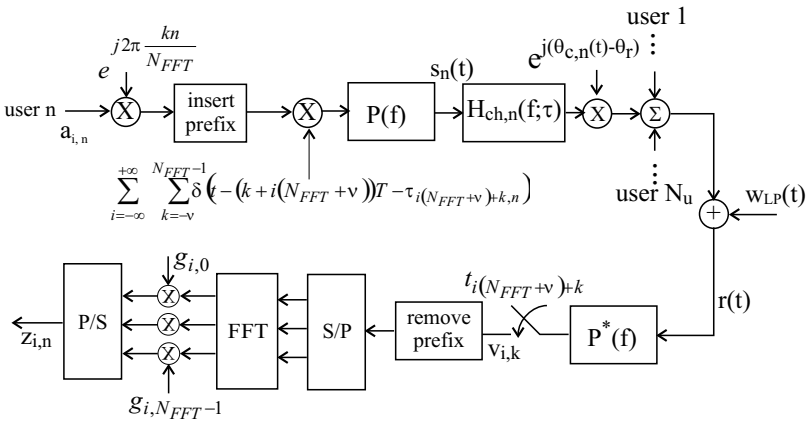

Figure 5.6: Transceiver structure for uplink OFDMA

the duration of the impulse response of the receiver filter and the timing errors are slowly varying as compared to the duration of the impulse response of the composite channel (consisting of the cascade of the transmit filter, the channel and the receiver filter) it is shown in section 2.4 that the time-domain samples $\mathbf{v}_i = [v_{i,-\nu} \dots v_{i,N_{FFT}-1}]^T$ at the output of the receiver filter yield

$$\begin{aligned} v_{i,k} &= \sum_{i=-\infty}^{+\infty} \sum_{k=-\nu}^{N_{FFT}-1} \sum_{n=0}^{N_{FFT}-1} s^n_{i',k'} \cdot \\ &\quad h_{eq,n}(t_{i(N_{FFT}+\nu)+k} - t_{i'(N_{FFT}+\nu)+k'}; t_{i(N_{FFT}+\nu)+k}) + w_{i,k} \end{aligned} \quad (5.27)$$

where $w_{i,k}$ is the matched filter output noise value at the instant $t_{i(N_{FFT}+\nu)+k}$, and $h_{eq,n}(t; t_{i(N_{FFT}+\nu)+k})$ is the impulse response of the equivalent time-varying filter whose Fourier transform with respect to the variable t is

$$\begin{aligned} H_{eq,n}(f; t_{i(N_{FFT}+\nu)+k}) &= H_n(f; t_{i(N_{FFT}+\nu)+k}) \cdot \\ &\quad e^{j(\phi_n(t_{i(N_{FFT}+\nu)+k}) - \Delta\theta_n(t_{i(N_{FFT}+\nu)+k}))} \cdot \\ &\quad e^{j2\pi f(\epsilon_{i(N_{FFT}+\nu)+k,n}T + \Delta\tau_{i(N_{FFT}+\nu)+k,n})} \end{aligned} \quad (5.28)$$

where $H_n(f;\tau) = H_{ch,n}(f;\tau)|P(f)|^2$. In (5.28), $\phi_n(t)$ and $\epsilon_{i(N_{FFT}+\nu)+k,n}T$ are respectively the carrier phase error and the timing error of the signal transmitted by user n, as defined in (2.26); the phase shift $\Delta\theta_n(t)$ and the time delay $\Delta\tau_{i(N_{FFT}+\nu)+k,n}$ depend on the channel characteristics and are defined in (2.25).

The receiver keeps the N_{FFT} samples outside the cyclic prefix for further processing, and applies these samples to the FFT. The FFT outputs are fed to one-tap equalisers with coefficients $g_{i,n}$ that scale and rotate the nth FFT output during the ith block, resulting in the samples $z_{i,n}$ (5.12) at the input of

the decision device, where $I_{i,i',n,n'}$ is given by (5.13) and

$$A_{i,i',n,n'} = \frac{1}{N_{FFT}} \sum_{k=0}^{N_{FFT}-1} \sum_{k'=-\nu}^{N_{FFT}-1} e^{-j2\pi \frac{kn-k'n'}{N_{FFT}}} \cdot h_{eq,n}(t_{i(N_{FFT}+\nu)+k} - t_{i'(N_{FFT}+\nu)+k'}; t_{i(N_{FFT}+\nu)+k}) \quad (5.29)$$

Similarly as in OFDM and downlink OFDMA, the samples $z_{i,n}$ can be decomposed into a useful component, intersymbol interference, intercarrier interference (which corresponds with the multiuser interference) and noise. The variance of the noise contribution is given by (5.15) and the interference powers are given by (5.17). Furthermore, the SNR can be defined as (5.16), considering the quantities $A_{i,i',n,n'}$ given by (5.29).

In the case of a sufficient cyclic prefix length, the quantities $A_{i,i',n,n'}$ (5.29) reduce to

$$A_{i,i',n,n'} = \delta_{i,i'} \frac{1}{\sqrt{N_{FFT}}} \sum_{k=0}^{N_{FFT}-1} e^{-j2\pi \frac{k(n-n')}{N_{FFT}}} G_{n'}(t_{i(N_{FFT}+\nu)+k}) \quad (5.30)$$

where

$$G_n(t_{i(N_{FFT}+\nu)+k}) = \frac{1}{T} \sum_{m=-\infty}^{+\infty} H_{eq,n}\left(\frac{n}{N_{FFT}T} + \frac{m}{T}; t_{i(N_{FFT}+\nu)+k}\right) \quad (5.31)$$

is the folded transfer function of the equivalent time-varying filter defined in (5.28), evaluated at the carrier frequencies $n/(N_{FFT}T)$.

5.4 Effect of Synchronisation Errors

In OFDM and downlink OFDMA, the signals corresponding to the different users are perfectly aligned at the transmitter. In uplink OFDMA, where each user generates one carrier signal, usually a timing misalignment between the individual carrier signals occurs when these signals reach the base station, because the different transmitter clocks are not perfectly synchronised. In the following, we assume that this misalignment is kept small, because the transmitter timing is derived from a synchronisation signal sent from the base station to the users.

Further, we assume that the length νT of the cyclic prefix is sufficiently longer than the duration T_{ch} of the impulse response of the composite channel with transfer function $H_{ch,n}(f;\tau)|P(f)|^2$, so that small timing errors do not cause interference between different OFDM(A) blocks. The situation for OFDM and downlink OFDMA is depicted in figure 5.7. As the transient from the previous block is limited to the first part (of duration T_{ch}) of the cyclic prefix, all receiver timings between the earliest and latest timing indicated in figure 5.7 provide a block of N_{FFT} samples that are not affected by interference from

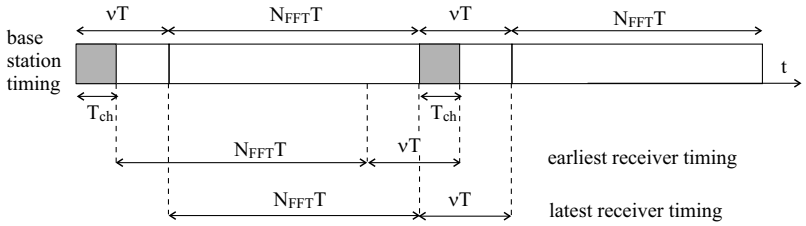

Figure 5.7: Earliest and latest possible timing instants at receiver for OFDM and downlink OFDMA, that do not cause ISI and ICI

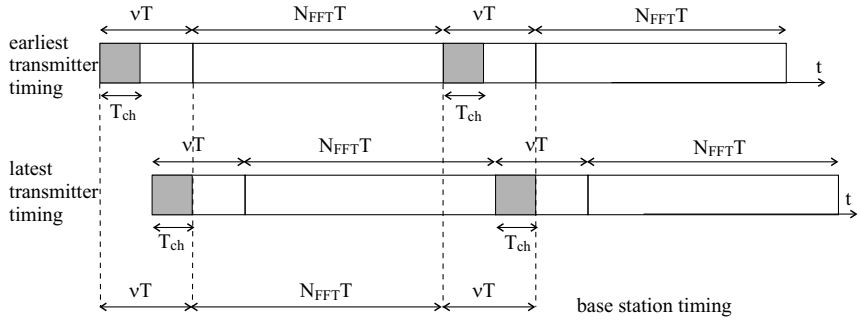

Figure 5.8: Earliest and latest possible timing instants at transmitter for uplink OFDMA, that do not cause ISI and ICI

other blocks. The case of uplink OFDMA is considered in figure 5.8. For each user, the transmitter timing should be between the earliest and latest timing indicated in figure 5.8, in order that the N_{FFT} samples to be processed at the basestation be free from interference from other blocks.

In this section, we investigate the effect of carrier phase errors and timing errors on the performance of OFDM and OFDMA systems. To clearly isolate the effect of synchronisation errors, we consider the case of an ideal channel, i.e., $H_{ch,n}(f;\tau) = 1, \forall n$. In this case, the channel dependent time delay $\Delta\tau_{i(N_{FFT}+\nu)+k,n}$ and phase shift $\Delta\theta_n(t)$ in (5.10) and (5.28) are zero. The effect of the synchronisation errors in the presence of a dispersive channel will be investigated in section 5.5.

5.4.1 Carrier Phase Errors

In this section, the sensitivity of OFDM and OFDMA to carrier phase errors is investigated in the absence of timing errors ($\epsilon_{i(N_{FFT}+\nu)+k,n} = 0$). In this case, (5.24) and (5.31) yield

$$G_n(t_{i(N_{FFT}+\nu)+k}) = e^{j\phi_n(t_{i(N_{FFT}+\nu)+k})} \tag{5.32}$$

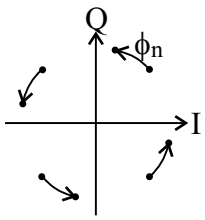

Figure 5.9: Influence of a constant phase rotation on the samples at the input of the decision device, $g_{i,n} = 1$

In the case of OFDM and downlink OFDMA, the different carriers exhibit the same carrier phase error $\phi_n(t) = \phi(t)$ as they are upconverted by the same carrier oscillator. In uplink OFDMA, all carriers exhibit different carrier phase errors, as they are upconverted by different carrier oscillators. In the following, the cases of a constant phase offset, a carrier frequency offset and carrier phase jitter are considered.

Constant Phase Offset

A constant mismatch between the carrier oscillators of the transmitter and the receiver introduces a constant phase offset $\phi_n(t) = \phi_n$. In OFDM and downlink OFDMA, the constant phase offset is the same for all carriers, i.e., $\phi_n = \phi$. Hence, this constant phase offset introduces a carrier-independent rotation of the FFT outputs as compared to a zero phase offset. In uplink OFDMA, where each carrier exhibit a different constant phase offset, each carrier is rotated over a different angle ϕ_n. However, neither in the case of OFDM or downlink OFDMA, nor for uplink OFDMA, the constant phase offset affects the orthogonality between the different carriers. Hence, no intercarrier interference is introduced and the quantities $A_{i,i',n,n'}$ (5.23) in the case of OFDM and downlink OFDMA reduce to $A_{i,i',n,n'} = \delta_{i,i'}\delta_{n,n'}\exp(j\phi)$, while in the case of uplink OFDMA the quantities $A_{i,i',n,n'}$ (5.29) reduce to $A_{i,i',n,n'} = \delta_{i,i'}\delta_{n,n'}\exp(j\phi_n)$. Hence, when no correction is applied ($g_{i,n} = 1$), the samples $z_{i,n}$ at the input of the decision device are rotated over a constant angle, as shown in figure 5.9. To compensate for the reduction of the noise margins introduced by the constant phase offset, the equaliser introduces a rotation over (an estimate of) the angle $-\phi$ for OFDM and downlink OFDMA (i.e., $(g_{MMSE})_{i,n} = C_n\exp(-j\phi)$) and over (an estimate of) the angle $-\phi_n$ for uplink OFDMA ($(g_{MMSE})_{i,n} = C_n\exp(-j\phi_n)$), where

$$C_n = \frac{\sqrt{\frac{N_{FFT}}{N_{FFT}+\nu}}\sqrt{E_{s,n}}}{N_0 + \frac{N_{FFT}}{N_{FFT}+\nu}E_{s,n}} \tag{5.33}$$

are the MMSE equaliser coefficients in the absence of carrier phase errors. Note that the MMSE equaliser depends of the carrier index n, but is independent of the block index i. The resulting samples at the input of the decision device

consist of the useful component disturbed by additive noise. The variance of the noise is given by (5.15). As we observe in (5.15), a phase rotation of the FFT outputs has no influence on the noise variance. Hence, a constant phase offset is compensated by the MMSE equaliser without loss of performance. In this case, the SNR is equal to $SNR_n(0)$, given by (5.21).

Carrier Frequency Offset

In section 2.3.2, it has been shown that the effect of a carrier frequency offset ΔF_n is twofold. First, a carrier frequency offset introduces a frequency shift of the transmitted signal. It is shown in chapter 3 that the frequency shift causes signal distortion and power loss, as a part of the received downconverted signal falls outside the bandwidth of the receiver filter. This frequency shift results in a reduction of the useful component in the receiver filter output samples $\mathbf{v}_i$ and the introduction of interference. In chapter 3, it has been shown that the degradation caused by the frequency shift is small when the carrier frequency offset is small as compared the bandwidth of the receiver filter, i.e., $\Delta F_n T \ll 1$. Further, a carrier frequency offset introduces a rotation at a constant speed of $2\pi\Delta F_n$ rad/s of the receiver filter output samples $\mathbf{v}_i$ (5.9). The rotating samples $\mathbf{v}_i$ are applied to the FFT. In the following, we will show that this rotation reduces the useful component and introduces ICI at the outputs of the FFT. As the FFT behaves like a bank of filters, each with a bandwidth in the order of $1/(N_{FFT}T)$, the frequency offset ΔF_n must satisfy $\Delta F_n T \ll 1/N_{FFT}$ in order to keep the degradation at the FFT outputs within reasonable bounds. Assuming $\Delta F_n T \ll 1/N_{FFT}$, the effect of the frequency shift at the output of the receiver filter will be neglected in the following analysis, i.e., only the rotation of the samples $\mathbf{v}_i$ will be taken into account.

A carrier frequency offset between the transmitter and receiver carrier oscillators introduces a carrier phase error that linearly increases with time: $\phi_n(t) = 2\pi\Delta F_n t + \phi_n(0)$. Without loss of generality, we assume that $\phi_n(0) = 0$.

In OFDM and downlink OFDMA, the carrier phase errors are the same for all carriers, i.e., $\Delta F_n = \Delta F, \forall n$. Let us investigate the nth FFT output during the ith OFDM block. Using (5.32), the quantities $A_{i,i',n,n'}$ (5.23) are given by

$$A_{i,i',n,n'} = \delta_{i,i'} e^{j2\pi\Delta FTi(N_{FFT}+\nu)} D\left(\frac{n'-n}{N_{FFT}} + \Delta FT\right) \tag{5.34}$$

where

$$D(x) = \frac{1}{N_{FFT}} \sum_{n=1}^{N_{FFT}-1} e^{j2\pi nx} = e^{j\pi(N_{FFT}-1)x} \frac{\sin \pi N_{FFT} x}{N_{FFT} \sin \pi x} \tag{5.35}$$

For small x, the approximations $\sin(\pi x) \approx \pi x$ holds, so that $D(x)$ is essentially a function of $N_{FFT}x$. As we observe in (5.34), the carrier frequency offset introduces a rotation of the FFT outputs at a constant speed of $2\pi\Delta FT(N_{FFT}+$

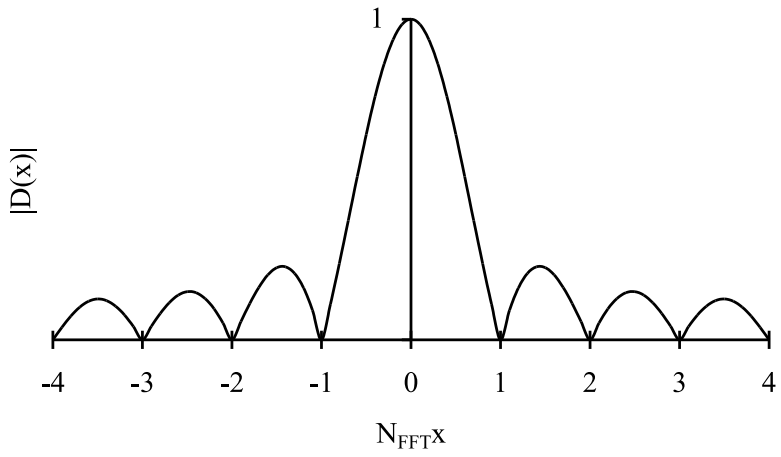

Figure 5.10: Shape of $|D(x)|$, $N_{FFT} = 8$

ν) rad/block. Observing the shape of $|D(x)|$ (see figure 5.10), it follows that the useful component $|A_{i,i,n,n}|$ at the FFT output is reduced as compared to the case of a zero carrier frequency offset. This useful component becomes zero when ΔF is a multiple of $1/(N_{FFT}T)$. In order to keep this reduction small, it is required that $|\Delta FT| \ll 1/N_{FFT}$. In addition, intercarrier interference (ICI) occurs ($|A_{i,i',n,n'}| \neq 0$ for $n' \neq n$). From the shape of $|D(x)|$ it follows that most of the ICI comes from the carriers that are nearest to the considered carrier.

The MMSE equaliser has equaliser coefficients

$$(g_{MMSE})_{i,n} = C_{\Delta F,n} e^{-j2\pi\Delta FTi(N_{FFT}+\nu)} D^*(\Delta FT) \tag{5.36}$$

where $C_{\Delta F,n}$ is a real-valued positive factor that is a function of ΔF and depends on the carrier index n. In (5.36), it is observed that the equaliser compensates for the systematic phase rotation of the FFT outputs. Furthermore, it follows from (5.36) and (5.23) that the useful component $I_{i,i,n,n}$ at the input of the decision device is real and positive. However, the equaliser is not able to eliminate the ICI ($I_{i,i',n,n'} \neq 0$ for $n' \neq n$). Hence, the OFDM and downlink OFDMA systems are degraded as compared to the case of a zero frequency offset. This degradation is caused by the rotation of the samples $\mathbf{v}_i$ at the output of the receiver filter and increases with increasing $|N_{FFT}\Delta FT|$.

When the energy per symbol is equal for all carriers, i.e., $E_{s,n} = E_s, n = 0, \ldots, N_{FFT} - 1$, it can be verified that the factor $C_{\Delta F,n}$ (in 5.36) and the resulting SNR (5.16) become independent of the carrier index n and block index i. In this case, the SNR (5.16) yields

$$SNR = \frac{SNR(0)|D(\Delta FT)|^2}{1 + SNR(0)(1 - |D(\Delta FT)|^2)} \tag{5.37}$$

where $SNR(0) = (N_{FFT}/(N_{FFT}+\nu))E_s/N_0$. The degradation (5.22) of the SNR as compared to $SNR(0)$ (5.21), introduced by the carrier frequency offset, is independent of the carrier index n and the block index i and is given by

$$Deg = -10\log\left(\frac{|D(\Delta FT)|^2}{1+SNR(0)(1-|D(\Delta FT)|^2)}\right) \tag{5.38}$$

In the case of uplink OFDMA, all carriers are affected by a different carrier frequency offset. In this case, the quantities $A_{i,i',n,n'}$ (5.23) yield

$$A_{i,i',n,n'} = \delta_{i,i'} e^{j2\pi\Delta F_{n'} Ti(N_{FFT}+\nu)} D\left(\frac{n'-n}{N_{FFT}} + \Delta F_{n'}T\right) \tag{5.39}$$

Hence, the contributions of the different transmitted carriers at the nth FFT output are rotating at different constant speeds of $2\pi\Delta F_{n'}T(N_{FFT}+\nu)$ rad/block. Assuming the basestation is able to estimate the different carrier frequency offsets $\Delta F_{n'}$, the MMSE equaliser for carrier n during the ith block is given by

$$(g_{MMSE})_{i,n} = C_{\Delta F,n} e^{-j2\pi\Delta F_n Ti(N_{FFT}+\nu)} D^*(\Delta F_n T) \tag{5.40}$$

where $C_{\Delta F,n}$ is a real-valued positive factor that is a function of $\Delta F_{n'}$, $n' = 0,\ldots,N_{FFT}-1$ and depends on the carrier index n. This factor, in general, differs from the corresponding factor in (5.36) for OFDM and downlink OFDMA. As we observe in (5.40), the equaliser compensates for the systematic phase rotation of the useful component. After equalisation, the contributions of the other carriers are still rotating at a constant speed of $2\pi(\Delta F_{n'} - \Delta F_n)T(N_{FFT}+\nu)$ rad/block. However, the magnitudes $|I_{i,i',n,n'}|$ of the interference terms are independent of the block index i. This implies that the resulting SNR is independent of the block index i but depends on the carrier index n. Furthermore, the SNR depends on the different carrier frequency offsets, i.e., $\Delta F_{n'}$, $n' = 0,\ldots,N_{FFT}-1$. When in uplink OFDMA all carriers are affected by the same carrier frequency offset, the results are the same as for OFDM and downlink OFDMA.

The degradation (5.38) is shown in figure 5.11. We observe that the OFDM(A) system is very sensitive to a carrier frequency offset. Hence, to obtain small degradations, the carrier frequency offset must be limited, i.e., $\Delta FT \ll 1/N_{FFT}$. In this case, the degradation is essentially proportional to $(N_{FFT}\Delta FT)^2$.

The OFDM(A) system is simulated in the absence of additive noise ($N_0 = 0$), for $N_{FFT} = 64$ carriers with QPSK modulation, the energy per symbol equal for all carriers ($E_{s,n} = E_s$) and all carriers exhibit the same carrier frequency offset $\Delta FT = 2.10^{-3}$. In figure 5.12, the scatter diagram is shown when no equaliser is present ($g_{i,n} = 1$). As we observe, the rotation at a speed $2\pi\Delta FT(N_{FFT}+\nu)$ rad/block of the samples $z_{i,n}$ at the input of the decision device introduces a systematic rotation of the constellation points in the scatter diagram. The

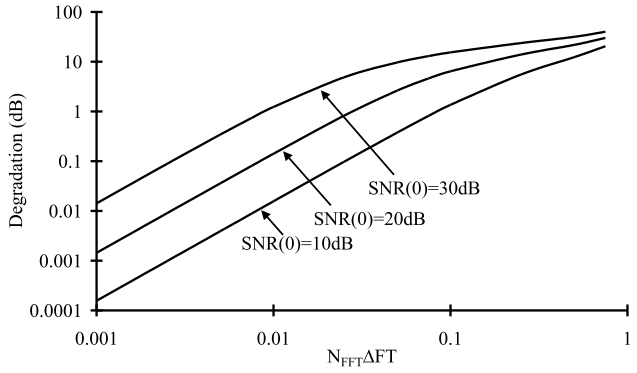

Figure 5.11: Carrier frequency offset, $E_{s,n} = E_s$

equaliser (5.36) compensates for the systematic phase rotation. In figure 5.13, the scatter diagram is shown for all carriers modulated and for the MMSE equaliser (5.36). The circular cloud in the scatter diagram can be explained as follows. As the ICI consists of a large number of uncorrelated contributions, it can be approximated by a (complex-valued) Gaussian noise variable. The contribution from the symbol $a_{i,n'}$ is proportional to $a_{i,n'} I_{i,i,n,n'}$. Assuming that $E[a_{i,n'}^2] = 0$ (which holds for M-PSK constellations with $M > 2$ and for M-QAM constellations), it follows that the real and imaginary parts of $a_{i,n'} I_{i,i,n,n'}$ are uncorrelated and have the same variance. Consequently, the ICI can be approximated by a Gaussian random variable whose real and imaginary parts have the same variance and are statistically independent. The distribution of such a complex-valued Gaussian random variable is rotationally invariant, which explains the circular shape of the clouds in the scatter diagram. In table 5.1, the mean square deviation of the samples at the input of the decision device is shown for the simulations of figure 5.13. As we observe, the theoretical results agree well with the simulation results.

When the degradation caused by the carrier frequency offset can not be tolerated, carrier frequency correction must be applied. In OFDM and downlink OFDMA the frequency offset is the same for all carriers. Hence, the carrier frequency can be corrected at the receiver in front of the FFT. When this correction is applied after the receiver filter, there is still the degradation caused by the frequency shift of the received signal with respect to the receiver filter. In uplink OFDMA, each carrier has a different frequency offset. The receiving base station can correct only the common frequency offset; differential frequency offsets should be corrected at the transmitters. When the base station has a fixed carrier for downconversion, the transmitters should correct the entire frequency offsets.

When the carrier frequency correction in the case of OFDM and downlink OFDMA is applied after the receiver filter, i.e., the systematic phase rotation

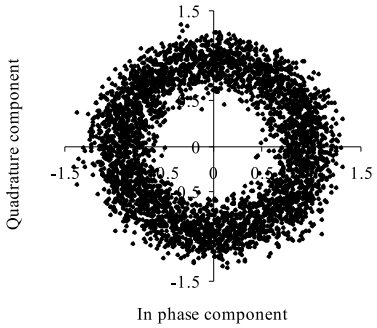

Figure 5.12: Carrier frequency offset, all carriers modulated, no equaliser ($g_{i,n} = 1$), $N_{FFT} = 64, \Delta FT = 2.10^{-3}, E_{s,n} = E_s$

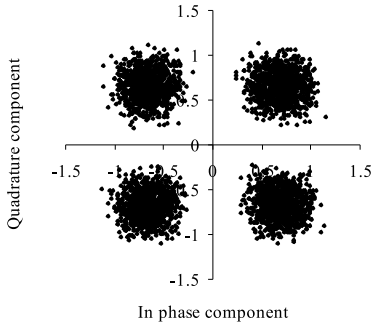

Figure 5.13: Carrier frequency offset, all carriers modulated, equaliser, $N_{FFT} = 64, \Delta FT = 2.10^{-3}, E_{s,n} = E_s$

Table 5.1: Mean square deviation of the samples at the input of the decision device

Theoretical	Simulations
$5.27E-2$	$5.33E-2$

is compensated in front of the FFT, the quantities $A_{i,i',n,n'}$ (5.23) are given by

$$A_{i,i',n,n'} = \delta_{i,i'}\delta_{n,n'}G_n(\Delta F) \tag{5.41}$$

where

$$G_n(\Delta F_n) = \frac{1}{T}\sum_{m=-\infty}^{+\infty} P\left(\frac{n}{N_{FFT}T} + \frac{m}{T}\right) P^*\left(\frac{n}{N_{FFT}T} + \frac{m}{T} + \Delta F\right) \tag{5.42}$$

Hence, the nth FFT output during the ith block contains only the useful data symbol $a_{i,n}$. This implies that a carrier frequency offset introduces no interference between symbols. Let us consider the case of the transmit and receiver filter being square-root raised-cosine filters with rolloff α (see appendix B). In this case, the transmit and receiver filter are bandwidth limited, i.e., $P(f) = 0$ for $|f| > (1+\alpha)/2T$, $0 \leq \alpha \leq 1$. The frequency interval $(1-\alpha)/2T \leq |f| \leq (1+\alpha)/2T$ is denoted the rolloff area. For carrier frequencies $n/(N_{FFT}T)$ inside $K(\Delta F) = [\min((1-\alpha)/2T; (1-\alpha)/2T - \Delta F)); \max((1+\alpha)/2T; (1+\alpha)/2T - \Delta F))]$, the sum (5.42) reduces to two terms, for which it can be verified that

$$|G_n(\Delta F)| \leq 1, \qquad \frac{n}{N_{FFT}T} \in K(\Delta F) \tag{5.43}$$

For carrier frequencies $n/(N_{FFT}T)$ outside the interval $K(\Delta F)$, the sum (5.42) reduces to only one term

$$G_n(\Delta F) = 1, \qquad \frac{n}{N_{FFT}T} nin K(\Delta F) \tag{5.44}$$

The set of carriers that fall inside the interval $K(\Delta F)$ corresponds to the set of carriers inside the rolloff area extended with one or more carriers adjacent to the rolloff area that are affected by the frequency shift. Figure 5.14 shows the amplitude of the FFT outputs as function of the carrier index. Hence, for carrier frequencies $n/(N_{FFT}T)$ outside $K(\Delta F)$, the frequency shift has no influence on the FFT outputs, which implies that these carriers are not degraded. For carrier frequencies $n/(N_{FFT}T)$ inside $K(\Delta F)$, the frequency shift causes a reduction of the amplitude of the useful component. This amplitude reduction, however, is small when the carrier frequency offset is small. The one-tap equaliser at the FFT output is not able to compensate for the reduction of the amplitude of the useful component without enhancing the noise power level. Hence, carriers $n/(N_{FFT}T)$ inside $K(\Delta F)$ are degraded. The degradation (5.22) of the SNR as compared to $SNR_n(0)$ (5.21) caused by the carrier frequency offset yields $Deg_n = -10log(|G_n(\Delta F)|^2)$. This degradation is caused by the frequency shift and depends on the product ΔFT. Figure 5.15 shows the degradation for $n = N_{FFT}/2$ where the reduction of the amplitude, hence the degradation is maximum (see figure 5.14). As we observe, the degradation is small when the carrier frequency offset is small, i.e., $\Delta FT \ll 1$. This degradation is independent of the number of carriers, and only depends on ΔFT (see (5.42)).

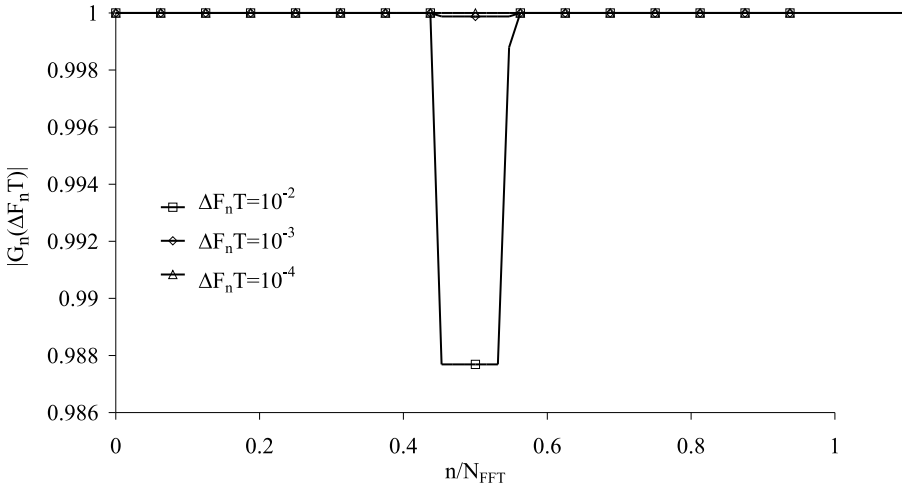

Figure 5.14: Reduction of the amplitude caused by the frequency shift of the transmitted signal, $N_{FFT} = 64$

Carrier Phase Jitter

To get rid of a carrier frequency offset and a constant phase offset, the total phase to be used by the carrier oscillator is estimated from the received signal by means of a synchronisation algorithm. In this case, the resulting phase error is called 'carrier phase jitter', and can be modelled as a zero-mean stationary random process with jitter power spectral density $S_{\phi,n}(f)$ and jitter variance $\sigma^2_{\phi,n}$.

In OFDM and downlink OFDMA, the phase jitter is the same for all carriers, i.e., $\phi_n(t) = \phi(t)$, $n = 0, \ldots, N_{FFT}-1$. We assume that for small jitter variances $\sigma^2_\phi \ll 1$, the approximation $\exp(j\phi(t)) \approx 1 + j\phi(t)$ can be used. In this case, the quantities $A_{i,i',n,n'}$ (5.23) reduce to

$$A_{i,i',n,n'} = \delta_{i,i'} \left(\delta_{n,n'} + \frac{1}{N_{FFT}} \sum_{k=0}^{N_{FFT}-1} j\phi(t_{i(N_{FFT}+\nu)+k}) e^{-j2\pi \frac{k(n-n')}{N_{FFT}}} \right) \quad (5.45)$$

Because of the random nature of the carrier phase jitter, self-interference is introduced. When the carrier phase jitter rapidly varies as compared to the averaging time of the MMSE equaliser, the equaliser is not able to track the jitter. The equaliser then averages the variations caused by the carrier phase jitter. As for small jitter variances, the average of $\exp(j\phi(t))$ can be approximated by $E[\exp(j\phi(t))] \approx E[1 + j\phi(t)] = 1$, the MMSE equaliser is essentially the same as in the absence of synchronisation errors and yields $(g_{MMSE})_{i,n} = C_n$, where C_n is given by (5.33). The resulting powers of the average useful component,

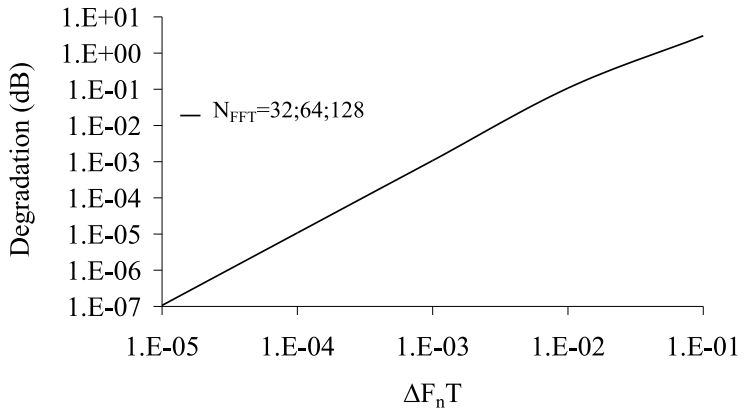

Figure 5.15: Carrier frequency offset, systematic rotation compensated in front of FFT, $n = N_{FFT}/2, \alpha = 0.1$

the self-interference, the intercarrier interference (5.17) and the noise (5.15) are given by

$$\begin{aligned} P_{U,n} &= |C_n|^2 \\ P_{SI,n} &= |C_n|^2 \int_{-\infty}^{+\infty} S_\phi(f)|D(fT)|^2 df \\ P_{ICI,n} &= |C_n|^2 \sum_{n'=0;n'\neq n}^{N_{FFT}-1} \frac{E_{s,n'}}{E_{s,n}} \int_{-\infty}^{+\infty} S_\phi(f) \left| D\left(\frac{n'-n}{N_{FFT}} + fT\right)\right|^2 df \\ E[|W_{i,n}|^2] &= N_0|C_n|^2 \end{aligned} \tag{5.46}$$

where $D(x)$ is defined in (5.35). We observe from (5.46) that the powers of the average useful component, the self-interference, the intercarrier interference and the noise depend on the carrier index n, but are independent of the block index i. When the energy per symbol is equal for all carriers, i.e., $E_{s,n} = E_s$ $(n = 0, ..., N_{FFT} - 1)$, the factor C_n becomes independent of the carrier index n, i.e., $C_n = C$. In this case, the intercarrier interference becomes independent of the carrier index n and is given by

$$P_{ICI} = |C|^2 \int_{-\infty}^{+\infty} S_\phi(f)(1 - |D(fT)|^2) df \tag{5.47}$$

When the energy per symbol is the same for all carriers, it follows from figure 5.16, the second equation of (5.46) and (5.47) that the self-interference and the intercarrier interference mainly consist of the low frequency components $(|f| < 1/(N_{FFT}T))$ and the high frequency components $(|f| > 1/(N_{FFT}T))$ of the jitter spectrum $S_\phi(f)$, respectively. Furthermore, the sum of the powers of the self-interference and the intercarrier interference becomes independent

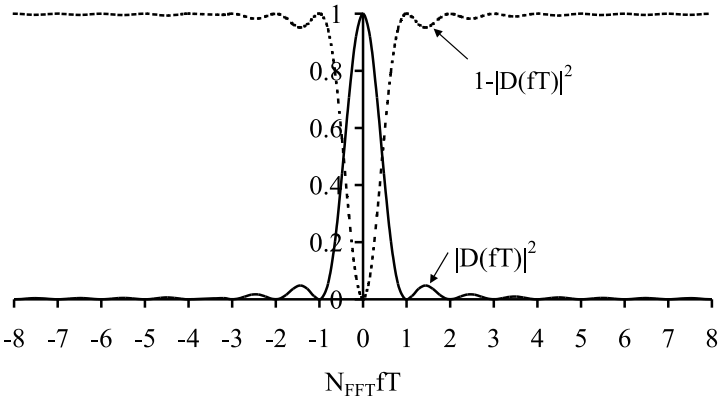

Figure 5.16: The weight functions $|D(fT)|^2$ and $(1-|D(fT)|^2)$, $N_{FFT}=16$

of the spectral contents of the jitter and of the number of carriers, but only depends on the jitter variance σ_ϕ^2, given by

$$\sigma_\phi^2 = \int_{-\infty}^{+\infty} S_\phi(f)df \tag{5.48}$$

In this case, the degradation (5.22) of the SNR, caused by the carrier phase jitter, is independent of the spectral contents of the jitter and the number of carriers, but only depends on the jitter variance:

$$Deg = 10\log\left(1+SNR(0)\sigma_\phi^2\right) \tag{5.49}$$

where $SNR(0) = (N_{FFT}/(N_{FFT}+\nu))E_s/N_0$. Note that the degradation (5.49) is very similar to the degradation in the case of the single carrier systems (see (3.22) and (4.25)).

In the case of uplink OFDMA, all carriers are affected by different carrier phase jitter processes. Assuming the jitter variances are small, the quantities $A_{i,i',n,n'}$ (5.23) can be approximated by

$$A_{i,i',n,n'} = \delta_{i,i'}\left(\delta_{n,n'} + \frac{1}{N_{FFT}}\sum_{k=0}^{N_{FFT}-1} j\phi_{n'}(t_{i(N_{FFT}+\nu)+k})e^{-j2\pi\frac{k(n-n')}{N_{FFT}}}\right) \tag{5.50}$$

Similarly as for OFDM and downlink OFDMA, the MMSE equaliser essentially equals (5.33) for small jitter variances. The powers of the average useful component and the noise are the same as for OFDM and downlink OFDMA and are given by (5.46). The powers of the self-interference and the intercarrier

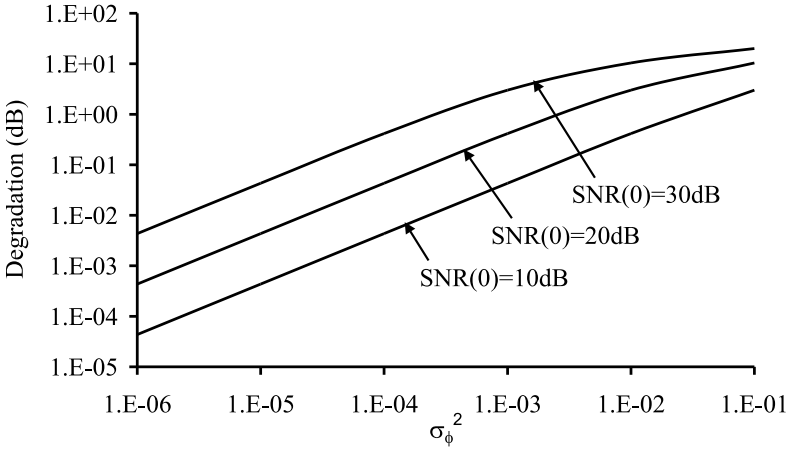

Figure 5.17: Carrier phase jitter, all carriers modulated, $E_{s,n} = E_s$

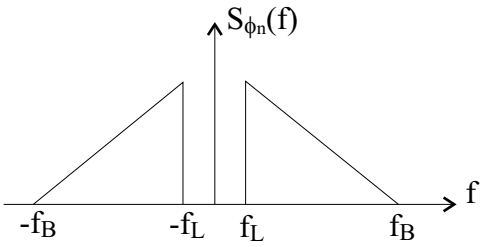

Figure 5.18: Jitter spectrum

interference are given by

$$P_{SI,n} = |C_n|^2 \int_{-\infty}^{+\infty} S_{\phi,n}(f)|D(fT)|^2 df$$

$$P_{ICI,n} = |C_n|^2 \sum_{n'=0;n'\neq n}^{N_{FFT}-1} \frac{E_{s,n'}}{E_{s,n}} \int_{-\infty}^{+\infty} S_{\phi,n'}(f) \left| D\left(\frac{n'-n}{N_{FFT}} + fT\right) \right|^2 df \quad (5.51)$$

When all jitter processes in the case of uplink OFDMA have the same jitter spectrum $S_{\phi,n}(f) = S_\phi(f)$ and, hence, the same jitter variance $\sigma^2_{\phi,n} = \sigma^2_\phi$, the results for uplink OFDMA are the same as for OFDM and downlink OFDMA.

In figure 5.17, the degradation (5.49) is shown as function of the jitter variance when the energy per symbol the same for all carriers ($E_{s,n} = E_s$, $n = 0, \ldots, N_{FFT} - 1$). In this case, the degradation is independent of the number of carriers. For a small jitter variance, the degradation is essentially proportional to σ^2_ϕ.

The OFDM(A) system is simulated in the absence of additive noise ($N_0 = 0$),

for $N_{FFT} = 64$ carriers with QPSK modulation and the energy per symbol equal for all carriers ($E_{s,n} = E_s, n = 0, \ldots, N_{FFT}-1$). All carriers are affected by the same carrier phase jitter process with a jitter spectrum having the shape shown in figure 5.18, with jitter variance $\sigma_\phi^2 = 5.10^{-3}$ rad^2. Figures 5.19 and 5.20 show the scatter diagram for $f_L = 0, f_B = 1/(N_{FFT}T)$ and $f_L = 2/(N_{FFT}T), f_B = 4/(N_{FFT}T)$, respectively. Although the mean-square deviation of the samples at the input of the decision device is independent of the spectral contents of the jitter, the scatter diagrams differ significantly. This can be explained as follows. When $f_L = 0, f_B = 1/(N_{FFT}T)$, it follows from figure 5.16, (5.46) and (5.47) that the dominant interference term is the self-interference. In this case, the jitter gives rise to a random phase rotation of the useful component (see (5.45) with $i = i', n = n'$). Hence, the scatter diagram shows mainly an angular displacement of the constellation points. When $f_L = 2/(N_{FFT}T), f_B = 4/(N_{FFT}T)$, the dominant interference term is the intercarrier interference. As the intercarrier interference term has uncorrelated real and imaginary parts, of which the variances are equal, the scatter diagram shows circular clouds. In table 5.2, the mean square deviation of the samples at the input of the decision device is shown for the simulations of figures 5.19 and 5.20. As we observe, the simulation results agree well with the theoretical results.

Not All Carriers Modulated

In section 5.4.2, we will show that a performance degradation in the presence of a timing offset can be avoided by modulating not all N_{FFT} carriers. Carriers that are not used for data transmission have zero amplitude. Denoting the number of modulated carriers by N_{carr}, the relation between the symbol rate R_s and the sampling rate $1/T$ becomes: $1/T = R_s(N_{FFT}+\nu)/N_{carr}$. Assuming that the energy per symbol equals E_s for those carriers that are modulated, the degradations (5.38) and (5.49) represent upper bounds when $N_{carr} < N_{FFT}$. These upper bounds are very tight when the fraction of unmodulated carriers is small.

5.4.2 Timing Errors

In this section, we investigate the sensitivity of OFDM and OFDMA to timing errors in the absence of carrier phase errors ($\phi_n(t) = 0$). As explained in section 5.4, we will assume that the cyclic prefix is sufficiently long to cope with the timing errors, so that the N_{FFT} samples per block that are processed by the receiver are not affected by interference from other blocks. In this case, (5.24) yields

$$G_n(t_{i(N_{FFT}+\nu)+k}) = \frac{1}{T}\sum_{m=-\infty}^{+\infty}\left|P\left(\frac{n}{N_{FFT}T}+\frac{m}{T}\right)\right|^2 e^{j2\pi\epsilon_{i(N_{FFT}+\nu)+k}\left(\frac{n}{N_{FFT}}+m\right)} \tag{5.52}$$

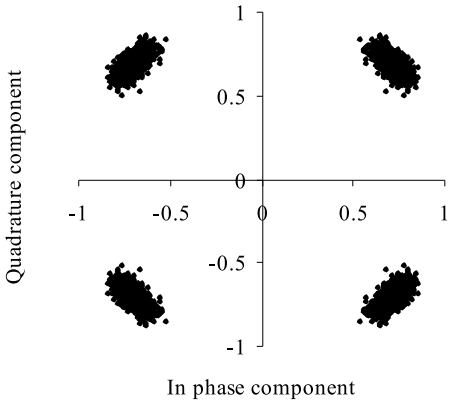

Figure 5.19: Carrier phase jitter, all carriers modulated, $E_{s,n} = E_s, f_L = 0, f_B = 1/(N_{FFT}T), N_{FFT} = 64, \sigma_\phi^2 = 5.10^{-3}$ rad^2

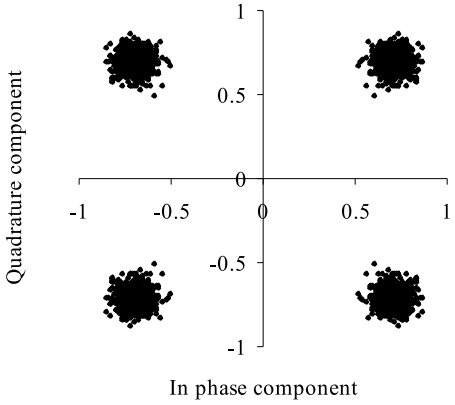

Figure 5.20: Carrier phase jitter, all carriers modulated, $E_{s,n} = E_s, f_L = 21/(N_{FFT}T), f_B = 4/(N_{FFT}T), N_{FFT} = 64, \sigma_\phi^2 = 5.10^{-3}$ rad^2

Table 5.2: Mean square deviation of the samples at the input of the decision device

	Theoretical	Simulations
$f_L = 0, f_B = 1/(N_cT) = R_s$	$5E-3$	$5.025E-3$
$fL = 2/(N_cT) = 2R_s, fB = 4/(N_cT) = 4R_s$	$5E-3$	$5.000E-3$

In the case of OFDM and downlink OFDMA, the contributions of the different transmitted carriers are aligned at the basestation. Hence, the timing errors are the same for all contributions. In uplink OFDMA, a misalignment between the contributions of the different users can occur. In this case, the different contributions exhibit a different timing error. For the transmit and receiver filter, we consider a square-root raised-cosine filter with rolloff α. In the following, the cases of a constant timing offset, a clock frequency offset and timing jitter are considered.

Constant Timing Offset

In the case of a constant timing offset $\epsilon_{i(N_{FFT}+\nu)+k,n} = \epsilon_n$ is independent of the block index i.

For OFDM and downlink OFDMA, where the contributions of the different carriers are aligned ($\epsilon_n = \epsilon$), the quantities $A_{i,i',n,n'}$ (5.23) are given by

$$A_{i,i',n,n'} = \delta_{i,i'}\delta_{n,n'}G_n \tag{5.53}$$

where

$$G_n = \frac{1}{T}\sum_{m=-\infty}^{+\infty}\left|P\left(\frac{n}{N_{FFT}T}+\frac{m}{T}\right)\right|^2 e^{j2\pi\left(\frac{n}{N_{FFT}}+m\right)\epsilon} \tag{5.54}$$

Hence, the nth FFT output during the ith block contains only the useful data symbol $a_{i,n}$, which indicates that a constant timing offset does not introduce any interference between symbols. The quantity G_n (5.54) satisfies the relationship $G_n(\epsilon+\Delta) = \exp(j2\pi n\Delta/N_{FFT})G_n(\epsilon)$, where Δ is an integer. Considering the phase rotation $\exp(j2\pi n\Delta/N_{FFT})$ at the nth FFT output can be compensated by the one-tap equaliser, a constant timing offset of an integer number of samples introduces no performance degradation as compared to the case of a zero timing offset. Hence, in our analysis, we restrict our attention to a constant timing offset in the interval $\epsilon \in [-0.5, 0.5]$.

The transmit and receiver filter, which are square-root raised-cosine filters with rolloff α, are bandwidth limited, i.e., $P(f) = 0, |f| > (1+\alpha)/2T, 0 \le \alpha \le 1$. The frequency interval $(1-\alpha)/2T \le |f| \le (1+\alpha)/2T$ is denoted the rolloff area. For carrier frequencies $n/(N_{FFT}T)$ inside this rolloff area, the sum (5.54) consists of two terms for which it can be verified that

$$|G_n| < 1, \qquad \frac{n}{N_{FFT}T} \notin \left[\frac{1-\alpha}{2T}, \frac{1+\alpha}{2T}\right] \tag{5.55}$$

For carrier frequencies $n/(N_{FFT}T)$ outside the rolloff area, the sum (5.54) reduces to only one term

$$G_n = e^{j2\pi\epsilon\frac{\mathrm{mod}(x;N_{FFT})}{N_{FFT}}}, \qquad \frac{n}{N_{FFT}T} \notin \left[\frac{1-\alpha}{2T}, \frac{1+\alpha}{2T}\right] \tag{5.56}$$

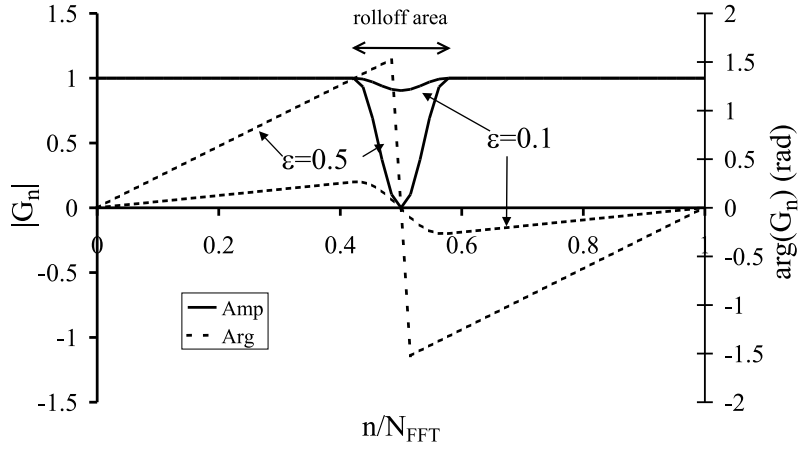

Figure 5.21: Dependency of $|G_n|$ and $\arg(G_n)$ on the carrier index n, $\alpha = 0.1$

where $\mathrm{mod}(x; N_{FFT})$ denotes the modulo-N_{FFT} reduction of x, yielding a result in $(-N_{FFT}/2, N_{FFT}/2)$. From (5.55), (5.56) and figure 5.21, it follows that for carrier frequencies $n/(N_{FFT}T)$ outside the rolloff area, the corresponding FFT output exhibits a constant amplitude $|G_n| = 1$ and is rotated over an angle $2\pi\epsilon\mathrm{mod}(n; N_{FFT})/N_{FFT}$ as compared to the case of a zero timing offset. For carrier frequencies $n/(N_{FFT}T)$ inside the rolloff area, the corresponding FFT output is rotated over some angle and the amplitude is reduced as compared to the case of a zero timing offset. The MMSE equaliser has equaliser coefficients

$$(g_{MMSE})_{i,n} = C_{\epsilon,n} G_n^* \tag{5.57}$$

where $C_{\epsilon,n}$ is a real-valued positive factor that depends on the timing offset ϵ and the carrier index n. Hence, for carrier frequencies $n/(N_{FFT}T)$ outside the rolloff area, where $|G_n| = 1$, the rotation of the FFT output is compensated by the equaliser without loss of performance, by rotating the FFT output over (an estimate of) the angle $-2\pi\epsilon\mathrm{mod}(n; N_{FFT})/N_{FFT}$. As the amplitude of the carriers outside the rolloff area is reduced as compared to a zero timing offset, the equaliser can not compensate the effect of the constant timing offset without increasing the noise power level. Hence, the carriers inside the rolloff area are degraded. The degradation (5.22) of the SNR as compared to $SNR_n(0)$ (5.21) caused by the constant timing offset yields $Deg_n = -10\log(|G_n|^2)$. The degradation of the OFDM and downlink OFDMA systems caused by a constant timing offset can be avoided by not using for data transmission the carriers inside the rolloff area, i.e., their amplitude is set to zero.

In uplink OFDMA, a constant misalignment between the contributions of the different users can occur. Hence, the timing offset en of the contributions of the different carriers depends on the carrier index n. In this case, the quantity

G_n in (5.53) is given by

$$G_n = \frac{1}{T} \sum_{m=-\infty}^{+\infty} \left| P\left(\frac{n}{N_{FFT}T} + \frac{m}{T} \right) \right|^2 e^{j2\pi\left(\frac{n}{N_{FFT}}+m\right)\epsilon_n} \tag{5.58}$$

Similarly as for OFDM and downlink OFDMA, the constant timing offset introduces a phase rotation over the angle $2\pi\epsilon_n \mathrm{mod}(n; N_{FFT})/N_{FFT}$ for carrier frequencies $n/(N_{FFT}T)$ outside the rolloff area and a rotation over some angle and a reduction of the amplitude for carrier frequencies $n/(N_{FFT}T)$ inside the rolloff area. Hence, similarly as for OFDM and downlink OFDMA, the effect of the constant timing offsets on the uplink OFDMA system can be compensated without loss of performance when the carriers inside the rolloff area are not used.

Clock Frequency Offset

In the case the receiver of each user (downlink OFDM(A)) or the transmitter of each user (uplink OFDM(A)) has a free-running clock with a relative clock frequency offset $\Delta T_n/T$ as compared to the frequency $1/T$ of the network reference clock signal, the timing error linearly increases with time: $\epsilon_{i(N_{FFT}+\nu)+k,n} = (k+i(N_{FFT}+\nu))\Delta T_n/T+\epsilon_{0,n}$. Hence, an increasing misalignment between the samples $s_{i(N_{FFT}+\nu)+k,n}$ at the transmitter and the samples $v_{i(N_{FFT}+\nu)+k,n}$ at the receiver is introduced. In OFDM and downlink OFDMA, the contributions of the different carriers are aligned and are transmitted using the same transmitter clock. Hence, the contributions of the different carriers exhibit the same clock frequency offset $\Delta T/T$. In uplink OFDMA, the contributions of the different carriers, in general, are affected by a different clock frequency offset.

To compensate for the increasing misalignment in OFDM and downlink OFDMA, the receiver can perform a coarse synchronisation. In this coarse synchronisation algorithm, the receiver removes ($\Delta T < 0$) or duplicates ($\Delta T > 0$) receiver filter output samples at the boundaries of the OFDM(A) blocks, such that the N_{FFT} successive samples kept for further processing are located in the region where interference from other blocks is absent. In the case of uplink OFDMA, the coarse synchronisation is performed at the transmitter, which receives timing information broadcast by the base station. The number of samples in the cyclic prefix is increased ($\Delta T > 0$) or reduced ($\Delta T < 0$), such that the N_{FFT} successive samples selected by the base station for further processing are not affected by interference from other blocks. Considering these coarse synchronisation algorithms for downlink and uplink OFDM(A), the resulting timing error can be written as: $\tilde{\epsilon}_{i(N_{FFT}+\nu)+k,n} = k\Delta T_n/T + \epsilon_{i,n}$, where $\epsilon_{i,n}$ does not vary over the considered OFDM(A) block.

In OFDM and downlink OFDMA, the quantities $\mathrm{A}_{i,i',n,n'}$ (5.23) reduce to

$$\begin{aligned} A_{i,i',n,n'} &= \delta_{i,i'} \frac{1}{T} \sum_{m=-\infty}^{+\infty} \left| P\left(\frac{n}{N_{FFT}T} + \frac{m}{T}\right) \right|^2 e^{j2\pi\epsilon_{i,n'}\left(\frac{n'}{N_{FFT}}+m\right)} \cdot \\ & \quad D\left(\frac{n'-n}{N_{FFT}} + \left(\frac{n'}{N_{FFT}} + m\right)\frac{\Delta T}{T}\right) \end{aligned} \tag{5.59}$$

where $D(x)$ is defined in (5.35). Let us consider the case that only carriers outside the rolloff area are modulated. For these carriers, the quantities $A_{i,i',n,n'}$ (5.59) yield

$$A_{i,i',n,n'} = \delta_{i,i'} e^{j2\pi\epsilon_{i,n'}\frac{\mathrm{mod}(n';N_{FFT})}{N_{FFT}}} D\left(\frac{n'-n}{N_{FFT}} + \left(\frac{\mathrm{mod}(n';N_{FFT})}{N_{FFT}}\right)\frac{\Delta T}{T}\right) \tag{5.60}$$

From (5.60) we observe that the contribution of the n'th transmitted carrier introduces non-zero interference at the nth output of the FFT ($A_{i,i,n,n'} \neq 0$ for $n' \neq n$). Furthermore, taking into account the shape of $D(x)$ (5.35), the useful component $A_{i,i,n,n}$ is attenuated as compared to the case of a zero clock frequency offset. In addition, the complex exponential in (5.60) indicates a phase rotation of the useful component. Hence, a clock frequency offset introduces intercarrier interference and an attenuation of the useful component at the output of the FFT.

The MMSE equaliser coefficients are given by

$$(g_{MMSE})_{i,n} = C_{\Delta T,n} D^*\left(\frac{\mathrm{mod}(n;N_{FFT})}{N_{FFT}}\frac{\Delta T}{T}\right) e^{-j2\pi\epsilon_{i,n}\frac{\mathrm{mod}(n;N_{FFT})}{N_{FFT}}} \tag{5.61}$$

where $C_{\Delta T,n}$ is a real-valued positive factor that depends on the clock frequency offset $\Delta T/T$ and the carrier index n. The MMSE equaliser compensates for the systematic phase rotation of the useful component $A_{i,i,n,n}$. However, the equaliser is not able to eliminate the ICI ($I_{i,i',n,n'} \neq 0$ for $n' \neq n$ see (5.13)). The powers of the average useful component, the intercarrier interference (5.17) and the noise (5.15) are independent of the block index i and yield

$$\begin{aligned} P_{U,n} &= |C_{\Delta T,n}|^2 \left(\left| D\left(\frac{\mathrm{mod}(n;N_{FFT})}{N_{FFT}}\frac{\Delta T}{T}\right)\right|^2\right)^2 \\ P_{ICI,n} &= |C_{\Delta T,n}|^2 \left| D\left(\frac{\mathrm{mod}(n;N_{FFT})}{N_{FFT}}\frac{\Delta T}{T}\right)\right|^2 \cdot \\ & \quad \sum_{n'=0;n'\neq n}^{N_{FFT}-1} \frac{E_{s,n'}}{E_{s,n}} \left| D\left(\frac{n'-n}{N_{FFT}} + \frac{\mathrm{mod}(n';N_{FFT})}{N_{FFT}}\frac{\Delta T}{T}\right)\right|^2 \\ E[|W_{i,n}|^2] &= N_0 |C_{\Delta T,n}|^2 \left| D\left(\frac{\mathrm{mod}(n;N_{FFT})}{N_{FFT}}\frac{\Delta T}{T}\right)\right|^2 \end{aligned} \tag{5.62}$$

When the carriers inside the rolloff are not used (i.e., $E_{s,n} = 0$ for carriers inside the rolloff), the summation over n' in the intercarrier interference power term (5.62) corresponds to the summation over the carriers outside the rolloff. From (5.62) it follows that the OFDM and downlink OFDMA systems are degraded as compared to the case of a zero clock frequency offset. The degradation (5.22) of the SNR as compared to $SNR_n(0)$ (5.21) caused by the clock frequency offset depends on the carrier index n and is given by

$$Deg_n = -10\log\left|D\left(\frac{\mathrm{mod}(n;N_{FFT})}{N_{FFT}}\frac{\Delta T}{T}\right)\right|^2 \qquad (5.63)$$
$$+10\log\left(1+\sum_{n'=0;n'\neq n}^{N_{FFT}-1} SNR_{n'}(0)\left|D\left(\frac{n'-n}{N_{FFT}}+\frac{\mathrm{mod}(n';N_{FFT})}{N_{FFT}}\frac{\Delta T}{T}\right)\right|^2\right)$$

where $SNR_{n'}(0)$ is given by (5.21). Let us assume that the energy per symbol is equal for all carriers outside the rolloff, i.e., $E_{s,n} = E_s$ for $n/(N_{FFT}T)$ outside the rolloff area. In this case, the degradation is given by (5.63), with $E_{s,n'}$ replaced by E_s and the summation index n' $(\neq n)$ ranging over an interval such that $n'/(N_{FFT}T)$ is outside the rolloff area. An upper bound on this degradation is obtained by extending the summation interval, such that n' $(\neq n)$ ranges from 0 to $N_{FFT} - 1$. This yields

$$Deg_n \leq -10\log\left|D\left(\frac{\mathrm{mod}(n;N_{FFT})}{N_{FFT}}\frac{\Delta T}{T}\right)\right|^2 \qquad (5.64)$$
$$+10\log\left(1+\sum_{n'=0;n'\neq n}^{N_{FFT}-1} SNR(0)\left|D\left(\frac{n'-n}{N_{FFT}}+\frac{\mathrm{mod}(n';N_{FFT})}{N_{FFT}}\frac{\Delta T}{T}\right)\right|^2\right)$$

where $SNR(0) = (N_{FFT}/(N_{FFT}+\nu))E_s/N_0$. The above upper bound is reached when the transmit pulse has zero rolloff ($\alpha = 0$), in which case no rolloff area is present. The degradation (5.64) yields an accurate approximation for the actual degradation when the rolloff area is small. Considering the nature of $D(x)$ (5.35), the degradation (5.64) is a function of the product $N_{FFT}\Delta T/T$ when n/N_{FFT} is a fixed value.

Let us define the average (over the FFT outputs) powers of the average useful component, the intercarrier interference and the noise (5.62) by

$$\overline{P}_X = \frac{1}{N_{FFT}}\sum_{n=0}^{N_{FFT}-1} P_{X,n}, \qquad X = U, ICI, noise \qquad (5.65)$$

The average SNR is defined as the ratio of the average power of the average useful component to the sum of the average powers of the intercarrier interference and the noise. The average SNR is independent of the carrier index n and the block index i. We assume that all carriers outside the rolloff area are modulated and have their energy per symbol equals E_s. The amplitude for the carriers inside

the rolloff area is set to zero. In a similar way as for the degradation (5.63), an upper bound on the degradation of the average SNR as compared to the case of a zero clock frequency offset is found. This yields

$$Deg_{Av} \leq -10\log\left(\sum_{n=0}^{N_{FFT}-1} Y_n^2\right) + 10\log\left(\sum_{n=0}^{N_{FFT}-1} Y_n - SNR(0)\sum_{n=0}^{N_{FFT}-1} Y_n^2\right) \tag{5.66}$$

where

$$\begin{aligned} Y_n &= X_{\Delta T,n}\left|D\left(\frac{\mathrm{mod}(n;N_{FFT})}{N_{FFT}}\frac{\Delta T}{T}\right)\right|^2 \qquad (5.67)\\ X_{\Delta T,n}^{-1} &= 1+SNR(0)\sum_{n'=0}^{N_{FFT}-1}\left|D\left(\frac{n'-n}{N_{FFT}}+\frac{\mathrm{mod}(n';N_{FFT})}{N_{FFT}}\frac{\Delta T}{T}\right)\right|^2 \end{aligned}$$

The upper bound (5.66) on the degradation is a function of the product $N_{FFT}\Delta T/T$.

In uplink OFDMA, the contributions transmitted by the different users exhibit a different clock frequency offset. In this case, the quantities $A_{i,i',n,n'}$ (5.29) yield

$$\begin{aligned} A_{i,i',n,n'} &= \delta_{i,i'}\frac{1}{T}\sum_{m=-\infty}^{+\infty}\left|P\left(\frac{n'}{N_{FFT}T}+\frac{m}{T}\right)\right|^2 e^{j2\pi\epsilon_{i,n'}\left(\frac{n'}{N_{FFT}}+m\right)}\cdot\\ &\quad D\left(\frac{n'-n}{N_{FFT}}+\left(\frac{n'}{N_{FFT}}+m\right)\frac{\Delta T_{n'}}{T}\right) \end{aligned} \tag{5.68}$$

A similar analysis as for OFDM and downlink OFDMA shows that a clock frequency offset introduces an attenuation and rotation of the useful component and intercarrier interference at the outputs of the FFT. For carriers outside the rolloff area, the quantities $A_{i,i',n,n'}$ (5.68) are given by

$$A_{i,i',n,n'} = \delta_{i,i'}e^{j2\pi\epsilon_{i,n'}\frac{\mathrm{mod}(n';N_{FFT})}{N_{FFT}}}D\left(\frac{n'-n}{N_{FFT}}+\left(\frac{\mathrm{mod}(n';N_{FFT})}{N_{FFT}}\right)\frac{\Delta T_{n'}}{T}\right) \tag{5.69}$$

The MMSE equaliser coefficients for these carriers are given by (5.57), where $C_{\Delta T,n}$ is a real-valued positive factor that depends on the clock frequency offsets $\Delta T_n/T, n = 0, ..., N_{FFT}-1$ and the carrier index n. In general, this factor differs from the corresponding factor $C_{\Delta T,n}$ for OFDM and uplink OFDMA. When the contributions of the different users are affected by the same clock frequency offset, the results for uplink OFDMA are the same as for OFDM and downlink OFDMA.

In the following, we consider the case that all contributions exhibit the same clock frequency offset $\Delta T/T$. The upper bound (5.64) on the degradation is shown as function of the carrier index n in figure 5.22. We observe that the

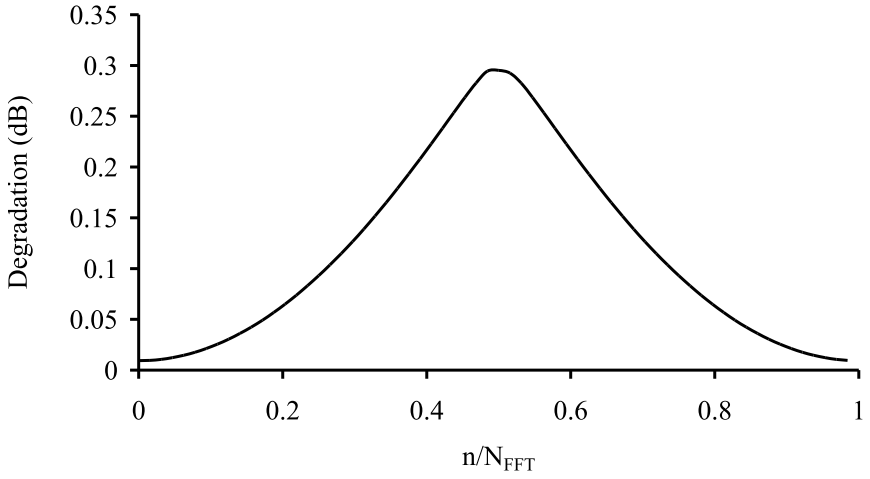

Figure 5.22: Clock frequency offset: dependency on the carrier index, $SNR(0) =$ 20 dB, $N_{FFT} = 64, N_{FFT}\Delta T/T = 10^{-2}$

Table 5.3: Mean square deviation of the samples at the input of the decision device

Theoretical	Simulations
$4.27E-2$	$4.09E-2$

maximum degradation occurs for $n = N_{FFT}/2$. In figure 5.23, the maximum degradation (at $n = N_{FFT}/2$) and the upper bound (5.66) on the degradation of the average SNR are shown as function of the product $N_{FFT}\Delta T/T$. As we observe in figure 5.23, the OFDM(A) system is very sensitive to a clock frequency offset. If we want to obtain small degradations, the clock frequency offset must be limited, i.e., $\Delta T/T \ll 1/N_{FFT}$. In this case, the degradation is essentially proportional to $(N_{FFT}\Delta T/T)^2$.

The OFDM(A) system has been simulated in the absence of additive noise ($N_0 = 0$), for $\alpha = 0, N_{FFT} = 64$ carriers modulated with QPSK symbols and assuming all carriers are modulated with data symbols having the same energy per symbol E_s. The clock frequency offset $\Delta T/T$ is the same for all carriers. In figure 5.24, the scatter diagram is shown for $\Delta T/T = 2.10^{-3}$, in the case of all carriers modulated. The displacement of the constellation points is caused by the dominating ICI component. The scatter diagram shows a circular cloud, as the ICI term has uncorrelated real and imaginary parts, each having the same variance. In table 5.3, the mean square deviation of the samples at the input of the decision device is shown for the simulations of figure 5.24. As we observe, the simulation results agree well with the theoretical results.

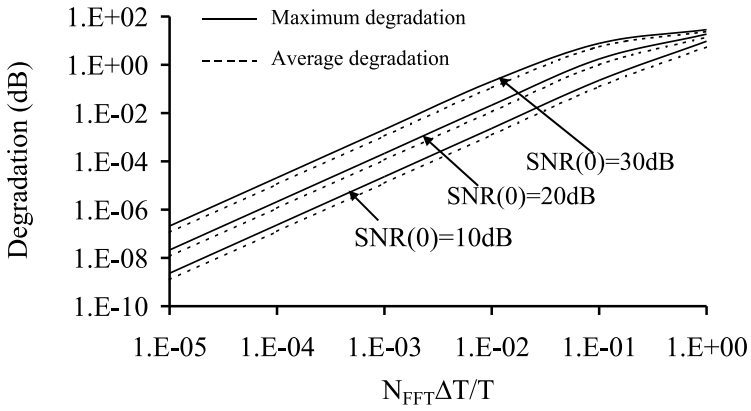

Figure 5.23: Clock frequency offset

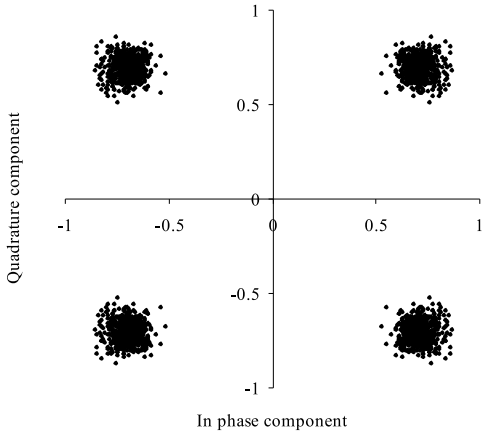

Figure 5.24: Clock frequency offset, all carriers modulated, MMSE equaliser, $\alpha = 0, N_{FFT} = 64, N_{FFT}\Delta T/T = 2.10^{-3}$

When the degradation caused by clock frequency offset can not be tolerated, timing correction must be applied. In OFDM and downlink OFDMA, all carriers have the same clock frequency offset. Hence, the timing can be corrected at the receiver by adjusting the sampling clock or by interpolating in front of the FFT. In uplink OFDMA, each carrier has a different clock frequency offset. As the receiving base station usually has a fixed clock, the clock frequency offsets should be corrected at the transmitters.

Timing Jitter

In order to get rid of a constant timing offset and a clock frequency offset, a timing synchronisation algorithm can be used to extract the timing instants. The residual timing error can be modelled as a zero-mean stationary random process with jitter power spectral density $S_{\epsilon,n}(\exp(j2\pi fT))$ and jitter variance $\sigma^2_{\epsilon,n}$.

In OFDM and downlink OFDMA, where the contributions of the different carriers are aligned, the timing jitter process $\epsilon_{i(N_{FFT}+\nu)+k}$ is the same for all transmitted carriers. For small jitter variances, the quantities $A_{i,i',n,n'}$ (5.23) can be approximated by

$$A_{i,i',n,n'} \approx \delta_{i,i'} \left(\delta_{n,n'} + j2\pi S_{n'} \frac{1}{N_{FFT}} \sum_{k=0}^{N_{FFT}-1} e^{-j2\pi \frac{k(n-n')}{N_{FFT}}} \epsilon_{i(N_{FFT}+\nu)+k} \right) \tag{5.70}$$

where

$$S_n = \frac{1}{T} \sum_{m=-\infty}^{+\infty} \left(\frac{n}{N_{FFT}T} + \frac{m}{T} \right) \left| P\left(\frac{n}{N_{FFT}T} + \frac{m}{T} \right) \right|^2 \tag{5.71}$$

Hence, timing jitter gives rise to interference at the output of the FFT. When the timing jitter rapidly varies as compared to the averaging time of the MMSE equaliser, the equaliser is not able to track the timing jitter. The equaliser averages the variations caused by the timing jitter. For small jitter variances, the average of $\exp(j2\pi\epsilon_{i(N_{FFT}+\nu)+k}\text{mod}(n;N_{FFT})/N_{FFT})$ can be approximated by $E[\exp(j2\pi\epsilon_{i(N_{FFT}+\nu)+k}\text{mod}(n;N_{FFT})/N_{FFT})] \approx E[1 + j2\pi\epsilon_{i(N_{FFT}+\nu)+k}\text{mod}(n;N_{FFT})/N_{FFT}] = 1$. Hence, the equaliser is essentially the same as in the absence of timing errors, i.e., $g_{i,n} \approx C_n$ where C_n is defined in (5.33). In this case, the powers of the average useful component, the self-interference, the intercarrier interference (5.17) and the noise (5.15) at the input of the decision device yield

$$\begin{aligned}
P_{U,n} &= |C_n|^2 \\
P_{SI,n} &= |C_n|^2 (2\pi)^2 |S_n|^2 \int_{-1/2T}^{+1/2T} S_\epsilon(e^{j2\pi fT}) |D(fT)|^2 df \\
P_{ICI,n} &= |C_n|^2 (2\pi)^2 \sum_{n'=0;n'\neq n}^{N_{FFT}-1} \frac{E_{s,n'}}{E_{s,n}} |S_{n'}|^2 \cdot \\
&\quad \int_{-1/2T}^{+1/2T} S_\epsilon(e^{j2\pi fT}) \left| D\left(fT - \frac{n-n'}{N_{FFT}} \right) \right|^2 df \\
E[|W_{i,n}|^2] &= N_0 |C_n|^2
\end{aligned} \tag{5.72}$$

As we observe in (5.72), the powers depend on the carrier index n, but not on the block index i. Hence, the resulting SNR (5.16) depends on the carrier index n, but is independent of the block index i. In the following, we assume that only

carriers outside the rolloff area are modulated, i.e., $E_{s,n} = 0$ for carriers inside the rolloff area. For carriers outside the rolloff area, the quantities (5.71) yield $S_n = \mathrm{mod}(n; N_{FFT})/N_{FFT}$. When $E_{s,n} = E_s$ for all carriers outside the rolloff area, the equaliser coefficients are independent of the carrier index n ($C_n = C$), and so are the powers of the average useful component and the noise. Let us define the average (over the FFT outputs) powers of the self-interference and the intercarrier interference by

$$\overline{P}_X = \frac{1}{N_{FFT}} \sum_{n=0}^{N_{FFT}-1} P_{X,n}, \qquad X = U, ICI \tag{5.73}$$

An upper bound on $\overline{P}_{SI}$ is obtained by assuming that for $n/(N_{FFT}T)$ inside the rolloff area, $P_{SI,n}$ is given by the second line of (5.72) (whereas the true $P_{SI,n}$ is zero). An upper bound on $\overline{P}_{ICI}$ is obtained by replacing in the third line of (5.68) $E_{s,n'}$ by E_s (instead of zero) for $n'/(N_{FFT}T)$ inside the rolloff area. This yields

$$\begin{aligned} \overline{P}_{SI} &\leq |C|^2 S_{N_{FFT}} \int_{-1/2T}^{+1/2T} S_\epsilon(e^{j2\pi fT}) |D(fT)|^2 df \\ \overline{P}_{ICI} &\leq |C|^2 S_{N_{FFT}} \int_{-1/2T}^{+1/2T} S_\epsilon(e^{j2\pi fT}) (1 - |D(fT)|^2) df \end{aligned} \tag{5.74}$$

where

$$S_{N_{FFT}} = \frac{(2\pi)^2}{N_{FFT}} \sum_{n=0}^{N_{FFT}-1} \left(\frac{\mathrm{mod}(n; N_{FFT})}{N_{FFT}} \right)^2 \tag{5.75}$$

and $D(x)$ is defined in (5.35). The upper bound is reached for a transmit pulse with zero rolloff ($\alpha = 0$). Considering figure 5.16, we observe that the average SI power and the average ICI power mainly consist of the low frequency components ($|f| < 1/(N_{FFT}T)$) and the high frequency components ($|f| > 1/(N_{FFT}T)$) of the jitter power spectral density $S_\epsilon(exp(j2\pi fT))$, respectively. Furthermore, the sum of the powers of the self-interference and the intercarrier interference becomes independent of the spectral contents of the jitter, but only depends on the jitter variance

$$\sigma_\epsilon^2 = \int_{-1/2T}^{+1/2T} S_\epsilon(e^{j2\pi fT}) df \tag{5.76}$$

The average SNR is defined as the ratio of the power of the average useful component to the sum of the average power of the self-interference and the intercarrier interference, and the noise power. The average SNR is independent of the carrier index n and the block index i. It can be verified that the sum (5.75) for a large number of carriers ($N_{FFT} \to \infty$), is independent of the number of carriers N_{FFT} and equals $S_{N_{FFT}} = \pi^2/3$. In this case, the upper bound on the degradation Deg_{Av} of the average SNR as compared to $SNR(0)$ (5.21) is independent of the number of carriers and of the spectral contents of the timing

jitter but only depends on the jitter variance, i.e.,

$$Deg_{Av} \leq 10 \log \left(1 + SNR(0) \frac{\pi^2}{3} \sigma_\epsilon^2 \right) \tag{5.77}$$

where $SNR(0) = (N_{FFT}/(N_{FFT}+\nu))E_s/N_0$. Further, for zero rolloff ($\alpha = 0$), it can be shown that for the case of uncorrelated timing jitter ($S_\epsilon(\exp(j2\pi fT)) = \sigma_\epsilon^2 T$), the upper bound on the degradation Deg_n (5.22) is the same for all carriers and given by the right hand side of (5.74). In addition, the maximum degradation Deg_{Max}, which is the maximum over all carriers and all jitter spectra, corresponds to the carrier index $n = N_{FFT}/2$ and the jitter power spectral density $S_\epsilon(\exp(j2\pi fT)) = \sigma_\epsilon^2 \delta(f)$ and is independent of the number of carriers

$$Deg_{Max} \leq 10 \log \left(1 + SNR(0) \pi^2 \sigma_\epsilon^2 \right) \tag{5.78}$$

The degradation (5.78) yields an upper bound on the actual maximum degradation when $\alpha \neq 0$ and the carriers inside the rolloff area are not modulated. The degradations (5.77) and (5.78) yield an accurate approximation for the actual degradations when the rolloff area is small.

In the case of uplink OFDMA, all transmitted carriers are affected by a different timing jitter process $\epsilon_{i(N_{FFT}+\nu)+k,n}$. For small jitter variances, the quantities $A_{i,i',n,n'}$ (5.23) can be approximated by

$$A_{i,i',n,n'} = \delta_{i,i'} \left(\delta_{n,n'} + j2\pi S_{n'} \frac{1}{N_{FFT}} \sum_{k=0}^{N_{FFT}-1} e^{-j2\pi \frac{k(n-n')}{N_{FFT}}} \epsilon_{i(N_{FFT}+\nu)+k,n'} \right) \tag{5.79}$$

Following a similar analysis as for OFDM and downlink OFDMA, it can be verified that the MMSE equaliser is essentially equal to C_n (5.33) for small jitter variances. The powers of the average useful component and the noise are identical as for OFDM and downlink OFDMA and are given by (5.72). The powers of the self-interference and the intercarrier interference yield

$$\begin{aligned} P_{SI,n} &= |C_n|^2 (2\pi)^2 |S_n|^2 \int_{-1/2T}^{+1/2T} S_{\epsilon,n}(e^{j2\pi fT}) |D(fT)|^2 df \\ P_{ICI,n} &= |C_n|^2 (2\pi)^2 \sum_{n'=0;n' \neq n}^{N_{FFT}-1} \frac{E_{s,n'}}{E_{s,n}} |S_{n'}|^2 \cdot \\ &\quad \int_{-1/2T}^{+1/2T} S_{\epsilon,n'}(e^{j2\pi fT}) \left| D\left(fT - \frac{n-n'}{N_{FFT}} \right) \right|^2 df \end{aligned} \tag{5.80}$$

It is clear that, when the different timing jitter processes have the same jitter power spectral density $S_\epsilon(\exp(j2\pi fT))$ and jitter variance σ_ϵ^2, the results are the same as for OFDM and downlink OFDMA. For small jitter variance, the degradation is essentially proportional to σ_ϵ^2.

In figure 5.25, the degradation of the average SNR (5.77) and the maximum degradation (5.78) at $SNR(0) = 20$ dB are shown as function of the jitter

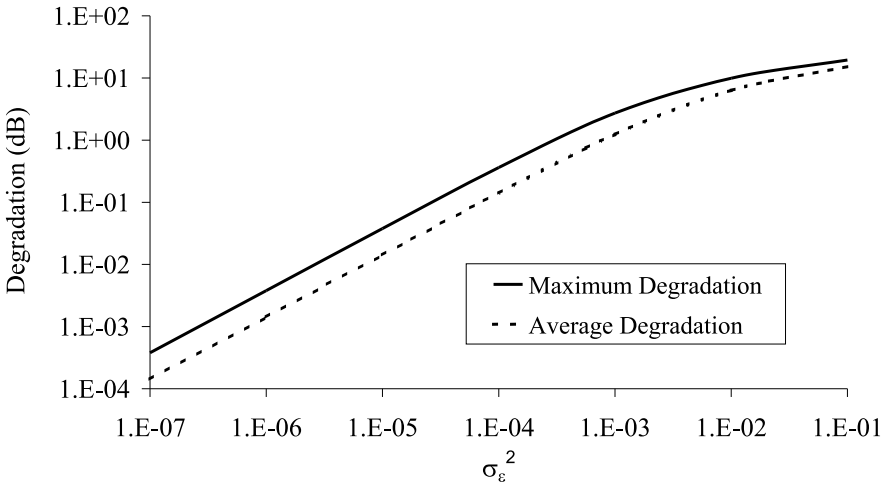

Figure 5.25: Timing jitter, $E_{s,n} = E_s$, all carriers outside rolloff modulated, MMSE equaliser, $N_{FFT} \to \infty, SNR(0) = 20$ dB

variance. These degradations are independent of the number of carriers. For small jitter variance, the degradations are essentially proportional to the jitter variance σ_ϵ^2.

We have simulated the OFDM(A) system in the absence of additive noise ($N_0 = 0$), for $\alpha = 0$, all $N_{FFT} = 64$ carriers are modulated with data symbols belonging to the QPSK constellation and the energy per symbol is equal for all carriers. The timing jitter is the same for all carriers. The shape of the jitter power spectral density is shown in figure 5.18, and the jitter variance σ_ϵ^2 equals 10^{-3} rad^2. In figures 5.26 and 5.27, the scatter diagrams are shown for $f_L = 0, f_B = 1/(N_{FFT}T)$ and $f_L = 1/(N_{FFT}T), f_B = 2/(N_{FFT}T)$, respectively. As is observed, the scatter diagrams differ considerably, although the mean-square deviation of the samples at the input of the decision device and the constellation points is the same for both cases. This can be explained as follows. In the case of $f_L = 0, f_B = 1/(N_{FFT}T)$, the dominant interference term is the self-interference. As the timing jitter is slowly varying, the timing jitter gives mainly rise to a random carrier-dependent phase rotation of the useful component. Hence, the samples at the input of the decision device show an angular displacement as compared to the constellation points. In the case of $f_L = 1/(N_{FFT}T), f_B = 2/(N_{FFT}T)$, the interference is dominated by the inter-carrier interference. This interference term has uncorrelated real and imaginary parts, each having the same variance. Hence, this term yields the circular clouds in the scatter diagram. In table 5.4, the mean square deviation of the samples at the input of the decision device is shown for the simulations of figures 5.26 and 5.27. As we observe, the simulation results agree well with the theoretical

results.

5.5 Dispersive Channel

In the previous section, we have investigated the effect of the synchronisation errors on the OFDM(A) system in the case of an ideal channel. In this section, we study the influence of the synchronisation errors in the presence of a dispersive channel. In our analysis, we assume that the channel transfer function is the same for all users. Furthermore, we consider the case of synchronous transmission, i.e., all carriers exhibit the same carrier phase errors and timing errors. The transmit and receiver filters are square-root raised-cosine filters with rolloff α. Furthermore, the cyclic prefix is able to cope with the dispersive channel and the timing errors, such that no interference between successive transmitted OFDM(A) blocks is introduced. We assume that the carriers inside the rolloff area are not used and all carriers outside the rolloff area are modulated and have the same energy per symbol E_s.

5.5.1 No Synchronisation Errors

In the case of a fixed dispersive channel, i.e., $H_{ch}(f;\tau) = H_{ch}(f)$, the quantity (5.14) for carriers outside the rolloff area and in the absence of synchronisation errors yields

$$A_{i,i',n,n'} = \delta_{i,i'}\delta_{n,n'}G_n \tag{5.81}$$

where

$$G_n = H_{ch}\left(\frac{\mathrm{mod}(n;N_{FFT})}{N_{FFT}T}\right) \tag{5.82}$$

We observe from (5.81) that the dispersive channel does not yield interference, but only causes a scaling and rotation of the FFT outputs, that depends on the channel characteristics. The MMSE equaliser has equaliser coefficients

$$(g_{MMSE})_{i,n} = C_{ch,n}G_n^* \tag{5.83}$$

where $C_{ch,n}$ is a real-valued positive factor that depends on the channel characteristics at the carrier frequency $n/(N_{FFT}T)$. The amplitude and phase of the equaliser coefficients (5.83) depend on the carrier index n. Note that the phase of the equaliser compensates for the phase rotation introduced by the channel. The signal-to-noise ratio (5.16) at the nth FFT output is given by

$$SNR_n(0) = \frac{N_{FFT}}{N_{FFT}+\nu}\frac{E_s}{N_0}|G_n|^2 \tag{5.84}$$

and the degradation (5.22) of the SNR as compared to SNR(0) (5.21) caused by the dispersive channel yields

$$Deg_n = -10\log|G_n|^2 \tag{5.85}$$

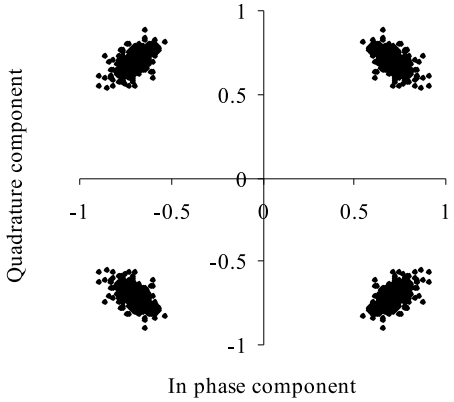

Figure 5.26: Timing jitter, all carriers modulated, $\alpha = 0, f_L = 0, f_B = 1/(N_{FFT}T), N_{FFT} = 64, \sigma_\epsilon^2 = 10^{-3}$ rad^2

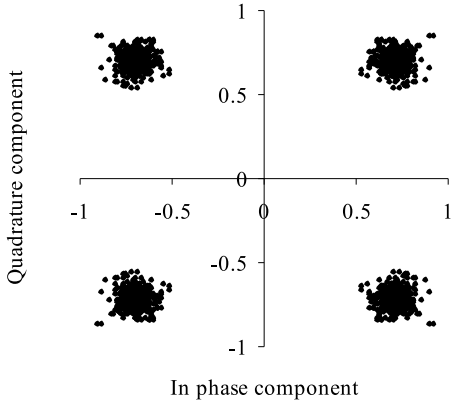

Figure 5.27: Timing jitter, all carriers modulated, $\alpha = 0, f_L = 1/(N_{FFT}T), f_B = 2/(N_{FFT}T), N_{FFT} = 64, \sigma_\epsilon^2 = 10^{-3}$ rad^2

Table 5.4: Mean square deviation of the samples at the input of the decision device

	Theoretical	Simulations
$f_L = 0, f_B = 1/(N_cT) = R_s$	$3.290E-3$	$3.205E-3$
$fL = 1/(N_cT) = R_s, fB = 2/(N_cT) = 2R_s$	$3.290E-3$	$3.285E-3$

Hence, the performance of the OFDM(A) system depends on the carrier index, but is independent of the block index i.

When the transfer function $H_{ch}(f;\tau)$ of a fading channel slowly varies as compared to the OFDM(A) block length, the channel transfer function during an OFDM(A) block can be viewed as a fixed channel. In this case, the former expressions for the fixed channel can be used, where the quantity (5.82) is replaced by

$$G_{n,i} = H_{ch}\left(\frac{\mathrm{mod}(n;N_{FFT})}{N_{FFT}T};t_{i(N_{FFT}+\nu)}\right) \tag{5.86}$$

In this case, the SNR (5.84) depends on the block index i.

In the following, we study the effect of the synchronisation errors on the performance of the OFDM(A) system in the presence of a fixed dispersive channel. In general, the synchronisation errors cause interference. Hence, it can be expected that the synchronisation errors give rise to a performance degradation as compared to the case of the dispersive channel without synchronisation errors. In the computations, we make use of a fixed dispersive channel with an exponentially decaying impulse response. The channel transfer function is given by

$$H_{ch}(f) = \frac{A}{a + j2\pi f} \tag{5.87}$$

where A is a constant of normalisation, such that the received energy per symbol is the same as the transmitted energy per symbol (for a fair comparison with the ideal channel $H_{ch}(f) = 1$) and a is the 3dB bandwidth of the channel. The amplitude of the channel transfer function (5.87) is maximum for $f = 0$ and decreases for increasing $|f|$. Figure 5.28 shows the degradation (5.85) as function of the carrier index n, for $N_{FFT} = 64$ and $SNR(0) = 20$ dB. As we observe, the maximum degradation occurs for $n = N_{FFT}/2$ (where the amplitude of the channel transfer function is minimum) and the minimum degradation occurs for $n = 0$ (where the amplitude of the channel transfer function is maximum). Note that, as for some carriers $|H_{ch}(n/(N_{FFT}T))| > 1$, the degradation for these carriers is negative. In the following, we consider in the figures only the degradations caused by the synchronisation errors for the carrier indices $n = 0$ and $n = N_{FFT}/2$, corresponding with the minimum and maximum degradation, respectively.

5.5.2 Carrier Phase Errors

In this section, we investigate the effect of the carrier phase errors on the OFDM(A) system in the presence of a dispersive channel, but in the absence of timing errors. In this case, the quantities (5.24) are given by

$$G_n(t_{i(N_{FFT}+\nu)+k}) = G_n e^{j\phi(t_{i(N_{FFT}+\nu)+k})} \tag{5.88}$$

where G_n is defined in (5.82). In the following, we separately consider the cases of a constant phase offset, a carrier frequency offset and carrier phase jitter.

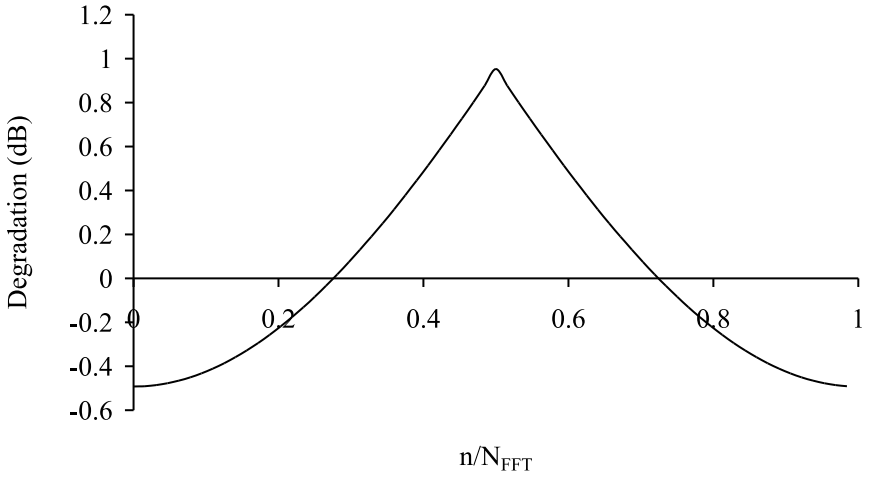

Figure 5.28: Degradation caused by the dispersive channel, $a = 5, N_{FFT} = 64$ and $SNR(0) = 20$ dB

Constant Phase Offset

In the case of the dispersive channel and in the presence of a constant phase offset, the quantities (5.23) reduce to

$$A_{i,i',n,n'} = \delta_{i,i'}\delta_{n,n'}G_n e^{j\phi} \tag{5.89}$$

Hence, the constant phase offset gives rise to a phase rotation of the FFT outputs over a carrier independent angle ϕ, as compared to the case of a zero phase offset. Furthermore, no intercarrier interference is introduced. Hence, a constant phase offset rotates the samples at the input of the decision device when no correction is applied ($g_{i,n} = 1$), resulting in a reduction of the noise margin, as shown in section 5.4.1. The MMSE equaliser compensates for this phase rotation:

$$(g_{MMSE})_{i,n} = C_{ch,n}e^{-j\phi} \tag{5.90}$$

where $C_{ch,n}$ are the MMSE equaliser coefficients in the absence of synchronisation errors, as defined in (5.83). The phase rotation of the FFT outputs over an angle $-\phi$ introduces no enhancement of the noise power level as compared to the case of a zero phase offset. Hence, a constant phase offset is compensated without loss of performance. These results correspond to the results found for the ideal channel in section 5.4.1.

Carrier Frequency Offset

In the case of a dispersive channel and a carrier frequency offset, the quantities (5.23) yield

$$A_{i,i',n,n'} = \delta_{i,i'} G_{n'} e^{j2\pi\Delta FTi(N_{FFT}+\nu)} D\left(\frac{n'-n}{N_{FFT}} + \Delta FT\right) \tag{5.91}$$

where $D(x)$ is defined in (5.35). Hence, a carrier frequency offset introduces a systematic phase rotation at a constant speed of $2\pi\Delta FT(N_{FFT}+\nu)$ rad/symbol of the samples at the output of the FFT. Furthermore, the carrier frequency offset causes a reduction of the useful component as compared to the case of a zero carrier frequency offset and introduces intercarrier interference. The MMSE equaliser for carriers outside the rolloff area has equaliser coefficients

$$(g_{MMSE})_{i,n} = C_{\Delta F,n} e^{-j2\pi\Delta F_n Ti(N_{FFT}+\nu)} G_n^* D^*(\Delta F_n T) \tag{5.92}$$

where $C_{\Delta F,n}$ is a real-valued positive factor that depends on the carrier frequency offset, the channel characteristics and the carrier index n. Hence, the equaliser compensates for the systematic phase rotation of the useful component. However, the equaliser is not able to eliminate the ICI. The resulting powers of the average useful component, the intercarrier interference power (5.17) and the noise (5.15) are independent of the block index i and yield

$$\begin{aligned} P_{U,n} &= |C_{\Delta F,n}|^2 \left(|G_n|^2 B_{0,0}\right)^2 \\ P_{ICI,n} &= |C_{\Delta F,n}|^2 |G_n|^2 B_{0,0} \sum_{n'=0;n'\neq n}^{N_{FFT}-1} \frac{E_{s,n'}}{E_{s,n}} |G_{n'}|^2 B_{n,n'} \\ E[|W_{i,n}|^2] &= N_0 |C_{\Delta F,n}|^2 |G_n|^2 B_{0,0} \end{aligned} \tag{5.93}$$

where $B_{n,n'}$ is given by

$$B_{n,n'} = \left| D\left(\frac{n'-n}{N_{FFT}} + \Delta FT\right) \right|^2$$

In (5.93), the energy per symbol $E_{s,n}$ equals $E_{s,n} = E_s$ for carriers outside the rolloff area and equals $E_{s,n} = 0$ for carriers inside the rolloff area. The resulting SNR (5.16) yields

$$SNR_n = \frac{SNR_n(0) B_{0,0}}{1 + \sum_{n'=0;n'\neq n}^{N_{FFT}-1} SNR_{n'}(0) B_{n,n'}} \tag{5.94}$$

where $SNR_n(0)$ is given by (5.84). It is observed in (5.94) that the SNR depends on the carrier index n. Furthermore, considering the SNR (5.84) in the absence of synchronisation errors, the carrier frequency offset gives rise to an additional degradation ΔDeg as compared to the case of a zero carrier frequency offset

$$\Delta Deg = -10 \log B_{0,0} + 10 \log \left(1 + \sum_{n'=0;n'\neq n}^{N_{FFT}-1} SNR_{n'}(0) B_{n,n'}\right) \tag{5.95}$$

An upper bound for the additional degradation can be found in a similar way as for the ideal channel. This yields

$$\Delta Deg \leq -10\log B_{0,0} + 10\log\left(1 + SNR(0)\sum_{n'=0;n'\neq n}^{N_{FFT}-1}|G_{n'}|^2 B_{n,n'}\right) \quad (5.96)$$

where $SNR(0) = (N_{FFT}/(N_{FFT}+\nu))E_s/N_0$. The upper bound is reached when the transmit pulse has zero rolloff ($\alpha = 0$). The upper bound on the additional degradation is a function of the product $N_{FFT}\Delta FT$ and the carrier index n. The upper bound on the additional degradation (5.96) yields an accurate approximation for the actual degradation when the rolloff area is small.

In figure 5.29, the upper bound (5.96) on the additional degradation is shown as function of the product $N_{FFT}\Delta FT$ for the fixed channel with transfer function (5.87), $SNR(0) = 20$ dB and for the carrier indices $n = 0$ and $n = N_{FFT}/2$, yielding the minimum and maximum degradation in the case of the dispersive channel without synchronisation errors, respectively. We observe that this additional degradation is essentially independent of the carrier index and the channel transfer function. In figure 5.30, the total degradation (i.e., the degradation of the SNR as compared to $SNR(0)$ caused by the dispersive channel and the carrier frequency offset) corresponding to the carrier $n = N_{FFT}/2$, i.e., the maximum total degradation, is shown as function of the product $N_{FFT}\Delta FT$, for the ideal channel and the dispersive channel and under the same conditions as for figure 5.29. For small frequency offsets, the total degradation is essentially independent of the carrier frequency offset. In this case, the effect of the carrier frequency offset is negligible as compared to the effect of the dispersive channel. For larger $N_{FFT}\Delta FT$, the total degradation essentially coincide with the degradation for the ideal channel: now the total degradation is mainly caused by the carrier frequency offset. Comparing these results with those found in section 5.4.1 for the case of the ideal channel, we observe that the influence of the carrier frequency offset is essentially the same in an ideal channel as in a dispersive channel.

Carrier Phase Jitter

In the case of a dispersive channel, the quantities (5.23) can be approximated for small jitter variance by

$$A_{i,i',n,n'} = \delta_{i,i'}G_{n'}\left(\delta_{n,n'} + \frac{1}{N_{FFT}}\sum_{k=0}^{N_{FFT}-1} j\phi(t_{i(N_{FFT}+\nu)+k})e^{-j2\pi\frac{k(n-n')}{N_{FFT}}}\right) \quad (5.97)$$

We observe from (5.97) that the carrier phase jitter introduces self-interference and intercarrier interference at the outputs of the FFT. When the carrier phase jitter rapidly varies as compared to the averaging time of the MMSE equaliser, the equaliser is not able to track the carrier phase jitter. The equaliser averages

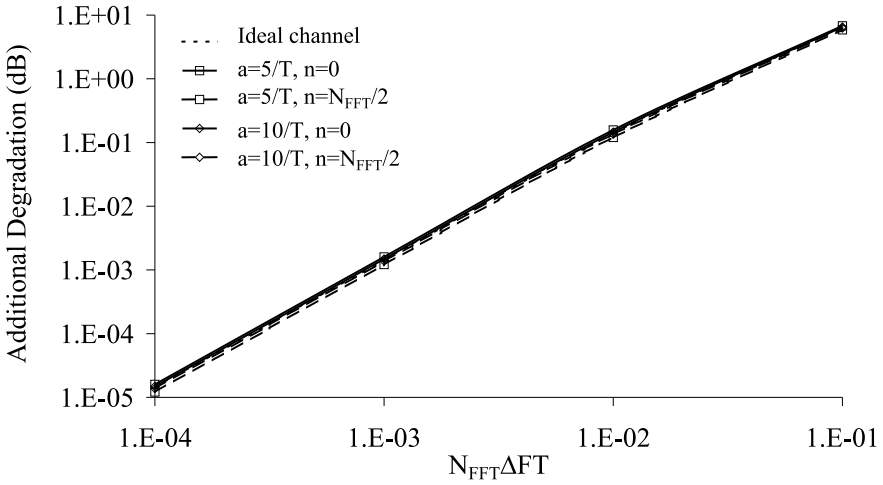

Figure 5.29: Additional degradation caused by carrier frequency offset, $SNR(0) = 20$ dB

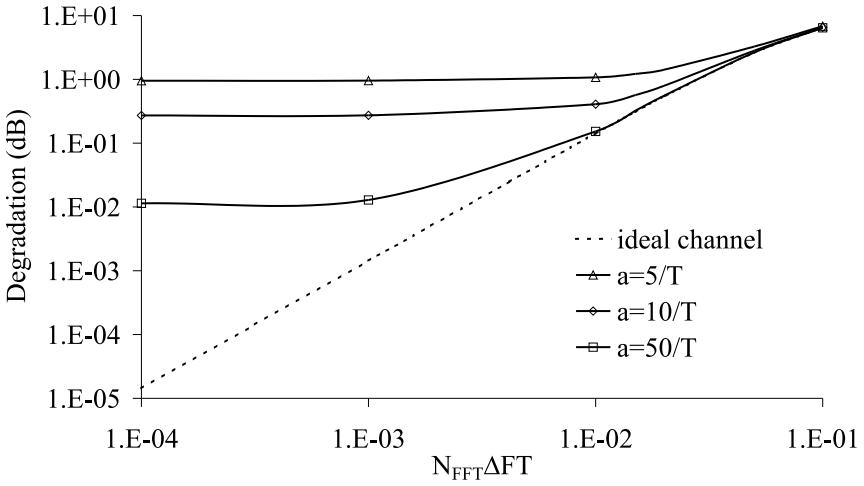

Figure 5.30: Maximum total degradation caused by dispersive channel and carrier frequency offset, $SNR(0) = 20$ dB

the variations caused by the carrier phase jitter. As for small jitter variances, the average of $\exp(j\phi(t))$ can be approximated by $E[\exp(j\phi(t))] \approx E[1+j\phi(t)] = 1$, the MMSE equaliser is essentially the same as in the absence of synchronisation errors and are given by (5.83). The powers of the average useful component, the self-interference, the intercarrier interference (5.17) and the noise (5.15) at the input of the decision device are independent of the block index i and are given by

$$\begin{aligned} P_{U,n} &= |C_{ch,n}|^2|G_n|^2 \\ P_{SI,n} &= |C_{ch,n}|^2|G_n|^2 B_{0,0} \\ P_{ICI,n} &= |C_{ch,n}|^2|G_n|^2 \sum_{n'=0;n'\neq n}^{N_{FFT}-1} \frac{E_{s,n'}}{E_{s,n}} |G_{n'}|^2 B_{n,n'} \\ E[|W_{i,n}|^2] &= N_0|C_{ch,n}|^2 \end{aligned} \tag{5.98}$$

where $B_{n,n'}$ is given by

$$B_{n,n'} = \int_{-\infty}^{+\infty} S_\phi(f) \left| D\left(\frac{n'-n}{N_{FFT}} + fT\right) \right|^2 df$$

and $D(x)$ is defined in (5.35). In (5.98), the energy per symbol $E_{s,n}$ equals $E_{s,n} = E_s$ for carriers outside the rolloff area and equals $E_{s,n} = 0$ for carriers inside the rolloff area. The resulting SNR (5.16) yields

$$SNR_n = \frac{SNR_n(0)}{1 + \sum_{n'=0;n'\neq n}^{N_{FFT}-1} SNR_{n'}(0) B_{n,n'}} \tag{5.99}$$

where $SNR_n(0)$ is given by (5.84). The SNR (5.99) is independent of the block index i. Considering the SNR (5.84) in the absence of synchronisation errors, the carrier phase jitter causes an additional degradation

$$\Delta Deg_n = 10 \log \left(1 + \sum_{n'=0;n'\neq n}^{N_{FFT}-1} SNR_{n'}(0) B_{n,n'} \right) \tag{5.100}$$

that depends on the carrier index n. An upper bound for the degradation can be found in a similar way as for the ideal channel. This yields

$$\Delta Deg_n \leq 10 \log \left(1 + SNR(0) \sum_{n'=0;n'\neq n}^{N_{FFT}-1} |G_{n'}|^2 B_{n,n'} \right) \tag{5.101}$$

where $SNR(0) = (N_{FFT}/(N_{FFT}+\nu))E_s/N_0$. The upper bound is reached when the transmit pulse has zero rolloff ($\alpha = 0$). It can be verified that the upper bound (5.101) on the additional degradation is essentially independent of N_{FFT} when the number of carriers is large. The upper bound (5.101) on the degradation yields an accurate approximation of the actual additional degradation when the rolloff area is small.

The upper bound (5.101) on the additional degradation caused by the carrier phase jitter is shown in figure 5.31 as function of the jitter variance, for the fixed dispersive channel with transfer function (5.87), a jitter power spectral density as shown in figure 5.16 with $f_L = 0, f_B = 2/(N_{FFT}T)$, for $SNR(0) = 20$ dB and for the carrier indices $n = 0$ and $n = N_{FFT}/2$, where the total degradation for the case of the dispersive channel without synchronisation errors is minimum and maximum, respectively. As is observed, the curves of the additional degradation in the case of the dispersive channel are essentially independent of the carrier index and the channel transfer function. In figure 5.32, the total degradation (i.e., the degradation of the SNR as compared to $SNR(0)$ caused by the dispersive channel and the carrier phase jitter) for the carrier $n = N_{FFT}/2$ is shown as function of the jitter variance under the same conditions as for figure 5.31. As is observed, the total degradation is essentially independent of the jitter variance for small jitter variances: the dominating effect is the dispersive channel. For larger jitter variances, the total degradation essentially coincides with the degradation for the ideal channel. Hence, for large jitter variances, the jitter becomes the dominating effect. Comparing the results in the case of a dispersive channel, we observe that the results are essentially the same as in the case of an ideal channel, considered in section 5.4.1.

5.5.3 Timing Errors

In this section, we investigate the influence of the timing errors on the OFDM(A) system in the presence of a dispersive channel, but in the absence of carrier phase errors. In this case, the quantities (5.24) yield

$$G_n(t_{i(N_{FFT}+\nu)+k}) = G_n e^{j2\pi\epsilon_{i(N_{FFT}+\nu)+k}\frac{\mathrm{mod}(n;N_{FFT})}{N_{FFT}}} \tag{5.102}$$

where G_n is defined by (5.82). In the following sections, we separately consider the cases of a constant timing offset, a clock frequency offset and timing jitter.

Constant Timing Offset

Taking into account that there are no carriers modulated in the rolloff area, the quantities (5.23) yield

$$A_{i,i',n,n'} = \delta_{i,i'}\delta_{n,n'}G_n e^{j2\pi\epsilon\frac{\mathrm{mod}(n;N_{FFT})}{N_{FFT}}} \tag{5.103}$$

Hence, the timing offset introduces a carrier dependent phase rotation of the FFT outputs as compared to a zero timing offset. The equaliser that minimises the MSE has equaliser coefficients $(g_{MMSE})_{i,n} = C_{ch,n}\exp(-j2\pi\epsilon\mathrm{mod}(n;N_{FFT})/N_{FFT})$, where $C_{ch,n}$ are the MMSE equaliser coefficients in the absence of synchronisation errors, as defined in (5.83). A phase rotation of the FFT outputs causes no noise power level enhancement as compared to the case of a zero timing offset. Hence, the OFDM(A) system is

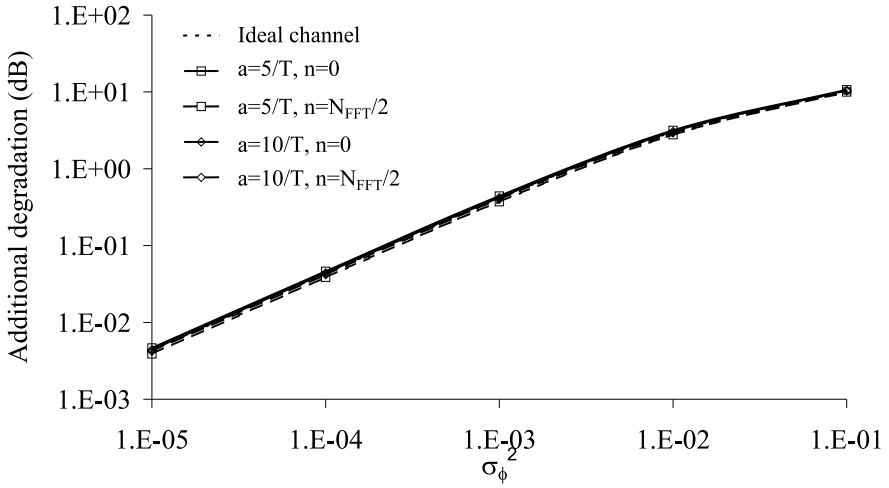

Figure 5.31: Additional degradation caused by carrier phase jitter, $N_{FFT} = 64, SNR(0) = 20$ dB

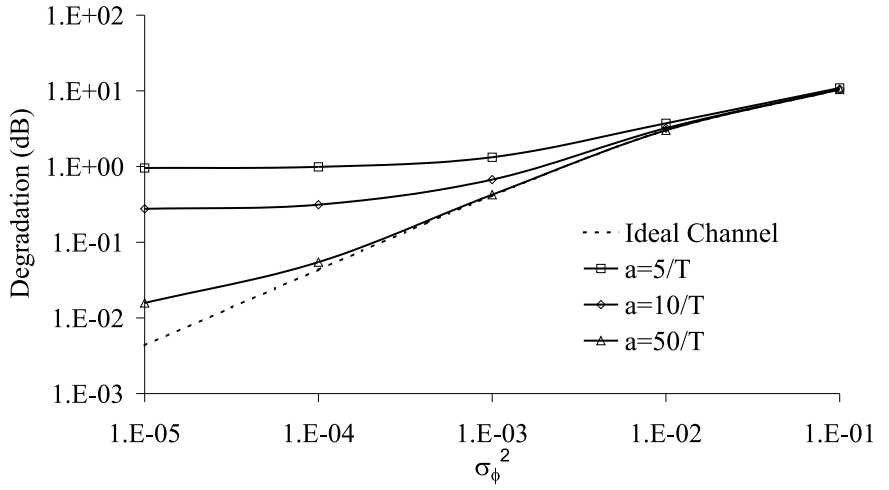

Figure 5.32: Maximum total degradation caused by dispersive channel and carrier phase jitter, $N_{FFT} = 64, SNR(0) = 20$ dB

not degraded by a constant timing offset, as compared to the case of a zero timing offset. It can be verified that carriers inside the rolloff area are subjected to a performance degradation caused by the constant timing offset. To avoid this degradation, the carriers inside the rolloff area should not be used. These results are very similar to the results obtained for an ideal channel (section 5.4.2).

Clock Frequency Offset

When the increasing misalignment of the FFT blocks, caused by the clock frequency offset $\Delta T/T$, is compensated by a coarse synchronisation algorithm as described in section 5.4.2, the resulting timing error is given by $\tilde{\epsilon}_{i(N_{FFT}+\nu)+k} = k\Delta T/T + \epsilon_i$. Hence, the quantities (5.23) for the carriers outside the rolloff area are given by

$$A_{i,i',n,n'} = \delta_{i,i'} G_{n'} e^{j2\pi\epsilon_i \frac{\mathrm{mod}(n';N_{FFT})}{N_{FFT}}} D\left(\frac{n'-n}{N_{FFT}} + \left(\frac{\mathrm{mod}(n';N_{FFT})}{N_{FFT}}\right)\frac{\Delta T}{T}\right) \tag{5.104}$$

where $D(x)$ is defined in (5.35). It is observed from (5.104) that a clock frequency offset introduces intercarrier interference. Furthermore, the useful component is subjected to a phase rotation and amplitude reduction as compared to the case of a zero clock frequency offset. The MMSE equaliser for the carriers outside the rolloff has equaliser coefficients

$$(g_{MMSE})_{i,n} = C_{\Delta T,n} G_n^* D^* \left(\frac{\mathrm{mod}(n;N_{FFT})}{N_{FFT}}\frac{\Delta T}{T}\right) e^{-j2\pi\epsilon_i \frac{\mathrm{mod}(n;N_{FFT})}{N_{FFT}}} \tag{5.105}$$

where $C_{\Delta T,n}$ is a real-valued positive factor that depends on the carrier index n and the clock frequency offset $\Delta T/T$. Hence, the equaliser is not able to eliminate the ICI. The powers of the average useful component, the intercarrier interference (5.17) and the noise (5.15) at the input of the decision device are independent of the block index i and yield

$$\begin{aligned} P_{U,n} &= |C_{\Delta T,n}|^2 |G_n|^2 B_{n,n}^2 \\ P_{ICI,n} &= |C_{\Delta T,n}|^2 B_{n,n} \sum_{n'=0;n'\neq n}^{N_{FFT}-1} \frac{E_{s,n'}}{E_{s,n}} |G_{n'}|^2 B_{n,n'} \\ E[|W_{i,n}|^2] &= N_0 |C_{\Delta T,n}|^2 B_{n,n} \end{aligned} \tag{5.106}$$

where

$$B_{n,n'} = \left| D\left(\frac{n'-n}{N_{FFT}} + \frac{\mathrm{mod}(n';N_{FFT})}{N_{FFT}}\frac{\Delta T}{T}\right)\right|^2$$

In (5.106), the energy per symbol $E_{s,n}$ equals $E_{s,n} = E_s$ for carriers outside the rolloff area and equals $E_{s,n} = 0$ for carriers inside the rolloff area. From (5.106) it follows that the OFDM(A) system is degraded as compared to the case of a

zero clock frequency offset. The resulting SNR (5.16) yields

$$SNR_n = \frac{SNR_n(0)B_{n,n}}{1 + \sum_{n'=0;n'\neq n}^{N_{FFT}-1} SNR_{n'}(0)B_{n,n'}} \tag{5.107}$$

where $SNR_n(0)$ is given by (5.84).The SNR depends on the carrier index n. Considering the SNR (5.84) in the absence of synchronisation errors, the OFDM(A) system suffers from an additional degradation ΔDeg caused by the clock frequency offset as compared to the case of a zero clock frequency offset

$$\Delta Deg = -10\log B_{n,n} + 10\log\left(1 + \sum_{n'=0;n'\neq n}^{N_{FFT}-1} SNR_{n'}(0)B_{n,n'}\right) \tag{5.108}$$

An upper bound for the degradation can be found in the same way as for the ideal channel. This yields

$$\Delta Deg \leq -10\log B_{n,n} + 10\log\left(1 + SNR(0)\sum_{n'=0;n'\neq n}^{N_{FFT}-1} |G_{n'}|^2 B_{n,n'}\right) \tag{5.109}$$

where $SNR(0) = (N_{FFT}/(N_{FFT}+\nu))E_s/N_0$. The upper bound is reached when the transmit pulse has zero rolloff ($\alpha = 0$). The upper bound (5.109) on the additional degradation depends on the carrier index and is a function of the product $N_{FFT}\Delta T/T$ when n/N_{FFT} is a fixed value. The upper bound (5.109) yields an accurate approximation for the actual additional degradation when the rolloff area is small.

In figure 5.33, the upper bound (5.103) on the additional degradation is shown as function of the product $N_{FFT}\Delta T/T$, for the dispersive channel (5.87), $SNR(0) = 20$ dB and for the carrier indices $n = 0$ and $n = N_{FFT}/2$, where the total degradation caused by the dispersive channel is minimum and maximum, respectively. As is observed, the additional degradation depends on the carrier index but is essentially independent of the channel transfer function. For $n = N_{FFT}/2$, the total degradation (i.e., the degradation of the SNR as compared to $SNR(0)$ caused by the dispersive channel and the clock frequency offset) is shown in figure 5.34, under the same conditions as figure 5.33. For a small clock frequency offset, the total degradation is essentially independent of the clock frequency offset. In this case, the effect of the clock frequency offset can be neglected as compared to the effect of the dispersive channel. For increasing clock frequency offset, the total degradation in the case of the dispersive channel essentially coincides with the degradation at $n = N_{FFT}/2$ in the case of the ideal channel. Hence, the clock frequency offset becomes the dominating effect. When we compare these results with the results found for an ideal channel (section 5.4.2), we observe that the results are very similar.

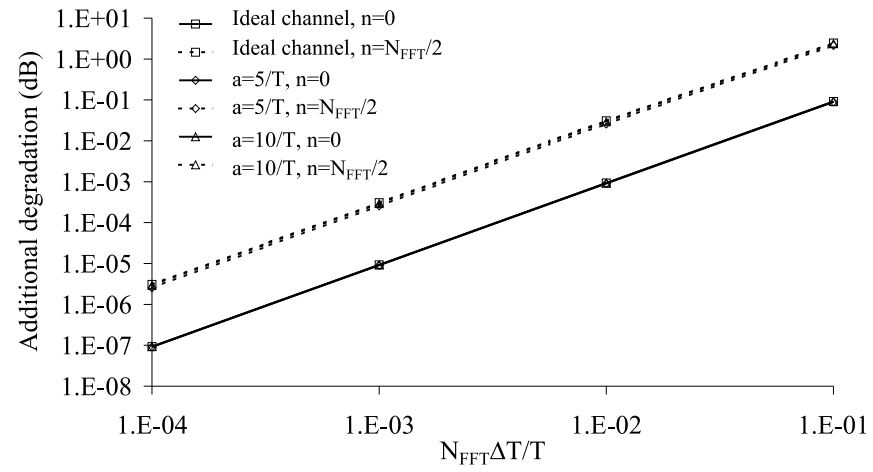

Figure 5.33: Additional degradation caused by clock frequency offset, $SNR(0) = 20$ dB

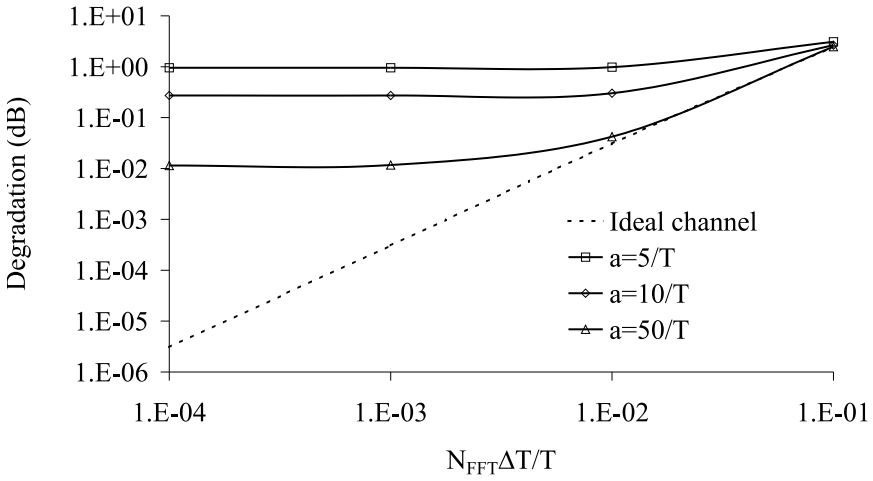

Figure 5.34: Maximum total degradation caused by dispersive channel and clock frequency offset, $SNR(0) = 20$ dB

Timing Jitter

In the case of a dispersive channel, the quantities (5.23) can be approximated for small jitter variances and slowly varying jitter by

$$A_{i,i',n,n'} \approx \delta_{i,i'} G_{n'} \left(\delta_{n,n'} + j2\pi S_{n'} \frac{1}{N_{FFT}} \sum_{k=0}^{N_{FFT}-1} e^{-j2\pi \frac{k(n-n')}{N_{FFT}}} \epsilon_{i(N_{FFT}+\nu)+k} \right) \tag{5.110}$$

The timing jitter introduces self-interference and intercarrier interference at the outputs of the FFT. Similarly as in section 5.4.2, it can be verified that when the timing jitter rapidly varies as compared to the averaging time of the equaliser and the jitter variances are small, the MMSE equaliser is essentially the same as in the absence of timing errors and is given by (5.83). The powers of the average useful component, the self-interference, the intercarrier interference (5.17) and the noise (5.15) at the input of the decision device are independent of the block index i and yield

$$\begin{aligned} P_{U,n} &= |C_{ch,n}|^2 \\ P_{SI,n} &= |C_{ch,n}|^2 (2\pi)^2 |G_n|^2 |S_n|^2 B_{0,0} \\ P_{ICI,n} &= |C_{ch,n}|^2 (2\pi)^2 |G_n|^2 \sum_{n'=0;n'\neq n}^{N_{FFT}-1} \frac{E_{s,n'}}{E_{s,n}} |S_{n'}|^2 |G_{n'}|^2 B_{n,n'} \\ E[|W_{i,n}|^2] &= N_0 |C_{ch,n}|^2 \end{aligned} \tag{5.111}$$

where $B_{n,n'}$ is given by

$$B_{n,n'} = \int_{-1/2T}^{+1/2T} S_\epsilon(e^{j2\pi fT}) \left| D\left(fT - \frac{n-n'}{N_{FFT}} \right) \right|^2 df$$

and $D(x)$ is defined in (5.35) and $S_n = \mathrm{mod}(n; N_{FFT})/N_{FFT}$ for carriers outside the rolloff. In (5.111), the energy per symbol $E_{s,n}$ equals $E_{s,n} = E_s$ for carriers outside the rolloff area and equals $E_{s,n} = 0$ for carriers inside the rolloff area. From (5.111) it follows that the OFDM(A) system is degraded as compared to the case of a zero clock frequency offset. The resulting SNR (5.16) yields

$$SNR_n = \frac{SNR_n(0)}{1 + (2\pi)^2 \sum_{n'=0;n'\neq n}^{N_{FFT}-1} SNR_{n'}(0) |S_{n'}|^2 B_{n,n'}} \tag{5.112}$$

where $SNR_n(0)$ is given by (5.84). The SNR depends on the carrier index n. Comparing (5.84) with (5.112), it is clear that the timing jitter introduces an additional degradation as compared to the case where no timing jitter is present. This yields

$$\Delta Deg_n = 10 \log \left(1 + (2\pi)^2 \sum_{n'=0;n'\neq n}^{N_{FFT}-1} SNR_{n'}(0) |S_{n'}|^2 B_{n,n'} \right) \tag{5.113}$$

The additional degradation depends on carrier index n. An upper bound for the degradation can be found in a similar way as for the ideal channel. This yields

$$\Delta Deg_n \leq 10 \log \left(1 + (2\pi)^2 SNR(0) \sum_{n'=0;n' \neq n}^{N_{FFT}-1} |G_{n'}|^2 |S_{n'}|^2 B_{n,n'} \right) \qquad (5.114)$$

The upper bound is reached when the transmit pulse has zero rolloff ($\alpha = 0$). It can be verified that the upper bound on the additional degradation is essentially independent of N_{FFT} when the number of carriers is large. The upper bound (5.114) on the additional degradation yields an accurate approximation for the actual additional degradation for the carriers outside the rolloff area when the rolloff area is small.

The upper bound (5.114) on the additional degradation is shown in figure 5.35 as function of the jitter variance, for the dispersive channel (5.87), $SNR(0) = 20$ dB, a jitter power spectral density as shown in figure 5.16 with $f_L = 0, f_B = 2/(N_{FFT}T)$ and for the carrier indices $n = 0$ and $n = N_{FFT}/2$, yielding the minimum and maximum total degradation, respectively. It is observed that the curves of the minimum and maximum additional degradation of the dispersive channel essentially coincide with the minimum and maximum degradation in the case of the ideal channel, respectively. Hence, the additional degradation depends on the carrier index, but is essentially independent of the channel transfer function. Furthermore, the total degradation (i.e., the degradation of the SNR as compared to $SNR(0)$ caused by the dispersive channel and the timing jitter) for the carrier $n = N_{FFT}/2$ is shown in figure 5.36 under the same conditions as for figure 5.35. For small jitter variances, the total degradation is essentially independent of the jitter variance: the degradation is mainly caused by the dispersive channel. For increasing jitter variances, the curves of the total degradation in the dispersive channels essentially coincide with the curve of the degradation at $n = N_{FFT}/2$ in the case of the ideal channel. In this case, the timing jitter becomes the dominating effect. When comparing the results in the case of a dispersive channel and an ideal channel (see section 5.4.2), we observe that the results are very similar.

5.6 Conclusions and Remarks

In this chapter, we have investigated the sensitivity of OFDM, uplink OFDMA and downlink OFDMA to synchronisation errors. The cyclic prefix of these systems is assumed to be sufficiently long, to cope with channel dispersion and timing misalignment. First we have considered an ideal transmission channel, and have computed the corresponding SNR degradation caused by synchronisation errors, as compared to the SNR for perfect synchronisation. We have shown that OFDM, downlink OFDMA and uplink OFDMA yield essentially the same degradation. Further, we have found that the SNR degradations on a

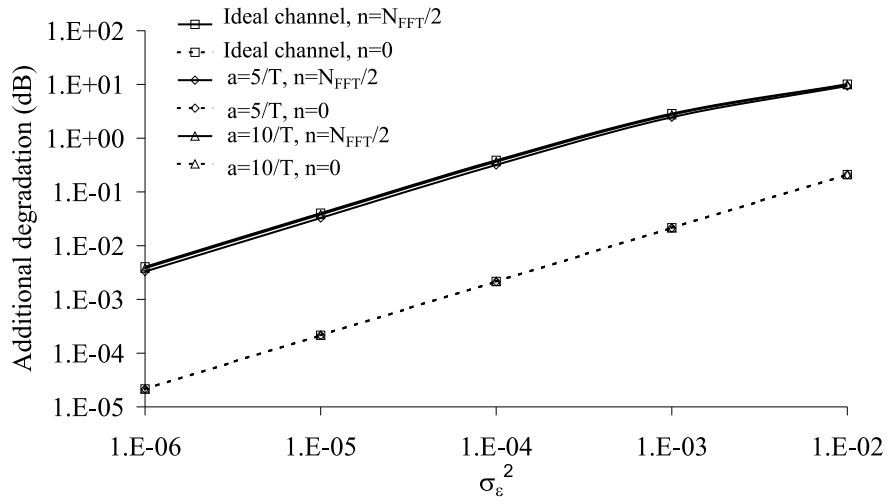

Figure 5.35: Maximum total degradation caused by dispersive channel and timing jitter, $N_{FFT} = 64, SNR(0) = 20$ dB

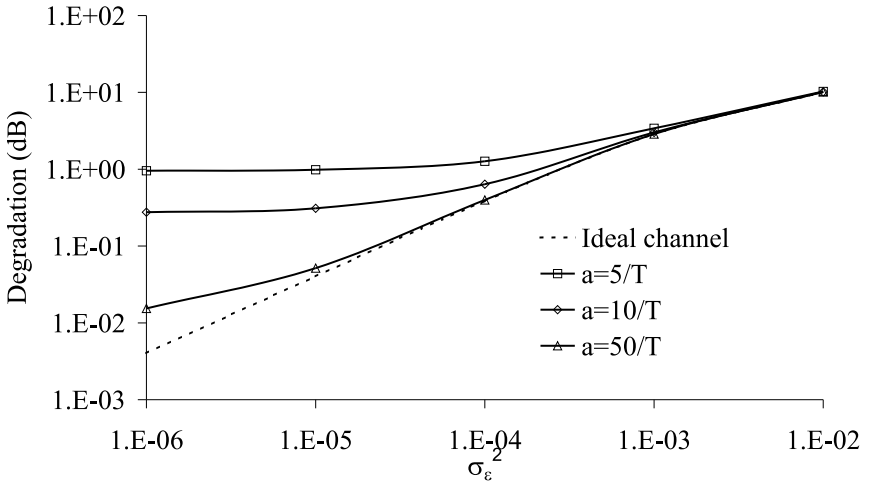

Figure 5.36: Maximum total degradation caused by dispersive channel and timing jitter, $N_{FFT} = 64, SNR(0) = 20$ dB

dispersive channel and over an ideal channel, as compared to the SNR on the respective channels without synchronisation errors, are nearly the same. This indicates that the results pertaining to the ideal channel are also relevant to more realistic channels. These results are briefly summarised in Table 5.5. A more extended discussion is presented below.

Assuming that all compensations of the effect of synchronisation errors are carried out by one-tap equalisers at the outputs of the FFT, the synchronisation errors affect the OFDM(A) system in the following way.

- A constant carrier phase offset only yields a phase rotation of the FFT outputs, which is compensated by the equaliser without loss of performance.
- A constant timing offset introduces a carrier-dependent phase rotation of the FFT outputs that correspond to carriers outside the rolloff area. The rotation of these carriers is compensated by the equaliser without performance degradation. The carriers inside the rolloff are affected not only by a phase rotation but also by an attenuation. The compensation of this attenuation yields a performance loss. This degradation can be avoided by not using the carriers in the rolloff area.
- A (relative) carrier frequency offset ΔFT yields a rotation at a speed of $2\pi\Delta FT$ rad/sample at the input of the FFT. This rotation gives rise to a degradation that is the same for all carriers, and is proportional to $(N_{FFT}\Delta FT)^2$. If this degradation can not be tolerated, frequency offset correction must be applied at the transmitter (uplink) or in front of the FFT at the receiver (downlink).
- A (relative) clock frequency offset $\Delta T/T$ yields a degradation that depends on the carrier index and is proportional to $(N_{FFT}\Delta T/T)^2$. If this degradation can not be tolerated, timing correction must be applied at the transmitter (uplink) or in front of the FFT at the receiver (downlink).
- Carrier phase jitter gives rise to a degradation that is essentially independent of the jitter spectrum shape, the number of carriers and the carrier index, provided that the modulated carriers have the same power. The degradation is proportional to the jitter variance. The scatter diagram at the input of the decision device does depend on the jitter spectrum shape. Low-frequency jitter ($|f| < 1/(N_{FFT}T)$) yields mainly self-interference, causing an angular displacement in the scatter diagram. High-frequency jitter ($|f| > 1/(N_{FFT}T)$) gives rise to intercarrier interference, yielding a circular cloud in the scatter diagram.
- Timing jitter gives rise to a degradation that is essentially independent of the jitter spectrum shape and the number of carriers, provided that the modulated carriers have the same power. The degradation depends on the carrier index, and is proportional to the jitter variance. The dependence

Table 5.5: Overview of the effect of synchronisation errors on the OFDM(A) system for all carriers modulated

constant phase offset	- no degradation
constant timing offset	- no degradation
carrier frequency offset	- strong degradation, proportional to $(N_{FFT}\Delta FT)^2$ - degradation independent of carrier index
clock frequency offset	- strong degradation, proportional to $(N_{FFT}\Delta T/T)^2$ - degradation depends on carrier index
carrier phase jitter	- degradation independent of N_{FFT} and spectral contents of jitter, proportional to σ_ϕ^2 - degradation independent of carrier index - scatter diagram depends on spectral contents jitter
jitter timing jitter	- degradation independent of spectral contents jitter and essentially independent of N_{FFT} for large N_{FFT}, proportional to σ_ϵ^2 - degradation depends on carrier index - scatter diagram depends on spectral contents jitter

of the scatter diagram at the input of the decision device on the jitter spectrum shape is similar to the case of carrier phase jitter.

The research leading to the results in this chapter has originated in a number of scientific papers. In [Ste98b], we have investigated the effect of carrier phase jitter on OFDMA, and a comparison with OFDM and conventional FDMA has been carried out [Ste97b]. In [Ste00] we have presented an overview of the sensitivity of OFDM to all types of synchronisation errors considered in this chapter.

It should be mentioned that some results on the sensitivity of OFDM to synchronisation errors were already available when we started the research for this thesis.

- In [Pol93], [Pol95a], [Pol96] and [Pol98], the impact of carrier phase errors on OFDM performance has been investigated in terms of the SNR degradation, and some comparisons with conventional single-carrier modulation have been made. In [Pol94], the sensitivity of OFDM to clock frequency offset has been considered. However, these papers mainly consider transmission over an ideal channel, whereas in our work also the dispersive channel is investigated. Moreover, in [Pol96], the effect of the frequency translation of the received OFDM signal with respect to the receive filter

has not been properly taken into account; the correct analysis is given in our section 5.4.1.

- In [Zog96] the effect of timing jitter on OFDM performance has been investigated. However, the jitter is assumed to be constant over an OFDM block, whereas in our work a less restrictive jitter model is assumed. In addition in [Zog96] the degradation of the carriers in the rolloff area, caused by timing offset, is not taken into account.

- In [Tom98], the sensitivity of OFDM to timing jitter has been considered. However, in spite of the small timing jitter, the authors do not consider any linearisation, so the resulting expressions are quite complicated and hard to interpret. The linearisation carried out in this work yields simple expressions from which the effect of various parameters is easily derived.

Chapter 6

Multicarrier CDMA

6.1 Introduction

In chapter 5, the orthogonal frequency division multiplexing (OFDM) technique, consisting of a number of orthogonal carriers, has been presented. However, OFDM still needs to be extended with a multiple access technique in order to support different users. A possible solution to separate the users is to use spreading sequences, i.e., to use CDMA as a multiple access technique. Recently, some new techniques for high data rate communications, based on a combination of a multicarrier technique and CDMA were proposed [Har97], [Faz97], [Faz00], [Faz93], [Yee93], [Cho93], [VBl98], [DaS93], [Van93], [Lin99]. The proposed techniques can be classified into two categories.

- In the multicarrier CDMA (MC-CDMA) technique [Faz93], [Yee93], [Cho93], [VBl98], the original data stream is first multiplied with the spreading sequence and then modulated on the different carriers, as shown in figure 6.1: as the chips belonging to the same symbol interval are modulated on different carriers, the spreading is done in the frequency domain. In MC-CDMA, the carriers satisfy the orthogonality condition with minimum frequency separation, similarly as in the OFDM technique (see figure 6.1). Hence, the transmitter and receiver can be implemented using fast Fourier transforms (FFT).

- In the other category, the serial-to-parallel converted data stream is multiplied with the spreading sequence and then the chips belonging to the same symbol interval modulate the same carrier, as shown in figure 6.2: the spreading is done in the time domain. Two schemes belong to this group: multicarrier DS-CDMA (MC-DS-CDMA) [DaS93] and multitone CDMA (MT-CDMA) [Van93]. In the MC-DS-CDMA technique, the carriers are chosen orthogonal with minimum frequency separation, similarly

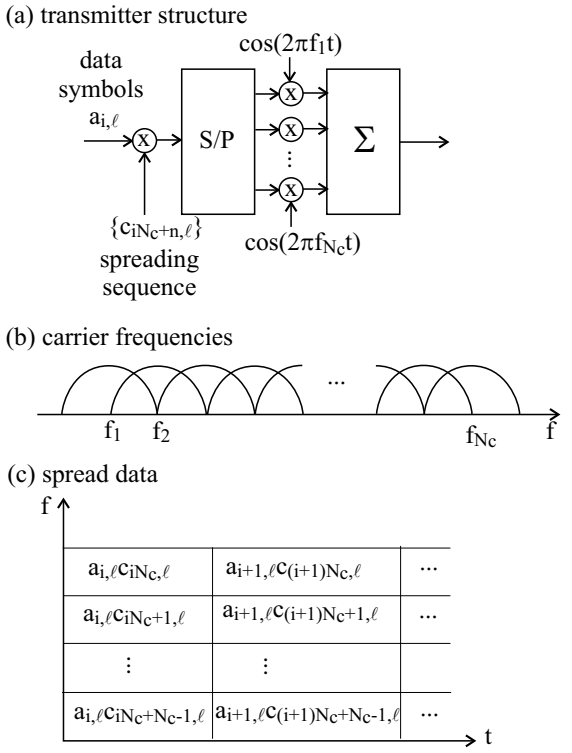

Figure 6.1: Spreading in the frequency domain (MC-CDMA)

as in the OFDM technique (see figure 6.2). Hence an FFT can be used to modulate the spread data. In the MT-CDMA technique, the carriers are not orthogonal (see figure 6.2).

In this work, only the MC-CDMA technique will be considered. The MC-CDMA technique has been investigated in the context of high data rate communications over dispersive channels and has been proposed for mobile radio communication [Faz93]. As all MC-CDMA user signals occupy the whole system bandwidth, MC-CDMA is less vulnerable to channel dispersion than MC-DS-CDMA. Unlike MC-CDMA, MT-CDMA is affected by multiuser interference when the channel is ideal.

In this chapter, we investigate the sensitivity of the MC-CDMA system to synchronisation errors for both downlink and uplink transmission. The chapter is organised as follows: in section 6.2, the transmitter of the MC-CDMA system is introduced. The receiver of the MC-CDMA system is derived in section 6.3, for both downlink and uplink MC-CDMA. In section 6.4, we separately consider the influence of carrier phase errors and timing errors in the case of an ideal channel. The effect of the synchronisation errors in the presence of a dispersive

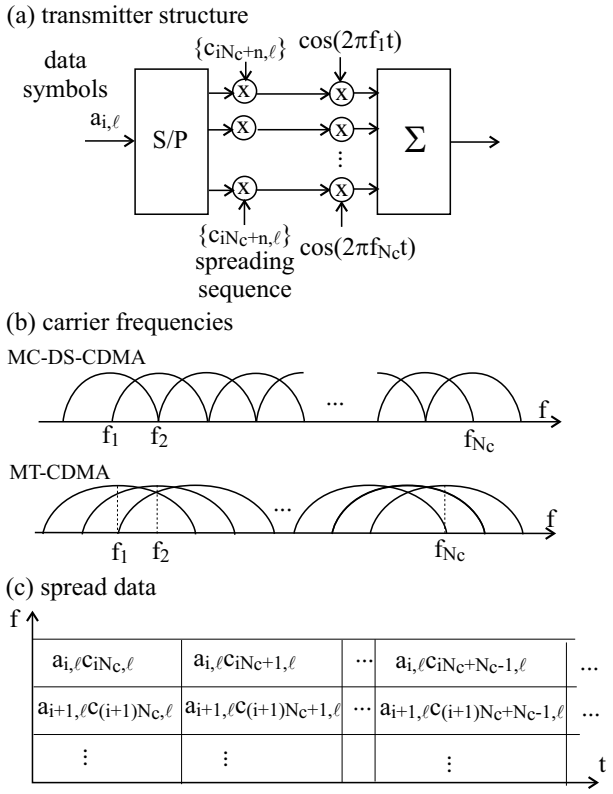

Figure 6.2: Spreading in the time domain (MC-DS-CDMA, MT-CDMA)

channel is investigated in section 6.5. The results are discussed in section 6.6.

6.2 The MC-CDMA Transmitter for a Single User

The conceptual block diagram of the MC-CDMA transmitter is shown in figure 6.3 for a single user [Har97], [Faz97], [Faz00], [Faz93], [Yee93], [Cho93], [VBl98]. Without loss of generality, the terminology for the uplink is used. The data symbols $\{a_{i,\ell}\}$ are generated at a rate R_s, where $a_{i,\ell}$ denotes the ith symbol transmitted by the user ℓ. Each data symbol is multiplied with a spreading sequence $\mathbf{c}_{i,\ell}$ of rate $N_c R_s$ (N_c is the spreading factor): $\mathbf{c}_{i,\ell} = (1/\sqrt{N_c})[c_{iN_c,\ell} \dots c_{iN_c+N_c-1,\ell}]^T$, where $c_{iN_c+n,\ell}$ is the nth chip during the ith symbol interval, of the sequence belonging to the user ℓ. In this work, we restrict our attention to two types of orthogonal spreading sequences, i.e., Walsh-Hadamard (WH) and overlay sequences, that have been discussed in section

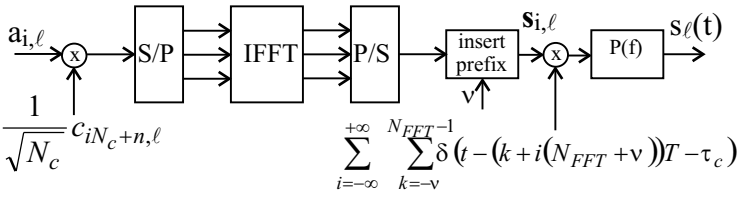

Figure 6.3: Conceptual block diagram of the MC-CDMA transmitter for a single user

2.4.3. The resulting sequence $\mathbf{b}_{i,\ell} = [b_{iN_c,\ell} \dots b_{iN_c+N_c-1,\ell}]^T$ is given by

$$\mathbf{b}_{i,\ell} = \mathbf{c}_{i,\ell} a_{i,\ell} \tag{6.1}$$

Each of the N_c components of $\mathbf{b}_{i,\ell}$ will be modulated on a different carrier. As in OFDM, these carriers are orthogonal by a proper selection of the carrier spacing: this spacing equals the per carrier chip rate ($= R_s$). In chapter 5, we have shown that the carriers inside the rolloff area are severely affected by some types of timing errors. To avoid this degradation, only carriers outside the rolloff area are used. Assuming that N_{FFT} carriers are available and square-root raised-cosine filters with rolloff α are used at the transmitter and the receiver, the number N_c of carriers actually used satisfies $N_c \leq (1-\alpha)N_{FFT}$. The N_c components of $\mathbf{b}_{i,\ell}$ are modulated on carriers outside the rolloff area (see figure 6.4) by using an IFFT of length N_{FFT}. This results in the sequence $\mathbf{s}_{i,\ell} = [s_{iN_{FFT},\ell} \dots s_{iN_{FFT}+N_{FFT}-1,\ell}]^T$, given by

$$\mathbf{s}_{i,\ell} = \mathbf{F}\mathbf{Q}\mathbf{b}_{i,\ell} = \mathbf{F}\mathbf{Q}\mathbf{c}_{i,\ell} a_{i,\ell} \tag{6.2}$$

which denotes the ith MC-CDMA block of the ℓth user. In (6.2), $\mathbf{F}_{k,n} = (1/\sqrt{N_{FFT}}) \exp(j2\pi kn/N_{FFT})$ denotes the $N_{FFT} \times N_{FFT}$ matrix of the inverse FFT and $\mathbf{Q}$ is an $N_{FFT} \times N_c$ matrix given by

$$\mathbf{Q} = \begin{pmatrix} \mathbf{I}_{N_c/2} & \mathbf{0}_{N_c/2 \times N_c/2} \\ \mathbf{0}_{(N_{FFT}-N_c) \times N_c/2} & \\ \mathbf{0}_{N_c/2 \times N_c/2} & \mathbf{I}_{N_c/2} \end{pmatrix} \tag{6.3}$$

In (6.3), $\mathbf{I}_K$ is the identity matrix of dimension $K \times K$, and $\mathbf{0}_{K \times M}$ is a $K \times M$ matrix containing only zeroes.

As in OFDM, each MC-CDMA block is preceded by a cyclic prefix of ν samples, in order to avoid interference between successive blocks and between carriers when transmitting over a dispersive channel. The resulting transmitted samples during the ith block are $\{s_{i(N_{FFT}+\nu)+n,\ell} | n = -\nu, \dots, N_{FFT}-1\}$, where the first ν samples are a duplication of the last ν samples, $\{s_{i(N_{FFT}+\nu)+n,\ell} | n = -\nu, \dots, -1\} = \{s_{i(N_{FFT}+\nu)+n,\ell} | n = N_{FFT}-\nu, \dots, N_{FFT}-1\}$. After normalisation such that the energy per symbol transmitted by user ℓ equals $E_{s,\ell}$, where $E_{s,\ell} = E[|a_{i,\ell}|^2]$, the resulting time-domain sequence $\mathbf{s}_{i,\ell} =$

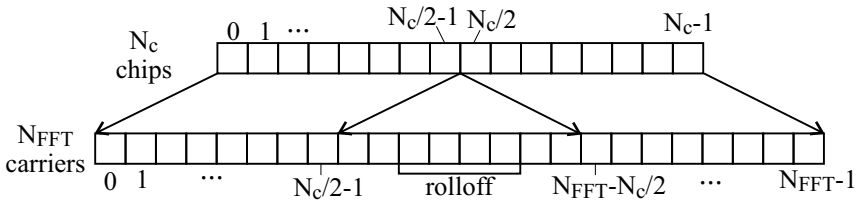

Figure 6.4: Mapping of the chips on the carriers

$[s_{i(N_{FFT}+\nu)-n,\ell} \cdots s_{i(N_{FFT}+\nu)+N_{FFT}-1,\ell}]^T$ yields

$$\mathbf{s}_{i,\ell} = \sqrt{\frac{N_{FFT}}{N_{FFT}+\nu}}\mathbf{\Omega}\mathbf{F}\mathbf{Q}\mathbf{c}_{i,\ell}a_{i,\ell} \tag{6.4}$$

where

$$\mathbf{\Omega} = \begin{pmatrix} \mathbf{0} & \mathbf{I}_{\nu} \\ \mathbf{I}_{N_{FFT}} & \end{pmatrix} \tag{6.5}$$

Hence, the transmitter converts one data symbol into a block of $N_{FFT}+\nu$ samples using the linear transformation $\mathbf{T}_{tr,i,\ell}$ (2.1), i.e.,

$$\mathbf{T}_{tr,i,\ell} = \sqrt{\frac{N_{FFT}}{N_{FFT}+\nu}}\mathbf{\Omega}\mathbf{F}\mathbf{Q}\mathbf{c}_{i,\ell} \tag{6.6}$$

The sequence $\mathbf{s}_{i,\ell}$ (6.4) is multiplied with the transmit clock signal that has a frequency $1/T = R_s(N_{FFT}+\nu)$. The resulting signal is applied to a transmit filter, which is a unit-energy square-root Nyquist filter with transfer function $P(f)$ (e.g., a square-root raised cosine filter with rolloff α), resulting in the complex baseband signal $s_\ell(t)$:

$$s_{i,\ell}(t) = \sum_{i=-\infty}^{+\infty} \sum_{k=-\nu}^{N_{FFT}-1} s_{i(N_{FFT}+\nu)+k,\ell}\, p(t-(k+i(N_{FFT}+\nu))T - \tau_c) \tag{6.7}$$

where τ_c is a time delay representing the transmit clock phase. Note that the MC-CDMA signal consists of N_c carriers, each of which has a chip rate that equals the original symbol rate R_s. The signal $s_\ell(t)$ is upconverted, yielding a real-valued bandpass signal that is transmitted over the channel.

6.3 Multiple Users

When different users are present, multiuser interference (MUI) can occur. Depending on the type of communication system, the spreading sequences must be chosen carefully as only a limited amount of MUI is allowed. In a stand-alone system, i.e., with only one basestation communicating with multiple users,

orthogonal sequences like Walsh-Hadamard sequences can be used. These sequences have the advantage that no MUI is introduced in a non-dispersive channel.

When the system supports a large number of users, e.g., as in mobile radio communication, the covered area is partitioned into a number of hexagonal cells. Each cell contains a basestation communicating with the users present in the same cell. In such a system, we can distinguish two types of multiuser interference: intracell interference, caused by the users of the same cell, and intercell interference, caused by users in other cells. To limit the intracell interference, users of the same cell can use orthogonal Walsh-Hadamard sequences. All cells make use of the same set of orthogonal sequences, but in each cell these orthogonal sequences are multiplied with a random sequence that is common to all users of the same cell. Different cells are assigned different random sequences, otherwise the interference between adjacent cells (intercell interference) would be too high. This combination of an orthogonal sequence with a random sequence is called an overlay sequence. The construction of the overlay sequences is described in section 2.4.3. In the case of a non-dispersive channel, no intracell interference is introduced, as the signals belonging to the different users of the same cell are orthogonal. However, as different cells are assigned different, uncorrelated random sequences, the overlay sequences belonging to different cells are not orthogonal. Therefore, the signals belonging to users of different cells introduce an amount of intercell interference, even in the case of an ideal channel.

In this section, we will investigate the influence of intracell interference for both uplink and downlink MC-CDMA. As a reference for the frequencies and phases of the clock signal and the carrier oscillator, we use the frequencies and phases of the network synchronisation reference signal, provided by the basestation. As in downlink MC-CDMA the signals transmitted to the different users are synchronised at the base station, the timing errors of the different signals are the same. Furthermore, as all transmitted signals are upconverted by the same carrier oscillator, they exhibit the same carrier phase error. In uplink MC-CDMA, each user generates a local clock signal and a local carrier oscillator of which the frequencies and phases are estimated from a network synchronisation reference signal. Hence, the signals transmitted by the different users exhibit a different carrier phase error and timing error. In the following, we separately consider downlink and uplink MC-CDMA.

6.3.1 Downlink MC-CDMA

First, we consider the case of downlink MC-CDMA. To reduce the complexity of the transmitter at the basestation, the transmitter is implemented as shown in figure 6.5, with only one inverse FFT generating all user signals. The number of active users equals N_u. The transmitted time-domain sequence

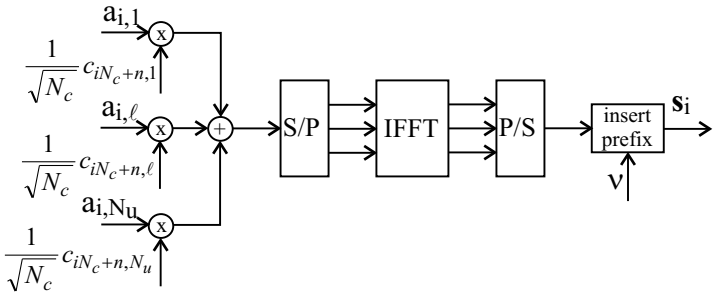

Figure 6.5: Transmitter for downlink MC-CDMA

$\mathbf{s}_i = [s_{i(N_{FFT}+\nu)-\nu} \ldots s_{i(N_{FFT}+\nu)+N_{FFT}-1}]^T$, is given by

$$\mathbf{s}_i = \sum_{\ell=1}^{N_u} \mathbf{s}_{i,\ell} \tag{6.8}$$

where $\mathbf{s}_{i,\ell}$ follows from (6.4). The sequence $\mathbf{s}_i$ is multiplied with the transmit clock signal, consisting of a periodic sequence of Dirac impulses, and applied to the transmit filter $P(f)$, which is a unit-energy square-root Nyquist filter (2.3), yielding

$$s(t) = \sum_{i=-\infty}^{+\infty} \sum_{k=-\nu}^{N_{FFT}-1} s_{i(N_{FFT}+\nu)+k} p(t - (k + i(N_{FFT} + \nu))T - \tau_c) \tag{6.9}$$

where τ_c is a time delay that represents the transmit clock phase. The transfer function of the dispersive channel from the basestation to the receiver of user ℓ is given by $H_{ch,\ell}(f;\tau)$. The output of the dispersive channel is disturbed by additive white Gaussian noise (AWGN) $w_{LP}(t)$ with uncorrelated real and imaginary parts, each having a power spectral density (psd) of $N_0/2$. Furthermore, the signal is affected by the carrier phase difference $\theta_c - \hat{\theta}_{r,\ell}(t)$, where θ_c is the phase of the upconverting carrier at the transmitter and $\hat{\theta}_{r,\ell}(t)$ is the estimated optimum carrier phase for downconversion at the receiver (see (2.10)), resulting in the complex baseband signal $r_\ell(t)$ after downconversion. The receiver block diagram of user ℓ is shown in figure 6.6. At the receiver of user ℓ, the signal $r_\ell(t)$ is applied to the receiver filter, which is matched to the transmit filter, and sampled at the instants $\hat{t}_{i(N_{FFT}+\nu)+k,\ell} = t_{i(N_{FFT}+\nu)+k,\ell} + \epsilon_{i(N_{FFT}+\nu)+k,\ell} T$, where $t_{i(N_{FFT}+\nu)+k,\ell} = (k + i(N_{FFT} + \nu))T + \tau^{\ell}_{r,i(N_{FFT}+\nu)+k}$ are the optimum sampling instants (see (2.10)) and $\epsilon_{i(N_{FFT}+\nu)+k,\ell}$ is the normalised timing error of the kth sample of the ith MC-CDMA block at the receiver of user ℓ.

Assuming the channel transfer function $H_{ch,\ell}(f;\tau)$ and the carrier phase difference $\theta_c - \hat{\theta}_{r,\ell}(t)$ are slowly varying as compared to the duration of the sampling interval T, the samples $\mathbf{v}_{i,\ell} = [v_{i(N_{FFT}+\nu)-\nu,\ell} \ldots v_{i(N_{FFT}+\nu)+N_{FFT}-1,\ell}]^T$ at the

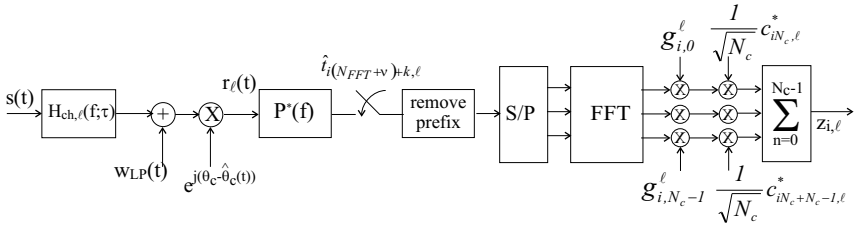

Figure 6.6: Channel and receiver structure for downlink MC-CDMA

output of the receiver filter yield

$$\begin{aligned} v_{i(N_{FFT}+\nu)+k,\ell} &= \sum_{i=-\infty}^{+\infty} \sum_{k'=-\nu}^{N_{FFT}-1} s_{i'(N_{FFT}+\nu)+k'} \cdot \\ &\quad h_{eq,\ell}(t_{i(N_{FFT}+\nu)+k,\ell} - t_{i'(N_{FFT}+\nu)+k',\ell}; t_{i(N_{FFT}+\nu)+k,\ell}) \\ &+ \quad w_{i(N_{FFT}+\nu)+k,\ell} \end{aligned} \tag{6.10}$$

where $w_{i(N_{FFT}+\nu)+k,\ell}$ is the value of the matched filter output noise at the instant $\hat{t}_{i(N_{FFT}+\nu)+k,\ell}$, originating from the noise contribution $w_{LP}(t)$, and $h_{eq,\ell}(t; t_{i(N_{FFT}+\nu)+k,\ell})$ is the impulse response of the equivalent time-varying channel corresponding to user ℓ, with transfer function as defined in (2.21)

$$\begin{aligned} H_{eq,\ell}(f; t_{i(N_{FFT}+\nu)+k,\ell}) &= H_\ell(f; t_{i(N_{FFT}+\nu)+k,\ell}) \cdot \\ &\quad e^{j(\phi_\ell(t_{i(N_{FFT}+\nu)+k,\ell}) - \Delta\theta_\ell(t_{i(N_{FFT}+\nu)+k,\ell}))} \cdot \\ &\quad e^{j2\pi f(\epsilon_{i(N_{FFT}+\nu)+k,\ell} T + \Delta\tau_{i(N_{FFT}+\nu)+k,\ell})} \end{aligned} \tag{6.11}$$

In (6.11), $\phi(t)$ is the carrier phase error; the phase shift $\Delta\theta_\ell(t_{i(N_{FFT}+\nu)+k})$ and the time delay $\Delta\tau_{i(N_{FFT}+\nu)+k,\ell}$ depend on the channel characteristics, and $H_\ell(f; t_{i(N_{FFT}+\nu)+k,\ell})$ is the transfer function of the cascade of the transmit filter, the dispersive channel and the receiver filter, i.e., $H_\ell(f;\tau) = H_{ch,\ell}(f;\tau)|P(f)|^2$.

The receiver removes from each MC-CDMA block the ν samples corresponding to the cyclic prefix, and keeps the remaining N_{FFT} samples for further processing. As shown in appendix D.2, the MMSE receiver structure consists of an FFT of length N_{FFT} followed by one-tap equalisers. As only the carriers outside the rolloff are modulated, only the corresponding FFT outputs are followed by one-tap equalisers. The equaliser coefficient $g_{i,n}^\ell$ scales and rotates the $M(n)$th FFT output during the ith MC-CDMA block, where $M(n)$ denotes the index of the carrier that contains the nth chip of the MC-CDMA block. The N_c equaliser outputs are multiplied with the spreading sequence of the considered user and summed, to obtain the samples $z_{i,\ell}$ at the input of the decision device. Defining the matrix $\mathbf{D}_{i,\ell}$ as the diagonal matrix of order $N_c \times N_c$ of the equaliser coefficients, i.e., $(\mathbf{D}_{i,\ell})_{n,n'} = \delta_{n,n'} g_{i,n}^\ell$, and $\mathbf{A}^\dagger$ as the Hermitian of the matrix $\mathbf{A}$, the samples $z_{i,\ell}$ yield

$$z_{i,\ell} = \mathbf{c}_{i,\ell}^\dagger \mathbf{D}_{i,\ell} \mathbf{Q}^\dagger \mathbf{F}^\dagger \Xi \mathbf{v}_{i,\ell} \tag{6.12}$$

where $\mathbf{\Xi} = (\mathbf{0} \quad \mathbf{I}_{N_{FFT}})$ is a $N_{FFT} \times (N_{FFT} + \nu)$ matrix. Hence, the received samples $\mathbf{v}_{i,\ell}$ are demodulated using the linear transformation $\mathbf{b}_{i,\ell}$ (2.5), where $\mathbf{b}_{i,\ell} = \mathbf{c}_{i,\ell}^{\dagger}\mathbf{D}_{i,\ell}\mathbf{Q}^{\dagger}\mathbf{F}^{\dagger}\mathbf{\Xi}$ is a vector of order $1 \times (N_{FFT} + \nu)$. The sample $z_{i,\ell}$ at the input of the decision device is decomposed into four contributions:

$$\begin{aligned} z_{i,\ell} &= \sqrt{\frac{N_{FFT}}{N_{FFT}+\nu}} a_{i,\ell} I_{i,i,\ell,\ell} + \sqrt{\frac{N_{FFT}}{N_{FFT}+\nu}} \sum_{i'=-\infty;i'\neq i}^{+\infty} a_{i',\ell} I_{i,i',\ell,\ell} \\ &+ \sqrt{\frac{N_{FFT}}{N_{FFT}+\nu}} \sum_{i'=-\infty;i'\neq i}^{+\infty} \sum_{\ell'=1;\ell'\neq\ell}^{N_u} a_{i',\ell'} I_{i,i',\ell,\ell'} + W_{i,\ell} \end{aligned} \tag{6.13}$$

where

$$I_{i,i',\ell,\ell'} = \frac{1}{N_c} \sum_{n,n'=0}^{N_c-1} c^*_{iN_c+n,\ell} c_{i'N_c+n',\ell'} g^{\ell}_{i,n} A^{\ell}_{i,i',n,n'} \tag{6.14}$$

$$\begin{aligned} A^{\ell}_{i,i',n,n'} &= \frac{1}{N_{FFT}} \sum_{k=0}^{N_{FFT}-1} \sum_{k'=-\nu}^{N_{FFT}-1} e^{-j2\pi \frac{kM(n)-k'M(n')}{N_{FFT}}} \cdot \\ &\quad h_{eq}(t_{i(N_{FFT}+\nu)+k,\ell} - t_{i'(N_{FFT}+\nu)+k',\ell}; t_{i(N_{FFT}+\nu)+k,\ell}) \end{aligned} \tag{6.15}$$

The quantity $I_{i,i',\ell,\ell'}$ represents the contribution of the symbol $a_{i',\ell'}$ to the input of the decision device of the ℓth user during the ith MC-CDMA block. In (6.13), the first contribution is the useful component. This contribution can be further decomposed into an average useful component $E[I_{i,i,\ell,\ell}]$, and a zero-mean fluctuation $I_{i,i,\ell,\ell} - E[I_{i,i,\ell,\ell}]$ about its average, i.e., the self-interference (SI). The second contribution ($i' \neq i, \ell' = \ell$) is the intersymbol interference (ISI), caused by other symbols from the same user. The third contribution ($\ell' \neq \ell$) denotes the multiuser interference (MUI). The last contribution is the additive noise term with variance

$$E[|W_{i,\ell}|^2] = N_0 \frac{1}{N_c} \sum_{n=0}^{N_c-1} |g^{\ell}_{i,n}|^2 \triangleq N_0 \sigma^2_{i,\ell} \tag{6.16}$$

The performance of the MC-CDMA system is measured by the signal-to-noise ratio (SNR) (2.59), which is the ratio of the power of the average useful component to the sum of the powers of the self-interference, the intersymbol interference, the multiuser interference and the noise. This yields

$$SNR_{i,\ell} = \frac{\frac{N_{FFT}}{N_{FFT}+\nu} E_{s,\ell} P_{U,i,\ell}}{N_0 \sigma^2_{i,\ell} + \frac{N_{FFT}}{N_{FFT}+\nu} E_{s,\ell} (P_{SI,i,\ell} + P_{ISI,i,\ell} + P_{MUI,i,\ell})} \tag{6.17}$$

where

$$\begin{aligned} P_{U,i,\ell} &= |E[I_{i,i,\ell,\ell}]|^2 \\ P_{SI,i,\ell} &= E[|I_{i,i,\ell,\ell} - E[I_{i,i,\ell,\ell}]|^2] \\ P_{ISI,i,\ell} &= \sum_{i'=-\infty;i'\neq i}^{+\infty} E[|I_{i,i',\ell,\ell}|^2] \\ P_{MUI,i,\ell} &= \sum_{i'=-\infty}^{+\infty} \sum_{\ell'=1;\ell'\neq\ell}^{N_{FFT}-1} \frac{E_{s,\ell'}}{E_{s,\ell}} E[|I_{i,i',\ell,\ell'}|^2] \end{aligned} \tag{6.18}$$

The instantaneous SNR (6.17) depends on the block index i and the user index ℓ. In many cases of practical interest, the dependency of (6.17) on one or both indices disappears.

In the case of an ideal channel ($H_{ch,\ell}(f;\tau) = 1$) and in the absence of synchronisation errors, the receiver filter output samples are given by

$$v_{i(N_{FFT}+\nu)+k} = \sum_{\ell'=1}^{N_u} s_{i(N_{FFT}+\nu)+k,\ell'} + w_{i(N_{FFT}+\nu)+k}, \qquad k = -\nu, \ldots, N_{FFT}-1 \tag{6.19}$$

where $w_{i(N_{FFT}+\nu)+k}$ is Gaussian with $E[w_{i(N_{FFT}+\nu)+k} w^*_{i'(N_{FFT}+\nu)+k'}] = N_0\delta_{k-k'}\delta_{i-i'}$, and $s_{i(N_{FFT}+\nu)+k,\ell'}$ is given by (6.4). Removing the cyclic prefix and applying the remaining samples to the FFT yields the following expression for the $M(n)$th FFT output $y_{i,M(n)}$:

$$y_{i,M(n)} = \sqrt{\frac{N_{FFT}}{N_{FFT}+\nu}} \sum_{\ell'=1}^{N_u} \frac{1}{\sqrt{N_c}} c_{iN_c+n,\ell'} a_{i,\ell'} + W_{i,M(n)} \tag{6.20}$$

with $E[W_{i,M(n)} W^*_{i',M(n')}] = N_0\delta_{n-n'}\delta_{i-i'}$. The equaliser coefficients do not depend on the carrier index nor the time index: $g_{i,M(n)} = g_{0,0}$. The corresponding quantity $z_{i,\ell}$ at the input of the decision device is determined by

$$\begin{aligned} \frac{z_{i,\ell}}{g_{0,0}} &= \frac{1}{\sqrt{N_c}} \sum_{n=0}^{N_c-1} y_{i,M(n)} c^*_{iN_c+n,\ell} \\ &= \sqrt{\frac{N_{FFT}}{N_{FFT}+\nu}} \left(a_{i,\ell} + \sum_{\ell'=1;\ell'\neq\ell}^{N_u} a_{i,\ell'} \frac{1}{N_c} \sum_{n=0}^{N_c-1} c^*_{iN_c+n,\ell} c_{iN_c+n,\ell'} \right) \\ &+ \frac{1}{\sqrt{N_c}} \sum_{n=0}^{N_c-1} W_{i,M(n)} c^*_{iN_c+n,\ell} \end{aligned} \tag{6.21}$$

The third term in (6.21) is a noise contribution with variance equal to N_0. The second term in (6.21) is MUI; this term is zero when the spreading sequences are orthogonal:

$$\frac{1}{N_c} \sum_{n=0}^{N_c-1} c^*_{iN_c+n,\ell} c_{iN_c+n,\ell'} = \delta_{\ell-\ell'} \tag{6.22}$$

The resulting SNR is independent of the symbol index i and is given by

$$SNR_\ell(0) = \frac{N_{FFT}}{N_{FFT}+\nu}\frac{E_{s,\ell}}{N_0} \tag{6.23}$$

The factor $N_{FFT}/(N_{FFT}+\nu)$ in (6.23) accounts for the loss in power efficiency, that results from not using the ν samples that are contained in the cyclic prefix.

In the presence of a dispersive channel or synchronisation errors, the SNR is reduced as compared to $SNR_\ell(0)$. The degradation of the SNR as compared to $SNR_\ell(0)$ (expressed in dB), caused by the presence of a dispersive channel and the synchronisation errors, is given by

$$Deg_{i,\ell} = -10\log\left(\frac{P_{U,i,\ell}}{\sigma^2_{i,\ell} + SNR_\ell(0)(P_{SI,i,\ell}+P_{ISI,i,\ell}+P_{MUI,i,\ell})}\right) \tag{6.24}$$

For a sufficient cyclic prefix length, i.e., when the duration of the impulse response $h_{eq,\ell}(t; t_{i(N_{FFT}+\nu)+k,\ell})$ does not exceed the duration of the cyclic prefix, no intersymbol interference is introduced ($I_{i,i',\ell,\ell'} = 0$, for $i' \neq i$, i.e., $P_{ISI,\ell} = 0$). From appendix D it follows that the quantities (6.15) reduce to

$$A^\ell_{i,i',n,n'} = \delta_{i,i'}\frac{1}{N_{FFT}}\sum_{k=0}^{N_{FFT}-1} e^{-j2\pi\frac{k(M(n)-M(n'))}{N_{FFT}}} G_{n',\ell}(t_{i(N_{FFT}+\nu)+k,\ell}) \tag{6.25}$$

where

$$G_{n,\ell}(t_{i(N_{FFT}+\nu)+k}) = \frac{1}{T}\sum_{m=-\infty}^{+\infty} H_{eq,\ell}\left(\frac{M(n)}{N_{FFT}T} + \frac{m}{T}; t_{i(N_{FFT}+\nu)+k,\ell}\right) \tag{6.26}$$

is the folded transfer function of the equivalent time-varying filter (6.11) belonging to user ℓ, evaluated at the frequencies $n/(N_{FFT}T)$.

The computation complexity of the expressions (6.18) strongly increases for an increasing spreading factor N_c. To reduce this computation complexity, we present accurate approximations for (6.18), that make use of the simplified expressions from appendix C.

6.3.2 Uplink MC-CDMA

In uplink MC-CDMA, the transmitter of each user derives a clock signal and a carrier oscillator signal from a network synchronisation reference signal. Hence, the transmitter of user ℓ has a user dependent, time-varying carrier phase $\theta_{c,\ell}(t)$ and clock phase $\tau_{i(N_{FFT}+\nu)+k,\ell}$ (see (2.25)). The time-domain sequence $\mathbf{s}_{i,\ell} = [s_{i(N_{FFT}+\nu)-\nu,\ell} \cdots s_{i(N_{FFT}+\nu)+N_{FFT}-1,\ell}]^T$, transmitted by user ℓ is multiplied with the transmit clock signal and applied to the transmit filter, yielding

$$s_\ell(t) = \sum_{i=-\infty}^{+\infty}\sum_{k=-\nu}^{N_{FFT}-1} s_{i(N_{FFT}+\nu)+k,\ell}\, p(t-(k+i(N_{FFT}+\nu))T - \tau_{i(N_{FFT}+\nu)+k,\ell}) \tag{6.27}$$

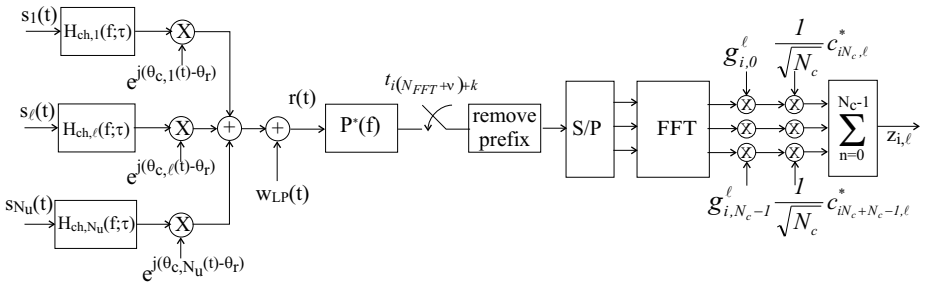

Figure 6.7: Channel and receiver structure for uplink MC-CDMA

The transfer function of the dispersive channel from the transmitter of user ℓ to the basestation is denoted as $H_{ch,\ell}(f;\tau)$. The output of the dispersive channel is affected by the carrier phase difference $\theta_{c,\ell}(t)-\theta_r$, where θ_r is the carrier phase of the oscillator used by the basestation. At the basestation, the received signal $r(t)$ consists of the contributions from the signals transmitted by the N_u active users, disturbed by AWGN $w_{LP}(t)$. The signal $r(t)$ is applied to the receiver filter and sampled at the instants $t_{i(N_{FFT}+\nu)+k} = (k+i(N_{FFT}+\nu))T+\tau_r$, where τ_r is the time delay corresponding to the clock phase of the basestation clock. Assuming the channel transfer functions $H_{ch,\ell}(f;\tau)$ and the carrier phase differences $\theta_c - \hat{\theta}_{r,\ell}(t)$ of the different users vary slowly as compared to the sampling duration T, and the timing phases $\tau_{i(N_{FFT}+\nu)+k,\ell}$ vary slowly as compared to the duration of the composite channel impulse response with transfer function $H_\ell(f;\tau) = H_{ch,\ell}(f;\tau)|P(f)|^2$, the samples $\mathbf{v}_i = [v_{i(N_{FFT}+\nu)-\nu} \ldots v_{i(N_{FFT}+\nu)+N_{FFT}-1}]^T$ at the output of the receiver filter yield

$$\begin{aligned} v_{i(N_{FFT}+\nu)+k} &= \sum_{i=-\infty}^{+\infty} \sum_{k'=-\nu}^{N_{FFT}-1} \sum_{\ell=1}^{N_u} s_{i'(N_{FFT}+\nu)+k',\ell} \cdot \\ &\quad h_{eq,\ell}(t_{i(N_{FFT}+\nu)+k} - t_{i'(N_{FFT}+\nu)+k'}; t_{i(N_{FFT}+\nu)+k}) \\ &+ \quad w_{i(N_{FFT}+\nu)+k} \end{aligned} \tag{6.28}$$

where $w_{i(N_{FFT}+\nu)+k}$ is the value of the matched filter output noise at the instant $t_{i(N_{FFT}+\nu)+k}$ and $h_{eq,\ell}(t; t_{i(N_{FFT}+\nu)+k})$ is the impulse response of the equivalent time-varying channel. The Fourier transform of the equivalent time-varying channel $h_{eq,\ell}(t; t_{i(N_{FFT}+\nu)+k})$ is given by (6.11), where the carrier phase error $\phi_\ell(t)$ and the timing error $\epsilon_{i(N_{FFT}+\nu)+k,\ell}T$ are defined in (2.25) and the phase shift $\Delta\theta_\ell(t_{i(N_{FFT}+\nu)+k})$ and the time delay $\Delta\tau_{i(N_{FFT}+\nu)+k,\ell}$ depend on the channel characteristics.

Let us concentrate on the detection of the data symbols transmitted by user ℓ. The corresponding block diagram of the receiver is shown in figure 6.7. The receiver removes the ν samples corresponding to the cyclic prefix, and keeps the remaining N_{FFT} samples for further processing. The receiver demodulates the selected samples using an FFT. The outputs of the FFT are applied to one-tap

equalisers with equaliser coefficients $g_{i,n}^{\ell}$. The outputs of the one-tap equalisers are multiplied with the spreading sequence of the considered user ℓ and summed, to obtain the samples $z_{i,\ell}$ at the input of the decision device. The samples $z_{i,\ell}$ are given by (6.13), where $W_{i,\ell}$ is a zero-mean complex-valued additive Gaussian noise term with variance (6.16) and

$$I_{i,i',\ell,\ell'} = \frac{1}{N_c} \sum_{n,n'=0}^{N_c-1} c^*_{iN_c+n,\ell} c_{i'N_c+n',\ell'} g_{i,n}^{\ell} A_{i,i',n,n'}^{\ell'} \tag{6.29}$$

with $A_{i,i',n,n'}^{\ell}$ being defined in (6.15). Similarly as for downlink communication, the samples $z_{i,\ell}$ can be decomposed into an average useful component, a self-interference component, intersymbol interference, multiuser interference and additive Gaussian noise. Furthermore, as in downlink MC-CDMA, the SNR is defined as (6.23), where the quantity $I_{i,i',\ell,\ell'}$ is now given by (6.29).

6.4 Effect of Synchronisation Errors

We have shown in chapter 5 that the use of a large number of carriers makes a multicarrier system very sensitive to some types of synchronisation errors. These synchronisation errors are classified in two categories: carrier phase errors and timing errors. To clearly isolate the effect of the synchronisation errors, we consider the case of an ideal channel, i.e., $H_{ch,\ell}(f;\tau) = 1, \forall \ell$. Hence, the phase shift $\Delta\theta_{\ell}(t_{i(N_{FFT}+\nu)+k})$ and the time delay $\Delta\tau_{i(N_{FFT}+\nu)+k,\ell}$ equal zero. The effect of a dispersive channel is investigated in section 6.5.

In downlink MC-CDMA, the MC-CDMA blocks transmitted to the different users are aligned in time, while in uplink MC-CDMA, a timing misalignment of the MC-CDMA blocks transmitted by the different users is present. However, it is assumed that this misalignment is kept small, because the base station sends timing correction information to the different users; this situation is similar to uplink OFDMA, described in section 5.4. Further, we assume that the length of the cyclic prefix is sufficiently long, so that small timing errors do not cause interference from other MC-CDMA blocks (see figure 5.8) to the N_{FFT} samples selected for further processing. Hence, as no interblock interference is present during the observed part of the block, the quantities (6.14) yield $I_{i,i',\ell,\ell'} = 0$ for $i' \neq i$. The transmit and receiver filter are square-root raised-cosine filters with rolloff α. In the following, we separately consider the cases of carrier phase errors and timing errors.

6.4.1 Carrier Phase Errors

In this section, we investigate the sensitivity of downlink and uplink MC-CDMA to carrier phase errors in the absence of timing errors ($\epsilon_{i(N_{FFT}+\nu)+k,\ell} = 0$). In

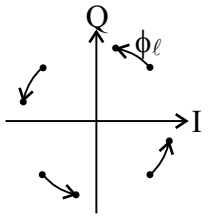

Figure 6.8: Influence of a constant phase offset on the constellation points, $g_{i,n}^{\ell} = 1$

this case, (6.26) yields

$$G_{n,\ell}(t_{i(N_{FFT}+\nu)+k}) = e^{j\phi_\ell(t_{i(N_{FFT}+\nu)+k})} \tag{6.30}$$

In the case of downlink MC-CDMA, the different user signals exhibit the same carrier phase error $\phi_\ell(t) = \phi(t)$ $\ell = 1, \ldots, N_u$, while in uplink MC-CDMA, the signals transmitted by the different users exhibit different carrier phase errors $\phi_\ell(t)$ $\ell = 1, \ldots, N_u$. In the following, we separately consider the case of a constant phase offset, a carrier frequency offset and carrier phase jitter.

Constant Phase Offset

A constant mismatch between the phases of the carrier oscillators at the basestation and the receiver of user ℓ (downlink) or the transmitter of user ℓ and the basestation (uplink) introduces a constant phase offset $\phi_\ell(t) = \phi_\ell$. In downlink communication, where the carrier phase error $\phi_\ell = \phi$ is the same for all user signals, this constant phase offset introduces a carrier-independent rotation over an angle ϕ of the contributions of all users at the FFT outputs, as compared to the case of a zero phase offset. However, the constant phase offset does not affect the orthogonality between the contributions corresponding to the different users, i.e., no MUI is introduced. This means that, when the equaliser applies no correction ($g_{i,n}^{\ell} = 1$), for both downlink and uplink MC-CDMA, the samples $z_{i,\ell}$ (6.13) at the input of the decision device are rotated over an angle ϕ, as shown in figure 6.8. To avoid the reduction of the noise margins, this phase rotation is corrected by the equaliser: the equaliser rotates the FFT outputs over (an estimate of) the angle $-\phi$, i.e., $(g_{MMSE})_{i,n}^{\ell} = C_\ell e^{-j\phi}$ where

$$C_\ell = \frac{\sqrt{\frac{N_{FFT}}{N_{FFT}+\nu}}\sqrt{E_{s,\ell}}}{N_0 + \frac{N_{FFT}}{N_{FFT}+\nu}E_{s,\ell}} \tag{6.31}$$

In (6.31), C_ℓ is the value of the MMSE equaliser coefficient in the absence of synchronisation errors. The MMSE equaliser in the presence of a constant phase offset is independent of the block index i and of the carrier index n.

In uplink communication, the contribution from the signal transmitted by user ℓ at the output of the FFT is rotated over an angle ϕ_ℓ. Similarly as in downlink MC-CDMA, a constant phase offset introduces no MUI but only yields a rotation over an angle ϕ_ℓ of the sample $z_{i,\ell}$ (6.13) at the input of the decision device when no correction is applied ($g_{i,n}^{\ell} = 1$). The equaliser compensates for the phase rotation of the samples $z_{i,\ell}$, i.e., $(g_{MMSE})_{i,n}^{\ell} = C_\ell e^{-j\phi_\ell}$, where C_ℓ is given by (6.31). Similarly as in downlink MC-CDMA, the MMSE equaliser coefficients are independent of the block index i and the carrier index n.

The resulting samples at the input of the decision device, for both downlink and uplink MC-CDMA, consist of the useful component disturbed by additive noise. The variance of the noise is given by (6.16). As the phase rotation applied to the FFT outputs does not enhance the noise power level (6.16), a constant phase offset is compensated by the one-tap equalisers without loss of performance. In this case, the SNR is equal to $SNR_\ell(0)$ from (6.23).

Carrier Frequency Offset

As shown in section 2.3.2, the effect of a carrier frequency offset ΔF_ℓ is twofold. First, a frequency shift of the transmitted signal is introduced. As a part of the received downconverted signal falls outside the bandwidth of the receiver filter, this frequency shift introduces signal distortion and power loss. Hence, this frequency shift results in a reduction of the useful component and the introduction of interference at the receiver filter output. In chapter 3, it is shown that the degradation caused by this frequency shift is small when the carrier frequency offset is small as compared to the bandwidth of the receiver filter, i.e., $\Delta F_\ell T \ll 1$. Further, a carrier frequency offset introduces a phase rotation at a constant speed of $2\pi\Delta F_\ell$ rad/s of the receiver filter output samples $\mathbf{v}_{i,\ell}$ (6.10). The rotating samples are applied to the FFT. In the following, we will show that this rotation reduces the useful component and introduces MUI at the input of the decision device. As the FFT behaves like a bank of filters, each with a bandwidth in the order of $1/(N_{FFT}T)$, the frequency offset ΔF_ℓ must satisfy $\Delta F_\ell T \ll 1/N_{FFT}$ in order to keep the degradation at the input of the decision device within reasonable limits. Assuming $\Delta F_\ell T \ll 1/N_{FFT}$, the frequency shift of the signal at the input of the receiver will be ignored in the following analysis, i.e., only the rotation of the samples $\mathbf{v}_{i,\ell}$ will be taken into account.

A carrier frequency offset between the carrier oscillators of the basestation and the receiver of user ℓ (downlink) or the transmitter of user ℓ and the basestation (uplink) introduces a carrier phase error that linearly increases with time $\phi_\ell(t) = 2\pi\Delta F_\ell t + \phi_\ell(0)$. Without loss of generality, we assume $\phi_\ell(0) = 0$.

In downlink communication, the contributions of the signals transmitted to the different users exhibit the same carrier frequency offset. Assuming the carrier phase error is slowly varying as compared to T, i.e., $\Delta F_\ell \ll 1/T$, the

quantities $I_{i,i',\ell,\ell'}$ (6.14) are given by

$$I_{i,i',\ell,\ell'} = \delta_{i,i'} e^{j2\pi\Delta F_\ell i(N_{FFT}+\nu)} \frac{1}{N_c} \sum_{n,n'=0}^{N_c-1} c^*_{iN_c+n,\ell} c_{iN_c+n',\ell'} g^\ell_{i,n} B_{n,n',\ell} \quad (6.32)$$

where

$$\begin{aligned} B_{n,n',\ell} &= D\left(\frac{M(n)-M(n')}{N_{FFT}} + \Delta F_\ell T\right) \\ D(x) &= \frac{1}{N_{FFT}} \sum_{n=1}^{N_{FFT}-1} e^{j2\pi nx} = e^{j\pi(N_{FFT}-1)x} \frac{\sin \pi N_{FFT} x}{N_{FFT} \sin \pi x} \end{aligned} \quad (6.33)$$

For small x, the approximations $\sin(\pi x) \approx \pi x$ holds, so that $D(x)$ is essentially a function of $N_{FFT}x$. In (6.32) we observe that the contributions of the different users at the input of the decision device are rotating at a constant speed of $2\pi\Delta F_\ell T(N_{FFT}+\nu)$ rad/symbol when $g^\ell_{i,n} = 1$. Hence, this rotation must be compensated by the equaliser. Assuming the receiver of user ℓ can estimate the carrier frequency offset ΔF_ℓ, the MMSE equaliser for both Walsh-Hadamard sequences and overlay sequences has equaliser coefficients

$$(g_{MMSE})^\ell_{i,n} = C^n_{\Delta F,\ell} e^{-j2\pi\Delta F_\ell T i(N_{FFT}+\nu)} D^*(\Delta F_\ell T) \quad (6.34)$$

where $C^n_{\Delta F,\ell}$ is a real-valued positive factor that depends on the carrier frequency offset ΔF_ℓ, the carrier index n and the user index ℓ, but is independent of the block index i. In (6.34) we observe that the equaliser compensates for the systematic phase rotation of the received samples $z_{i,\ell}$. However, the equaliser (6.34) is not able to eliminate the MUI ($I_{i,i',\ell,\ell'} \neq 0$ for $\ell' \neq \ell$). Let us consider the case of the maximum load ($N_u = N_c$). This is the worst case, as the multiuser interference power is maximum. When the rolloff area is small and the spreading factor is essentially equal to the number of carriers, i.e., $N_c \approx N_{FFT}$, the factor $C^n_{\Delta F,\ell}$ is essentially independent of the carrier index n: $C^n_{\Delta F,\ell} \approx C_{\Delta F,\ell}$. In this case, the powers of the average useful component, the self-interference, the multiuser interference and the noise are independent of the block index i and yield

$$\begin{aligned} P_{U,\ell} &= |C_{\Delta F,\ell}|^2 \left(|B_{0,0,\ell}|^2\right)^2 \\ P_{SI,\ell} &= |C_{\Delta F,\ell}|^2 |B_{0,0,\ell}|^2 \frac{1}{N_c^2} \sum_{n,n'=0;n'\neq n}^{N_c-1} |B_{n,n',\ell}|^2 \\ P_{MUI,\ell} &= |C_{\Delta F,\ell}|^2 |B_{0,0,\ell}|^2 \sum_{\ell'=1;\ell'\neq\ell}^{N_c} \frac{1}{N_c^2} \frac{E_{s,\ell'}}{E_{s,\ell}} \sum_{n,n'=0;n'\neq n}^{N_c-1} |B_{n,n',\ell}|^2 \\ E[|W_{i,\ell}|^2] &= N_0 |C_{\Delta F,\ell}|^2 |B_{0,0,\ell}|^2 \end{aligned} \quad (6.35)$$

Hence, the MC-CDMA system is degraded as compared to the case of a zero carrier frequency offset. In the interference powers (6.35), the summation over

n and n' corresponds to the summation over the N_c modulated carriers. To simplify the expressions, we add non-negative terms for the unmodulated carriers by extending the summation to all N_{FFT} available carriers. This yields an upper bound for the powers of the self-interference and the multiuser interference power, i.e.,

$$\begin{aligned} P_{SI,\ell} &\leq |C_{\Delta F,\ell}|^2 |D(\Delta F_\ell T)|^2 \frac{1}{N_c}(1 - |D(\Delta F_\ell T)|^2) \\ P_{MUI,\ell} &\leq |C_{\Delta F,\ell}|^2 |D(\Delta F_\ell T)|^2 (1 - |D(\Delta F_\ell T)|^2) \frac{1}{N_c} \sum_{\ell'=1;\ell'\neq\ell}^{N_c} \frac{E_{s,\ell'}}{E_{s,\ell}} \end{aligned} \quad (6.36)$$

Considering this upper bound (6.36) for the interference powers, an upper bound for the degradation (6.24) of the SNR as compared to $SNR_\ell(0)$ (6.23), caused by the carrier frequency offset can be found. This yields

$$Deg_\ell \leq -10 \log \left(\frac{|D(\Delta F_\ell T)|^2}{1 + (1 - |D(\Delta F_\ell T)|^2) \frac{1}{N_c} \sum_{\ell'=1;\ell'\neq\ell}^{N_c} SNR_{\ell'}(0)} \right) \quad (6.37)$$

The upper bound in (6.36) and (6.37) is reached when $\alpha = 0$ and all carriers are modulated ($N_c = N_{FFT}$). The degradation (6.37) depends on the user index ℓ. Considering the nature of $D(x)$, the degradation is a function of $N_{FFT}\Delta F_\ell T$. This upper bound (6.37) yields an accurate approximation for the actual degradation when the rolloff area is small and $N_c \approx N_{FFT}$. For the maximum load ($N_u = N_c$), the degradation (6.37) is independent of the spreading factor when all users have the same symbol energy ($E_{s,\ell} = E_s$).

In uplink communication, the contributions of the signals transmitted by the different users are affected by a different carrier frequency offset. Assuming the carrier phase errors are slowly varying as compared to T, i.e., $\Delta F_\ell \ll 1/T$ ($\ell = 1, \ldots, N_u$) the quantities $I_{i,i',\ell,\ell'}$ (6.14) are given by

$$I_{i,i',\ell,\ell'} = \delta_{i,i'} e^{j2\pi\Delta F_{\ell'} i(N_{FFT}+\nu)} \frac{1}{N_c} \sum_{n,n'=0}^{N_c-1} c^*_{iN_c+n,\ell} c_{iN_c+n',\ell'} g^\ell_{i,n} B_{n,n',\ell'} \quad (6.38)$$

In (6.38), we observe that the contributions of the different users ℓ' at the input of the decision device are rotating at a different constant speed of $2\pi\Delta F_{\ell'} T(N_{FFT} + \nu)$ rad/symbol when $g^\ell_{i,n} = 1$. Assuming the basestation can estimate the carrier frequency offsets ΔF_ℓ ($\ell = 1, \ldots, N_u$) the MMSE equaliser for both Walsh-Hadamard sequences and overlay sequences is given by (6.34), where $C_{\Delta F,\ell}$ is a real-valued positive factor that depends on the carrier frequency offsets $\Delta F_{\ell'}$ ($\ell' = 1, \ldots, N_u$) and the user index ℓ, but is independent of the carrier index n and the block index i. This factor in general is different from the factor for downlink MC-CDMA. In (6.38), it is observed that the equaliser compensates for the systematic phase rotation of the useful component. Contributions of other users are still rotating at a constant speed of $2\pi(\Delta F_{\ell'} - \Delta F_\ell)T(N_{FFT} + \nu)$ rad/symbol. Similar as in downlink MC-CDMA,

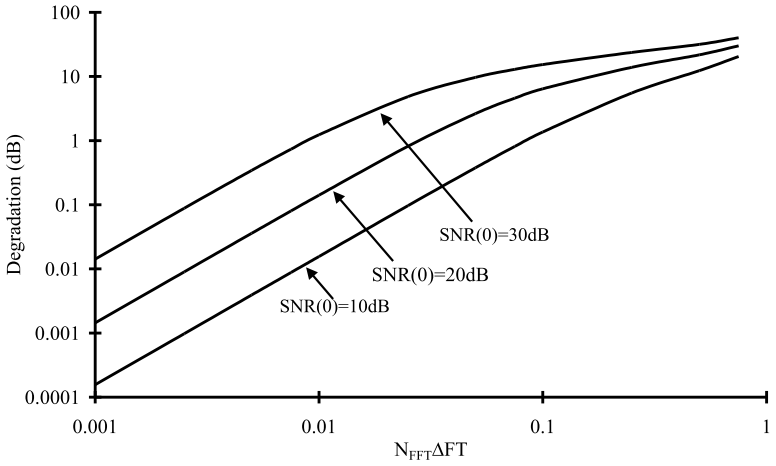

Figure 6.9: Carrier frequency offset, $N_u = N_c$

an upper bound for the degradation (6.24) can be found by adding non-negative terms to the interference powers. This yields

$$Deg_\ell \leq -10 \log \left(\frac{|D(\Delta F_\ell T)|^2}{1 + \frac{1}{N_c} \sum_{\ell'=1;\ell' \neq \ell}^{N_c} SNR_{\ell'}(0)(1 - |D(\Delta F_{\ell'} T)|^2)} \right) \quad (6.39)$$

Similarly as for downlink MC-CDMA, the upper bound is reached when $\alpha = 0$ and all carriers are modulated ($N_c = N_{FFT}$). The degradation (6.39) depends on the user index ℓ and is a function of $N_{FFT}\Delta F_\ell T$ ($\ell = 1, \ldots, N_u$). It is clear that when in uplink MC-CDMA the signals transmitted by the different users are affected by the same carrier frequency offset $\Delta F_{\ell'} = \Delta F_\ell$ ($\ell' = 1, \ldots, N_u$), the results for uplink MC-CDMA are the same as for downlink MC-CDMA.

In figure 6.9, the degradation (6.37) is shown for the maximum load (i.e., $N_u = N_c$) and all users having the same energy per symbol $E_{s,\ell} = E_s$ and the same carrier frequency offset ΔF. We observe a high sensitivity of the MC-CDMA system to the carrier frequency offset. As expected, to obtain small degradations, only small frequency offsets are allowed, i.e., $\Delta FT \ll 1/N_{FFT}$. In this case, the degradation is essentially proportional to $(N_{FFT}\Delta FT)^2$. The degradation of figure 6.9 yields an upper bound when the carriers in the rolloff area are not modulated.

The MC-CDMA system is simulated in the absence of additive noise ($N_0 = 0$), the data symbols belong to the QPSK constellation, for $\alpha = 0, N_c = N_{FFT} = 64$, all users having the same energy per symbol $E_{s,\ell} = E_s$ and the same carrier frequency offset $\Delta FT = 2.10^{-3}$, in the case of Walsh-Hadamard sequences and overlay sequences. Figures 6.10(a)-(b) show the scatter diagrams for the Walsh-Hadamard sequences and the overlay sequences, respectively, assuming

that there is no equaliser ($g_{i,n}^{\ell} = 1$). As we observe, the rotation at a speed $2\pi\Delta F_{\ell'} T(N_{FFT} + \nu)$ rad/symbol of the samples at the input of the decision device introduces a systematic phase rotation in the scatter diagram. To avoid this systematic rotation of the constellation points, the equaliser (6.34) must rotate the FFT outputs over an angle $-2\pi\Delta FTi(N_{FFT} + \nu) - \arg(D(\Delta FT))$ rad. The resulting scatter diagrams are shown in figures 6.11(a)-(b). We observe that the scatter diagrams for the Walsh-Hadamard sequences and the overlay sequences are essentially the same. The cloud in the scatter diagram has a circular shape, as the multiuser interference has uncorrelated real and imaginary parts, each having the same variance. In table 6.1, the mean square deviation of the samples at the input of the decision device is shown for the simulations of the scatter diagrams of figures 6.11. We observe that the simulation results and the theoretical results agree well.

To get rid of the strong degradation caused by carrier frequency offset, carrier frequency correction should be applied at the transmitter (uplink) or in front of the FFT at the receiver (downlink).

Carrier Phase Jitter

When a carrier synchronisation algorithm is used to get rid of the constant phase offset and the carrier frequency offset, the residual phase error can be modelled as a zero-mean stationary jitter process with spectral density $S_{\phi,\ell}(f)$ and variance $\sigma_{\phi,\ell}^2$.

In downlink MC-CDMA, the phase jitter is the same for all signals transmitted to all users. We assume slowly varying phase jitter, so the bandwidth f_B of the jitter spectrum $S_\phi(f)$ needs to be $f_B T \ll 1$. For small jitter variances, i.e., $\sigma_\phi^2 \ll 1$, we can use the approximation $\exp(j\phi(t)) \approx 1 + j\phi(t)$. The quantities $I_{i,i',\ell,\ell'}$ (6.14) reduce to

$$I_{i,i',\ell,\ell'} = \delta_{i,i'} \frac{1}{N_c} \sum_{n,n'=0}^{N_c-1} c_{iN_c+n,\ell}^{*} c_{iN_c+n',\ell'} g_{i,n}^{\ell} \cdot \left(\delta_{n,n'} + \frac{1}{N_{FFT}} \sum_{k=0}^{N_{FFT}-1} j\phi(t_{i(N_{FFT}+\nu)+k}) e^{-j2\pi \frac{k(M(n)-M(n'))}{N_{FFT}}} \right) \tag{6.40}$$

When the carrier phase jitter rapidly varies as compared to the averaging time of the MMSE equaliser, the equaliser is not able to track the jitter. The equaliser then averages the variations caused by the carrier phase jitter. As for small jitter variances, the time average of $\exp(j\phi(t))$ can be approximated by $E[\exp(j\phi(t))] \approx E[1 + j\phi(t)] = 1$, the MMSE equaliser is essentially the same as in the absence of synchronisation errors, and is given by C_ℓ from (6.31). The resulting powers of the average useful component, the self-interference, the multiuser interference and the noise are independent of the block index i and

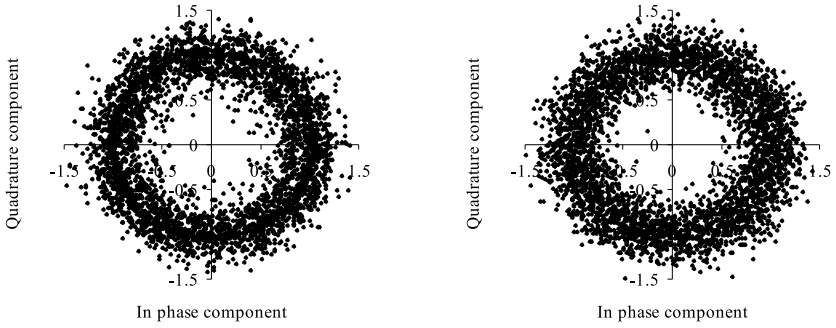

(a) (b)

Figure 6.10: Carrier frequency offset, $N_u = N_c, g_{i,n}^{\ell} = 1, \alpha = 0, N_c = N_{FFT} = 64, \Delta FT = 2.10^{-3}$ (a) Walsh-Hadamard sequences (b) overlay sequences

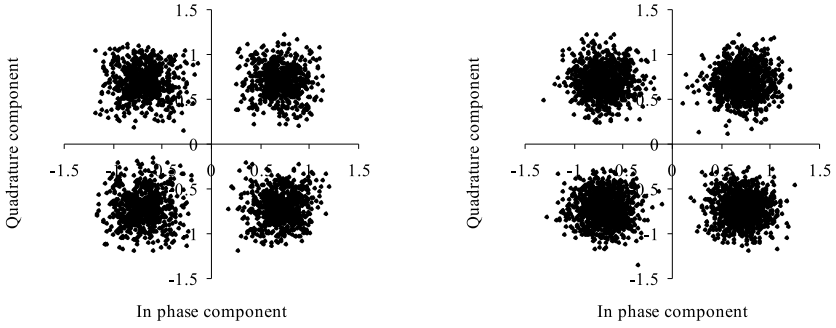

(a) (b)

Figure 6.11: Carrier frequency offset, $N_u = N_c$, MMSE equaliser, $\alpha = 0, N_c = N_{FFT} = 64, \Delta FT = 2.10^{-3}$ (a) Walsh-Hadamard sequences (b) overlay sequences

Table 6.1: Mean square deviation of the samples at the input of the decision device

	Theoretical	Simulations
Walsh-Hadamard	$5.568E-2$	$5.503E-2$
overlay	$5.568E-2$	$5.527E-2$

yield

$$\begin{aligned} P_{U,\ell} &= |C_\ell|^2 \\ P_{SI,\ell} &= |C_\ell|^2 \frac{1}{N_c}\left(\frac{1}{N_c}\sum_{n,n'=0}^{N_c-1}|B_{n,n'}|^2 + (N_c-1)B_{0,0}\right) \\ P_{MUI,\ell} &= |C_\ell|^2 \frac{1}{N_c}\sum_{\ell'=1;\ell'\neq\ell}^{N_u}\frac{E_{s,\ell'}}{E_{s,\ell}}\left(\frac{1}{N_c}\sum_{n,n'=0}^{N_c-1}|B_{n,n'}|^2 - B_{0,0}\right) \\ E[|W_{i,\ell}|^2] &= N_0|C_\ell|^2 \end{aligned} \tag{6.41}$$

where

$$B_{n,n'} = \int_{-\infty}^{+\infty} S_\phi(f)\left|D\left(fT + \frac{M(n)-M(n')}{N_{FFT}}\right)\right|^2 df$$

and $D(x)$ is defined in (6.33). In the interference powers of (6.41), the summation over n and n' corresponds with the summation over the N_c modulated carriers. To simplify the expressions (6.41), we extend the summation to all N_{FFT} available carriers. This yields an upper bound for the interference powers, i.e.,

$$\begin{aligned} P_{SI,\ell} &\leq |C_\ell|^2 \frac{1}{N_c}\Bigg(\int_{-\infty}^{+\infty} S_\phi(f)|D(fT)|^2 df \\ &+ \frac{1}{N_c}\int_{-\infty}^{+\infty} S_\phi(f)(1-|D(fT)|^2)df\Bigg) \\ P_{MUI,\ell} &\leq |C_\ell|^2 \frac{1}{N_c}\sum_{\ell'=1;\ell'\neq\ell}^{N_u}\frac{E_{s,\ell'}}{E_{s,\ell}}\int_{-\infty}^{+\infty} S_\phi(f)(1-|D(fT)|^2)df \end{aligned} \tag{6.42}$$

The upper bound is reached for $\alpha = 0$ and all carriers modulated (i.e., $N_c = N_{FFT}$). From (6.42) and figure 6.12 it follows that the self-interference and the multiuser interference mainly consist of the low frequency components ($|f| < 1/(N_{FFT}T)$) and the high frequency components ($|f| > 1/(N_{FFT}T)$) of the jitter spectrum $S_\phi(f)$, respectively. For the highest load ($N_u = N_c$) and all users exhibiting the same energy per symbol $E_{s,\ell} = E_s$, the sum of the powers of the self-interference and the multiuser interference (6.42) is independent of the spectral contents of the jitter, the spreading factor N_c and the number of carriers N_{FFT} and only depends on the jitter variance σ_ϕ^2, given by

$$\sigma_\phi^2 = \int_{-\infty}^{+\infty} S_\phi(f)df \tag{6.43}$$

In this case, the lower bound for the SNR (6.17) is equal for all users, is independent of the block index i, and yields

$$SNR \geq \frac{SNR(0)}{1 + SNR(0)\sigma_\phi^2} \tag{6.44}$$

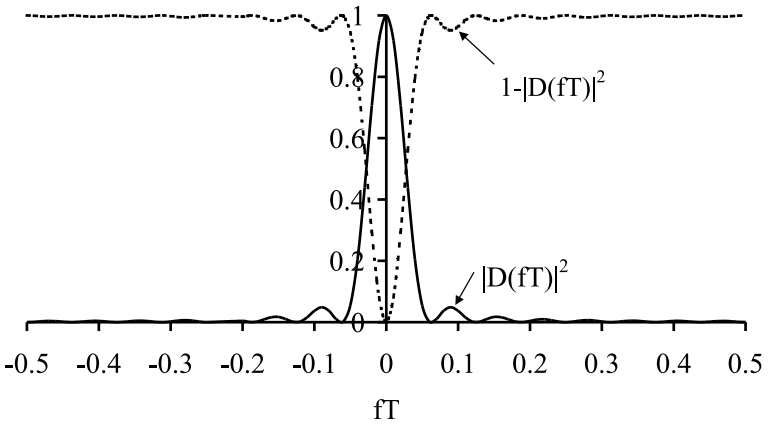

Figure 6.12: The weight functions $|D(fT)|^2$ and $1 - |D(fT)|^2$, $N_c = 16$

and the upper bound for the degradation (6.24) of the SNR as compared to SNR(0) (6.23), caused by the carrier phase jitter is given by

$$Deg \leq 10 \log \left(1 + SNR(0)\sigma_\phi^2\right) \tag{6.45}$$

where $SNR(0) = (N_{FFT}/(N_{FFT} + \nu))E_s/N_0$. The upper bound in (6.45) is reached when $\alpha = 0$ and all carriers are modulated ($N_c = N_{FFT}$). This upper bound (6.45) yields an accurate approximation for the actual degradation when the rolloff area is small and $N_c \approx N_{FFT}$. The degradation (6.45) is independent of the spreading factor.

When $N_u < N_c$, the sum of the powers of the self-interference and the multiuser interference (6.42) does depend on the shape of the jitter spectrum. Let us consider the following cases.

1. When all jitter power is in the interval $|f| < 1/(N_{FFT}T)$, the MUI power is negligibly small as compared to the SI power. The degradation of the SNR is essentially independent of the number N_u of active users, and equal to (6.45).

2. Decreasing by some amount the jitter power in the interval $|f| < 1/(N_{FFT}T)$ and simultaneously increasing by the same amount the jitter power in the interval $|f| > 1/(N_{FFT}T)$, yields a decrease of the SI power and an increase of the MUI power. As $N_u < N_c$, the sum of the powers of the SI and the MUI is reduced, so that the degradation of the SNR is smaller that for case (1).

3. The smallest degradation of the SNR is obtained when all jitter power is in the interval $|f| > 1/(N_{FFT}T)$, in which case the SI power is essentially

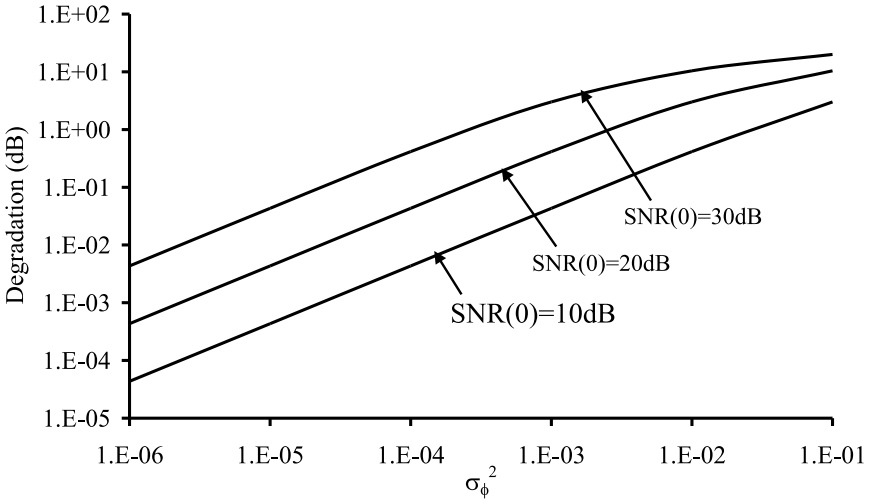

Figure 6.13: Carrier phase jitter, $N_u = N_c$

zero. The degradation of the SNR is essentially zero for $N_u = 1$, and is given by (6.45) for $N_u \to N_c$.

In uplink MC-CDMA, the contributions of the signals transmitted by the different users exhibit a different carrier phase jitter process. Assuming the phase jitter is slowly varying and the jitter variance is small, a similar approximation as for downlink MC-CDMA reduces the quantities $I_{i,i',\ell,\ell'}$ (6.29) to

$$I_{i,i',\ell,\ell'} = \delta_{i,i'} \frac{1}{N_c} \sum_{n,n'=0}^{N_c-1} c^*_{iN_c+n,\ell} c_{iN_c+n',\ell'} g^{\ell}_{i,n} \cdot \left(\delta_{n,n'} + \frac{1}{N_{FFT}} \sum_{k=0}^{N_{FFT}-1} j\phi_{\ell'}(t_{i(N_{FFT}+\nu)+k}) e^{-j2\pi \frac{k(M(n)-M(n'))}{N_{FFT}}} \right) \quad (6.46)$$

A similar analysis can be done as for downlink MC-CDMA. When in uplink MC-CDMA the different carrier phase jitter processes have the same jitter spectrum $S_{\phi,\ell'}(f) = S_\phi(f)$ $(\ell' = 1, \ldots, N_u)$, the results are the same as for downlink MC-CDMA.

In figure 6.13, the degradation (6.45) is shown for the maximum load ($N_u = N_c$) as function of the jitter variance. For small jitter variance, the degradation is essentially proportional to σ^2_ϕ. The results of figure 6.13 yield an upper bound when the carriers inside the rolloff area are not modulated. In figure 6.14, the degradation is shown as function of the load for various values of $f_L T$ and $f_B T$, assuming $\sigma^2_\phi = -40$ dB rad^2 and $SNR(0) = 25$ dB. The degradations of figures 6.13 and 6.14 are independent of the spreading factor and the number of carriers.

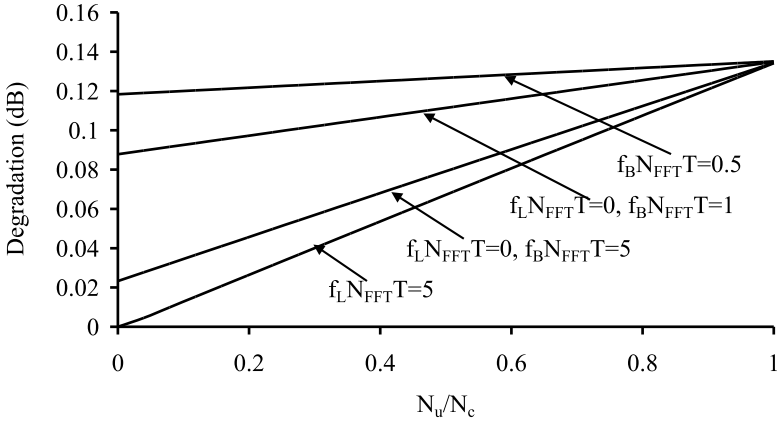

Figure 6.14: Degradation as function of the load, $\sigma_\phi^2 = -40$ dB rad^2, $SNR(0) = 25$ dB

- For $f_B N_{FFT} T = 0.5$, most jitter power is within the interval $|f| < 1/(N_{FFT}T)$. The degradation is essentially independent of the number of users and of the bandwidth f_L of the phase-locked loop (PLL) ($f_L < f_B$).

- For $f_L N_{FFT} T = 5$, most jitter power is within the interval $|f| > 1/(N_{FFT}T)$. The degradation is independent of the jitter bandwidth f_B ($f_B > f_L$), and assumes its minimum value.

- For $f_L N_{FFT} T = 0$ and $f_B N_{FFT} T \geq 1$, phase jitter is present in both intervals $|f| < 1/(N_{FFT}T)$ and $|f| > 1/(N_{FFT}T)$. When $f_B N_{FFT} T$ increases, the self-interference decreases and the multiuser interference increases; the net effect is a reduction of the degradation.

We have simulated the MC-CDMA system in the absence of additive noise ($N_0 = 0$), assuming the data symbols belong to the QPSK constellation. We consider $\alpha = 0$, $N_c = N_{FFT} = 64$, the maximum load ($N_u = N_c$) and all users having the same energy per symbol $E_{s,\ell} = E_s$. The jitter spectrum for all users is shown in figure 6.15 with $\sigma_\phi^2 = 5.10^{-3}$ rad^2. Figures 6.16(a)-(b) and 6.17(a)-(b) show the scatter diagrams for $f_L = 0, f_B = 1/(N_c T)$ and $f_L = 2/(N_c T), f_B = 4/(N_c T)$, respectively. As $N_u = N_c$, the mean-square deviation of the samples at the input of the decision device from the constellation points is the same for all scatter diagrams and equals σ_ϕ^2. However, the scatter diagrams of figures 6.16 and 6.17 differ considerably. As we observe, the results for the Walsh-Hadamard sequences and the overlay sequences are the same. When $f_L = 0, f_B = 1/(N_c T)$, the jitter mainly introduces self-interference: the jitter gives rise to a random fluctuation of the useful component. Hence, the scatter diagram shows an angular displacement of the samples at the input of the

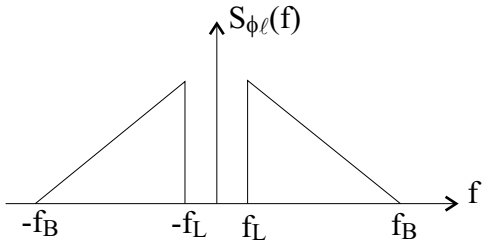

Figure 6.15: Jitter spectrum

decision device. When $f_L = 2/(N_cT), f_B = 4/(N_cT)$, the phase jitter mainly introduces multiuser interference. The term of the multiuser interference has uncorrelated real and imaginary parts, each having the same variance, so that the cloud in the scatter diagram has a circular shape. In table 6.2, the mean square deviation of the samples at the input device is shown for the simulations of the scatter diagrams of figures 6.16 and 6.17. As we observe, the simulation results and the theoretical results agree well.

6.4.2 Timing Errors

In this section, we investigate the sensitivity of downlink and uplink MC-CDMA to timing errors in the absence of carrier phase errors ($\phi_\ell(t) = 0$). We assume that the cyclic prefix is sufficiently long, so that in the presence of timing errors the N_{FFT} samples per block processed by the receiver are not affected by interference from other blocks. As only carriers outside the rolloff area are modulated, (6.26) yields

$$G_{n,\ell}(t_{i(N_{FFT}+\nu)+k}) = e^{j2\pi\epsilon_{i(N_{FFT}+\nu)+k,\ell}\frac{\mathrm{mod}(M(n);N_{FFT})}{N_{FFT}}} \tag{6.47}$$

In the case of downlink MC-CDMA, the signals transmitted to the different users are aligned at the basestation. Hence, the timing errors are the same for all contributions. In uplink MC-CDMA, a misalignment between the FFT frames transmitted by the different users can occur. Hence, the contributions of the different users exhibit a different timing error. In the following, we separately consider the case of a constant timing offset, a clock frequency offset and timing jitter.

Constant Timing Offset

In the case of downlink MC-CDMA where the contributions of the different users exhibit the same constant timing offset $\epsilon_{\ell'} = \epsilon_\ell$ ($\ell' = 1, \ldots, N_u$), the quantities

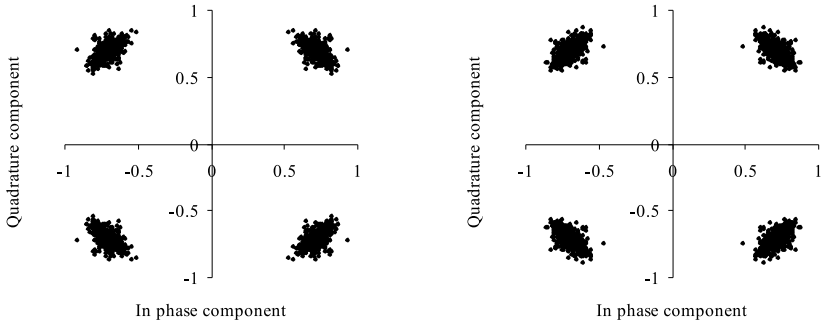

Figure 6.16: Carrier phase jitter, $N_u = N_c, f_L = 0, f_B = 1/(N_cT), \alpha = 0, N_c = 64, \sigma_\phi^2 = 5.10^{-3}$ rad^2 (a) Walsh-Hadamard sequences (b) overlay sequences

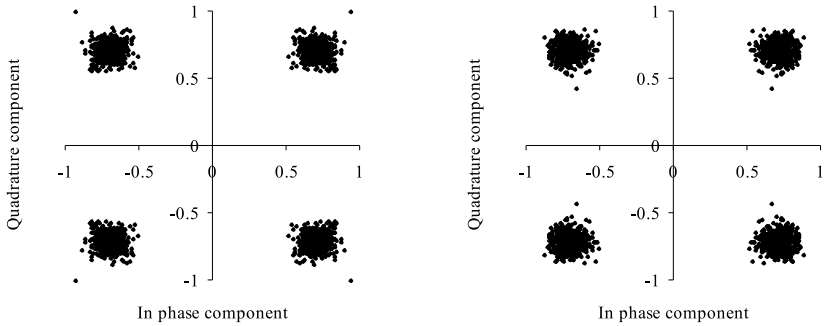

Figure 6.17: Carrier phase jitter, $N_u = N_c, f_L = 2/(N_cT), f_B = 4/(N_cT), \alpha = 0, N_c = 64, \sigma_\phi^2 = 5.10^{-3}$ rad^2 (a) Walsh-Hadamard sequences (b) overlay sequences

Table 6.2: Mean square deviation of the samples at the input of the decision device

		Theoretical	Simulations
$f_L = 0,$	Walsh-Hadamard	$5E-3$	$4.988E-3$
$f_B = 1/(N_cT) = R_s$	overlay	$5E-3$	$5.030E-3$
$fL = 2/(N_cT) = 2R_s,$	Walsh-Hadamard	$5E-3$	$5.013E-3$
$fB = 4/(N_cT) = 4R_s$	overlay	$5E-3$	$5.022E-3$

$I_{i,i',\ell,\ell'}$ (6.14) reduce to

$$I_{i,i',\ell,\ell'} = \delta_{i,i'} \frac{1}{N_c} \sum_{n,n'=0}^{N_c-1} c^*_{iN_c+n,\ell} c_{iN_c+n',\ell'} g^{\ell}_{i,n} G_{n,\ell} \tag{6.48}$$

As only carriers outside the rolloff area are modulated, the quantity $G_{n,\ell}$ yields

$$G_{n,\ell} = e^{j2\pi\epsilon_\ell \frac{\text{mod}(M(n);N_{FFT})}{N_{FFT}}} \tag{6.49}$$

where $\text{mod}(x; N_{FFT})$ denotes the modulo-N_{FFT} reduction of x, yielding a result in $(-N_{FFT}/2, N_{FFT}/2)$. Hence, the constant timing offset introduces a pure phase rotation of the FFT outputs. This carrier dependent phase rotation is compensated by the one-tap equaliser without enhancing the noise power level (6.16), thus without performance loss, by rotating the FFT outputs over the angle $-2\pi\epsilon_\ell \text{mod}(M(n); N_{FFT})/N_{FFT}$.

In the case of uplink MC-CDMA, where the contributions of the signals transmitted by the different users exhibit a different timing error $\epsilon_{\ell'}$ $\ell' = 1, \ldots, N_u$, the quantities $I_{i,i',\ell,\ell'}$ (6.14) reduce to

$$I_{i,i',\ell,\ell'} = \delta_{i,i'} \frac{1}{N_c} \sum_{n,n'=0}^{N_c-1} c^*_{iN_c+n,\ell} c_{iN_c+n',\ell'} g^{\ell}_{i,n} G_{n,\ell'} \tag{6.50}$$

where $G_{n,\ell}$ is given by (6.49). Let us consider the case of one disturbing user. We assume that the transmitter and receiver clocks of user '0' are perfectly synchronised, i.e., $\epsilon_0 = 0$. Further, the MC-CDMA blocks of the disturbing user '1' are shifted over an interval ϵT as compared to the MC-CDMA blocks of the considered user, as shown in figure 6.18, i.e., $\epsilon_1 = \epsilon$. In figure 6.19, the degradation of the uplink MC-CDMA system is shown as function of the misalignment between the MC-CDMA blocks of the two users, for both users having the same energy per symbol, an MMSE equaliser and $SNR(0)$=20 dB. As we observe in figure 6.19, the performance of the uplink MC-CDMA system is strongly degraded. This degradation can be explained as follows: the rotation over a carrier dependent angle $2\pi\epsilon \text{mod}(M(n); N_{FFT})/N_{FFT}$ of the contributions of the disturbing user at the FFT outputs can be viewed as if the disturbing user makes use of the spreading sequence $\tilde{c}_{iN_c+n,1} = c_{iN_c+n,1} \exp(j2\pi\epsilon \text{mod}(M(n); N_{FFT})/N_{FFT})$. The FFT outputs are multiplied with the spreading sequence $\mathbf{c}_{i,0}$ of the considered user, and the resulting terms are summed. As the sequence $\tilde{\mathbf{c}}_{i,1}$ of the disturbing user is no longer orthogonal with the spreading sequence $\mathbf{c}_{i,0}$ of the considered user, MUI is introduced. For small timing offsets, the sequence $\tilde{\mathbf{c}}_{i,1}$ only slightly differs from the original spreading sequence $\mathbf{c}_{i,1}$ and is nearly orthogonal to the spreading sequence $\mathbf{c}_{i,0}$ of the considered user. Hence, only a small degradation is introduced. For larger misalignments between the blocks of the different users, the sequence $\tilde{\mathbf{c}}_{i,1}$ differs considerably from the original spreading sequence $\mathbf{c}_{i,1}$. In this case, the sequence $\tilde{\mathbf{c}}_{i,1}$ can be viewed as random with respect to $\mathbf{c}_{i,0}$, which means that a significant degradation is introduced.

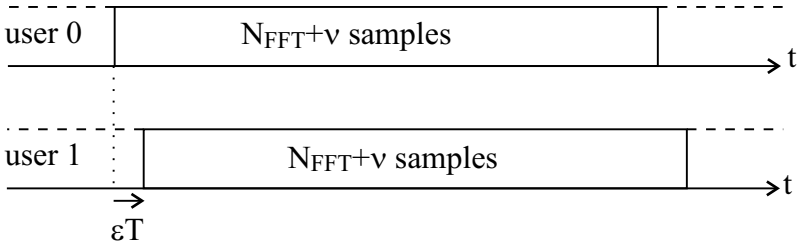

Figure 6.18: Misalignment of the MC-CDMA blocks

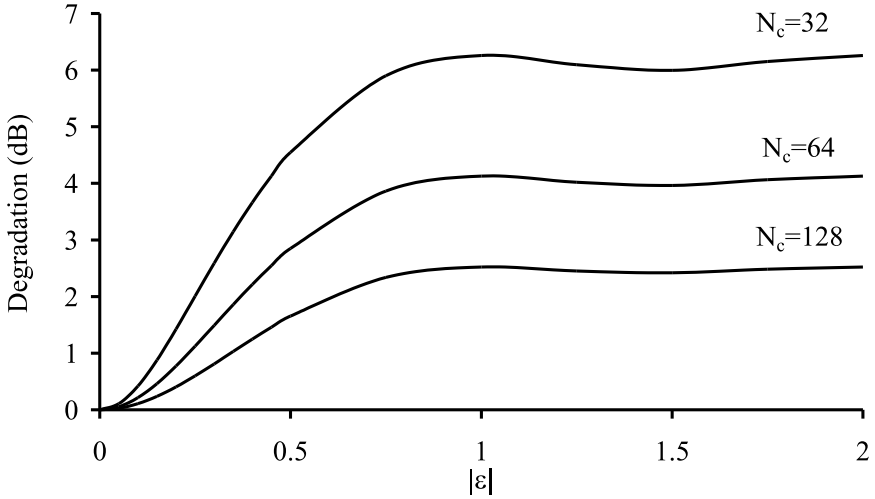

Figure 6.19: Influence of a constant timing offset in uplink MC-CDMA, one disturbing user, MMSE equaliser, $E_{s,\ell} = E_s, \alpha = 0, N_{FFT} = N_c, SNR(0) = 20$ dB

Because of the large sensitivity of uplink MC-CDMA to timing misalignments between the signals transmitted by the different users, the transmitters should be synchronised within a small fraction of the sampling interval T.

Clock Frequency Offset

In the case of a clock frequency offset, the timing error linearly increases with time $\epsilon_{i(N_{FFT}+\nu)+k,\ell} = (k + i(N_{FFT} + \nu))\Delta T_\ell/T + \epsilon_{0,\ell}$, where $\Delta T_\ell/T$ is the relative clock frequency offset. This yields an increasing misalignment between the samples $s_{i(N_{FFT}+\nu)+k,\ell}$ at the transmitter and the samples $v_{i(N_{FFT}+\nu)+k,\ell}$ at the receiver. Similarly as in OFDM(A), the increasing misalignment could be compensated by using a coarse synchronisation algorithm at the receiver, which involves duplication or removing samples at regular intervals (see section 5.4.2).

In downlink MC-CDMA, the contributions of the different users are aligned at the basestation. Hence, the contributions of the different users at the receiver of user ℓ exhibit the same clock frequency offset $\Delta T_{\ell'}/T = \Delta T_\ell/T$ ($\ell' = 1, \ldots, N_u$). The resulting timing error after coarse synchronisation yields $\tilde{\epsilon}_{i(N_{FFT}+\nu)+k,\ell} = k\Delta T_\ell/T + \epsilon_{i,\ell}$, where $\epsilon_{i,\ell}$ is constant over a MC-CDMA block and depends on the block index i. In uplink MC-CDMA, the contributions of the different users exhibit a different clock frequency offset $\Delta T_\ell/T$ ($\ell = 1, \ldots, N_u$). The resulting timing errors after coarse synchronisation at the transmitters yield $\tilde{\epsilon}_{i(N_{FFT}+\nu)+k,\ell} = k\Delta T_\ell/T + \epsilon_{i,\ell}$ ($\ell = 1, \ldots, N_u$), where $\epsilon_{i,\ell}$ is constant over a MC-CDMA block and depends on the block index i and the user index ℓ.

In the case of downlink MC-CDMA, the contributions of the different users are affected by the same timing error $\tilde{\epsilon}_{i(N_{FFT}+\nu)+k,\ell} = k\Delta T_\ell/T + \epsilon_{i,\ell}$. As only carriers outside the rolloff area are modulated, the quantities (6.14) yield

$$I_{i,i',\ell,\ell'} = \delta_{i,i'} \frac{1}{N_c} \sum_{n,n'=0}^{N_c-1} c^*_{iN_c+n,\ell} c_{iN_c+n',\ell'} g^\ell_{i,n} e^{j2\pi\epsilon_{i,\ell}\frac{\mathrm{mod}(M(n');N_{FFT})}{N_{FFT}}} B_{n,n',\ell} \tag{6.51}$$

where

$$B_{n,n',\ell} = D\left(\frac{M(n) - M(n')}{N_{FFT}} + \frac{\mathrm{mod}(M(n');N_{FFT})}{N_{FFT}}\frac{\Delta T_\ell}{T}\right)$$

and $D(x)$ is defined in (6.33). As we observe from (6.51), the contribution $I_{i,i,\ell,\ell'}$ is nonzero for $\ell' \neq \ell$. Furthermore, the useful contribution $I_{i,i,\ell,\ell}$ is attenuated as compared to the case of a zero clock frequency offset, and exhibits a random fluctuation when the overlay spreading sequences are used. Hence, a clock frequency offset introduces a reduction of the useful component, self-interference and multiuser interference. The MMSE equaliser has equaliser coefficients

$$(g_{MMSE})^\ell_{i,n} = C_{\Delta T_\ell,n} e^{-j2\pi\epsilon_{i,\ell}\frac{\mathrm{mod}(M(n);N_{FFT})}{N_{FFT}}} D^*\left(\frac{\mathrm{mod}(M(n);N_{FFT})}{N_{FFT}}\frac{\Delta T_\ell}{T}\right) \tag{6.52}$$

where $C_{\Delta T_\ell,n}$ is a real-valued positive factor that depends on the clock frequency offset ΔT_ℓ, the user index ℓ and the carrier index n. With these equaliser coefficients, we observe in (6.51) that the equaliser is not able to eliminate the MUI ($I_{i,i',\ell,\ell'} \neq 0$ for $\ell' \neq l$). Hence, the MC-CDMA system is degraded as compared to the case of a zero clock frequency offset.

In uplink MC-CDMA, the contributions of the different users exhibit a different timing error $\tilde{\epsilon}_{i(N_{FFT}+\nu)+k,\ell} = k\Delta T_\ell/T + \epsilon_{i,\ell}$ ($\ell = 1, \ldots, N_u$). As only carriers outside the rolloff area are modulated, the quantities $I_{i,i',\ell,\ell'}$ (6.14) yield

$$I_{i,i',\ell,\ell'} = \delta_{i,i'} \frac{1}{N_c} \sum_{n,n'=0}^{N_c-1} c^*_{iN_c+n,\ell} c_{iN_c+n',\ell'} g^\ell_{i,n} e^{j2\pi\epsilon_{i,\ell'}\frac{\mathrm{mod}(M(n');N_{FFT})}{N_{FFT}}} B_{n,n',\ell'} \tag{6.53}$$

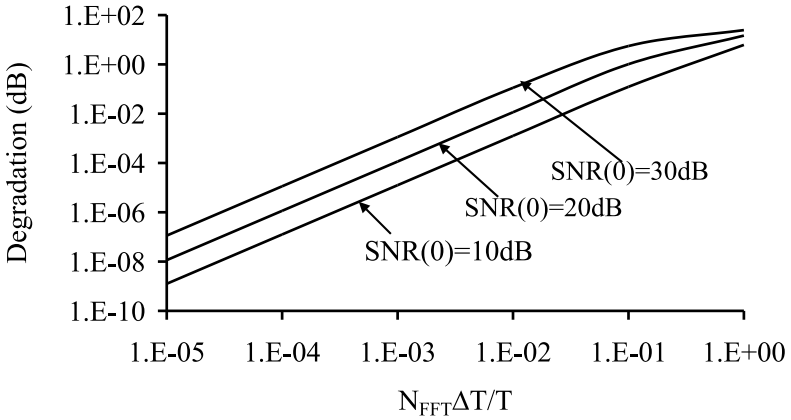

Figure 6.20: Clock frequency offset, $\alpha = 0, N_{FFT} = N_c, N_u = N_c$, downlink

A similar analysis as for downlink MC-CDMA shows us that a clock frequency offset introduces self-interference and multiuser interference and degrades the uplink MC-CDMA system. Because of the timing misalignment between the blocks from different users, the degradation is much worse than in downlink MC-CDMA (see also section on constant timing offset).

In figure 6.20, the degradation of the downlink MC-CDMA system is shown, for all users having the same energy per symbol $E_{s,\ell} = E_s$. We assume $\alpha = 0, N_{FFT} = N_c$ and the maximum load $N_u = N_c$. The degradation is a function of the product $N_{FFT}\Delta T/T$. As we observe in figure 6.20, the MC-CDMA system is very sensitive to a clock frequency offset. As expected, in order to obtain a small degradation, the clock frequency offset must be limited, i.e., $\Delta T/T \ll 1/N_{FFT}$. In this case, the degradation is essentially proportional to $(N_{FFT}\Delta T/T)^2$. The degradation of figure 6.20 yields an upper bound for the degradation when the carriers in the rolloff are not modulated.

We have simulated the downlink MC-CDMA system in the absence of additive noise ($N_0 = 0$), assuming the data symbol belongs to the QPSK constellation. We consider $\alpha = 0, N_{FFT} = N_c = 64, \Delta T/T = 10^{-2}$ and all users have the same energy per symbol $E_{s,\ell} = E_s$. In figures 6.21 (a)-(b), the scatter diagram is shown for the maximum load, for both Walsh-Hadamard sequences and overlay sequences. It is assumed that the equaliser minimises the MSE. We observe that the scatter diagrams for the Walsh-Hadamard sequences and the overlay sequences are the same. The circular cloud in the scatter diagram is introduced by the dominating MUI contribution: this term has uncorrelated real and imaginary parts, each having the same variance. In table 6.3, the mean square deviation of the samples at the input device is shown for the simulations of the scatter diagrams of figure 6.21. As we observe, the simulation results and the theoretical results agree well.

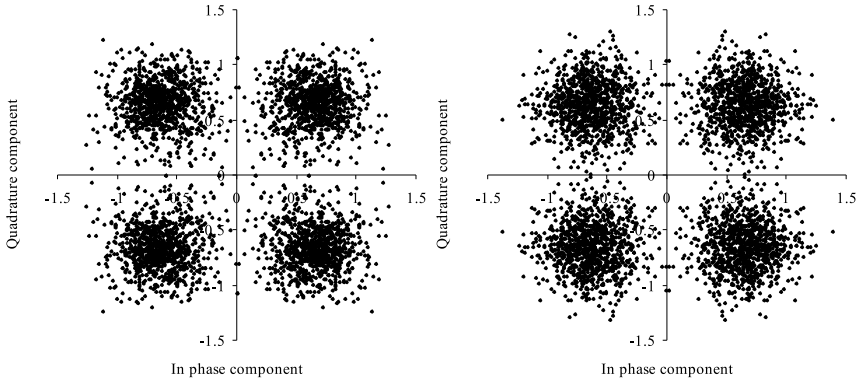

(a) (b)

Figure 6.21: Clock frequency offset, $N_u = N_c$, MMSE equaliser, $\alpha = 0, N_{FFT} = N_c = 64, \Delta T/T = 10^{-2}$ (a) Walsh-Hadamard sequences (b) overlay sequences

Table 6.3: Mean square deviation of the samples at the input of the decision device

	Theoretical	Simulations
Walsh-Hadamard	$1.036E-1$	$1.075E-1$
overlay	$1.036E-1$	$0.992E-1$

When the degradation caused by clock frequency offset can not be tolerated, timing correction should be applied at the transmitter (uplink) or in front of the FFT at the receiver (downlink).

Timing Jitter

When a clock synchronisation mechanism is used to extract the timing instants, we get rid of a constant timing offset and a clock frequency offset. The residual timing error can be modelled as a zero-mean stationary random process with jitter power spectral density $S_{\epsilon,\ell}(\exp(j2\pi fT))$ and jitter variance $\sigma^2_{\epsilon,\ell}$.

In downlink MC-CDMA, the timing jitter $\epsilon_{i(N_{FFT}+\nu)+k,\ell}$ is the same for the contributions of all users, as the MC-CDMA blocks are aligned at the basestation. Assuming the timing error is slowly varying as compared to T and the jitter variances are small, i.e., $\sigma^2_{\epsilon,\ell} \ll 1$, the quantities $I_{i,i',\ell,\ell'}$ (6.14) can be

approximated by

$$I_{i,i',\ell,\ell'} \approx \delta_{i,i'} \frac{1}{N_c} \sum_{n,n'=0}^{N_c-1} c^*_{iN_c+n,\ell} c_{iN_c+n',\ell'} g^{\ell}_{i,n} \cdot \left(\delta_{n,n'} + j2\pi S_{n'} \frac{1}{N_{FFT}} \sum_{k=0}^{N_{FFT}-1} e^{-j2\pi \frac{k(M(n)-M(n'))}{N_{FFT}}} \epsilon_{i(N_{FFT}+\nu)+k,\ell} \right) \tag{6.54}$$

As only carriers outside the rolloff area are modulated, the quantity S_n in (6.54) yields

$$S_n = \frac{\mathrm{mod}(M(n); N_{FFT})}{N_{FFT}} \tag{6.55}$$

When the timing jitter rapidly varies as compared to the averaging time of the MMSE equaliser, the equaliser is not able to track the timing jitter. The equaliser averages the variations caused by the timing jitter. For small jitter variances, the time average of $\exp(j2\pi\epsilon_{i(N_{FFT}+\nu)+k}\mathrm{mod}(M(n); N_{FFT})/N_{FFT})$ can be approximated by $E[\exp(j2\pi\epsilon_{i(N_{FFT}+\nu)+k}\mathrm{mod}(M(n); N_{FFT})/N_{FFT})] \approx E[1 + j2\pi\epsilon_{i(N_{FFT}+\nu)+k}\mathrm{mod}(M(n); N_{FFT})/N_{FFT}] = 1$. Hence, the equaliser is essentially the same as in the absence of timing errors, i.e., $(g_{MMSE})^{\ell}_{i,n} \approx C_\ell$ where C_ℓ is defined in (6.31). The resulting powers of the average useful component, the self-interference, the multiuser interference (6.18) and the noise (6.17) are independent of the block index i and yield

$$\begin{aligned}
P_{U,\ell} &= |C_\ell|^2 \\
P_{SI,\ell} &= |C_\ell|^2 \frac{(2\pi)^2}{N_c^2} \left(\sum_{n,n'=0;n'\neq n}^{N_c-1} |S_{n'}|^2 B_{n,n',\ell} \right. \\
&+ \left. \left(\left| \sum_{n=0}^{N_c-1} S_n \right|^2 - \sum_{n=0}^{N_c-1} |S_n|^2 \right) B_{0,0,\ell} \right) \\
P_{MUI,\ell} &= |C_\ell|^2 \frac{(2\pi)^2}{N_c^2} \sum_{\ell'=1;\ell'\neq\ell}^{N_u} \frac{E_{s,\ell'}}{E_{s,\ell}} \left(\sum_{n,n'=0;n'\neq n}^{N_c-1} |S_{n'}|^2 B_{n,n',\ell} \right. \\
&- \left. \frac{1}{N_c-1} \left(\left| \sum_{n=0}^{N_c-1} S_n \right|^2 - \sum_{n=0}^{N_c-1} |S_n|^2 \right) B_{0,0,\ell} \right) \\
E[|W_{i,\ell}|^2] &= N_0 |C_\ell|^2
\end{aligned} \tag{6.56}$$

where

$$B_{n,n',\ell} = \int_{-1/2T}^{+1/2T} S_{\epsilon,\ell}(e^{j2\pi fT}) \left| D\left(fT - \frac{M(n') - M(n)}{N_{FFT}} \right) \right|^2 df$$

and $D(x)$ is defined in (6.33). In the interference powers in (6.56), the summations over n (and n') corresponds to the summation over the N_c modulated

carriers. By extending the summation to all N_{FFT} available carriers, an upper bound for the interference powers can be found. This yields

$$\begin{aligned} P_{SI,\ell} &\leq |C_\ell|^2 S_{N_{FFT}} \frac{1}{N_c} \int_{-1/2T}^{+1/2T} S_{\epsilon,\ell}(e^{j2\pi fT})(1-|D(fT)|^2)df \\ P_{ICI,\ell} &\leq |C_\ell|^2 S_{N_{FFT}} \frac{1}{N_c-1} \sum_{\ell'=1;\ell'\neq\ell}^{N_u} \frac{E_{s,\ell'}}{E_{s,\ell}} \cdot \\ &\quad \left(\int_{-1/2T}^{+1/2T} S_\epsilon(e^{j2\pi fT}) - \frac{1}{N_c} \int_{-1/2T}^{+1/2T} S_{\epsilon,\ell}(e^{j2\pi fT})(1-|D(fT)|^2)df \right) \end{aligned} \tag{6.57}$$

where

$$S_{N_{FFT}} = \frac{(2\pi)^2}{N_c} \sum_{n=0}^{N_{FFT}-1} \left(\frac{\mathrm{mod}(n; N_{FFT})}{N_{FFT}} \right)^2 \tag{6.58}$$

The upper bound in (6.57) is reached for $\alpha = 0$ and all carriers modulated, i.e., $N_c = N_{FFT}$. As we observe from (6.57) and figure 6.12, the upper bound for the SI power depends on the high frequency components ($|f| > 1/(N_{FFT}T)$) of the jitter. Furthermore, for large N_c, the upper bound for the multiuser interference power is essentially independent of the spectral contents of the jitter. From (6.57) it also follows that the sum of the SI power and the MUI power increases with the number of active users N_u. For large N_u, the SI power is negligible as compared to the MUI power. For the maximum load $N_u = N_c$ and when all users exhibit the same energy per symbol, this sum is independent of the spectral contents of the jitter and only depends on the jitter variance $\sigma^2_{\epsilon,\ell}$, given by

$$\sigma^2_{\epsilon,\ell} = \int_{-1/2T}^{+1/2T} S_{\epsilon,\ell}(e^{j2\pi fT})df \tag{6.59}$$

For the maximum load, the interference is dominated by the MUI. For a large number of carriers ($N_{FFT} \to \infty$), the sum $S_{N_{FFT}}$ (6.58) equals $S_{N_{FFT}} = (N_{FFT}/N_c)\pi^2/3$. Hence, when the number of unmodulated carriers is small, i.e., $N_c \approx N_{FFT}$, the quantity $S_{N_{FFT}}$ (6.58) is essentially independent of the number of carriers and of the spreading factor. In this case, the upper bound for the degradation (6.24) of the SNR depends only on the jitter variance, i.e.,

$$Deg_\ell \leq 10 \log \left(1 + SNR(0) \frac{\pi^2}{3} \sigma^2_{\epsilon,\ell} \right) \tag{6.60}$$

where $SNR(0) = (N_{FFT}/(N_{FFT}+\nu))E_s/N_0$. The upper bound for the degradation (6.60) yields an accurate approximation of the actual degradation when the rolloff area is small and the spreading factor is almost equal to the number of carriers, i.e., $N_c \approx N_{FFT}$.

In uplink MC-CDMA, the contributions of the signals transmitted by the different users exhibit a different timing jitter process. In this case, assuming

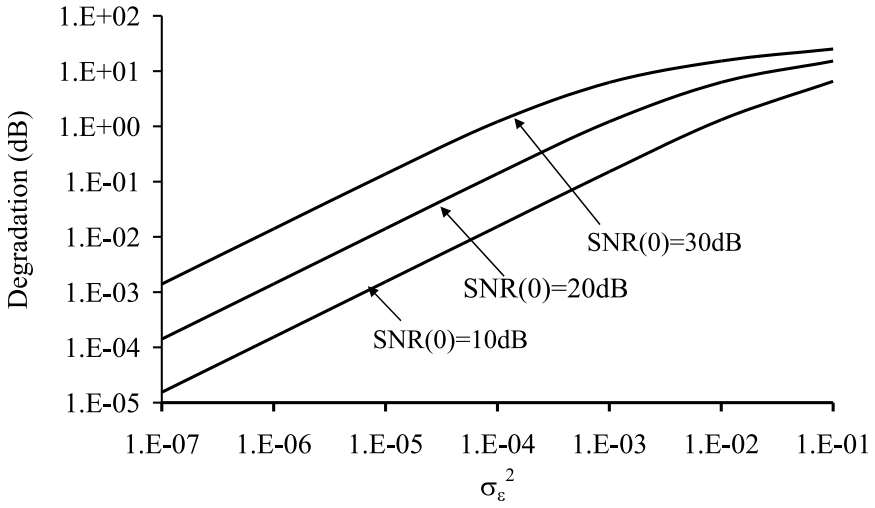

Figure 6.22: Timing jitter, $E_{s,\ell} = E_s, N_u = N_c, N_{FFT\rightarrow\infty, N_c \approx N_{FFT}}$

slowly varying timing jitter and small jitter variances, the quantities $I_{i,i',\ell,\ell'}$ (6.14) can be approximated by

$$I_{i,i',\ell,\ell'} \approx \delta_{i,i'} \frac{1}{N_c} \sum_{n,n'=0}^{N_c-1} c^*_{iN_c+n,\ell} c_{iN_c+n',\ell'} g^{\ell}_{i,n} \cdot \left(\delta_{n,n'} + j2\pi S_{n'} \frac{1}{N_{FFT}} \sum_{k=0}^{N_{FFT}-1} e^{-j2\pi \frac{k(M(n)-M(n'))}{N_{FFT}}} \epsilon_{i(N_{FFT}+\nu)+k,\ell'} \right) \quad (6.61)$$

Following a similar analysis as for downlink MC-CDMA, the power of the MUI yields

$$P_{MUI,\ell} = |C_\ell|^2 \frac{(2\pi)^2}{N_c^2} \sum_{\ell'=1;\ell'\neq\ell}^{N_u} \frac{E_{s,\ell'}}{E_{s,\ell}} \left(\sum_{n,n'=0;n'\neq n}^{N_c-1} |S_{n'}|^2 B_{n,n',\ell'} - \frac{1}{N_c - 1} \left(\left| \sum_{n=0}^{N_c-1} S_n \right|^2 - \sum_{n=0}^{N_c-1} |S_n|^2 \right) B_{0,0,\ell'} \right) \quad (6.62)$$

The powers of the average useful component, the self-interference and the noise are the same as for downlink MC-CDMA and are given by (6.56). It is clear that when the timing jitter processes have the same jitter spectrum $S_\epsilon(\exp(j2\pi fT))$, the results are the same as for downlink MC-CDMA.

In figure 6.22, the degradation (6.60) is shown as function of the jitter variance. This degradation is independent of the number of carriers and the spreading factor. For small jitter variance, the degradation is essentially proportional

to σ_ϵ^2. The degradation of figure 6.22 yields an upper bound for the degradation in the case where the carriers in the rolloff area are not modulated.

We have simulated the MC-CDMA system in the absence of additive noise ($N_0 = 0$), assuming the data symbols belong to the QPSK constellation. We consider $\alpha = 0, N_{FFT} = N_c = 64$; all users have the same energy per symbol $E_{s,\ell} = E_s$, and the same jitter spectrum $S_\epsilon(\exp(j2\pi fT))$ of figure 6.15 with jitter variance $\sigma_\epsilon^2 = 10^{-3}$ rad^2. In figures 6.23 (a)-(b) and 6.24 (a)-(b), the scatter diagrams are shown for $f_L = 0, f_B = 1/(N_cT)$ and $f_L = 1/(N_cT), f_B = 2/(N_cT)$, respectively. We observe that the results for the Walsh-Hadamard sequences are the same as for the overlay sequences. As expected, the scatter diagrams do not depend on the spectral contents of the timing jitter. All scatter diagrams show a circular cloud, as the dominating MUI term has uncorrelated real and imaginary parts, each having the same variance. In table 6.4, the mean square deviation of the samples at the input device is shown for the simulations of the scatter diagrams of figures 6.23 and 6.24. As we observe, the simulation results and the theoretical results agree well.

6.5 Dispersive Channel

In the previous section, the sensitivity of the MC-CDMA system to synchronisation errors has been investigated in the case of an ideal channel. In this section, we will consider the case of a dispersive channel. In our analysis, we consider the case of synchronous transmission, i.e., all users exhibit the same carrier phase errors and timing errors. The channel transfer function is assumed to be the same for all users. This situation is typical for downlink MC-CDMA. The cyclic prefix is able to counteract the effects of the dispersive channel, i.e., neither intersymbol interference nor interference between the different carriers is introduced. We assume the maximum load ($N_u = N_c$) and all users exhibit the same energy per symbol $E_{s,\ell} = E_s$. Maximum load corresponds to the worst case, as the multiuser interference power is the largest. Furthermore, we consider both Walsh-Hadamard sequences and overlay sequences.

6.5.1 No Synchronisation Errors

Similarly as for the OFDM(A) system, the quantities (6.25) reduce for a fixed channel $H_{ch}(f;\tau) = H_{ch}(f)$ and in the absence of synchronisation errors to

$$A_{i,i',n,n'} = \delta_{i,i'}\delta_{n,n'}G_n \tag{6.63}$$

As only the carriers outside the rolloff area are modulated, the quantity G_n in (6.63) yields

$$G_n = H_{ch}\left(\frac{\mathrm{mod}(M(n);N_{FFT})}{N_{FFT}T}\right) \tag{6.64}$$

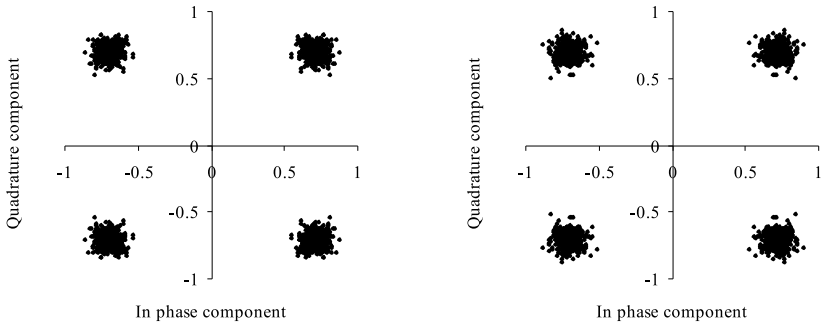

Figure 6.23: Timing jitter, $N_u = N_c, f_L = 0, f_B = 1/(N_cT), \alpha = 0, N_{FFT} = N_c = 64, \sigma_\epsilon^2 = 10^{-3}$ rad^2 (a) Walsh-Hadamard sequences (b) overlay sequences

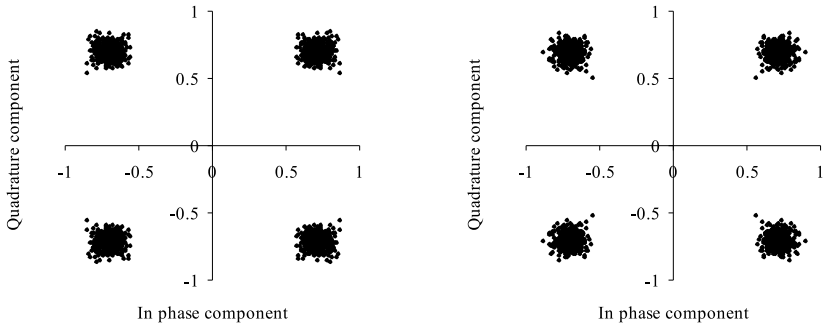

Figure 6.24: Timing jitter, $N_u = N_c, f_L = 1/(N_cT), f_B = 2/(N_cT), \alpha = 0, N_{FFT} = N_c = 64, \sigma_\epsilon^2 = 10^{-3}$ rad^2 (a) Walsh-Hadamard sequences (b) overlay sequences

Table 6.4: Mean square deviation of the samples at the input of the decision device

		Theoretical	Simulations
$f_L = 0,$	Walsh-Hadamard	$3.290E-3$	$3.299E-3$
$f_B = 1/(N_cT) = R_s$	overlay	$3.290E-3$	$3.266E-3$
$fL = 1/(N_cT) = R_s,$	Walsh-Hadamard	$3.290E-3$	$3.275E-3$
$fB = 2/(N_cT) = 2R_s$	overlay	$3.290E-3$	$3.278E-3$

Hence, in the presence of a sufficient cyclic prefix length, the dispersive channel introduces a scaling and rotation of the FFT outputs, that is related to the channel characteristics. The MMSE equaliser has equaliser coefficients

$$(g_{MMSE})_{i,n}^{\ell} = C_{ch,n} G_n^* \tag{6.65}$$

where $C_{ch,n}$ is a real-valued positive factor that depends on the carrier index and the channel characteristics, but is independent of the user index ℓ and the block index i. The MMSE equaliser compensates for the phase rotation of the FFT outputs and applies a carrier dependent scaling of the FFT outputs. However, as the resulting scaled FFT output has an amplitude that in generally depends on the carrier index, multiuser interference is introduced after correlation with the spreading sequences. The resulting signal-to-noise ratio (6.17) is independent of the user index ℓ and the block index i and yields

$$SNR = \frac{SNR(0) \sum_{n=0}^{N_c-1} X_n |G_n|^2}{\sum_{n=0}^{N_c-1} X_n} \tag{6.66}$$

where $SNR(0) = \frac{N_{FFT}}{N_{FFT}+\nu} \frac{E_s}{N_0}$ and

$$X_n^{-1} = 1 + SNR(0)|G_n|^2 \tag{6.67}$$

The degradation (6.24) of the SNR as compared to $SNR(0)$ (6.23), caused by the dispersive channel is given by

$$Deg = -10 \log \sum_{n=0}^{N_c-1} X_n |G_n|^2 + 10 \log \sum_{n=0}^{N_c-1} X_n \tag{6.68}$$

Hence, the performance of the MC-CDMA system is independent of the user index ℓ and the block index i. When the rolloff area is small and the spreading factor is almost equal to the number of carriers, i.e., $N_c \approx N_{FFT}$, the degradation (6.68) is essentially independent of the number of carriers and of the spreading factor.

For large E_s/N_0, the equaliser coefficients (6.65) can be shown to converge to the zero-forcing equaliser coefficients $(g_{zero})_{i,n}^{\ell}$ that eliminate the MUI. The zero-forcing equaliser coefficients are given by

$$(g_{zero})_{i,n}^{\ell} = \frac{1}{G_n} \tag{6.69}$$

This indicates that for large E_s/N_0 the MMSE equaliser essentially eliminates the MUI. The residual MUI at the input of the decision device can be neglected as compared to the noise.

In the case of a fading channel with transfer function $H_{ch}(f;\tau)$ that slowly varies as compared to the MC-CDMA block length, the channel can be viewed during an MC-CDMA block as a fixed channel. Similarly as for the OFDM(A)

system, the expressions for a fixed channel can be used where the quantity (6.64) is replaced by

$$G_{n,i} = H_{ch}\left(\frac{\mathrm{mod}(M(n); N_{FFT})}{N_{FFT}T}; t_{i(N_{FFT}+\nu)}\right) \tag{6.70}$$

Taking into account the stationary nature of the fading channel, the quantity (6.70) is stationary with respect to the block index i. The resulting SNR (6.66) depends on the block index i and can be viewed as a instantaneous SNR during the considered MC-CDMA block.

Let us briefly consider uplink MC-CDMA in the absence of synchronisation errors. The main difference with downlink communication is that the N_u user signals reach the base station over different channels. Assuming a sufficiently long guard interval to cope with channel dispersion, the $M(n)$th FFT output at the base station receiver during the ith MC-CDMA block can be represented as

$$y_{i,M(n)} = \frac{1}{\sqrt{N_c}} \sum_{\ell=1}^{N_u} a_{i,\ell'} c_{iN_c+n,\ell'} G_{n,i}^{\ell'} \tag{6.71}$$

where $G_{n,i}^{\ell'}$ is given by an expression similar to (6.70). In (6.71) we have neglected the noise contribution. The detection of the symbol $a_{i,\ell}$ is based upon the quantity $z_{i,\ell}$, given by

$$z_{i,\ell} = \frac{1}{\sqrt{N_c}} \sum_{n=0}^{N_c-1} c_{iN_c+n,\ell}^{*} g_{n,i}^{\ell} y_{i,M(n)} \triangleq \sum_{\ell=1}^{N_u} a_{i,\ell'} I_{i,i,\ell,\ell'} \tag{6.72}$$

where

$$I_{i,i,\ell,\ell'} = \frac{1}{N_c} \sum_{n=0}^{N_c-1} c_{iN_c+n,\ell}^{*} c_{iN_c+n,\ell'} g_{n,i}^{\ell} G_{n,i}^{\ell'} \tag{6.73}$$

can be interpreted as the correlation of the sequences $\{c_{iN_c+n,\ell}(g_{i,n}^{\ell})^*\}$ and $\{c_{iN_c+n,\ell'}(G_{i,n}^{\ell'})^*\}$. For arbitrary $G_{i,n}^{\ell'}$, the equaliser coefficients $\{g_{i,n}^{\ell} | n = 0, \ldots, N_c - 1\}$ do not provide sufficient degrees of freedom to yield $I_{i,i,\ell,\ell'} = 0$ for all $N_u - 1$ values of ℓ' that differ from ℓ. Note that for downlink MC-CDMA, (6.71) and (6.72) are still valid, but with $G_{i,n}^{\ell'} = G_{i,n}^{\ell}$; in this case $g_{i,n}^{\ell} = 1/G_{i,n}^{\ell}$ yields $I_{i,i,\ell,\ell'} = 0$ for $\ell' \neq \ell$. Hence, the fact that the user signals are sent over different dispersive channels in uplink MC-CDMA gives rise to inevitable MUI; in fact, the same situation occurs on ideal channels when the transmitted user signals are not aligned in time (see section 6.4.2). To counteract the MUI in uplink MC-CDMA, a much more sophisticated receiver structure is needed [Ver98]. However, as this type of receivers is beyond the scope of the present work, we restrict our attention to downlink MC-CDMA.

In the following sections, we will investigate the effect of the synchronisation errors on the downlink MC-CDMA system in the presence of a dispersive channel. As the synchronisation errors in general cause interference between

the different carriers, it can be expected that in the presence of synchronisation errors, the MC-CDMA system is subjected to an additional degradation as compared to the absence of synchronisation errors. In our computations, we make use of the fixed dispersive channel with transfer function defined in (5.87).

6.5.2 Carrier Phase Errors

In this section, we study the influence of the carrier phase errors on the MC-CDMA system in the presence of a dispersive channel, but in the absence of timing errors. In this case, the quantities (6.26) are given by

$$G_n(t_{i(N_{FFT}+\nu)+k}) = G_n e^{j\phi(t_{i(N_{FFT}+\nu)+k})} \tag{6.74}$$

where G_n is defined in (6.64). In the following sections, we separately consider a constant phase offset, a carrier frequency offset and carrier phase jitter.

Constant Phase Offset

In the presence of a dispersive channel and a constant phase offset, the quantities (6.25) yield

$$A_{i,i',n,n'} = \delta_{i,i'}\delta_{n,n'}G_n e^{j\phi} \tag{6.75}$$

A constant phase offset introduces a phase rotation of the FFT outputs over a carrier independent angle ϕ as compared to the case of a zero phase offset. As is observed in (6.75), a constant phase offset causes no interference between the different carriers. Hence, a constant phase offset yields a rotation of the samples at the input of the decision device as compared to the case of a zero phase offset when no correction is applied ($g_{i,n}^{\ell} = 1$). This results in a reduction of the noise margins, as depicted in figure 6.8. The MMSE equaliser compensates for the phase rotation: $(g_{MMSE})_{i,n}^{\ell} = C_{ch,n}\exp(-j\phi)$, where $C_{ch,n}$ are the MMSE equaliser coefficients in the absence of synchronisation errors, defined in (6.65). As a phase rotation over an angle $-\phi$ of the FFT outputs introduces no enhancement of the noise power level as compared to a zero phase offset, a constant phase offset causes no performance degradation. These results correspond with the results found in the case of an ideal channel (section 6.4.1).

Carrier Frequency Offset

In the case of a dispersive channel, the quantities (6.14) in the presence of a carrier frequency offset ΔF can be written as

$$\begin{aligned} I_{i,i',\ell,\ell'} &= \delta_{i,i'} e^{j2\pi\Delta F_\ell i(N_{FFT}+\nu)} \frac{1}{N_c} \sum_{n,n'=0}^{N_c-1} c^*_{iN_c+n,\ell} c_{iN_c+n',\ell'} g_{i,n}^{\ell} G_{n'} \cdot \\ &\quad D\left(\frac{M(n)-M(n')}{N_{FFT}} + \Delta FT\right) \end{aligned} \tag{6.76}$$

where $D(x)$ is defined in (6.33). In (6.76) it is observed that a carrier frequency offset introduces a phase rotation of the FFT outputs at a constant speed of $2\pi\Delta FT(N_{FFT}+\nu)$ rad/symbol. Furthermore, a carrier frequency offset causes a reduction of the amplitude of the useful component and introduces interference between the different carriers, which results in additional multiuser interference, as compared to the case of a zero carrier frequency offset. For the maximum load, the MMSE equaliser yields

$$(g_{MMSE})_{i,n}^{\ell} = CX_{\Delta F,n}e^{-j2\pi\Delta FTi(N_{FFT}+\nu)}G_n^* D^*(\Delta FT) \tag{6.77}$$

where C is a real-valued positive factor that is independent of the carrier index n, the user index ℓ , the block index i and the carrier frequency offset ΔF, and

$$X_{\Delta F,n}^{-1} = 1 + SNR(0)\sum_{n'=0}^{N_c-1}|G_{n'}|^2\left|D\left(\frac{M(n')-M(n)}{N_{FFT}}+\Delta FT\right)\right|^2 \tag{6.78}$$

Hence, the equaliser compensates for the systematic phase rotation of the FFT outputs. However, the equaliser is not able to eliminate the interference between the carriers, such that additional MUI is introduced as compared to the case of a zero carrier frequency offset. The resulting SNR (6.17) is independent of the block index i and the user index ℓ, and is given by

$$SNR = \frac{SNR(0)|D(\Delta FT)|^2\frac{1}{N_c}\sum_{n=0}^{N_c-1}|G_n|^2X_{\Delta F,n}}{1+SNR(0)|D(\Delta FT)|^2\frac{1}{N_c}\sum_{n=0}^{N_c-1}|G_n|^2X_{\Delta F,n}} \tag{6.79}$$

From (6.79) and (6.66) it follows that a carrier frequency offset introduces an additional degradation as compared to the SNR (6.66) in the absence of synchronisation errors. When the rolloff area is small and the spreading factor is almost equal to the number of carriers, i.e., $N_c \approx N_{FFT}$, the SNR (6.79) is a function of the product $N_{FFT}\Delta FT$, and is essentially independent of the spreading factor.

Figure 6.25 shows the additional degradation caused by the carrier frequency offset as function of the product $N_{FFT}\Delta FT$ for $\alpha = 0, N_c = N_{FFT}$, the fixed channel with transfer function (5.87) and $SNR(0) = 20$ dB. As we observe, the additional degradation caused by the carrier frequency offset in the presence of a dispersive channel is essentially the same as the degradation caused by the carrier frequency offset in the case of the ideal channel. In figure 6.26, the total degradation (i.e., the degradation as compared to $SNR(0)$ (6.23), caused by the carrier frequency offset and the dispersive channel) is shown under the same conditions as in figure 6.25. For small carrier frequency offsets, the total degradation is essentially independent of the carrier frequency offset: the total degradation is mainly caused by the dispersive channel. For increasing carrier frequency offsets, the curves corresponding to the dispersive channel and the ideal channel coincide. In this case, the carrier frequency offset has become the main cause of degradation. Hence, the influence of a carrier frequency offset in the case of a dispersive channel is essentially the same as in the case of an ideal channel (section 6.4.1).

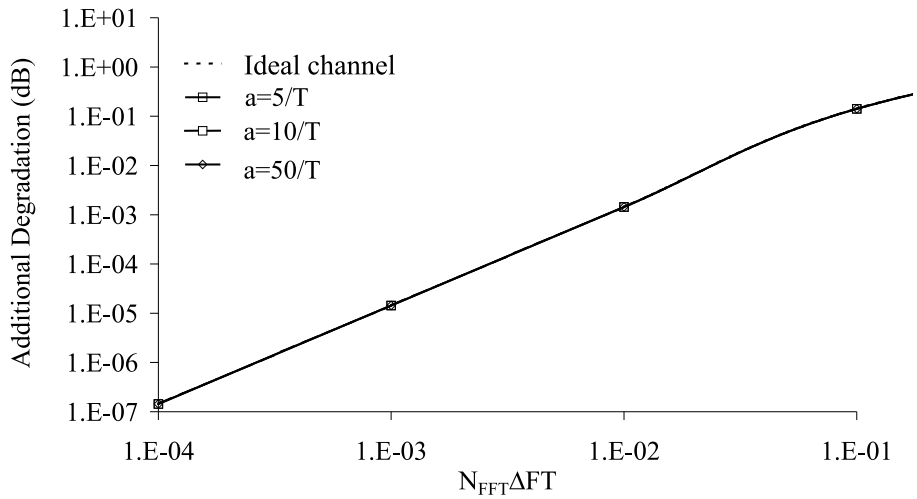

Figure 6.25: Additional degradation caused by carrier frequency offset, $\alpha = 0, N_c = N_{FFT}, SNR(0) = 20$ dB

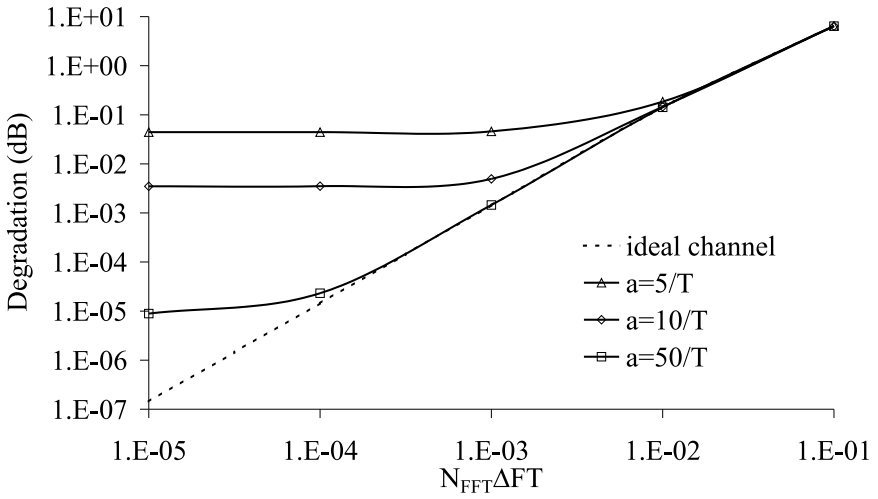

Figure 6.26: Maximum total degradation caused by dispersive channel and carrier frequency offset, $\alpha = 0, N_c = N_{FFT}, SNR(0) = 20$ dB

Carrier Phase Jitter

In the case of a dispersive channel, the quantities (6.14) can be approximated for small jitter variances by

$$I_{i,i',\ell,\ell'} = \delta_{i,i'} \frac{1}{N_c} \sum_{n,n'=0}^{N_c-1} c^*_{iN_c+n,\ell} c_{iN_c+n',\ell'} g^{\ell}_{i,n} G_{n'} \cdot \left(\delta_{n,n'} + \frac{1}{N_{FFT}} \sum_{k=0}^{N_{FFT}-1} j\phi(t_{i(N_{FFT}+\nu)+k}) e^{-j2\pi \frac{k(M(n)-M(n'))}{N_{FFT}}} \right) \tag{6.80}$$

When the carrier phase jitter rapidly varies as compared to the averaging time of the MMSE equaliser, the equaliser is not able to track the carrier phase jitter. The equaliser averages the variations caused by the carrier phase jitter. As for small jitter variances, the time average of $\exp(j\phi(t))$ can be approximated by $E[\exp(j\phi(t))] \approx E[1 + j\phi(t)] = 1$, the MMSE equaliser is essentially the same as in the absence of synchronisation errors and is given by (6.65). In this case, the SNR (6.17) is independent of the block index i and the user index ℓ and can be written as

$$SNR = \frac{SNR(0) \frac{1}{N_c} \sum_{n=0}^{N_c-1} |G_n|^2 X_n}{\left(\frac{1}{N_c} \sum_{n=0}^{N_c-1} X_n \right) \left(\frac{1}{N_c} \sum_{n=0}^{N_c-1} |G_n|^2 X_n \right) + Y} \tag{6.81}$$

where X_n is given by (6.67),

$$Y = SNR(0) \frac{1}{N_c} \sum_{n,n'=0}^{N_c-1} X_n^2 |G_n|^2 |G_{n'}|^2 \cdot \int_{-\infty}^{+\infty} S_\phi(f) \left| D\left(fT + \frac{M(n) - M(n')}{N_{FFT}} \right) \right|^2 df \tag{6.82}$$

and $D(x)$ is defined in (6.33). Considering (6.66) and (6.81), it is clear that the carrier phase jitter introduces an additional degradation ΔDeg as compared to the SNR (6.66) in the absence of synchronisation errors

$$\Delta Deg = 10 \log \left(1 + \frac{Y}{\left(\frac{1}{N_c} \sum_{n=0}^{N_c-1} X_n \right) \left(\frac{1}{N_c} \sum_{n=0}^{N_c-1} |G_n|^2 X_n \right)} \right) \tag{6.83}$$

As is observed from (6.83), the performance of the MC-CDMA system is independent of the user index ℓ and the block index i. When the rolloff area is small and the spreading factor is nearly equal to the number of carriers, i.e., $N_c \approx N_{FFT}$, the SNR (6.81) and the degradation (6.83) are essentially independent of the number of carriers and the spreading factor, but only depend on the jitter variance σ^2_ϕ (6.43). In figure 6.27, the additional degradation (6.83) is

shown as function of the jitter variance, for $\alpha = 0, N_c = N_{FFT}$, the dispersive channel (5.87), assuming a jitter power spectral density as shown in figure 6.15 with $f_L = 0, f_B = 2/(N_c T)$ and $SNR(0) = 20$ dB. It can be observed that the additional degradation caused by the carrier phase jitter in the presence of the dispersive channel is essentially the same as the degradation caused by the carrier phase jitter in the case of the ideal channel. The total degradation (i.e., the degradation as compared to $SNR(0)$ (6.23), caused by the carrier phase jitter and the dispersive channel) is shown in figure 6.28, under the same conditions as is figure 6.27. For small jitter variances, the total degradation is essentially independent of the jitter variance. Hence, the degradation is mainly caused by the dispersive channel. For increasing jitter variances, the curves of the dispersive channel and the ideal channel coincide: the total degradation is mainly caused by the carrier phase jitter. The degradation of figures 6.27 and 6.28 is essentially independent of the number of carriers and the spreading factor, but only depends on the jitter variance σ_ϕ^2 (6.43). Hence, the influence of carrier phase jitter in the case of a dispersive channel is essentially the same as in the case of an ideal channel (section 6.4.1).

6.5.3 Timing Errors

In this section, the sensitivity of the MC-CDMA system to timing errors is investigated in the presence of a dispersive channel, but in the absence of carrier phase errors. As only carriers outside the rolloff area are modulated, the quantities (6.26) yield

$$G_n(t_{i(N_{FFT}+\nu)+k}) = G_n e^{j2\pi\epsilon_{i(N_{FFT}+\nu)+k}\frac{\text{mod}(M(n);N_{FFT})}{N_{FFT}}} \tag{6.84}$$

where G_n is defined by (6.64). In the following sections, we separately consider the cases of a constant timing offset, a clock frequency offset and timing jitter.

Constant Timing Offset

We assume that the cyclic prefix is extended, similarly as for the OFDM(A) system (see figure 5.33), such that the cyclic prefix not only counteracts the effects of the dispersive channel, but also is able to cope with small timing offsets. As only carriers outside the rolloff area are modulated, the quantities (6.25) in the presence of a dispersive channel are given by

$$A_{i,i',n,n'} = \delta_{i,i'}\delta_{n,n'} G_n e^{j2\pi\epsilon\frac{\text{mod}(M(n);N_{FFT})}{N_{FFT}}} \tag{6.85}$$

It is observed in (6.85) that a constant timing offset introduces a carrier dependent phase rotation of the FFT outputs as compared to the case of a zero timing offset. Furthermore, the constant timing offset causes no interference between the different carriers. The MMSE equaliser has equaliser coefficients $(g_{MMSE})_{i,n}^{\ell} = C_{ch,n}\exp(-j2\pi\epsilon\text{mod}(M(n);N_{FFT})/N_{FFT})$, where $C_{ch,n}$ are the

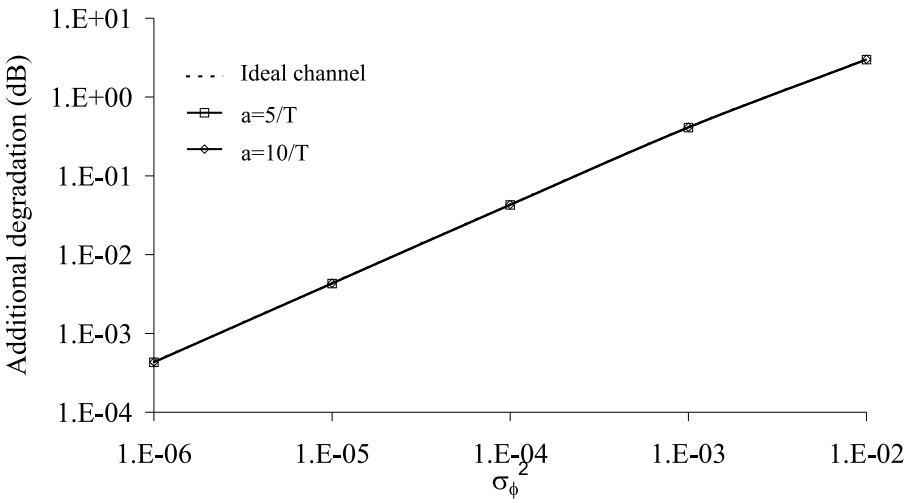

Figure 6.27: Additional degradation caused by carrier phase jitter, $\alpha = 0, N_c = N_{FFT} = 64, SNR(0) = 20$ dB

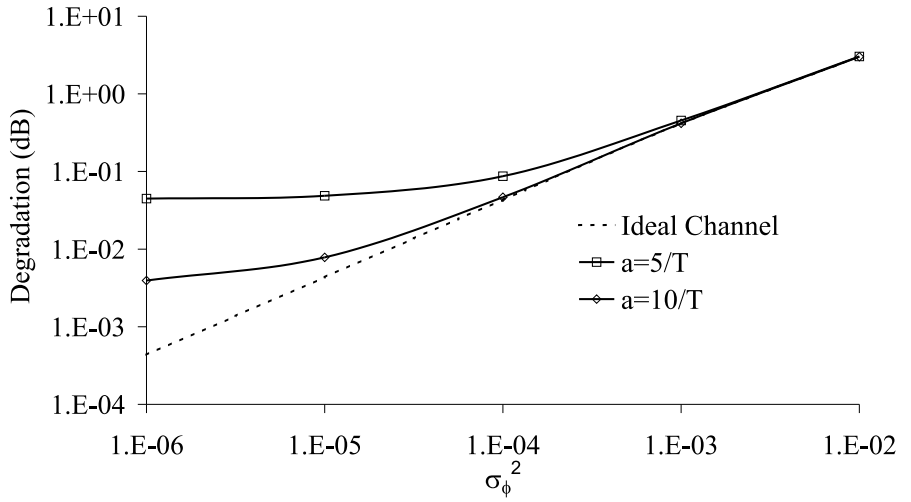

Figure 6.28: Maximum total degradation caused by dispersive channel and carrier phase jitter, $\alpha = 0, N_c = N_{FFT} = 64, SNR(0) = 20$ dB

MMSE equaliser coefficients in the absence of synchronisation errors, as defined in (6.65). As a phase rotation of the FFT outputs introduces no enhancement of the noise power level as compared to the case of a zero timing offset, the MC-CDMA system is not degraded by a constant timing offset. These results are very similar as the results found for the case of the ideal channel (section 6.4.2).

Clock Frequency Offset

When the increasing misalignment of the transmitted and received MC-CDMA blocks is compensated by means of the coarse synchronisation algorithm and the resulting timing error is, similarly as in section 6.4.2, given by $\tilde{\epsilon}_{i(N_{FFT}+\nu)+k} = k\Delta T/T + \epsilon_i$, the quantities (6.25) in the case of a dispersive channel are given by

$$A_{i,i',n,n'} = \delta_{i,i'} G_{n'} e^{j2\pi\epsilon_i \frac{\mathrm{mod}(M(n');N_{FFT})}{N_{FFT}}} B_{n,n'} \tag{6.86}$$

where

$$B_{n,n'} = D\left(\frac{M(n) - M(n')}{N_{FFT}} + \frac{\mathrm{mod}(M(n');N_{FFT})}{N_{FFT}}\frac{\Delta T}{T}\right)$$

and $D(x)$ is defined in (6.33). Hence, a clock frequency offset introduces interference between the different carriers. Furthermore, the useful component is subjected to a phase rotation and amplitude reduction as compared to the case of a zero clock frequency offset. In the case of the maximum load ($N_u = N_c$), the MMSE equaliser has equaliser coefficients

$$(g_{MMSE})^{\ell}_{i,n} = C X_{\Delta T,n} G^*_n B^*_{n,n} e^{-j2\pi\epsilon_i \frac{\mathrm{mod}(M(n);N_{FFT})}{N_{FFT}}} \tag{6.87}$$

where C is a real-valued positive factor that is independent of the block index i, the carrier index n, the user index ℓ and the clock frequency offset ΔT, and

$$X^{-1}_{\Delta T,n} = 1 + SNR(0) \sum_{n'=0}^{N_c-1} |G_{n'}|^2 |B_{n,n'}|^2 \tag{6.88}$$

The equaliser compensates for the phase rotation of the useful component but is not able to eliminate the interference. The resulting SNR (6.17) is independent of the block index i and the user index ℓ and equals

$$SNR = \frac{SNR(0)\frac{1}{N_c}\sum_{n=0}^{N_c-1} X_{\Delta T,n}|G_n|^2|B_{n,n}|^2}{1 + SNR(0)\frac{1}{N_c}\sum_{n=0}^{N_c-1} X_{\Delta T,n}|G_n|^2|B_{n,n}|^2} \tag{6.89}$$

From (6.66) and (6.89) it follows that the SNR (6.86) in the presence of a clock frequency offset is reduced as compared to the SNR (6.66) without synchronisation errors. Hence, a clock frequency offset introduces an additional degradation as compared to (6.66). When the rolloff area is small and the spreading factor is nearly equal to the number of carriers, i.e., $N_c \approx N_{FFT}$, the SNR (6.89) is

a function of the product $N_{FFT}\Delta T/T$, and is essentially independent of the spreading factor.

The additional degradation is shown in figure 6.29 as function of the product $N_{FFT}\Delta T/T$, for $\alpha = 0, N_c = N_{FFT}$, the dispersive channel (5.87) and $SNR(0) = 20$ dB. As is observed, the additional degradation caused by the clock frequency offset in the presence of the dispersive channel is essentially the same as the degradation caused by the clock frequency offset in the case of the ideal channel. The total degradation (i.e., the degradation as compared to $SNR(0)$ (6.23) caused by the clock frequency offset and the dispersive channel) is shown in figure 6.30, under the same conditions as in figure 6.29. For small clock frequency offsets, the total degradation is essentially independent of the clock frequency offset. The total degradation in this case is mainly caused by the dispersive channel. For increasing clock frequency offset, the curves of the dispersive channel and the ideal channel coincide: the total degradation is mainly caused by the clock frequency offset. Hence, the influence of a clock frequency offset in the case of a dispersive channel is essentially the same as in the case of an ideal channel (section 6.4.2).

Timing Jitter

For a dispersive channel, the quantities (6.14) can be approximated for small jitter variances and slowly varying jitter by

$$I_{i,i',\ell,\ell'} \approx \delta_{i,i'} \frac{1}{N_c} \sum_{n,n'=0}^{N_c-1} c^*_{iN_c+n,\ell} c_{iN_c+n',\ell'} g^{\ell}_{i,n} G_{n'} \cdot \left(\delta_{n,n'} + j2\pi S_{n'} \frac{1}{N_{FFT}} \sum_{k=0}^{N_{FFT}-1} e^{-j2\pi \frac{k(M(n)-M(n'))}{N_{FFT}}} \epsilon_{i(N_{FFT}+\nu)+k} \right) \tag{6.90}$$

where S_n is given by (6.55). Hence, the timing jitter will introduce self-interference and interference between the different carriers, similarly as for the case of the ideal channel. When the timing jitter rapidly varies as compared to the averaging time of the MMSE equaliser, the equaliser is not able to track the timing jitter. The equaliser averages the variations caused by the timing jitter. For small jitter variances, the time average of $\exp(j2\pi\epsilon_{i(N_{FFT}+\nu)+k}\mathrm{mod}(M(n);N_{FFT})/N_{FFT})$ can be approximated by $E[\exp(j2\pi\epsilon_{i(N_{FFT}+\nu)+k}\mathrm{mod}(M(n);N_{FFT})/N_{FFT})] \approx E[1 + j2\pi\epsilon_{i(N_{FFT}+\nu)+k}\mathrm{mod}(M(n);N_{FFT})/N_{FFT}] = 1$. Hence, the MMSE equaliser is essentially the same as in the absence of timing errors and is given by (6.65). The resulting SNR (6.17) is independent of the block index i and the user index ℓ and yields

$$SNR = \frac{SNR(0)\frac{1}{N_c}\sum_{n=0}^{N_c-1}|G_n|^2 X_n}{\left(\frac{1}{N_c}\sum_{n=0}^{N_c-1} X_n\right)\left(\frac{1}{N_c}\sum_{n=0}^{N_c-1}|G_n|^2 X_n\right) + Y} \tag{6.91}$$

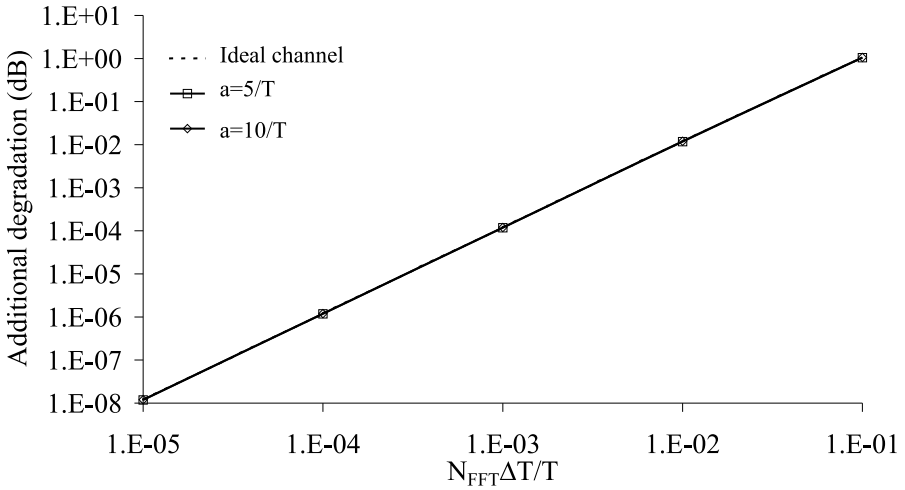

Figure 6.29: Additional degradation caused by clock frequency offset, $\alpha = 0, N_c = N_{FFT}, SNR(0) = 20$ dB

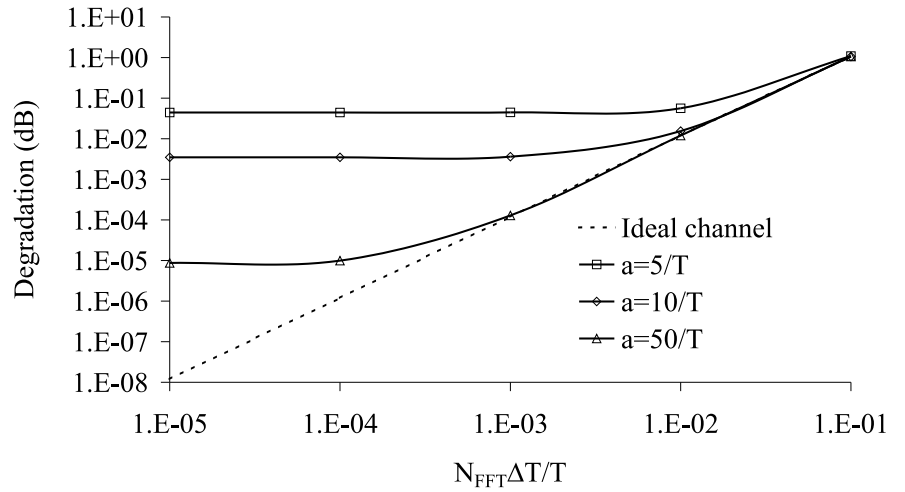

Figure 6.30: Maximum total degradation caused by dispersive channel and clock frequency offset, $\alpha = 0, N_c = N_{FFT}, SNR(0) = 20$ dB

where X_n is given by (6.67),

$$Y = SNR(0)\frac{1}{N_c}\sum_{n,n'=0}^{N_c-1} X_n^2|G_n|^2|G_{n'}|^2 S_{n'}^2 \cdot \int_{-1/2T}^{+1/2T} S_\epsilon(e^{j2\pi fT})\left|D\left(fT + \frac{M(n)-M(n')}{N_{FFT}}\right)\right|^2 df \quad (6.92)$$

and $D(x)$ is defined in (6.33). Considering (6.66) and (6.92), the SNR in the absence and in the presence of timing jitter, respectively, it is clear that the timing jitter introduces an additional degradation ΔDeg as compared to SNR (6.66) in the absence of synchronisation errors

$$\Delta Deg = 10\log\left(1 + \frac{Y}{\left(\frac{1}{N_c}\sum_{n=0}^{N_c-1} X_n\right)\left(\frac{1}{N_c}\sum_{n=0}^{N_c-1}|G_n|^2 X_n\right)}\right) \quad (6.93)$$

As is observed from (6.93), the performance of the MC-CDMA system is independent of the user index ℓ and the block index i. When the rolloff area is small and the spreading factor is nearly equal to the number of carriers, i.e., $N_c \approx N_{FFT}$, the SNR (6.91) and the degradation (6.93) are essentially independent of the number of carriers and the spreading factor, but only depend on the jitter variance σ_ϵ^2 (6.59).

Figure 6.31 shows the additional degradation (6.90) as function of the jitter variance, for $\alpha = 0, N_c = N_{FFT}$, the dispersive channel (5.87), a jitter power spectral density as shown in figure (6.37 with $f_L = 0, f_B = 2/(N_cT)$ and $SNR(0) = 20$ dB. It follows from figure 6.31 that the additional degradation caused by the timing jitter in the presence of the dispersive channel is essentially the same as the degradation caused by the timing jitter in the case of the ideal channel. In figure 6.32, the total degradation i.e., the degradation as compared to $SNR(0)$ (6.23) caused by the timing jitter and the dispersive channel) is shown under the same conditions as in figure 6.31. For small jitter variances, the total degradation is essentially independent of the jitter variance: the dominating effect is the dispersive channel. For increasing jitter variances, the curves of the dispersive channel and the ideal channel coincide. In this case, the total degradation is mainly caused by the timing jitter. The degradation of figures 6.31 and 6.32 is essentially independent of the number of carriers and the spreading factor, but only depends on the jitter variance σ_ϵ^2 (6.59). Hence, the influence of timing jitter in the case of a dispersive channel is essentially the same as in the case of an ideal channel (section 6.4.2).

6.6 Conclusions and Remarks

In this chapter, we have investigated the sensitivity of MC-CDMA to synchronisation errors. The cyclic prefix is assumed to be sufficiently long to cope with

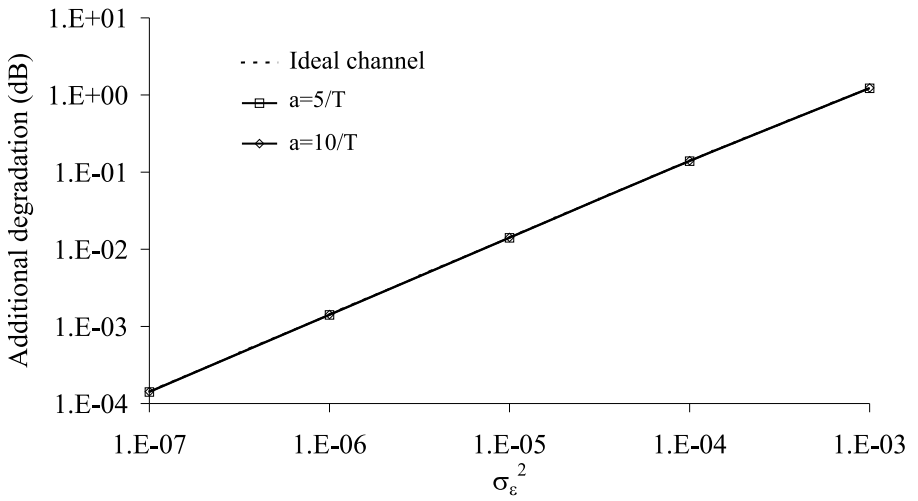

Figure 6.31: Additional degradation caused by timing jitter, $\alpha = 0, N_c = N_{FFT} = 64, SNR(0) = 20$ dB

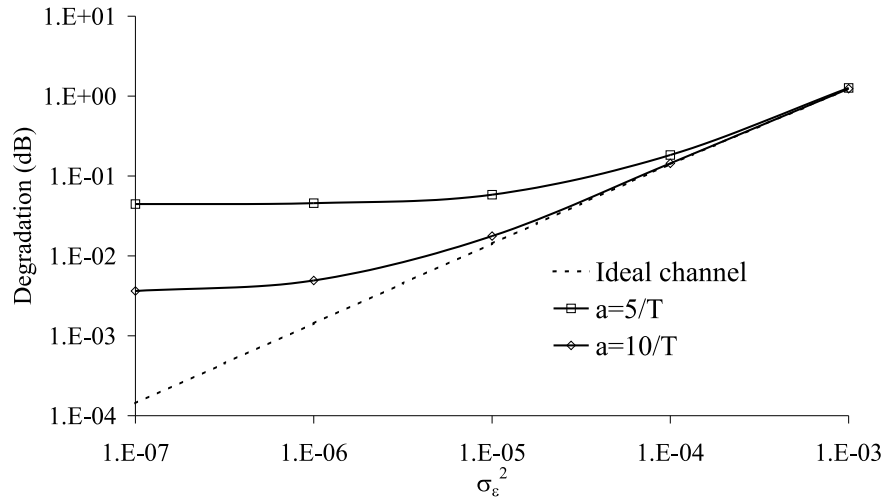

Figure 6.32: Maximum total degradation caused by dispersive channel and timing jitter, $\alpha = 0, N_c = N_{FFT} = 64, SNR(0) = 20$ dB

Table 6.5: Overview of the effect of synchronisation errors on downlink MC-CDMA for the maximum load

constant phase offset	- no degradation
constant timing offset	- no degradation
carrier frequency offset	- strong degradation, proportional to $(N_{FFT}\Delta FT)^2$ - degradation independent of carrier index
clock frequency offset	- strong degradation, proportional to $(N_{FFT}\Delta T/T)^2$ - degradation depends on carrier index
carrier phase jitter	- degradation independent of N_c and spectral contents of jitter, proportional to σ_ϕ^2 - scatter diagram depends on spectral contents jitter
jitter timing jitter	- degradation independent of spectral contents jitter and essentially independent of N_c for large N_c, proportional to σ_ϵ^2 - scatter diagram depends on spectral contents jitter

channel dispersion and timing misalignment. The considered receiver makes use of one-tap equalisers at the FFT outputs to compensate the effect of synchronisation errors and channel dispersion. In the absence of synchronisation errors, this type of receiver is able to suppress the multiuser interference in downlink MC-CDMA on dispersive channels. However, a much more complicated type of receiver is required to combat multiuser interference in uplink MC-CDMA on dispersive channels, even in case of perfect synchronisation. As such receivers are beyond the scope of this work, we have concentrated mainly on downlink MC-CDMA. We have found that downlink transmission over an ideal channel and over a dispersive channel yields nearly the same SNR degradation caused by synchronisation errors, as compared to the SNR on the respective channels with perfect synchronisation. Hence, results valid for the ideal channel are also relevant to more realistic channels. These results for downlink MC-CDMA are briefly summarised in Table 6.5, and a more detailed discussion if given below. In the case of uplink MC-CDMA on an ideal channel, the degradations caused by carrier phase offset, carrier frequency offset, carrier phase jitter and timing jitter are essentially the same as for downlink MC-CDMA, whereas timing offset and clock frequency offset are much more harmful to uplink MC-CDMA than to downlink MC-CDMA.

Assuming that all compensations of the effect of synchronisation errors are carried out by the one-tap equalisers at the outputs of the FFT, the synchronisation errors affect the full-load ($N_u = N_c$) downlink MC-CDMA system in the following way.

- A constant carrier phase offset only yields a phase rotation at the FFT outputs, which is compensated by the equaliser without loss of performance.
- As no carriers in the rolloff area are modulated, a constant timing offset gives rise to a carrier-dependent phase rotation of the FFT outputs, which is compensated by the equaliser without loss of performance.
- A (relative) carrier frequency offset ΔFT yields a degradation that is proportional to $(N_{FFT}\Delta FT)^2$. If this degradation can not be tolerated, frequency correction must be applied in front of the FFT at the receiver.
- A (relative) clock frequency offset $\Delta T/T$ gives rise to a degradation that is proportional to $(N_{FFT}\Delta T/T)^2$. If this degradation can not be tolerated, timing correction must be applied in front of the FFT at the receiver.
- Carrier phase jitter yields a degradation that is essentially independent of the number of carriers, provided that all users have the same transmit power and the same jitter spectrum. The degradation is proportional to the jitter variance. The scatter diagram at the input of the decision device does depend on the jitter spectrum shape. Low-frequency jitter ($|f| < 1/(N_{FFT}T)$) gives rise to mainly self-interference, causing an angular displacement in the scatter diagram. High-frequency jitter ($|f| > 1/(N_{FFT}T)$) yields mainly multiuser interference, corresponding to a circular cloud in the scatter diagram.
- Timing jitter gives rise to a degradation with similar properties as the degradation caused by carrier phase jitter. The main difference is the scatter diagram: irrespective of the jitter spectrum shape, multiuser interference is dominant over self-interference, so that the resulting scatter diagram shows a circular cloud.

The results obtained in this chapter have been published in a number of scientific papers. In [Ste97a], [Ste98d] and [Ste99a] we have studied the effect of the carrier phase errors on MC-CDMA performance. A comparison between MC-CDMA and orthogonal CDMA regarding their sensitivity to carrier phase errors is presented in [Ste99e]. In [Ste99b] we have investigated how timing errors affect MC-CDMA performance. In [Ste99c] and [Ste99d] we have introduced the equivalent time-varying channel impulse response that incorporates the synchronisation errors, to determine the degradation in MC-CDMA. An overview of MC-CDMA sensitivity to synchronisation errors can be found in [Ste99f]. In the above papers, the performance degradation caused by synchronisation errors has been determined analytically; this is in contrast with other authors (e.g., [Tom96]) who use mainly computer simulations to determine the system performance in the presence of synchronisation errors.

Chapter 7

Comparison of the Modulation Techniques

7.1 Introduction

So far, a number of single carrier and multicarrier modulation techniques have been presented and the effect of synchronisation errors on their performance has been investigated. In this chapter, the sensitivity of these modulation techniques will be compared. However, to allow a fair comparison between the different modulation techniques, we assume that all considered systems are able to accommodate up to N users, each user operating at a data rate R_s. In addition, to simplify the comparison, we consider the case of synchronous transmission, i.e., the signals of the different users are synchronised such that all users exhibit the same carrier phase errors and timing errors. The transmit and receiver filters are square-root raised-cosine filters with rolloff α.

In this chapter, we consider three types of multicarrier systems and compare them with their single carrier equivalents. A description of the considered multicarrier systems and their single carrier counterparts is presented in section 7.2. In section 7.3, the comparison of the sensitivities to synchronisation errors of the considered systems will be discussed. In section 7.4 conclusions are drawn.

7.2 Multicarrier Systems and their Single Carrier Equivalents

In this section, we consider three multicarrier systems, based on the OFDM, OFDMA and MC-CDMA techniques and present a single carrier equivalent

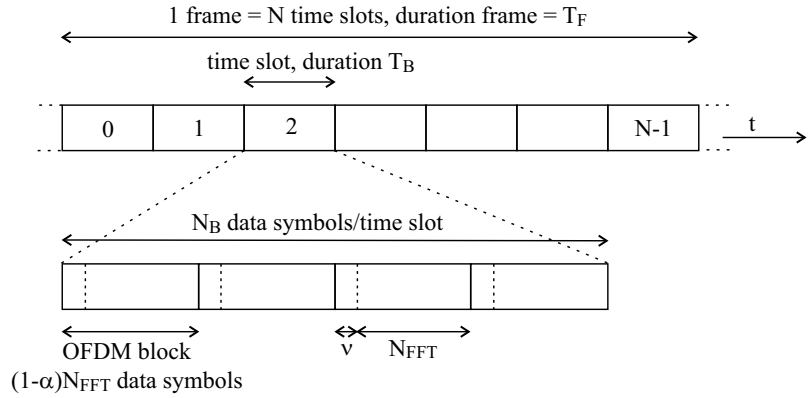

Figure 7.1: The OFDM/TDMA technique

for each of the considered multicarrier systems. The first multicarrier technique makes use of the OFDM modulation technique, combined with TDMA as the multiple access technique (OFDM/TDMA). Its single carrier counterpart consists of the conventional single carrier communication technique, combined with the TDMA multiple access technique (SC/TDMA). Next, we consider the OFDMA technique and its single carrier equivalent, consisting of the conventional single carrier communication technique, combined with the FDMA multiple access technique (SC/FDMA). The last multicarrier technique that is considered is the MC-CDMA technique, which is the multicarrier counterpart of the DS-CDMA technique.

7.2.1 OFDM/TDMA and SC/TDMA

In the OFDM/TDMA technique, where OFDM is used as the modulation technique and TDMA as an access technique, the time axis is partitioned into a number of non-overlapping time slots, as shown in figure 7.1. The time slots are grouped into frames of N time slots. During each frame, a user is assigned a time slot. Each time slot consists of a burst of OFDM blocks, during which N_B data symbols are transmitted. Considering N_{FFT} as the number of carriers and ν as the number of samples in the cyclic prefix, each OFDM block consists of $N_{FFT} + \nu$ samples. Assuming the carriers inside the rolloff area are not modulated, i.e., in each OFDM block $N_{carr} \leq (1-\alpha)N_{FFT}$ symbols are transmitted, the number of OFDM blocks necessary to transmit N_B data symbols per time slot equals N_B/N_{carr}. Furthermore, for a given data rate R_s per user, the bandwidth occupied by the OFDM/TDMA system equals $B = (1 + \nu/N_{FFT})NR_s$ Hz. The corresponding sampling rate equals $1/T = (N_{FFT} + \nu)NR_s/N_{carr}$ Hz. An overview of the system parameters is shown in table 7.1. The performance of the OFDM/TDMA technique has been investigated in chapter 5.

Similarly to the OFDM/TDMA technique, the time axis in the case of the

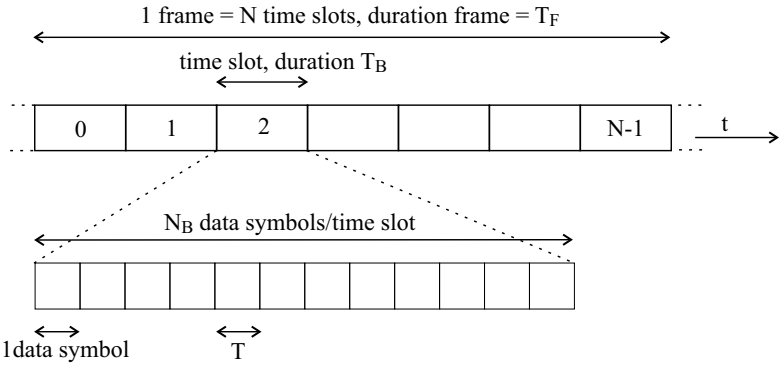

Figure 7.2: The SC/TDMA technique

Table 7.1: Comparison of the system parameters of OFDM/TDMA and SC/TDMA

	OFDM/TDMA	SC/TDMA
data rate per user (symb/s)	R_s	R_s
number of users	N	N
number of data symbols per time slot	N_B	N_B
system bandwidth (Hz)	$B = \left(1 + \frac{\nu}{N_{FFT}}\right) NR_s$	$B = (1+\alpha)NR_s$
sampling rate (Hz)	$\frac{1}{T} = (N_{FFT} + \nu)\frac{NR_s}{N_{carr}}$	$\frac{1}{T} = NR_s$
duration time slot T_B (s)	$T_B = \frac{N_B}{NR_s}$	$T_B = \frac{N_B}{NR_s}$
duration frame T_F (s)	$T_F = \frac{N_B}{R_s}$	$T_F = \frac{N_B}{R_s}$

SC/TDMA technique is partitioned into a number of non-overlapping time slots, that are grouped into frames of N time slots. In each frame, a user is assigned a time slot, during which the user can transmit a burst of N_B data symbols, as shown in figure 7.2. The bandwidth occupied by the SC/TDMA technique equals $B = (1+\alpha)NR_s$ Hz. Furthermore, the sampling rate equals $1/T = NR_s$ Hz. Table 7.1 shows an overview of the SC/TDMA system parameters. The performance of the SC/TDMA technique has been investigated in chapter 3.

When $n \ll N_{FFT}, \alpha \approx 1$ and $N_{carr} \approx N_{FFT}$, it is observed from table 7.1 that OFDM/TDMA and SC/TDMA occupy approximately the same bandwidth $B \approx NR_s$ Hz. Furthermore, the sampling rate is approximately the same for both techniques and equals $1/T = NR_s$ Hz. The duration of a time slot, hence the duration of a frame, is the same for both techniques when the number of data symbols N_B transmitted during a time slot is the same.

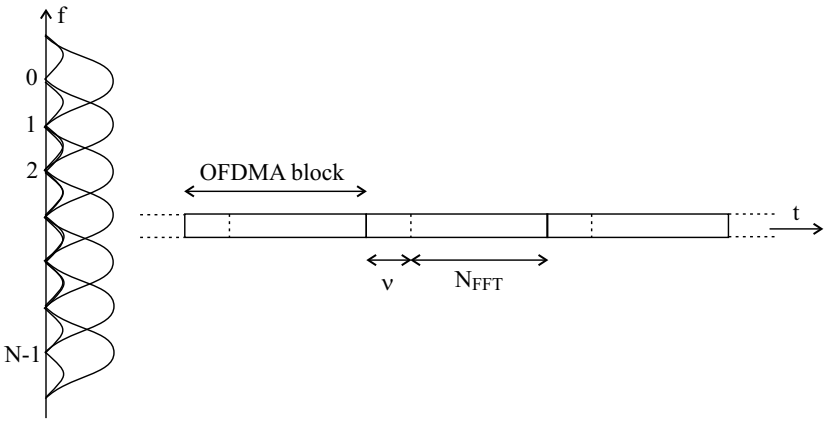

Figure 7.3: The OFDMA technique

7.2.2 OFDMA and SC/FDMA

In the OFDMA technique, the available bandwidth is partitioned into a number of subchannels that spectrally overlap, as shown in figure 7.3. By adequately selecting the carrier spacing, the carriers are made orthogonal. Each user is assigned a different carrier. For N_{FFT} the number of carriers and n the number of samples in the cyclic prefix, the OFDMA block consists of $N_{FFT}+\nu$ samples. During one OFDMA block, one data symbol per user is transmitted. When the carriers inside the rolloff area are not used, i.e., the number of modulated carriers equals $N \leq (1-\alpha)N_{FFT}$, the bandwidth occupied by the OFDMA system equals $B = (1+\nu/N_{FFT})NR_s$ Hz. Furthermore, the sampling rate is equal to $1/T = (1+\nu/N_{FFT})NR_s/(1-\alpha)$ Hz. A summary of the system parameters for the OFDMA system is shown in table 7.2. The performance of the OFDMA system has been investigated in chapter 5.

Similarly to the OFDMA technique, the available bandwidth in the case of the SC/FDMA technique is partitioned into a number of subchannels. However, unlike the carriers in the OFDMA technique, the carriers in the SC/FDMA technique do not spectrally overlap, as shown in figure 7.4. Each user is assigned a different carrier, on which the data stream of the considered user is transmitted as described in chapter 3: the data symbols are transmitted sequentially. The bandwidth occupied by the SC/FDMA technique is given by $(1+\alpha)NR_s$ Hz, and the corresponding sampling rate is $1/T = R_s$ Hz. Table 7.2 shows an overview of the SC/FDMA system parameters. The performance of the SC/FDMA technique has been investigated in chapter 3.

Assuming that $n \ll N_{FFT}, \alpha \ll 1$ and $N \approx N_{FFT}$, we observe in table 7.2 that the system bandwidths of the OFDMA technique and the SC/FDMA technique are approximately the same and equal to $B \approx NR_s$ Hz. Furthermore, the sampling rate of the OFDMA technique is about N times as large as the

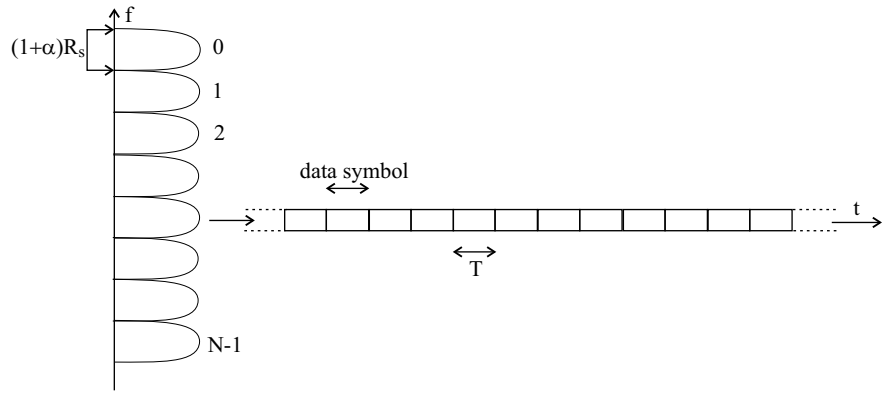

Figure 7.4: The SC/FDMA technique

Table 7.2: Comparison of the system parameters of OFDMA and SC/FDMA

	OFDMA	SC/FDMA
data rate per user (symb/s)	R_s	R_s
number of users	N	N
system bandwidth (Hz)	$B = \left(1 + \frac{\nu}{N_{FFT}}\right) NR_s$	$B = (1+\alpha)NR_s$
sampling rate (Hz)	$\frac{1}{T} = (N_{FFT} + \nu)R_s$	$\frac{1}{T} = R_s$

sampling rate of its single carrier equivalent, the SC/FDMA technique.

7.2.3 MC-CDMA and DS-CDMA

In the MC-CDMA technique, where OFDM is used as the modulation technique and CDMA as the multiple access technique, the available bandwidth is partitioned into a number (N_{FFT}) of spectrally overlapping subchannels. The data symbols of a user (generated at a rate R_s) are multiplied with a spreading sequence that has a rate N_cR_s and the resulting sequence is mapped on the carriers, as shown in figure 7.5. In each MC-CDMA block, one data symbol per user is transmitted. We assume that the carriers inside the rolloff area are not modulated, i.e., the spreading factor N_c is smaller than or equal to the number of carriers outside the rolloff area: $N_c \leq (1-\alpha)N_{FFT}$. Each MC-CDMA block consists of $N_{FFT} + \nu$ samples, where ν is the number of samples in the cyclic prefix. All users are assigned different spreading sequences. When using orthogonal sequences or overlay sequences, the signals of the different users are orthogonal. In this case, up to N_c users can be accommodated without introducing severe interference between the users. Hence, the maximum number of users N equals the spreading factor N_c: $N = N_c$. The bandwidth occupied by the MC-CDMA technique equals $B = (1+\nu/N_{FFT})NR_s$ Hz, and the sampling rate is $1/T = (N_{FFT}+\nu)R_s$ Hz. A summary of the MC-CDMA system param-

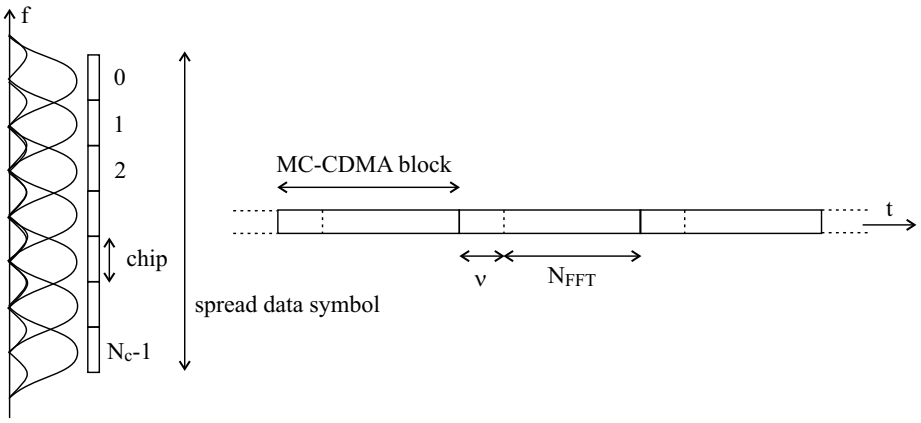

Figure 7.5: The MC-CDMA technique

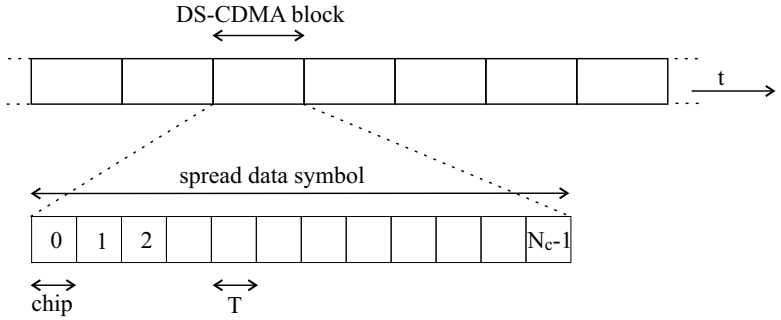

Figure 7.6: The DS-CDMA technique

eters is shown in table 7.3. The MC-CDMA performance has been investigated in chapter 6.

Similarly to the MC-CDMA technique, the data symbols in the DS-CDMA technique (generated at a rate R_s) are multiplied with a spreading sequence that has a rate $N_c R_s$. However, unlike the MC-CDMA technique, the resulting sequence is transmitted in the time domain, as shown in figure 7.6. During one DS-CDMA block, one data symbol per user is transmitted. Similarly as in the MC-CDMA system, we consider the cases of orthogonal sequences and overlay sequences, which means that up to N_c users can be accommodated. Consequently, the maximum number of active users equals the spreading factor, i.e., $N = N_c$. The DS-CDMA system occupies a bandwidth $B = (1 + \alpha)NR_s$ Hz. Furthermore, the sampling rate equals $1/T = NR_s$ Hz. In table 7.3, an overview of the DS-CDMA system parameters is shown. The DS-CDMA system performance has been investigated in chapter 4.

Considering the case that $\nu \ll N_{FFT}, \alpha \ll 1$ and $N \approx N_{FFT}$, we observe in

Table 7.3: Comparison of the system parameters of MC-CDMA and DS-CDMA

	MC-CDMA	DS-CDMA
data rate per user (symb/s)	R_s	R_s
number of users	N	N
system bandwidth (Hz)	$B = \left(1 + \frac{\nu}{N_{FFT}}\right) NR_s$	$B = (1+\alpha)NR_s$
sampling rate (Hz)	$\frac{1}{T} = (N_{FFT} + \nu)R_s$	$\frac{1}{T} = NR_s$

table 7.3 that the bandwidths occupied by the MC-CDMA technique and the DS-CDMA technique are approximately the same and equal to $B \approx NR_s$ Hz. Furthermore, it is observed that the sampling rates of the MC-CDMA technique and the DS-CDMA technique are approximately the same and yield $1/T \approx NR_s$ Hz. Comparing the bandwidth of the MC-CDMA technique and the DS-CDMA technique with the bandwidth of the other considered systems (OFDM/TDMA, SC/TDMA, OFDMA and SC/FDMA), we observe that the system bandwidth is approximately the same for all considered systems and yields $B \approx NR_s$ Hz.

7.3 Effect of Synchronisation Errors

In this section, we compare the sensitivity of the systems described in section 7.2 to carrier phase and timing synchronisation errors. To clearly isolate the effect of the synchronisation errors, we consider the transmission over an ideal channel. Furthermore, we consider the case of synchronous transmission, i.e., the signals transmitted to/by the different users are synchronised such that all users exhibit the same carrier phase error and timing error. In addition, we assume that all users have the same energy per symbol and that the system works at a full load, i.e., the number of active users equals N. In the following, we separately consider the effect of the carrier phase errors and the timing errors.

7.3.1 Carrier Phase Errors

In this section, we compare the effect of the carrier phase errors on the systems of section 7.2, in the absence of timing errors. We consider the cases of a constant phase offset, a carrier frequency offset and carrier phase jitter.

Constant Phase Offset

A constant mismatch of the phase between the carrier oscillators at the transmitter and the receiver yields a constant phase offset ϕ. As shown in chapter 3 (SC/TDMA and SC/FDMA), chapter 4 (DS-CDMA), chapter 5 (OFDM/TDMA and OFDMA) and chapter 6 (MC-CDMA), a constant phase offset introduces a phase rotation over an angle ϕ of the samples at the input

Table 7.4: Overview of the effect of a constant phase offset.

	Constant Phase Offset
SC/TDMA	no degradation
DS-CDMA	no degradation
SC/FDMA	no degradation
OFDM/TDMA	no degradation
MC-CDMA	no degradation
OFDMA	no degradation

of the decision device for all systems when no equaliser is used. Hence, a constant phase offset results in a reduction of the noise margins if no precaution is taken. A one-tap equaliser is able to compensate for the systematic phase rotation of the samples at the input of the decision device without enhancing the noise power level. Consequently, for any of the systems of section 7.2 a constant phase offset introduces no performance degradation. The results are summarised in table 7.4.

Carrier Frequency Offset

A constant mismatch of the frequency between the carrier oscillators at the transmitter and the receiver introduces a carrier phase error that linearly increases with time: $\phi(t) = 2\pi\Delta Ft + \phi(0)$. The effect of this carrier frequency offset is twofold. First, a carrier frequency offset introduces a frequency shift of the downconverted received signal. This results in signal distortion and power loss at the receiver filter output, as a part of the received signal falls outside the bandwidth of the receiver filter. This effect results in an attenuation of the useful component and the introduction of interference at the receiver filter output. Further, the carrier frequency offset introduces a rotation at a constant speed of $2\pi\Delta F$ rad/s of the receiver filter output samples. In single carrier systems, the receiver filter output samples are applied to a one-tap equaliser (see figures 3.1 and 4.2). In the SC/TDMA system and the SC/FDMA system, the equaliser is followed by the decision device, while in the DS-CDMA system, the receiver correlates the equaliser output with the spreading sequence of the considered user and applies the correlator output to the decision device. The one-tap equaliser is able to compensate for the systematic rotation of the receiver filter output samples without enhancing the noise power level. However, the equaliser is not able to correct for the reduction of the useful component without enhancing the noise power level, or to eliminate the interference. Hence, the single carrier systems are degraded as compared to the case of a zero carrier frequency offset. In chapter 3 and 4, it is shown that the effect of the interference is negligible as compared to the effect of the reduction of the useful component. Hence, the degradation is mainly caused by the effect of the reduction of the useful component. The degradation is a function of the product ΔFT; for given ΔFT the degradation for SC/TDMA, SC/FDMA and DS-CDMA are the same.

In multicarrier systems, the rotating receiver filter output samples are applied to the FFT, followed by one-tap equalisers that scale and rotate the FFT outputs (see figures 5.2 and 6.6). The rotation of the receiver filter output samples gives rise to an additional reduction of the useful component and additional interference at the FFT outputs. Furthermore, the FFT outputs are rotating at a constant speed of $2\pi(N_{FFT} + \nu)\Delta FT$ rad/block. The one-tap equalisers are able to compensate for the systematic rotation of the FFT outputs without loss of performance. However, the equaliser is not able to correct for the reduction of the useful component without enhancing the noise power level, or to eliminate the interference. Hence, the multicarrier systems are degraded as compared to the case of a zero carrier frequency offset. The degradation at the output of the receiver filter (caused by the frequency shift of the downconverted received signal) is negligibly small as compared to the degradation at the FFT outputs (caused by the rotation of the receiver filter output samples). In chapters 5 and 6, an upper bound on the degradation is given by (5.38) and (6.36), for the OFDM(A) system and the MC-CDMA system, respectively. When the rolloff is small (so that the number of modulated carriers is close to N_{FFT}), this upper bound yields an accurate approximation of the actual degradation. This upper bound is a function of the product $N_{FFT}\Delta FT$; for given $N_{FFT}\Delta FT$, the upper bounds for OFDM(A) and MC-CDMA are the same. A small degradation requires $\Delta FT \ll N_{FFT}$. The degradation strongly increases for an increasing number of carriers. Hence, the multicarrier systems are very sensitive to a carrier frequency offset. To get rid of the degradation caused by the rotation of the filter output samples, the carrier frequency offset should be corrected in front of the FFT. When this correction is applied after the receiver filter, the frequency shift of the downconverted received signal introduces only a degradation of the carriers inside the rolloff area, and of some carriers adjacent to the rolloff area. This degradation is independent of the number of carriers and only depends on the receiver filter bandwidth. When the affected carriers are not used, no degradation is introduced by a carrier frequency offset, provided that the systematic phase rotation is compensated in front of the FFT.

In figure 7.7, the performance degradation is shown as function of the carrier frequency offset relative to the symbol rate R_s, for $N = 64$ users, $\alpha = 0.1$ and $SNR(0) = 20$ dB. As we observe, all multicarrier systems are much more sensitive to a carrier frequency offset than are the single carrier systems.

- As the sampling rates $1/T$ for SC/TDMA and DS-CDMA are the same (see table 7.1 and 7.3), these modulations yield the same degradation, which for given $\Delta F/R_s$ decreases with increasing number (N) of users. The sampling rate $1/T$ for SC/FDMA is N times as small as for SC/TDMA and DS-CDMA (see table 7.2), so that the degradation for the former modulation is larger than the degradation for the latter modulations; for given $\Delta F/R_s$ the degradation for SC/FDMA is independent of the number (N) of users.

- The degradation for OFDMA and MC-CDMA are essentially the same,

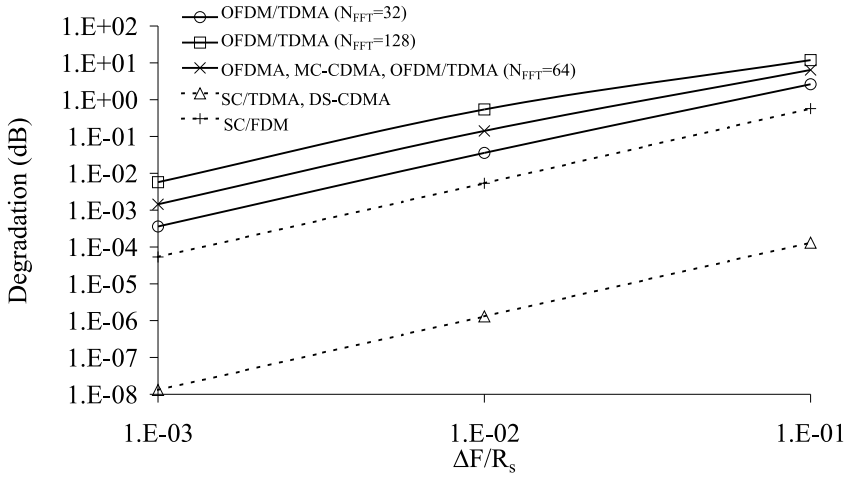

Figure 7.7: Effect of a carrier frequency offset, $N = 64, \alpha = 0.1, SNR(0) = 20$ dB.

Table 7.5: Overview of the effect of a carrier frequency offset.

	Carrier Frequency Offset
SC/TDMA	small degradation, increases with $(1/N)\Delta F/R_s$
DS-CDMA	small degradation, increases with $(1/N)\Delta F/R_s$
SC/FDMA	moderate degradation, increases with $\Delta F/R_s$
OFDM/TDMA	strong degradation, increases with $(N_{FFT}/N)\Delta F/R_s$
MC-CDMA	strong degradation, increases with $\Delta F/R_s$
OFDMA	strong degradation, increases with $\Delta F/R_s$

as these modulations yield the same sampling rate $1/T$ (see table 7.2 and 7.3) and essentially the same size of FFT ($N_{FFT} \approx N$); these degradations do not depend on N. When $N_{carr} \approx N_{FFT}$, the degradation for OFDM/TDMA is larger or smaller than the degradation for OFDMA and MC-CDMA, depending on whether $N_{FFT} > N$ or $N_{FFT} < N$; for given $\Delta F/R_s$, this degradation increases with increasing N_{FFT} and decreasing N.

Table 7.5 shows an overview of the results.

Carrier Phase Jitter

When a carrier synchronisation mechanism is used to adjust the carrier oscillator, we get rid of a carrier frequency offset and a constant phase offset. We can model the residual phase jitter as a zero-mean stationary random process with

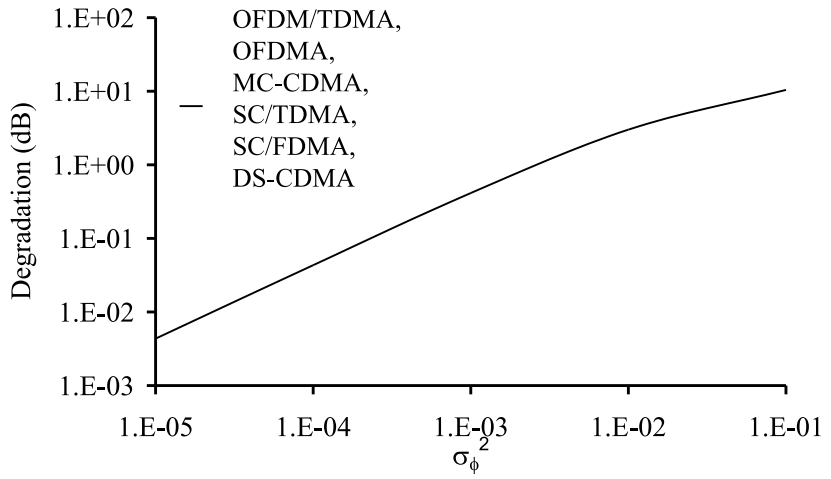

Figure 7.8: Effect of carrier phase jitter, $N = 64, SNR(0) = 20$ dB.

jitter power spectral density $S_\phi(f)$ and jitter variance σ_ϕ^2.

As shown in chapter 3 (SC/TDMA and SC/FDMA), chapter 4 (DS-CDMA), chapter 5 (OFDM/TDMA and OFDMA) and chapter 6 (MC-CDMA), the degradation caused by the carrier phase jitter is independent of the spectral contents of the jitter and of the number of carriers (OFDM/TDMA, OFDMA and MC-CDMA) and/or the spreading factor (DS-CDMA and MC-CDMA). For the multicarrier systems, the degradations (5.45) and (6.45) are an upper bound on the actual degradations in the case of OFDM(A) and MC-CDMA, respectively. However, this upper bound yields an accurate approximation for the actual degradation when the rolloff area is small. Considering (3.23), (4.27), (5.45) and (6.45) and for given $SNR(0)$, all considered systems exhibit the same sensitivity to the carrier phase jitter when the jitter variance is the same. Figure 7.8 shows the performance degradation caused by the carrier phase jitter.

The shape of the scatter diagrams in general depends on the spectral contents of the jitter.

- For the SC/TDMA system and the SC/FDMA system, the shape of the scatter diagram does not depend on the jitter spectrum, and the samples at the input of the decision device experience a pure (random) phase rotation, as shown in figure 3.7.

- All other systems yield a scatter diagram that depends on the spectral contents of the jitter. For jitter with mainly low frequency components ($|f| < (N/N_{FFT})R_s$ for OFDM/TDMA, $|f| < R_s$ for OFDMA, MC-CDMA and DS-CDMA), the jitter causes mainly an angular displacement of the samples at the input of the decision device (see figures 4.10, 5.16 and

Table 7.6: Overview of the effect of carrier phase jitter.

	Carrier Frequency Offset
SC/TDMA	- degradation is independent of N and spectral contents of jitter and only depends on jitter variance - scatter diagram independent of spectral contents jitter
DS-CDMA	- degradation is independent of N, N_c and spectral contents of jitter and only depends on jitter variance - scatter diagram depends on spectral contents jitter
SC/FDMA	- degradation is independent of N and spectral contents of jitter and only depends on jitter variance - scatter diagram independent of spectral contents jitter
OFDM/TDMA	- degradation is independent of N, N_{FFT} and spectral contents of jitter and only depends on jitter variance - scatter diagram depends on spectral contents jitter
MC-CDMA	- degradation is independent of N, N_c and spectral contents of jitter and only depends on jitter variance - scatter diagram depends on spectral contents jitter
OFDMA	- degradation is independent of N, N_{FFT} and spectral contents of jitter and only depends on jitter variance - scatter diagram depends on spectral contents jitter

6.18). Jitter with mainly high frequency components ($|f| > (N/N_{FFT})R_s$ for OFDM/TDMA, $|f| > R_s$ for OFDMA, MC-CDMA and DS-CDMA) gives rise to a scatter diagram at the input of the decision device that shows circular clouds (see figures 4.11, 5.17 and 6.19). When these modulations are affected by the same jitter spectrum, they yield identical scatter diagram.

An overview of these results can be found in table 7.6.

7.3.2 Timing Errors

In this section, we compare the effect of the timing errors on the systems of section 7.2 in the absence of carrier phase errors. We consider the cases of a constant timing offset, a clock frequency offset and timing jitter.

Constant Timing Offset

A constant mismatch between the optimum timing instants and the estimated timing instants results in a constant timing offset $\epsilon_k T = \epsilon T$. In chapter 3 (SC/TDMA and SC/FDMA) and chapter 4 (DS-CDMA), it is shown that for the considered single carrier systems, a constant timing offset yields a performance degradation. This performance degradation is mainly caused by the

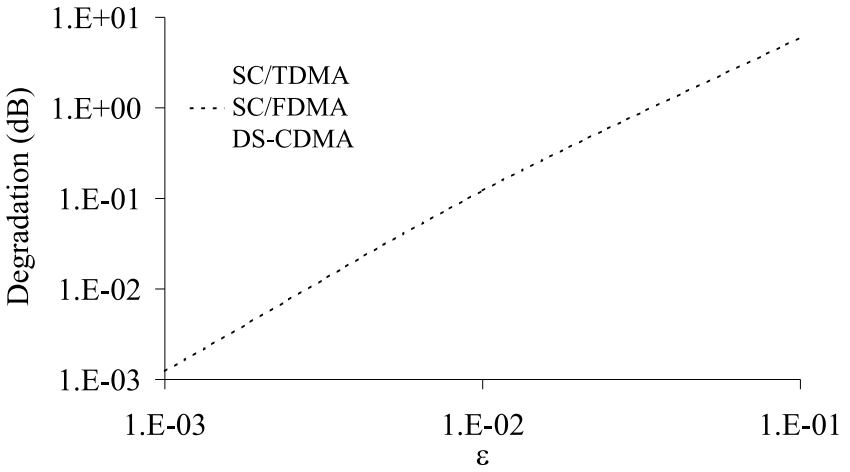

Figure 7.9: Effect of timing offset, $N = 64, \alpha = 0.1, SNR(0) = 20$ dB.

interference (ISI in the case of SC/TDMA and SC/FDMA, MUI in the case of DS-CDMA) which is introduced by the timing error. Furthermore, it is shown that a constant timing offset $|\epsilon| > 0.5$ causes severe performance degradation as in this case either a decision is taken about an adjacent symbol instead of the correct symbol (conventional single carrier system) or each receiver output sample is multiplied with an adjacent chip instead of the correct chip (DS-CDMA system). The degradations of the SC/TDMA and SC/FDMA systems (3.32) and the DS-CDMA system (for the maximum load) (4.32) are the same, for the same relative timing offset ϵ. However, considering that the sampling rate $1/T$ of the SC/FDMA system is N times as small as in the SC/TDMA system and the DS-CDMA system, the SC/FDMA system is less sensitive to the same absolute constant timing offset ϵT. The degradation caused by the constant timing offset decreases with increasing rolloff.

In the multicarrier systems (OFDM/TDMA, OFDMA and MC-CDMA), the carriers inside the rolloff area are not used. Hence, assuming that the cyclic prefix is sufficiently long to cope with the timing error, a constant timing offset only introduces a carrier dependent phase rotation of the FFT outputs. As this phase rotation can be compensated by the one-tap equaliser without enhancement of the noise power level, a constant timing offset causes no performance degradation.

Figure 7.9 shows the degradation of the considered single carrier systems as a function of the relative timing offset ϵ. Table 7.7 shows an overview of these results.

Table 7.7: Overview of the effect of constant timing offset.

	Constant Timing Offset
SC/TDMA	- degradation decreases for increasing rolloff - timing offset must be $\|\epsilon\| < 0.5$
DS-CDMA	- degradation decreases for increasing rolloff - timing offset must be $\|\epsilon\| < 0.5$
SC/FDMA	- degradation decreases for increasing rolloff - timing offset must be $\|\epsilon\| < 0.5$
OFDM/TDMA	- no degradation when cyclic prefix is long enough
MC-CDMA	- no degradation when cyclic prefix is long enough
OFDMA	- no degradation when cyclic prefix is long enough

Clock Frequency Offset

A constant mismatch of the frequency between the transmitter and receiver sampling clocks gives rise to a timing error that linearly increases with time: $\epsilon_k = k\Delta T/T + \epsilon_0$. This clock frequency offset introduces an increasing misalignment between the transmitted time-domain samples and the received time-domain samples. This misalignment can be compensated by means of a coarse synchronisation algorithm, which involves duplicating ($\Delta T > 0$) or removing ($\Delta T < 0$) receiver filter output samples at regular intervals.

In the conventional single carrier communication system (chapter 3) and the DS-CDMA system (chapter 4), the residual timing error after coarse synchronisation slowly varies within the interval $[-0.5, 0.5]$. Hence, the performance depends on the considered symbol interval. Because of its slow variation, the residual timing error can be interpreted as a fixed timing offset that depends on the symbol index. At regular intervals, the resulting timing error is close to -0.5 or 0.5, in which case the single carrier systems are so severely degraded (see figure 7.9) that a clock frequency offset can not be tolerated.

In the OFDM(A) system (chapter 5) and the MC-CDMA system (chapter 6), the resulting timing error $\tilde{\epsilon}_{i(N_{FFT}+\nu)+k} = k\Delta T/T + \epsilon_i$ after coarse synchronisation consists of a contribution $k\Delta T/T$ that linearly increases with time, which is independent of the block index, and a constant contribution ei that depends on the block index. The constant contribution ei introduces a pure phase rotation of the FFT outputs outside the rolloff area, which can, similarly as for a constant timing offset, be compensated by the one-tap equalisers without enhancing the noise power level. The linearly increasing contribution $k\Delta T/T$ gives rise to a reduction of the useful component and the introduction of interference at the FFT outputs. Hence, the multicarrier systems are degraded by a clock frequency offset. In OFDM/TDMA and OFDMA, the degradation depends on the carrier index, but is independent of the block index and is maximum for carriers close to the rolloff area. In MC-CDMA, the degradation is independent of the user index and of the block index. The degradation (5.61)

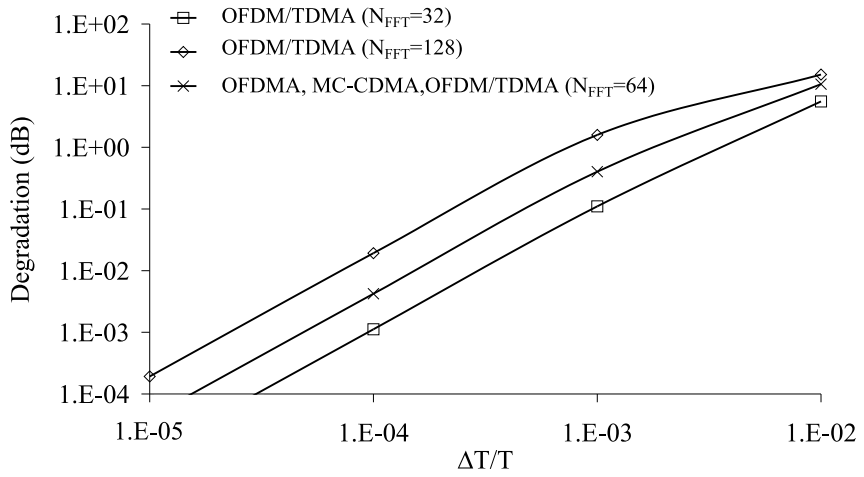

Figure 7.10: Effect of a clock frequency offset, $N = 64, \alpha = 0.1, SNR(0) = 20$ dB.

for OFDM/TDMA and OFDMA is an upper bound for the actual degradation. Similarly, an upper bound for the degradation in the MC-CDMA system can be defined. For given $N_{FFT}\Delta T/T$, the average (over the FFT outputs) degradation for OFDM(A) is essentially equal to the degradation for MC-CDMA. For all multicarrier systems, the upper bound on the degradation is a function of the product $N_{FFT}\Delta T/T$ and strongly increases for an increasing number of carriers.

Figure 7.10 shows the degradation of the multicarrier systems as a function of the normalised clock frequency offset $\Delta T/T$. For OFDM/TDMA and OFDMA, the average (over the FFT outputs) degradation is shown.

- As the sizes of the FFT for OFDMA and MC-CDMA are essentially the same ($N_{FFT} \approx N$), the average degradation for OFDMA is very close to the degradation for MC-CDMA; this degradation strongly increases with N, as $N_{FFT}\Delta T/T \approx N\Delta T/T$. The maximum degradation for OFDMA is somewhat larger than the degradation for MC-CDMA.

- For OFDM/TDMA, the size N_{FFT} of the FFT can be chosen independently of the number N of users. The degradation for OFDM/TDMA is larger or smaller than for OFDMA, depending on whether $N_{FFT} > N$ or $N_{FFT} < N$. The degradation is independent of N, but increases with increasing N_{FFT}.

Table 7.8 shows a summary of the results.

Table 7.8: Overview of the effect of clock frequency offset.

	Clock frequency Offset
SC/TDMA	- not tolerable
DS-CDMA	- not tolerable
SC/FDMA	- not tolerable
OFDM/TDMA	- strong degradation, increases with $N_{FFT}\Delta T/T$ - degradation depends on carrier index
MC-CDMA	- strong degradation, increases with $N\Delta T/T$ - degradation depends on user index
OFDMA	- strong degradation, increases with $N\Delta T/T$ - degradation depends on carrier index

Timing Jitter

When a timing synchronisation algorithm is used to adjust the sampling clock (or to control an interpolator), we get rid of a clock frequency offset and a constant timing offset. We can model the residual timing jitter ϵ_k as a zero-mean stationary random process with jitter power spectral density $S_\epsilon(\exp(j2\pi fT))$ and jitter variance σ_ϵ^2.

In chapter 3 (SC/TDMA and SC/FDMA) and chapter 4 (DS-CDMA), it is shown that the degradation caused by the timing jitter is independent of the spectral contents of the jitter but only depends on the jitter variance. Furthermore, in the case of the DS-CDMA system (for the maximum load), the degradation is independent of the spreading factor. The degradation also depends on the rolloff: the degradation decreases for increasing rolloff. For given jitter variance σ_ϵ^2, the degradations of the SC/TDMA system and SC/FDMA system (3.40) and the degradation of the DS-CDMA system in the case of the maximum load (4.38) are the same.

For the OFDM/TDMA and the OFDMA systems, the timing jitter introduces a degradation that depends on the carrier index. The average degradation (over all carriers) is independent of the spectral contents of the jitter but only depends on the jitter variance. Furthermore, the degradation is essentially independent of the number of carriers. In the considered OFDM/TDMA system and the OFDMA system, the carriers inside the rolloff are not used. Hence, the average degradation (5.71) is an upper bound on the actual average degradation. However, for a small rolloff area and for a large number of carriers, the upper bound (5.71) yields an accurate approximation of the actual average degradation. The scatter diagram depends on the spectral contents of the jitter. For jitter with mainly low frequency components ($|f| < 1/(N_{FFT}T) \approx (N/N_{FFT})R_s$), the scatter diagram shows mainly an angular displacement of the samples at the input of the decision device. Jitter with mainly high frequency components ($|f| > 1/(N_{FFT}T) \approx (N/N_{FFT})R_s$) gives rise to a scatter diagram at the input of the decision device with circular clouds.

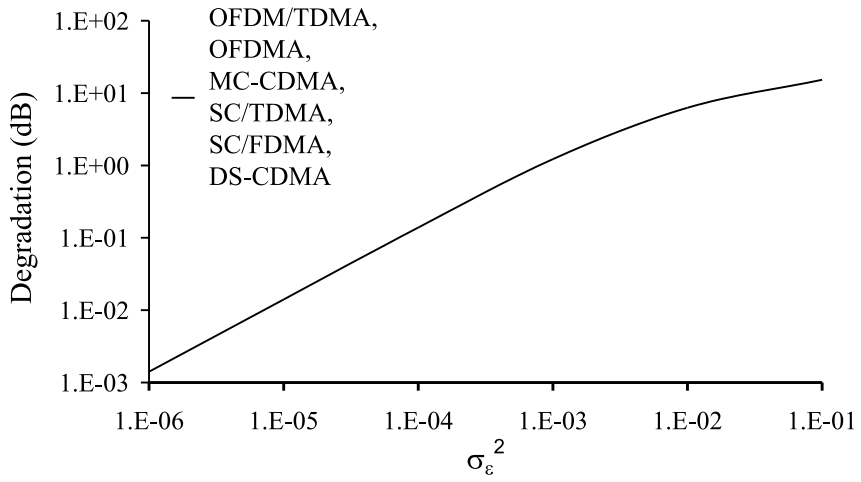

Figure 7.11: Effect of timing jitter, $N = 64, \alpha = 0, SNR(0) = 20$ dB.

In the MC-CDMA system of chapter 6, the timing jitter gives rise to a degradation that is independent of the spectral contents of the jitter but only depends on the jitter variance. Furthermore, the degradation is independent of the user index and essentially independent of the spreading factor and the FFT length N_{FFT}. Unlike the multicarrier systems of chapter 5, the scatter diagram for MC-CDMA is independent of the spectral contents of the jitter. The upper bound on the degradation of the MC-CDMA system (6.60) is equal to upper bound on the average degradation of the multicarrier systems of chapter 5 (5.71). This upper bound (6.60) yields an accurate approximation of the actual degradation when the rolloff area is small and the FFT length N_{FFT} is large.

Note that for $\alpha \to 0$, the degradations (3.41), (4.38) of the single carrier systems converge to the degradations (5.71) and (6.60) of the multicarrier systems, yielding

$$Deg = 10 \log \left(1 + SNR(0) \frac{\pi^2}{3} \sigma_\epsilon^2 \right) \tag{7.1}$$

Hence, all considered system exhibit essentially the same sensitivity to timing jitter. This degradation is independent of the number of users. The degradation caused by the timing jitter is shown in figure 7.11. The results are summarised in table 7.9.

7.4 Conclusions and Remarks

In this chapter, we have compared a number of multicarrier systems and their single carrier equivalents regarding their sensitivity to synchronisation errors. In

Table 7.9: Overview of the effect of timing jitter.

	Timing jitter
SC/TDMA	- degradation independent of spectral contents jitter, only depends on jitter variance - degradation decreases for increasing rolloff
DS-CDMA	- degradation independent of spectral contents jitter and spreading factor, only depends on jitter variance - degradation decreases for increasing rolloff
SC/FDMA	- degradation independent of spectral contents jitter, only depends on jitter variance - degradation decreases for increasing rolloff
OFDM/TDMA	- degradation independent of spectral contents jitter, essentially independent of number of carriers, depends only on carrier index and jitter variance - scatter diagram depends on spectral contents jitter
MC-CDMA	- degradation independent of spectral contents jitter and user index, essentially independent of number of carriers, depends only on jitter variance - scatter diagram independent of spectral contents jitter
OFDMA	- degradation independent of spectral contents jitter, essentially independent of number of carriers, depends only on carrier index and jitter variance - scatter diagram depends on spectral contents jitter

order to allow a fair comparison between the different systems, we have assumed that all systems are able to accommodate N users at a data rate R_s per user. In the comparison, we considered the case of synchronous transmission. All systems make use of one-tap equalisation to partially compensate the effect of the synchronisation errors: for DS-CDMA and MC-CDMA, equalisation is applied in front of the despreading, whereas for the other modulation techniques, equalisation is applied at the input of the decision device. The cyclic prefix in multicarrier systems is sufficiently long to cope with timing errors. The results can be summarised as follows:

- None of the systems is degraded by a constant phase offset.
- Multicarrier systems are much more sensitive to a carrier frequency offset than single carrier systems. The degradation of multicarrier systems and single carrier systems is an increasing function of $N_{FFT}\Delta FT$ and ΔFT, respectively.
- All systems exhibit the same sensitivity to carrier phase jitter. The degradation is independent of the spectral contents of the jitter, the FFT length N_{FFT} and of the spreading factor, but only depends on the jitter variance.

- Single carrier systems are degraded by a constant timing offset. In multicarrier systems, no degradation occurs when the carriers inside the rolloff area are not used.
- Single carrier and multicarrier systems are both very sensitive to a clock frequency offset. For single carrier systems, the degradation is so large that a clock frequency offset can not be tolerated: the clock frequency offset must be eliminated by adjusting the sampling clock or by interpolating between available receiver filter output samples.
- Timing jitter introduces a degradation that is essentially the same for all systems. The degradation is independent of the spectral contents of the jitter, essentially independent of the FFT length and of the spreading factor, but only depends on the jitter variance.

Given an acceptable amount of performance degradation, our results on the sensitivity of the various modulations can be used to derive requirements on the accuracy of carrier and timing synchronisation algorithms and on the stability of carrier and clock oscillators.

Chapter 8

Conclusions – Future Work

8.1 Achievements - Conclusions

The objective of this work was to study the effect of the synchronisation errors on multicarrier systems. In this work, we have investigated, using an equivalent time-varying model for a generic system for bandpass communication, the influence of carrier phase errors and timing errors on the signal-to-noise ratio (SNR) for a number of multicarrier systems, i.e., OFDM, OFDMA and MC-CDMA. The cyclic prefix is assumed to be sufficiently long such that, even in the presence of timing errors, no interference between data symbols transmitted during different blocks is present. At the receiver, each FFT output is applied to a one-tap MMSE equaliser. In this work, we have compared the different multicarrier systems for a given number of carriers (N_{FFT}) and a given sampling rate ($1/T$). The results for downlink communication in an ideal channel can be summarised as follows:

- A constant phase offset does not degrade the multicarrier systems.
- A constant timing offset causes no degradation of the multicarrier systems, provided that the carriers inside the rolloff area are not used.
- All considered multicarrier systems exhibit the same sensitivity to carrier frequency offsets. The degradation increases with $N_{FFT}\Delta FT$.
- The degradation caused by a clock frequency offset increases with $N_{FFT}\Delta T/T$. OFDM and OFDMA exhibit the same degradation, that depends on the carrier index. The degradation of MC-CDMA equals the average degradation (over the FFT outputs) of OFDM and OFDMA.
- Carrier phase jitter introduces a degradation that is independent of the number of carriers (N_{FFT}) and the spectral contents of the jitter, but only depends on the jitter variance.

- Timing jitter gives rise to a degradation that is independent of the number of carriers (for large N_{FFT}) and the spectral contents of the jitter, but only depends on the jitter variance. OFDM and OFDMA exhibit the same degradation, that depends on the carrier index. The degradation of MC-CDMA equals the average degradation (over the FFT outputs) of OFDM and OFDMA.

In uplink OFDM(A) over an ideal channel, the degradation is the same as in the downlink. Uplink MC-CDMA over an ideal channel yields the same degradation as in downlink MC-CDMA, provided that the transmitters of the different users are synchronised (i.e., there is no mutual clock frequency offset and no mutual constant timing offset). When the different users in uplink MC-CDMA are not mutually synchronised, the interference between the users can not be reduced sufficiently by the simple one-tap equalisers at the FFT outputs of the base station, such that the degradation is much larger than in downlink MC-CDMA.

In the case of a dispersive channel, the attenuation of the carriers depends on the carrier index, which implies that the sensitivity to the noise is larger than in the case of an ideal channel. In OFDM(A), a sufficient large cyclic prefix guarantees that there is no interference between the carriers, for both the uplink and the downlink. In MC-CDMA, interference between the different users appears at the FFT outputs. The simple one-tap equalisers at the FFT outputs are able to eliminate this interference in the case of downlink MC-CDMA (where the signals transmitted to the different users have reach the receiver via a common channel), but are not able to eliminate this interference in the case of uplink MC-CDMA (where the signals transmitted by the different users reach the base station via different channels).

Based on a number of numerical examples, we have shown that, in the case of uplink multicarrier transmission over a dispersive channel, the additional degradation caused by synchronisation errors is essentially the same as the degradation in the case of an ideal channel. This implies that the results obtained with the idea channel are applicable to more realistic channels.

Furthermore, we have made a comparison between the multicarrier systems and the single carrier systems with respect to their sensitivity to synchronisation errors in the case of an ideal channel. The results can be summarised as follows:

- For none of the systems, a constant phase offset causes a performance degradation.
- A constant timing offset introduces no degradation in the case of multicarrier systems, provided that the carriers inside the rolloff area are not used. A single carrier system is degraded by a constant timing offset.
- A carrier frequency offset gives rise to a degradation that increases with $N_{FFT}\Delta FT$ for multicarrier systems, while for single carrier systems, the degradation increases with ΔFT. For given ΔFT, the degradation is much larger for multicarrier systems than for single carrier systems.

- A clock frequency offset gives rise to a severe degradation in single carrier systems. Hence, a clock frequency offset can not be tolerated in single carrier systems. In multicarrier systems, the degradation increases with $N_{FFT}\Delta T/T$.
- Both single carrier and multicarrier systems exhibit the same sensitivity to carrier phase jitter and timing jitter, for given jitter variances σ_ϕ^2 and σ_ϵ^2.

The research on the effect of synchronisation errors on multicarrier systems that has resulted in this thesis has been published in a number of articles. In [Ste98b], we have investigated the effect of carrier phase jitter on an OFDMA system. A comparison of the sensitivities on an OFDM system, an OFDMA system and an FDMA system has been made in [Ste97b]. An overview of the effect of different types of carrier phase and clock errors on OFDM systems is presented in [Ste00]. In [Ste97a], [Ste99a], we have studied the effect of carrier phase jitter on the MC-CDMA system. The effect of timing errors on the MC-CDMA system has been investigated in [Ste99b]. The sensitivity of MC-CDMA to different types of carrier phase and clock errors has been studied in [Ste99c], [Ste99d], [Ste99f]. Furthermore, in [Ste99c], [Ste99d], the idea of including the different types of synchronisation errors into a single equivalent time-varying channel model has been introduced. In [Ste98b], we have made a comparison of the sensitivity of MC-CDMA and OFDM to carrier phase errors, while in [Ste99e], a comparison is made between MC-CDMA and OCDMA.

8.2 Future Work

In this work, we have investigated the effect of synchronisation errors on the performance of a number of multicarrier systems (OFDM(A), MC-CDMA). Our suggestions for future work are twofold: they pertain to the application of our analysis method to other multicarrier systems, and to the derivation and analysis of synchronisation algorithms for combinations of multicarrier modulation with CDMA.

8.2.1 Sensitivity of Other Multicarrier Systems

In this work, we have investigated the sensitivity of OFDM(A) and MC-CDMA to carrier phase and timing errors. The analysis method, based upon the equivalent time-varying channel model, can be used to compute the degradation of other multicarrier systems to synchronisation errors. Some examples of such multicarrier systems are discussed below.

- In the MC-CDMA system considered in this work, the number of carriers used equals the number of chips per symbol (N_c), whereas the number

of available carriers equals the FFT length N_{FFT}. When the carriers in the rolloff area are not used, we obviously have $N_c < N_{FFT}$. In practice, both Nc and N_{FFT} are usually selected to be powers of two. Hence, when $N_c < N_{FFT}$, the minimum FFT length equals $2N_c$, which indicates that only 50% of the available carriers are actually used. In [Ste99g], we have proposed a more flexible version of MC-CDMA, where the spreading factor N_c is not necessarily the same as the number of carriers actually used (N_{carr}). This allows us to select both N_c and N_{FFT} as powers of two, and to choose N_{carr} ($< N_{FFT}$) independently of N_c. In [Ste99h], we have already carried out some preliminary investigations regarding the sensitivity of this 'flexible' MC-CDMA to synchronisation errors, but more work remains to be done.

- The MC-CDMA system considered in this work is only one of the possible combinations of multicarrier modulation with CDMA. Other combinations that have been proposed are multicarrier direct-sequence CDMA (MC-DS-CDMA) [DaS93] and multitone CDMA (MT-CDMA) [Van93]; we have briefly described MC-DS-CDMA and MT-CDMA in section 6.1. It would be worthwhile to investigate the degradations caused by synchronisation errors to MC-DS-CDMA and MT-CDMA, and make the comparison with MC-CDMA.

- The MC-CDMA system considered in this work is only one of the possible combinations of multicarrier modulation with CDMA. Other combinations that have been proposed are multicarrier direct-sequence CDMA (MC-DS-CDMA) [DaS93] and multitone CDMA (MT-CDMA) [Van93]; we have briefly described MC-DS-CDMA and MT-CDMA in section 6.1. It would be worthwhile to investigate the degradations caused by synchronisation errors to MC-DS-CDMA and MT-CDMA, and make the comparison with MC-CDMA. The different multicarrier systems considered in this work are based upon the Fourier transform. However, the resulting individual carrier signals have rather high sidelobes in the frequency domain, which makes the multicarrier signals sensitive to carrier frequency offsets and narrowband interferers. This sensitivity can be reduced by replacing the Fourier transforms by a different transform (such as a wavelet transform) [Snd95], [Lou98a]. The generation of the transmitted signal and the demodulation of the received signal is accomplished by means of a bank of filters. In [Lou98b], the sensitivity to timing errors of a filter bank based multicarrier system has been studied in the context of baseband transmission. It would be of interest to study the effect of carrier phase errors (especially carrier frequency offset) in the case of bandpass transmission.

8.2.2 Synchronisation Algorithms

In this work, we have investigated the effect of synchronisation errors on the performance of multicarrier systems, but we have not specified the operation of

the synchronisation algorithms that provide the carrier and timing recovery.

In the case of OFDM, several algorithms for carrier and timing recovery have been proposed and analysed in the open literature. Basically, two classes of algorithms exist. The algorithms of the first class require some redundancy of the transmitted OFDM blocks (occasionally, OFDM blocks must be repeated) [Moo94], [Sch97], or the transmission of pilot symbols (that are known to the receiver) [War93], [Ste98a]. The algorithm of the second class provide carrier and timing recovery irrespective of the data symbol sequence, by exploiting the redundancy introduced by the cyclic prefix [vdB97]. To our knowledge, not much research has been carried out yet with respect to synchronisation algorithms for MC-CDMA or for other combinations of multicarrier modulation with CDMA. It would be of interest to derive synchronisation algorithms for these modulations and to investigate their performance. As a starting point, adaptations of the synchronisation algorithms for OFDM could be studied.

Appendix A

Bit Error Rate for QPSK

In this appendix, the bit error rate (BER) is derived for the case of the data symbols belonging to a QPSK constellation. Each QPSK data symbol ali,n has statistically independent in-phase and quadrature components $(a_{i,n}^{\ell})^I$ and $(a_{i,n}^{\ell})^Q$ that each represent one information bit: $a_{i,n}^{\ell} = (a_{i,n}^{\ell})^I + j(a_{i,n}^{\ell})^Q$. The bit error rate for QPSK is given by

$$BER = \frac{1}{2}\left[Pr\left((\hat{a}_{i,n}^{\ell})^I \neq (a_{i,n}^{\ell})^I\right) + Pr\left((\hat{a}_{i,n}^{\ell})^Q \neq (a_{i,n}^{\ell})^Q\right)\right] \tag{A.1}$$

where $Pr(x)$ is the probability of the event x.

Taking into account the QPSK decision rule illustrated in figure A.1, the probability that the in-phase component of the data symbol was detected incorrectly when the in-phase component of the transmitted data symbol equals $(a_{i,n}^{\ell})^I = \sqrt{2}/2$ is given by

$$Pr\left((\hat{a}_{i,n}^{\ell})^I \neq (a_{i,n}^{\ell})^I \middle| (a_{i,n}^{\ell})^I = +\frac{\sqrt{2}}{2}\right) = Pr\left(Re(z_{i,n}^{\ell}) < 0 \middle| (a_{i,n}^{\ell})^I = +\frac{\sqrt{2}}{2}\right) \tag{A.2}$$

where $z_{i,n}^{\ell}$ is given by (2.58). The sample $z_{i,n}^{\ell}$ can be decomposed into a useful component, interference and noise. The coefficient of the useful component $s_{i,n}^{\ell}$ is decomposed into an average component $E[s_{i,n}^{\ell}]$ and a zero-mean fluctuation $\Delta s_{i,n}^{\ell} = s_{i,n}^{\ell} - E[s_{i,n}^{\ell}]$, i.e. the self-interference.

$$z_{i,n}^{\ell} = a_{i,n}^{\ell} E[s_{i,n}^{\ell}] + a_{i,n}^{\ell} \Delta s_{i,n}^{\ell} + Int_{i,n}^{\ell} + W_{i,n}^{\ell} \sigma_{i,n}^{\ell} \tag{A.3}$$

In (A.3), the average useful component, the self-interference, the interference component and the noise component are uncorrelated. The noise component $W_{i,n}^{\ell}\sigma_{i,n}^{\ell}$ is uncorrelated with all transmitted symbols, from which it follows that the noise contribution is uncorrelated with the average useful component,

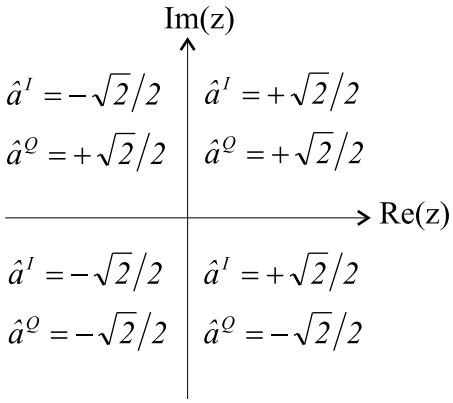

Figure A.1: Decision rule

the self-interference and the interference component. The interference component $Int_{i,n}^{\ell}$ consists of all contributions of symbols other than the considered symbol $a_{i,n}^{\ell}$ (ISI and MUI) and is therefore uncorrelated with the contributions that contain the considered symbol, as all transmitted symbols are assumed to be uncorrelated. Furthermore, the interference component has uncorrelated real and imaginary parts each having the same variance, as the in-phase and quadrature components of the associated data symbols are independent and have identical variance. It follows from the definition of $\Delta s_{i,n}^{\ell}$ that the self-interference component is uncorrelated with the average useful component.

In the following, we assume that the average coefficient $E[s_{i,n}^{\ell}]$ of the useful component is real and positive. This is accomplished by a proper selection of the vector $\mathbf{b}_{i,n}^{\ell}$ at the receiver (see figure 2.21). Considering (A.3) the probability (A.2) yields

$$Pr\left((\hat{a}_{i,n}^{\ell})^I \neq (a_{i,n}^{\ell})^I \middle| (a_{i,n}^{\ell})^I = +\frac{\sqrt{2}}{2}\right) = Pr\left(\frac{\sqrt{2}}{2}E[s_{i,n}^{\ell}] + \frac{\sqrt{2}}{2}Re(\Delta s_{i,n}^{\ell})\right.$$
$$\left. -(a_{i,n}^{\ell})^Q Im(\Delta s_{i,n}^{\ell}) + Re(\Delta Int_{i,n}^{\ell}) + Re(W_{i,n}^{\ell}\sigma_{i,n}^{\ell}) < 0 \middle| (a_{i,n}^{\ell})^I = \frac{\sqrt{2}}{2}\right) \quad \text{(A.4)}$$

As $(a_{i,n}^{\ell})^Q$ has zero mean, the quantities $\frac{\sqrt{2}}{2}Re(\Delta s_{i,n}^{\ell})$ and $(a_{i,n}^{\ell})^Q Im(\Delta s_{i,n}^{\ell})$ are uncorrelated. Assuming the quantity $Re(z_{i,n}^{\ell})$ can be modelled as a Gaussian variable with average m_I and variance σ_I^2, the probability (A.4) can be written as

$$Pr\left((\hat{a}_{i,n}^{\ell})^I \neq (a_{i,n}^{\ell})^I \middle| (a_{i,n}^{\ell})^I = +\frac{\sqrt{2}}{2}\right) = Q\left(\frac{m_I}{\sigma_I}\right) \quad \text{(A.5)}$$

where

$$\begin{aligned} m_I &= \frac{\sqrt{2}}{2} E[s_{i,n}^{\ell}] \\ \sigma_I^2 &= \frac{1}{2} E\left[\left(Re(\Delta s_{i,n}^{\ell})\right)^2\right] + \frac{1}{2} E\left[\left(Im(\Delta s_{i,n}^{\ell})\right)^2\right] \\ &+ E\left[\left(Re(\Delta Int_{i,n}^{\ell})\right)^2\right] + E\left[\left(Re(W_{i,n}^{\ell}\sigma_{i,n}^{\ell})\right)^2\right] \end{aligned} \tag{A.6}$$

and $Q(x)$ is the complementary error function

$$Q(x) = \int_x^{+\infty} \frac{1}{\sqrt{2\pi}} e^{-\frac{z^2}{2}} dz \tag{A.7}$$

The assumption that the quantity $Re(z_{i,n}^{\ell})$ can be modelled as a Gaussian variable holds only when the quantity $\sigma_{i,n}^{\ell}$ is non-random. Furthermore, as only small degradations of the system performance can be tolerated, the interference contribution and the self-interference contribution must be small as compared to the noise contribution. In this case, the disturbance of the average useful component is dominated by the noise contribution, which is a Gaussian variable. Therefore, the assumption that $Re(z_{i,n}^{\ell})$ can be modelled as a Gaussian variable is valid for small degradations and when the quantity $\sigma_{i,n}^{\ell}$ is non-random.

Now we consider the probability that the in-phase component of the data symbol was detected incorrectly when the in-phase component of the transmitted data symbol equals $(a_{i,n}^{\ell})^I = -\sqrt{2}/2$. Following the same reasoning as for the case of $(a_{i,n}^{\ell})^I = \sqrt{2}/2$, this probability yields

$$\begin{aligned} Pr\left((\hat{a}_{i,n}^{\ell})^I \neq (a_{i,n}^{\ell})^I \middle| (a_{i,n}^{\ell})^I = -\frac{\sqrt{2}}{2}\right) &= Pr\left(-\frac{\sqrt{2}}{2} E[s_{i,n}^{\ell}] - \frac{\sqrt{2}}{2} Re(\Delta s_{i,n}^{\ell})\right. \\ \left. -(a_{i,n}^{\ell})^Q Im(\Delta s_{i,n}^{\ell}) + Re(\Delta Int_{i,n}^{\ell}) + Re(W_{i,n}^{\ell}\sigma_{i,n}^{\ell}) > 0 \middle| (a_{i,n}^{\ell})^I = -\frac{\sqrt{2}}{2}\right) \\ = Q\left(\frac{m_I}{\sigma_I}\right) \end{aligned} \tag{A.8}$$

From (A.5) and (A.8) it follows that the conditional probabilities that the in-phase component was detected incorrectly are equal. Hence,

$$Pr\left((\hat{a}_{i,n}^{\ell})^I \neq (a_{i,n}^{\ell})^I\right) = Q\left(\frac{m_I}{\sigma_I}\right) \tag{A.9}$$

A similar analysis can be done for the probability that the quadrature component of the data symbol was detected incorrectly. We obtain

$$Pr\left((\hat{a}_{i,n}^{\ell})^Q \neq (a_{i,n}^{\ell})^Q\right) = Q\left(\frac{m_Q}{\sigma_Q}\right) \tag{A.10}$$

where

$$\begin{aligned} m_Q &= m_I = \frac{\sqrt{2}}{2} E[s_{i,n}^{\ell}] \\ \sigma_Q^2 &= \frac{1}{2} E\left[\left(Re(\Delta s_{i,n}^{\ell})\right)^2\right] + \frac{1}{2} E\left[\left(Im(\Delta s_{i,n}^{\ell})\right)^2\right] \\ &+ E\left[\left(Im(\Delta Int_{i,n}^{\ell})\right)^2\right] + E\left[\left(Im(W_{i,n}^{\ell}\sigma_{i,n}^{\ell})\right)^2\right] \end{aligned} \tag{A.11}$$

The interference term $Int_{i,n}^{\ell}$ and the noise term $\sigma_{i,n}^{\ell} W_{i,n}^{\ell}$ have uncorrelated real and imaginary parts with equal same variances. Considering $E[|x|^2] = E[(Re(x))^2] + E[(Im(x))^2]$, the variances σ_I^2 and σ_Q^2 are equal and yield

$$\sigma_I^2 = \sigma_Q^2 = \frac{1}{2}\left(E\left[\left|\Delta s_{i,n}^{\ell}\right|^2\right] + E\left[\left|\Delta Int_{i,n}^{\ell}\right|^2\right] + \left(\sigma_{i,n}^{\ell}\right)^2 E\left[\left|\Delta W_{i,n}^{\ell}\right|^2\right]\right) \tag{A.12}$$

From (A.8), (A.10) and (A.11) it follows that the probability of an erroneous detection of the in-phase component is equal to the probability of an erroneous detection of the quadrature component. Hence, the bit error rate (A.1) yields

$$BER_{i,n}^{\ell} = Q\left(\sqrt{SNR_{i,n}^{\ell}}\right) \tag{A.13}$$

where the signal-to-noise ratio is defined as

$$SNR_{i,n}^{\ell} = \frac{\left|E[s_{i,n}^{\ell}]\right|^2}{N_0\left(\sigma_{i,n}^{\ell}\right)^2 + E\left[\left|\Delta s_{i,n}^{\ell}\right|^2\right] + E\left[\left|\Delta Int_{i,n}^{\ell})\right|^2\right]} \tag{A.14}$$

In (A.14), we have made use of $E[|W_{i,n}^{\ell}|^2] = N_0$.

Appendix B

Square-Root Raised-Cosine Filter

In this work, it is assumed that the transmit filter $P(f)$ is a Nyquist filter with respect to the time interval T, i.e. the transmit pulse $p(t)$ satisfies (2.3). The receiver filter is matched to the transmit filter. The cascade of the transmit filter and the receiver filter has an impulse response $g(t)$ and its Fourier transform is $G(f) = |P(f)|^2$. These filters can be implemented as square-root raised-cosine filters with rolloff α, i.e. $P(f) = \sqrt{G(f)}\exp(j\Psi(f))$, where $\Psi(f)$ is an arbitrary phase function and $G(f)$ is given by (see also figure B.1):

$$G(f) = \begin{cases} T & |f|T \leq \frac{1-\alpha}{2} \\ \frac{T}{2}\left(1 - \sin\left(\frac{\pi}{\alpha}\left(|f|T - \frac{1}{2}\right)\right)\right) & \frac{1-\alpha}{2} \leq |f|T \leq \frac{1+\alpha}{2} \\ 0 & \text{otherwise} \end{cases} \tag{B.1}$$

The corresponding impulse response yields

$$g(t) = \frac{\sin\frac{\pi t}{T}}{\frac{\pi t}{T}} \frac{\cos\frac{\pi\alpha t}{T}}{1 - \left(\frac{2\alpha t}{T}\right)^2} \tag{B.2}$$

It is easily verified that the first order derivative $g'(t)$ at the instants $t = nT$ and the second order derivative $g''(t)$ at the instant $t = 0$ are given by

$$g'(nT) = \begin{cases} 0 & n = 0 \\ \frac{\pi}{T}\frac{\cos\pi n}{\pi n}\frac{\cos\pi\alpha n}{1-(2\alpha n)^2} & n \neq 0 \end{cases} \tag{B.3}$$

$$g''(0) = -(2\pi)^2 \int_{-\infty}^{+\infty} f^2 G(f) df = -\frac{1}{T^2}\left(\frac{\pi^2}{3} + \alpha^2(\pi^2 - 8)\right) \tag{B.4}$$

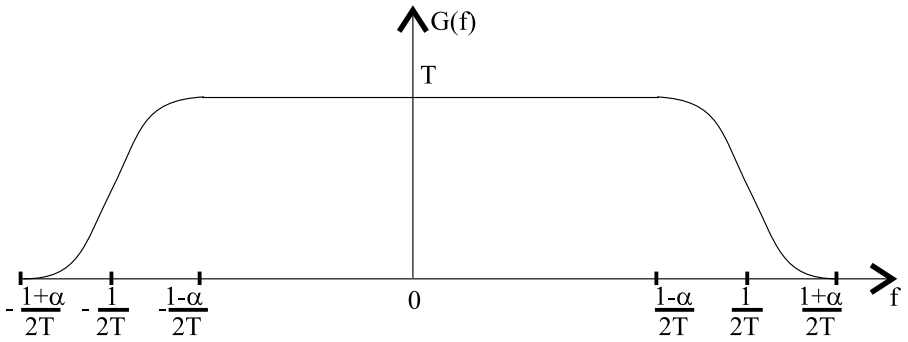

Figure B.1: Raised-cosine transfer function

Furthermore, the following expression is valid for the raised-cosine filter:

$$\begin{aligned}\sum_{n=-\infty}^{+\infty} T^2|g'(nT)|^2 &= (2\pi)^2T^2\int_{-\infty}^{+\infty} df G(f)\int_{-\infty}^{+\infty} df' f' G^*(f')\sum_{n=-\infty}^{+\infty} e^{j2\pi(f-f')nT} \\ &= (2\pi)^2T\sum_{n=-\infty}^{+\infty}\int_{-\infty}^{+\infty} df\, f\left(f+\frac{n}{T}\right)G(f)G^*\left(f+\frac{n}{T}\right) \\ &= \frac{\pi^2}{3}+\alpha^2(\pi^2-8)-\frac{\alpha\pi^2}{2} \qquad \text{(B.5)}\end{aligned}$$

Appendix C

Moments of Spreading Sequences

C.1 Introduction

In this work, the systems that make use of spreading sequences have a structure as shown in figure C.1. The data symbol $a_{i,\ell}$ of user ℓ is spread using the spreading sequence $\mathbf{c}_{i,\ell} = (1/\sqrt{N_c})[c_{iN_c,\ell} \dots c_{iN_c+N_c-1,\ell}]^T$. The number N_c of chips per symbol is called the spreading factor. The resulting sequence $\mathbf{c}_{i,\ell}a_{i,\ell}$ is applied to a linear transformation $\mathbf{T}_{tr,i,\ell}$ (2.1) that converts the spread data symbol into a block of M_s samples $\mathbf{s}_{i,\ell}$. The discrete-time sequence $\mathbf{s}_{i,\ell}$ is transmitted over the equivalent channel (see figure 2.17) with discrete time impulse response $h_{eq,\ell}(k; iM_s + m)$ (2.22). The sum of the different user signals is disturbed by additive white Gaussian noise (AWGN) $\mathbf{w}_{i,\ell}$ (see (2.24) and (2.30)). The resulting sequence $\mathbf{v}_{i,\ell}$ is applied to the receiver, that consists of a linear transformation $\mathbf{B}_{i,\ell}$, converting a block of M_s samples $\mathbf{v}_{i,\ell}$ into a block of N_c samples. The receiver correlates the outputs of the linear transformation $\mathbf{B}_{i,\ell}$ with the spreading sequence $\mathbf{c}_{i,\ell}$ of the considered user. The sample $z_{i,\ell}$ at the input of the decision device, used to make a decision about the transmitted data symbol $a_{i,\ell}$, is given by

$$z_{i,\ell} = \sum_{i'=-\infty}^{+\infty} \sum_{\ell'=1}^{N_u} a_{i',\ell'} I_{i,i',\ell,\ell'} + W_{i,\ell} \tag{C.1}$$

where $W_{i,\ell}$ is the contribution from the AWGN, i.e., $W_{i,\ell} = \mathbf{c}_{i,\ell}^{\dagger}\mathbf{B}_{i,\ell}\mathbf{w}_{i,\ell}$ and

$$I_{i,i',\ell,\ell'} = \frac{1}{N_c} \sum_{n,n'=0}^{N_c-1} c^*_{iN_c+n,\ell} c_{i'N_c+n',\ell'} A^{(\ell,\ell')}_{iN_c+n,i'N_c+n'} \tag{C.2}$$

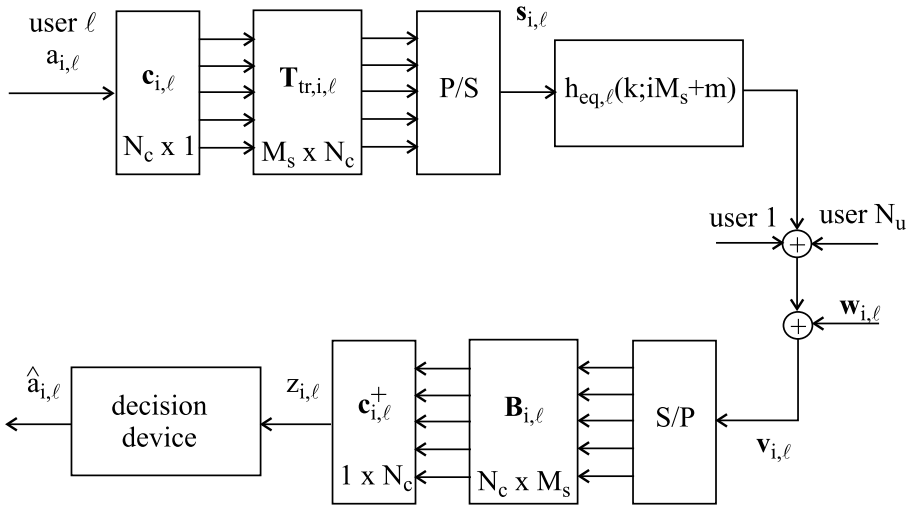

Figure C.1: Block diagram of a system using spreading sequences

The quantity $A^{(\ell,\ell')}_{iN_c+n,i'N_c+n'}$ is the transfer matrix taking into account the linear transformation $\mathbf{T}_{tr,i,\ell}$ at the transmitter, the dispersive channel including the synchronisation errors $h_{eq,\ell}(k;iM_s+m)$ and the linear transformation matrix $\mathbf{B}_{i,\ell}$ at the receiver. This yields

$$A^{(\ell,\ell')}_{iN_c+n,i'N_c+n'} = \left[\mathbf{B}_{i,\ell}\,(\mathbf{H}_{eq})^{\ell'}_{i,i'}\,\mathbf{T}_{tr,i',\ell'}\right]_{n,n'} \tag{C.3}$$

where $[(\mathbf{H}_{eq})^{\ell'}_{i,i'}]_{m,m'} = h_{eq,\ell'}((iM_s+m)-(i'M_s+m');iM_s+m)$ is the $M_s \times M_s$ matrix consisting of the discrete-time impulse response of the channel including the synchronisation errors. The quantities (C.3) can be viewed as random variables because of the presence of random synchronisation errors and/or a fading channel.

The samples $z_{i,\ell}$ (C.1) can be decomposed into a useful component $s_{i,\ell}a_{i,\ell}$ ($i'=i,\ell'=\ell$), intersymbol interference $ISI_{i,\ell}$ ($i'\neq i,\ell'=\ell$), multiuser interference $MUI_{i,\ell}$ ($\ell'\neq\ell$) and additive noise $W_{i,\ell}$. The coefficient $s_{i,\ell}$ of the useful component can be further decomposed into an average useful contribution $E[s_{i,\ell}]$ and a zero-mean fluctuation $\Delta s_{i,\ell} = s_{i,\ell} - E[s_{i,\ell}]$ about its average, i.e., the self-interference. Considering the data symbols are uncorrelated and have a unit-average energy, i.e., $E[a_{i,\ell}a^*_{i',\ell'}] = \delta_{i,i'}\delta_{\ell,\ell'}$, the average useful component and the powers of the self-interference, the intersymbol interference, the

multiuser interference and the noise yield

$$
\begin{aligned}
E[s_{i,\ell}] &= \frac{1}{N_c}\sum_{n,n'=0}^{N_c-1} E\left[A^{(\ell,\ell)}_{iN_c+n,iN_c+n'}\right] E\left[c^*_{iN_c+n,\ell}c_{iN_c+n',\ell}\right] \\
E\left[|\Delta s_{i,\ell}|^2\right] &= \frac{1}{N_c^2}\sum_{n,n'=0}^{N_c-1}\sum_{k,k'=0}^{N_c-1} E\left[A^{(\ell,\ell)}_{iN_c+n,iN_c+n'}\left(A^{(\ell,\ell)}_{iN_c+k,iN_c+k'}\right)^*\right]\cdot \\
&\quad E\left[c^*_{iN_c+n,\ell}c_{iN_c+n',\ell}c_{iN_c+k,\ell}c^*_{iN_c+k',\ell}\right] \\
&\quad - \left|\frac{1}{N_c}\sum_{n,n'=0}^{N_c-1} E\left[c^*_{iN_c+n,\ell}c_{iN_c+n',\ell}\right] E\left[A^{(\ell,\ell)}_{iN_c+n,iN_c+n'}\right]\right|^2 \\
E\left[|ISI_{i,\ell}|^2\right] &= \sum_{i'=-\infty;i'\neq i}^{+\infty}\frac{1}{N_c^2}\sum_{n,n'=0}^{N_c-1}\sum_{k,k'=0}^{N_c-1} \\
&\quad E\left[A^{(\ell,\ell)}_{iN_c+n,i'N_c+n'}\left(A^{(\ell,\ell)}_{iN_c+k,i'N_c+k'}\right)^*\right]\cdot \\
&\quad E\left[c^*_{iN_c+n,\ell}c_{i'N_c+n',\ell}c_{iN_c+k,\ell}c^*_{i'N_c+k',\ell}\right] \\
E\left[|MUI_{i,\ell}|^2\right] &= \sum_{i'=-\infty}^{+\infty}\sum_{\ell'=1;\ell'\neq\ell}^{N_u}\frac{1}{N_c^2}\sum_{n,n'=0}^{N_c-1}\sum_{k,k'=0}^{N_c-1} \\
&\quad E\left[A^{(\ell,\ell')}_{iN_c+n,i'N_c+n'}\left(A^{(\ell,\ell')}_{iN_c+k,i'N_c+k'}\right)^*\right]\cdot \\
&\quad E\left[c^*_{iN_c+n,\ell}c_{i'N_c+n',\ell'}c_{iN_c+k,\ell}c^*_{i'N_c+k',\ell'}\right] \\
E\left[|W_{i,\ell}|^2\right] &= \frac{1}{N_c}\sum_{n,n'=0}^{N_c-1} E[\tilde{w}_{iN_c+n,\ell}\tilde{w}^*_{iN_c+n',\ell'}]E\left[c^*_{iN_c+n,\ell}c_{iN_c+n',\ell}\right] \quad \text{(C.4)}
\end{aligned}
$$

We observe in (C.4) that the average useful component and the powers of the noise and the interference depend on two types of moments of the used spreading sequences. Moreover, it is clear that when the spreading factor N_c increases, the computation complexity of these terms, hence the SNR (2.59), rapidly increases. For computational purposes, it is desirable that the averages over the sequences in (C.4) are approximated by simple expressions. These approximations depend on the specific type of sequence that is used. In the following, we separately consider Walsh-Hadamard sequences, random sequences and overlay sequences, which are a combination of Walsh-Hadamard sequences and random sequences. For each of these types of sequences, we present expressions for the moments of the spreading sequences. Simulations are carried out to investigate the accuracy of the expressions.

C.2 Orthogonal Sequences

In this section, we consider the case of Walsh-Hadamard (WH) sequences. We assume the assignment of the WH sequences to the different users does not

change from one symbol interval to the next, i.e., all symbols of a user are spread with the same WH sequence. In this case, the chips are independent of the symbol index i: $c_{iN_c+n,\ell} = WH_{n,\ell}$ (2.24). As the assignment of the spreading sequences to the different users does not change from one symbol interval to the next, the performance of the user may depend on the sequence that is assigned to that user. Furthermore, the WH sequences contain no random components. Hence, the averaging over the chips in (C.4) can be omitted.

In the following, we introduce randomness by assuming that each of the N_c WH sequences can be assigned with a probability $1/N_c$ to the first user, each of the remaining $N_c - 1$ WH sequences can be assigned with a probability $1/(N_c - 1)$ to the second user, and so on. The resulting expressions (C.4) then become averages (over all users) of the expressions (C.4) for non-random WH sequences; the former expressions (that do not depend on the user index) will be used as approximation for the latter expressions, for any index. The moments of the chip sequences (averaging over all users) yield

$$E\left[c^*_{iN_c+n,\ell} c_{iN_c+n',\ell}\right] = \frac{1}{N_c} \sum_{m=0}^{N_c-1} WH_{n,m} WH_{n',m} \tag{C.5}$$

$$E\left[c^*_{iN_c+n,\ell} c_{i'N_c+n',\ell'} c_{iN_c+k,\ell} c^*_{i'N_c+k',\ell'}\right] = \tag{C.6}$$
$$\begin{cases} \frac{1}{N_c(N_c-1)} \sum_{m=0}^{N_c-1} \sum_{m'=0;m'\neq m}^{N_c-1} WH_{n,m} WH_{n',m'} WH_{k,m} WH_{k',m'} & \ell' \neq \ell \\ \frac{1}{N_c} \sum_{m=0}^{N_c-1} WH_{n,m} WH_{n',m} WH_{k,m} WH_{k',m} & \ell' = \ell \end{cases}$$

Considering the symmetry of the Hadamard matrix $\mathbf{H}_\gamma$ (2.42) and the orthogonality of the WH sequences, the average (C.5) reduces to

$$E\left[c^*_{iN_c+n,\ell} c_{iN_c+n',\ell}\right] = \delta_{n,n'} \tag{C.7}$$

Hence, the average useful component and the noise power in (C.4) yield

$$\begin{aligned} E[s_{i,\ell}] &= \frac{1}{N_c} \sum_{n=0}^{N_c-1} E\left[A^{(\ell,\ell)}_{iN_c+n,iN_c+n}\right] \\ E\left[|W_{i,\ell}|^2\right] &= \frac{1}{N_c} \sum_{n=0}^{N_c-1} E[\left|\tilde{w}_{iN_c+n,\ell}\right|^2] \end{aligned} \tag{C.8}$$

For $\ell' \neq \ell$, the sum (C.6) can be written as

$$\begin{aligned} &E\left[c^*_{iN_c+n,\ell} c_{i'N_c+n',\ell'} c_{iN_c+k,\ell} c^*_{i'N_c+k',\ell'}\right] = \\ &\frac{1}{N_c(N_c-1)} \Bigg(\sum_{m,m'=0}^{N_c-1} WH_{n,m} WH_{n',m'} WH_{k,m} WH_{k',m'} \\ &- \sum_{m=0}^{N_c-1} WH_{n,m} WH_{n',m} WH_{k,m} WH_{k',m} \Bigg) \end{aligned} \tag{C.9}$$

As the WH sequences are orthogonal, the first term in (C.9) reduces to

$$\sum_{m,m'=0}^{N_c-1} WH_{n,m}WH_{n',m'}WH_{k,m}WH_{k',m'} = N_c^2\delta_{n,n'}\delta_{k,k'} \tag{C.10}$$

The second term in (C.9) equals the sum for $\ell' = \ell$ in (C.6) and is a very complicated function of n, n', k and k'. In the following, we approximate this sum by

$$\frac{1}{N_c}\sum_{m=0}^{N_c-1} WH_{n,m}WH_{n',m}WH_{k,m}WH_{k',m} \approx \delta_{n,k}\delta_{n',k'} + \delta_{n,n'}\delta_{k,k'} - \delta_{n,n',k,k'} \tag{C.11}$$

where $\delta_{n,n',k,k'} = \delta_{n,n'}\delta_{k,k'}\delta_{n,k}$. In the simulations, it will be shown that the approximation (C.11) gives rise to very accurate results for the MUI power, while for the SI and the ISI power, this approximation yields a result of the same order as the actual SI and ISI power. Using (C.11), (C.6) reduces to

$$\begin{aligned} &E\left[c^*_{iN_c+n,\ell}c_{i'N_c+n',\ell'}c_{iN_c+k,\ell}c^*_{i'N_c+k',\ell'}\right] \approx \\ &\begin{cases} \delta_{n,k}\delta_{n',k'} - \frac{1}{N_c-1}(\delta_{n,n'}\delta_{k,k'} - \delta_{n,n',k,k'}) & \ell' \neq \ell \\ \delta_{n,k}\delta_{n',k'} + \delta_{n,n'}\delta_{k,k'} - \delta_{n,n',k,k'} & \ell' = \ell \end{cases} \end{aligned} \tag{C.12}$$

Hence the SI power, the MUI power and the ISI power (C.4) can be written as

$$\begin{aligned} E\left[|\Delta s_{i,\ell}|^2\right] &\approx \frac{1}{N_c^2}\Bigg(\sum_{n,n'=0;n'\neq n}^{N_c-1} E\left[\left|A^{(\ell,\ell)}_{iN_c+n,iN_c+n'}\right|^2\right] \\ &+ E\left[\left|\sum_{n=0}^{N_c-1} A^{(\ell,\ell)}_{iN_c+n,iN_c+n}\right|^2\right] - \left|E\left[\sum_{n=0}^{N_c-1} A^{(\ell,\ell)}_{iN_c+n,iN_c+n}\right]\right|^2\Bigg) \\ E\left[|ISI_{i,\ell}|^2\right] &\approx \sum_{i'=-\infty;i'\neq i}^{+\infty}\frac{1}{N_c^2}\Bigg(\sum_{n,n'=0,n'\neq n}^{N_c-1} E\left[\left|A^{(\ell,\ell)}_{iN_c+n,i'N_c+n'}\right|^2\right] \\ &+ E\left[\left|\sum_{n=0}^{N_c-1} A^{(\ell,\ell)}_{iN_c+n,i'N_c+n}\right|^2\right]\Bigg) \\ E\left[|MUI_{i,\ell}|^2\right] &\approx \sum_{i'=-\infty}^{+\infty}\sum_{\ell'=1;\ell'\neq\ell}^{N_u}\frac{1}{N_c^2}\Bigg(\sum_{n,n'=0}^{N_c-1} E\left[\left|A^{(\ell,\ell')}_{iN_c+n,i'N_c+n'}\right|^2\right] \\ &- \frac{1}{N_c-1}\Bigg(E\left[\left|\sum_{n=0}^{N_c-1} A^{(\ell,\ell')}_{iN_c+n,i'N_c+n}\right|^2\right] \\ &- \left|E\left[\sum_{n=0}^{N_c-1} A^{(\ell,\ell')}_{iN_c+n,i'N_c+n}\right]\right|^2\Bigg)\Bigg) \end{aligned} \tag{C.13}$$

C.3 Random Sequences

In this section, an expression for the averages over the chips for the case of the random sequences is presented, and the corresponding average useful component and the powers of the interference and the noise are given. Considering the chips are statistically independent, the moments in (C.4) yield

$$E\left[c^*_{iN_c+n,\ell}c_{iN_c+n',\ell}\right] = \delta_{n,n'} \tag{C.14}$$

$$E\left[c^*_{iN_c+n,\ell}c_{i'N_c+n',\ell'}c_{iN_c+k,\ell}c^*_{i'N_c+k',\ell'}\right] = \begin{cases}\delta_{n,k}\delta_{n',k'} & \ell' \neq \ell \\ \delta_{n,k}\delta_{n',k'} + \delta_{i,i'}(\delta_{n,n}\delta_{k,k'} - \delta_{n,n',k,k'}) & \ell' = \ell\end{cases} \tag{C.15}$$

from which it follows that the average useful component, the powers of the self-interference, the MUI power, the ISI power and the noise power from (C.4) reduce to

$$\begin{aligned}
E[s_{i,\ell}] &= \frac{1}{N_c}\sum_{n}^{N_c-1} E\left[A^{(\ell,\ell)}_{iN_c+n,iN_c+n}\right] \\
E\left[|\Delta s_{i,\ell}|^2\right] &= \frac{1}{N_c^2}\Bigg(\sum_{n,n'=0;n'\neq n}^{N_c-1} E\left[\left|A^{(\ell,\ell)}_{iN_c+n,iN_c+n'}\right|^2\right] \\
&+ E\left[\left|\sum_{n=0}^{N_c-1} A^{(\ell,\ell)}_{iN_c+n,iN_c+n}\right|^2\right] - \left|E\left[\sum_{n=0}^{N_c-1} A^{(\ell,\ell)}_{iN_c+n,iN_c+n}\right]\right|^2\Bigg) \\
E\left[|ISI_{i,\ell}|^2\right] &= \sum_{i'=-\infty;i'\neq i}^{+\infty}\frac{1}{N_c^2}\sum_{n,n'=0}^{N_c-1} E\left[\left|A^{(\ell,\ell)}_{iN_c+n,i';N_c+n'}\right|^2\right] \\
E\left[|MUI_{i,\ell}|^2\right] &= \sum_{i'=-\infty}^{+\infty}\sum_{\ell'=1;\ell'\neq\ell}^{N_u}\frac{1}{N_c^2}\sum_{n,n'=0}^{N_c-1} E\left[\left|A^{(\ell,\ell')}_{iN_c+n,i';N_c+n'}\right|^2\right] \\
E\left[|W_{i,\ell}|^2\right] &= \frac{1}{N_c}\sum_{n=0}^{N_c-1} E[\left|\tilde{w}_{iN_c+n,\ell}\right|^2]
\end{aligned} \tag{C.16}$$

C.4 Overlay Sequences

In this section, an expression is presented for the averages over the chips in the case of overlay sequences. The overlay sequence (2.44) consists of the product of a real-valued non-random WH sequence $\{WH_{n,\ell}\}$, that is assigned to a user ℓ, and a complex-valued random sequence $\{PN_{iN_c+n}\}$ (e.g., a complex-valued pseudo-noise sequence), that is the same for all users:

$$c_{iN_c+n,\ell} = WH_{n,\ell}PN_{iN_c+n} \tag{C.17}$$

The random sequence is statistically independent of the orthogonal sequence. Hence, the averages over the chips can be written as

$$E\left[c^*_{iN_c+n,\ell}c_{iN_c+n',\ell}\right] = E\left[PN^*_{iN_c+n}PN_{iN_c+n'}\right]E\left[WH_{n,\ell}WH_{n',\ell}\right] \tag{C.18}$$

$$\begin{aligned} E\left[c^*_{iN_c+n,\ell}c_{i'N_c+n',\ell'}c_{iN_c+k,\ell}c^*_{i'N_c+k',\ell'}\right] = \\ E\left[PN^*_{iN_c+n}PN_{i'N_c+n'}PN_{iN_c+k}PN^*_{i'N_c+k'}\right]\cdot \\ E\left[WH_{n,\ell}WH_{n',\ell'}WH_{k,\ell}WH_{k',\ell'}\right] \end{aligned} \tag{C.19}$$

Considering the averages over the chips for the random sequences (C.14), the average (C.18) yields

$$E\left[c^*_{iN_c+n,\ell}c_{iN_c+n',\ell}\right] = \delta_{n,n'} \tag{C.20}$$

Hence, the average useful component and the noise power in (C.4) yield

$$\begin{aligned} E[s_{i,\ell}] &= \frac{1}{N_c}\sum_{n=0}^{N_c-1} E\left[A^{(\ell,\ell)}_{iN_c+n,iN_c+n}\right] \\ E\left[|W_{i,\ell}|^2\right] &= \frac{1}{N_c}\sum_{n=0}^{N_c-1} E[\left|\tilde{w}_{iN_c+n,\ell}\right|^2] \end{aligned} \tag{C.21}$$

Furthermore, considering the random character of the chips $\{PN_{iN_c+n}\}$ and the approximation found in (C.12) for the WH sequences, the average over the chips in (C.19) can be written as

$$\begin{aligned} &E\left[c^*_{iN_c+n,\ell}c_{i'N_c+n',\ell'}c_{iN_c+k,\ell}c^*_{i'N_c+k',\ell'}\right] \approx \\ &\begin{cases} \delta_{n,k}\delta_{n',k'} - \frac{1}{N_c-1}\delta_{i,i'}(\delta_{n,n'}\delta_{k,k'} - \delta_{n,n',k,k'}) & \ell' \neq \ell \\ \delta_{n,k}\delta_{n',k'} + \delta_{i,i'}(\delta_{n,n'}\delta_{k,k'} - \delta_{n,n',k,k'}) & \ell' = \ell \end{cases} \end{aligned} \tag{C.22}$$

Hence, the self-interference power (C.4), the MUI power and the ISI power (C.5) yield

$$\begin{aligned}
E\left[|\Delta s_{i,\ell}|^2\right] &\approx \frac{1}{N_c^2}\Bigg(\sum_{n,n'=0;n'\neq n}^{N_c-1} E\left[\left|A^{(\ell,\ell)}_{iN_c+n,iN_c+n'}\right|^2\right] \\
&+ E\left[\left|\sum_{n=0}^{N_c-1} A^{(\ell,\ell)}_{iN_c+n,iN_c+n}\right|^2\right] - \left|E\left[\sum_{n=0}^{N_c-1} A^{(\ell,\ell)}_{iN_c+n,iN_c+n}\right]\right|^2\Bigg) \\
E\left[|ISI_{i,\ell}|^2\right] &\approx \sum_{i'=-\infty;i'\neq i}^{+\infty} \frac{1}{N_c^2} \sum_{n,n'=0}^{N_c-1} E\left[\left|A^{(\ell,\ell)}_{iN_c+n,i'N_c+n'}\right|^2\right] \\
E\left[|MUI_{i,\ell}|^2\right] &\approx \sum_{i'=-\infty}^{+\infty} \sum_{\ell'=1;\ell'\neq\ell}^{N_u} \frac{1}{N_c^2} \sum_{n,n'=0}^{N_c-1} E\left[\left|A^{(\ell,\ell')}_{iN_c+n,i'N_c+n'}\right|^2\right] \\
&- \sum_{\ell'=1;\ell'\neq\ell}^{N_u} \frac{1}{N_c^2(N_c-1)}\Bigg(E\left[\left|\sum_{n=0}^{N_c-1} A^{(\ell,\ell')}_{iN_c+n,i'N_c+n}\right|^2\right] \\
&- \left|E\left[\sum_{n=0}^{N_c-1} A^{(\ell,\ell')}_{iN_c+n,i'N_c+n}\right]\right|^2\Bigg)\Bigg) \qquad \text{(C.23)}
\end{aligned}$$

C.5 Simulation Results

To investigate the accuracy of the expressions (C.12), (C.15) and (C.23), a number of simulations are carried out. For the simulations, we consider a MC-CDMA system. The transmit and receiver filter are square-root raised cosine filters with rolloff $\alpha = 0$. The spreading factor N_c is chosen equal to the number of carriers. For all users, we consider the same time-invariant channel with exponentially decaying impulse response profile with parameter $a = 0.5T$:

$$h_{ch}(t) = \begin{cases} \sqrt{2a}e^{-at} & t \geq 0 \\ 0 & t < 0 \end{cases} \qquad \text{(C.24)}$$

We consider the case of no cyclic prefix ($\nu = 0$). Furthermore, it is assumed that all signals are synchronised, i.e., the signals are not disturbed by synchronisation errors. In addition, we assume that the signals at the receiver transmitted by the different users have the same signal energy. No equaliser is present, i.e., $(g^{\ell}_{i,n})_k = 1$ (2.51). In this case, we can concentrate on the effect of the sequences only. A simulation point represents the total interference power corresponding to a given assignment of sequences to the users; different simulation points correspond to different assignments.

Figures C.2(a)-(c) show the total interference power, which is the sum of the SI power, the MUI power and the ISI power, as function of the spreading factor N_c for the maximum load, i.e., the number N_u of active users equals N_c. From

the figures C.2(a)-(c), we observe that the fluctuation of the simulation results about their average is small, i.e., the simulation results only slightly deviate from their average. Furthermore, the average over the simulations and the total interference power obtained with expressions (C.13), (C.16) and (C.23) for the WH, the random and the overlay sequences, respectively, well correspond. Hence, the expressions (C.13), (C.16) and (C.23) yield a very accurate approximation for the actual total interference power. Furthermore, we observe from the figures C.2(a)-(c) that for an increasing spreading factor the total interference power for the maximum load becomes essentially independent of the spreading factor, in which case the interference power per user is inversely proportional to the spreading factor.

In figures C.3(a)-(c), the total interference power is shown as function of the load N_u/N_c. For the WH sequences and the overlay sequences (figures C.3(a) and C.3(c)), we observe that for a decreasing load, i.e., when the number of active users decreases, the simulation results strongly depend on the considered sequences. The average over the simulation results, however, agrees with the total interference power obtained with (C.13) and (C.23). The fluctuation of the simulation results about their average is smaller for the overlay sequences than for the orthogonal sequences, as the multiplication with the random sequences in the case of overlay sequences slightly mitigates the dependency of the used WH sequences. In the case of the random sequences (figure C.3(b)), the fluctuation of the simulation results about their average is very small. Furthermore, the correspondence between the average of the simulations and the interference power of (C.16) is very good.

The total interference power in the case of a single active user (SI + ISI, no MUI is present) is shown in figures C.4(a)-(c) as function of the spreading factor. In the case of the WH sequences, the simulation results strongly depend on the considered sequence. The average over the simulation results differs from the interference power in (C.13): the approximation (C.11) is not accurate for the sum of the SI and the ISI power, but yields a similar order of magnitude. However, comparing the total interference power levels from figure C.4(a) (SI + ISI) with those from figures C.2(a) and C.3(a) (SI + ISI + MUI), it is clear that the sum of the SI and the ISI power is negligible as compared to the MUI power when the load is sufficiently high. Hence, the approximation (C.11) gives rise to accurate results when the load is sufficiently high. For the random sequences (figure C.4(b)) and the overlay sequences (figure C.4(c)), the fluctuation of the simulation results about their average is very small. Furthermore, the average over the simulations agrees with the interference power from (C.16) and (C.23). As expected, the interference power (SI + ISI) is inversely proportional with the spreading factor. Considering these simulation results, we observe that the fluctuation of the simulation results about their average is small when the load is sufficiently high. Furthermore, the average over the simulations agrees with the total interference power obtained with (C.13), (C.16) and (C.23) for the WH, the random and the overlay sequences, respectively. We conclude that the expressions (C.13), (C.16) and (C.23) provide accurate approximations of the

actual total interference power when the load is sufficiently high.

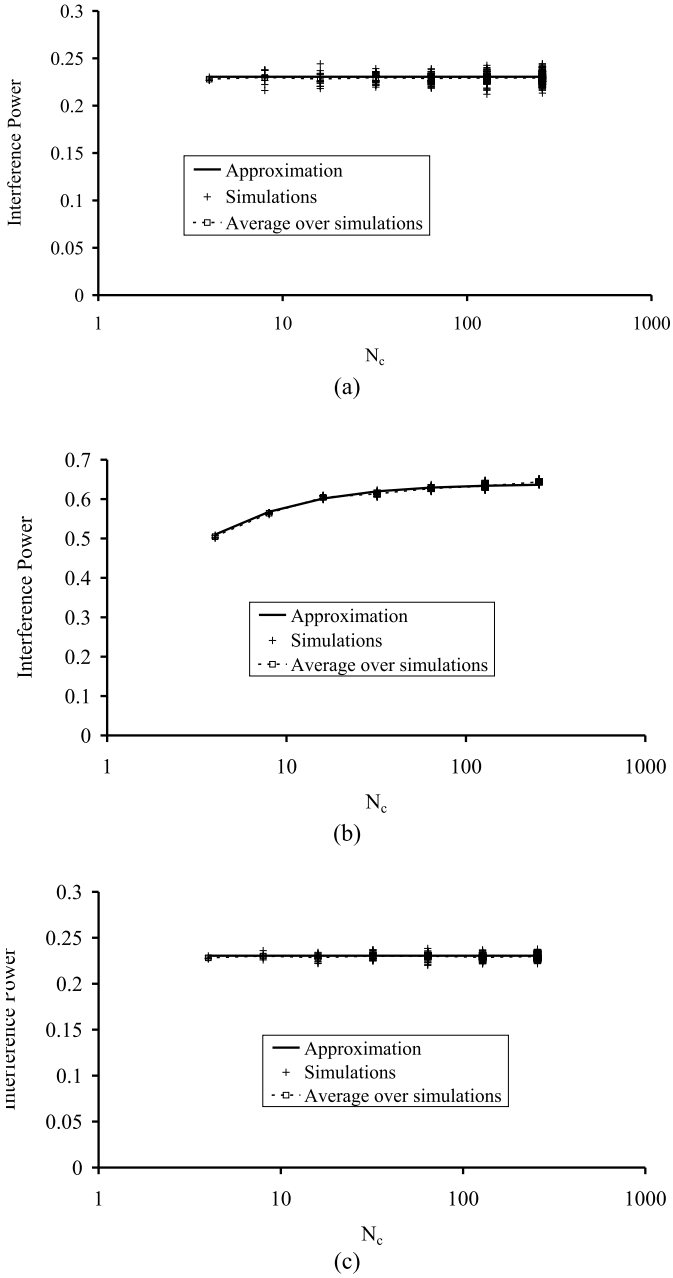

Figure C.2: Total interference power as function of the spreading factor for the maximum load, (a) orthogonal sequences, (b) random sequences, (c) overlay sequences.

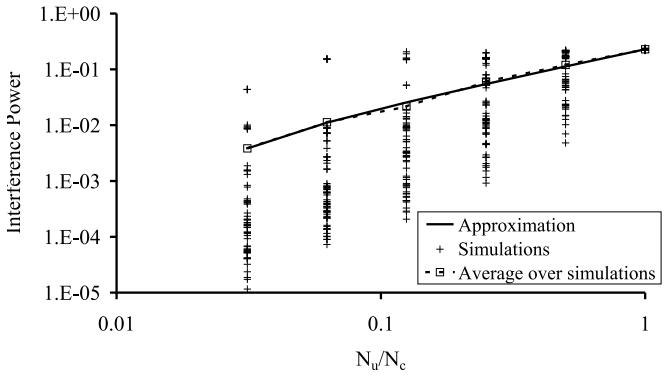

(a)

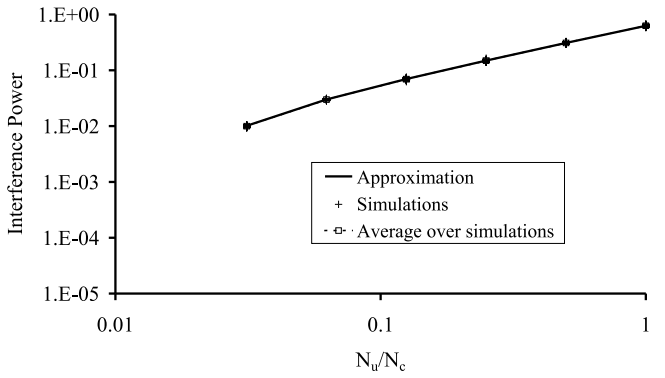

(b)

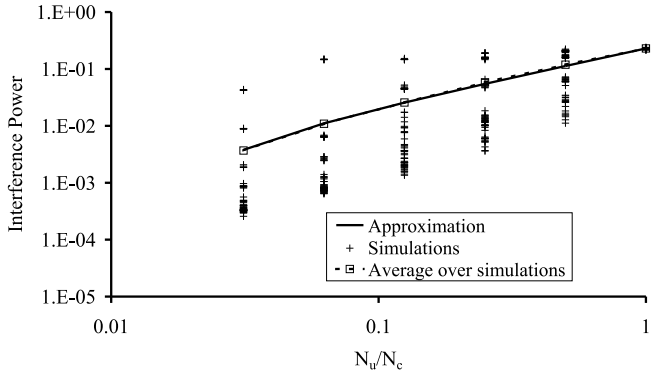

(c)

Figure C.3: Total interference power as function of the load for $N_c = 64$, (a) orthogonal sequences, (b) random sequences, (c) overlay sequences.

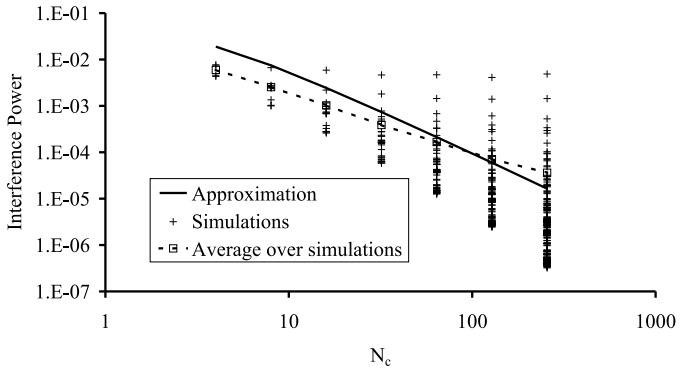

(a)

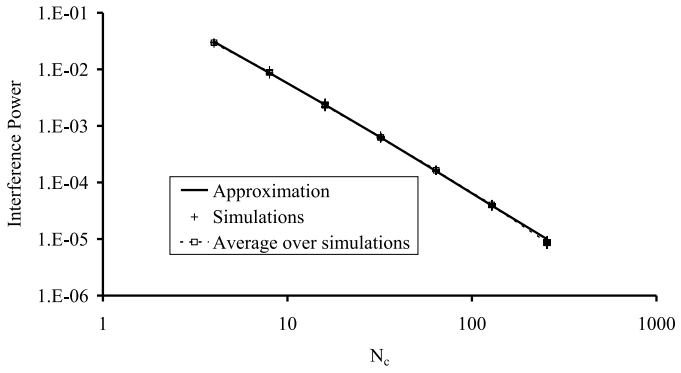

(b)

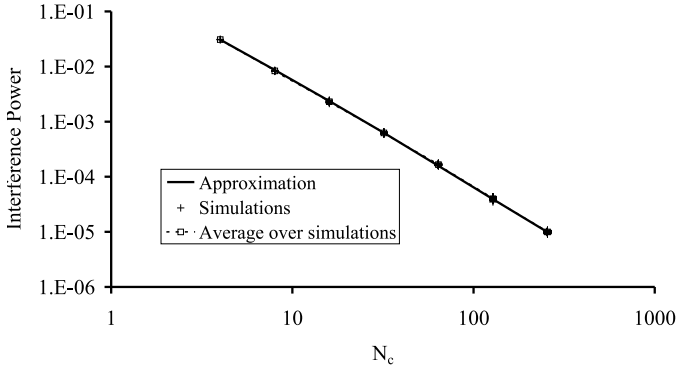

(c)

Figure C.4: Total interference power for one active user as function of the spreading factor, (a) orthogonal sequences, (b) random sequences, (c) overlay sequences.

Appendix D

Multicarrier Systems

D.1 Sufficient Cyclic Prefix Length

In this section, the relation between the sequence at the input of the IFFT at the transmitter side and the sequence at the output of the FFT at the receiver side of a multicarrier communication system is derived assuming a sufficient cyclic prefix length, i.e., the duration of the channel impulse response does not exceed the duration of the cyclic prefix. The block diagram of the multicarrier system is shown in figure D.1.

The N components of the input sequence $\mathbf{x}^{(i)} = [x_{i,0} \dots x_{i,N-1}]^T$ modulate the orthogonal carriers. To cope with the channel dispersion, each transmitted FFT frame is cyclically extended with a cyclic prefix, resulting in the time-domain sequence of length $N + \nu$, $\mathbf{s}^{(i)} = [s_{i,-\nu} \dots s_{i,N-1}]^T$

$$\mathbf{s}^{(i)} = \begin{pmatrix} \mathbf{0} & \mathbf{I}_\nu \\ & \mathbf{I}_N \end{pmatrix} \mathbf{F}\mathbf{x} \tag{D.1}$$

where

$$\mathbf{F}_{k,n} = \frac{1}{\sqrt{N}} e^{j2\pi \frac{kn}{N}}, \qquad k, n = 0, \dots, N-1 \tag{D.2}$$

is the matrix corresponding with the inverse FFT and $\mathbf{I}_M$ is the identity matrix of order $(M \times M)$. The transmitted samples are fed to a composite channel filter with impulse response $g(t)$ and Fourier transform $G(f)$. Disregarding the additive noise, the signal at the receiver is given by

$$r(t) = \sum_{k=-\nu}^{N-1} \sum_{i=-\infty}^{+\infty} s_{i,k} g(t - (k + i(N+\nu))T) \tag{D.3}$$

Without loss of generality, we can restrict our attention to the frame $i = 0$. In the following the index i is dropped. Evaluating the received signal in the

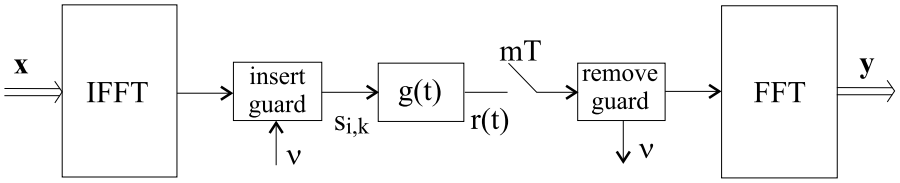

Figure D.1: Block diagram of a multicarrier structure.

interval $[0, NT]$, it is clear from figure D.2 that for the case of a sufficient cyclic prefix length (i.e., $g(t) = 0$ for $t < 0$ or $t > \nu T$), the other transmitted frames cause no interference. The signal (D.3) is sampled at the instants mT $(m = 0, 1, \ldots, N-1)$ resulting in the N samples $\mathbf{r} = [r_0 \ldots r_{N-1}]^T$

$$\mathbf{r} = \begin{pmatrix} \mathbf{0} & \mathbf{I}_N \end{pmatrix} \mathbf{\Gamma s} \tag{D.4}$$

where $\mathbf{\Gamma}_{k,k'} = g((k-k')T)$ is the matrix containing the samples of the composite channel impulse response $g(t)$. From (D.1) and (D.4) it follows that the samples r_m (for $m = 0, 1, \ldots, N-1$) yield

$$\begin{aligned} r_m &= \sum_{k=-\infty}^{+\infty} s_k g((m-k)T) \\ &= \frac{1}{\sqrt{N}} \sum_{n=0}^{N-1} x_n \int_{-\infty}^{+\infty} df G(f) e^{j2\pi mfT} \sum_{k=-\infty}^{+\infty} e^{j2\pi k\left(\frac{n}{N} - fT\right)} \\ &= \frac{1}{\sqrt{N}} \sum_{n=0}^{N-1} x_n e^{j2\pi \frac{nm}{N}} G_n \end{aligned} \tag{D.5}$$

where G_n is the folded channel transfer function evaluated at the carrier frequency n/NT:

$$G_n = \frac{1}{T} \sum_{\ell=-\infty}^{+\infty} G\left(\frac{n}{NT} + \frac{\ell}{T}\right) \tag{D.6}$$

The samples r_m are demodulated using the FFT, which results in the samples $\mathbf{y} = [y_0 \ldots y_{N-1}]^T$ given by

$$\mathbf{y} = \mathbf{F}^\dagger \mathbf{r} \tag{D.7}$$

where $\mathbf{F}^\dagger$ is the Hermitian of the matrix $\mathbf{F}$ (D.2). Substituting (D.4) and (D.1) into (D.7), we obtain

$$\mathbf{y} = \mathbf{D}\mathbf{x} \tag{D.8}$$

where

$$\mathbf{D} = \mathbf{F}^\dagger \begin{pmatrix} \mathbf{0} & \mathbf{I}_N \end{pmatrix} \mathbf{\Gamma} \begin{pmatrix} \mathbf{0} & \mathbf{I}_\nu \\ \mathbf{I}_N & \end{pmatrix} \mathbf{F} \tag{D.9}$$

Assuming a sufficient cyclic prefix length, $\mathbf{D}$ reduces to a diagonal matrix containing the folded channel transfer function evaluated at the carrier frequencies, $\mathbf{D}_{n,n'} = G_n \delta_{n,n'}$ $(n, n' = 0, \ldots, N-1)$.

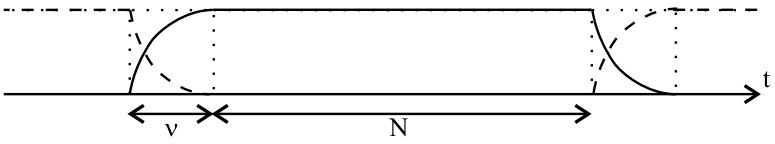

Figure D.2: The multicarrier signal.

A similar analysis can be done for a linear time-varying composite channel filter $g(t;\tau)$ with Fourier transform with respect to the time variable t $G(f;\tau)$. The signal at the receiver is now given by

$$r(t) = \sum_{k=-\nu}^{N-1} \sum_{i=-\infty}^{+\infty} s_{i,k} g(t - (k + i(N+\nu))T; t) \tag{D.10}$$

Considering the same assumptions as for the linear time-invariant filter, it is found that for a sufficient cyclic prefix length the samples r_k outside the cyclic prefix at the input of the FFT are given by

$$r_k = \frac{1}{\sqrt{N}} \sum_{n=0}^{N-1} x_n e^{j2\pi \frac{nk}{N}} G_n(kT), \qquad k = 0, 1, \ldots, N-1 \tag{D.11}$$

where $G_n(kT)$ is the folded channel transfer function of the linear time-varying filter at the instant kT evaluated at the carrier frequency n/NT.

$$G_n(kT) = \frac{1}{T} \sum_{\ell=-\infty}^{+\infty} G\left(\frac{n}{NT} + \frac{\ell}{T}; kT\right) \tag{D.12}$$

D.2 MMSE Filter

In this section, the MMSE filter for optimum detection and the corresponding receiver structure are derived for a multicarrier system with a cyclic prefix. Considering the demodulation of one FFT frame, it follows from (D.7) that the samples at the output of the FFT are given by

$$\mathbf{y} = \mathbf{D}\mathbf{x} + \mathbf{n} \tag{D.13}$$

where $\mathbf{n} = [n_0 \ldots n_{N-1}]^T$ is the vector of the additive noise samples and $\mathbf{D}$ is given by (D.9). The MMSE filter $\mathbf{H}_0$ that minimises the mean-square error $E[|\mathbf{H}_0\mathbf{y} - \mathbf{x}|^2]$, is given by

$$\begin{aligned} \mathbf{H}_0 &= E[\mathbf{x}\mathbf{y}^{dagger}]E[\mathbf{y}\mathbf{y}^{dagger}]^{-1} \\ &= \mathbf{R}_x\mathbf{D}^\dagger \left(\mathbf{D}\mathbf{R}_x\mathbf{D}^\dagger + \mathbf{R}_n\right)^{-1} \end{aligned} \tag{D.14}$$

where $\mathbf{R}_x = E[\mathbf{x}\mathbf{x}^\dagger]$ and $\mathbf{R}_n = E[\mathbf{n}\mathbf{n}^\dagger]$ are the autocorrelation matrices of the input samples $\mathbf{x}$ and the noise samples $\mathbf{n}$, respectively. A closed form of

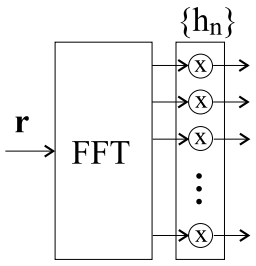

Figure D.3: MMSE receiver structure for a sufficient cyclic prefix length.

(D.14) is difficult to obtain, except for the maximum load, i.e., when all carriers are modulated. Taking into account that $\mathbf{F}\mathbf{F}^\dagger = \mathbf{I}_N$, assuming additive white Gaussian noise with psd N_0 ($\mathbf{R}_n = N_0\mathbf{I}_N$) and uncorrelated zero-mean input samples with variance $E[x_i^2] = \sigma_x^2$, the MMSE filter simplifies to

$$\mathbf{H}_0 = \sigma_x^2\mathbf{D}^\dagger\left(\sigma_x^2\mathbf{D}\mathbf{D}^\dagger + N_0\mathbf{I}_N\right)^{-1} \tag{D.15}$$

from which it follows that the receiver applies the FFT outputs to a $N \times N$ matrix filter $\mathbf{H}_0$.

For a sufficient cyclic prefix length, it follows from (D.9) that the matrix product $\mathbf{D}$ reduces to a diagonal matrix. In this case, the matrix filter $\mathbf{H}_0$ also reduces to a diagonal matrix with diagonal elements

$$h_n = \frac{\sigma_x^2 G_n^*}{\sigma_x^2|G_n|^2 + N_0} \tag{D.16}$$

The corresponding receiver structure consists of an FFT followed by one-tap equalisers that scale and rotate the FFT outputs, as shown in figure D.3.

Bibliography

[Ada98] F. Adachi, M. Sawahashi, H. Suda, "Wideband DS-CDMA for Next-Generation Mobile Communication Systems", *IEEE Communications Magazine*, Vol. 36, no. 9, Sep 1998, pp. 56-69

[Ali97] H. Alikhani, R. Bohnke, M. Suzuki, "BDMA Band Division Multiple Access - A New Air-Interface for 3rd Generation Mobile System in Europe", *Proceedings ACTS Summit*, Aalborg, Denmark, Oct 1997, pp. 482-488

[Bah99] A.R.S. Bahai, B.R. Saltzberg, *Multi-Carrier Digital Communications - Theory and Applications of OFDM*, Kluwer, 1999

[Bin90] J.A.C. Bingham, "Multicarrier Modulation for Data Transmission: An Idea Whose Time Has Come", *IEEE Communications Magazine*, Vol. 28, no 5, pp. 5-14, 1990

[Buc93] K. Bucket, M. Moeneclaey, "Timing Jitter Sensitivity Comparison of Narrowband M-PSK and Bandlimited DS/SS M-PSK Signals", *Proceedings IEEE Int. Conf. on Communications*, ICC'93, Geneve, May 1993, pp. 453-457

[Buc95] K. Bucket, M. Moeneclaey, "Effect of Random Carrier Phase and Timing Errors on the Detection of Narrowband M-PSK and Bandlimited DS/SS M-PSK Signals", *IEEE Transactions on Communications*, Vol. 43, no. 2/3/4, Feb/Mar/Apr 1995, pp. 1260-1263

[Cas91] E.F. Casas, C. Leung, "OFDM for Data Communications over Mobile Radio FM Channels - Part 1: Analysis and Experimental Results", *IEEE Transactions on Communications*, Vol. 39, no 5, May 1991, pp. 783-793

[Cha66] R.W. Chang, "Synthesis of Band-limited Orthogonal Signals for Multi-channel Data Transmission", *Bell System Technical Journal*, Vol. 45, pp. 1775-1796, 1966

[Chi95] A. Chini, M.S. El-Tanany, S.A. Mahmoud, "On the Performance of a Coded MCM over Multipath Rayleigh Fading Channels", *Proceedings ICC'95*, Seattle, WA, Jun 95, pp. 1689-1694

[Cho93] A. Chouly, A. Brajal, S. Jourdan, "Orthogonal Multicarrier Techniques Applied to Direct Sequence Spread Spectrum CDMA techniques", *Proceedings IEEE Globecom'93*, Houston, USA, Nov. 1993, pp. 1723-1728

[Chw91a] J.S. Chow, J.C. Tu, J.M. Cioffi, "A Discrete Multitone Transceiver for HDSL Applications", *IEEE Journal on Selected Areas in Communications*, Vol. 9, no 8, Aug 1991, pp. 895-908

[Chw91b] P.S. Chow, J.C. Tu, J.M. Cioffi, "Performance Evaluation of a Multichannel Transceiver System for ADSL and VHDSL", *IEEE Transactions on Communications*, Vol. 9, no 8, Aug 1991, pp. 909-919

[Dah98] E. Dahlman, B. Gudmundson, M. Nilsson, J. Skld, "UMTS/IMT-2000 Based on Wideband CDMA", *IEEE Communications Magazine*, Vol. 36, no. 9, Sep 1998, pp. 70-80

[DaS93] V.M. DaSilva, E.S. Sousa, "Performance of Orthogonal CDMA Sequences for Quasi-Synchronous Communication Systems", *Proceedings IEEE ICUPC'93*, Ottawa, Canada, Oct. 1993, pp. 995-999

[Eru93] L. Erup, F.M. Gardner, R.A. Harris, "Interpolation in Digital Modems - Part II: Implementation and Performance", *IEEE Transactions on Communications*, Vol. 41, no. 6, Jun 1993, pp. 998-1008

[ETSI96] ETSI, "*Radio Equipment and Systems, HIgh PErformance Radio Local Area Network (HIPERLAN) Type 1*", European Telecommunication Standard, ETS 300-652, Oct 1996

[ETSI97] European Telecommunications Standard, "*Radio Broadcast Systems: Digital Audio Broadcasting (DAB) to Mobile, Portable and Fixed Receivers*", European Telecommunications Standards Institute, ETS 300 401 2nd edition, Valbonne, France, 1997

[ETSI99] ETSI, "*Broadband Radio Access Networks (BRAN); HIPERLAN Type 2 Technical Specifications Part 1 - Physical Layer*", DTS/BRAN030003-1, Oct 1999

[Faz93] K. Fazel, L. Papke, "On the Performance of Convolutionally Sequenced CDMA/OFDM for Mobile Communication System", *Proceedings IEEE PIMRC'93*, Yokohama, Japan, Sep. 1993, pp. 468-472

[Faz97] "*Multi-Carrier Spread-Spectrum*", Eds. K. Fazel, G.P. Fettweis, Kluwer, 1997

[Faz00] "*Multi-Carrier Spread-Spectrum & Related Topics*", Eds. K. Fazel, S. Kaiser, Kluwer, 2000

[Fra80] L.E. Franks, "Carrier and Bit Synchronization in Data Communication - A Tutorial Review", *IEEE Transactions on Communications*, Vol. 28, no. 8, Aug. 1980, pp. 1107-1121

[Fre98] R.L. Freeman, *Telecommunications Transmission Handbook*, Wiley, New-York, 1998

[Gar93] F.M. Gardner, "Interpolation in Digital Modems - Part I: Fundamentals", *IEEE Transactions on Communications*, Vol. 41, no. 3, Mar 1993, pp. 501-507

[Har97] S. Hara, R. Prasad, "Overview of Multicarrier CDMA", *IEEE Communications Magazine*, Dec 1997, Vol. 35, No. 12, pp. 126-133

[Has98] A.A. Hassan, J.E. Hershey, G.J. Saulnier, *Perspectives in Spread Spectrum*, Kluwer, Boston, 1998

[Hir80] B. Hirosaki, "An Analysis of Automatic Equalisers for Orthogonally Multiplexed QAM Systems", *IEEE Transactions on Communications*, Vol. 28, no 1, Jan 1980, pp. 73-83

[Hir81] B. Hirosaki, "An Orthogonally Multiplexed QAM System Using the Discrete Fourier Transform", *IEEE Transactions on Communications*, Vol. 29, 1981, pp. 982-989

[IEEE97] IEEE 802.11, *IEEE Standard for Wireless LAN Medium Access Control (MAC) and Physical Layer (PHY) Specifications*, Nov 1997

[IEEE99] IEEE, "*Supplement to Standard for Telecommunications and Information Exchange Between Systems - LAN/MAN Specific Requirements - Part 11: Wireless MAC and PHY Specifications: High Speed Physical Layer in the 5-GHz Band*", P802.11a/D7.0, Jul 1999

[Kal89] I. Kalet, "The multitone Channel", *IEEE Transactions on Communications*, Vol. 37, no. 2, Feb. 1989, pp. 119-124

[Kni98] D.N. Knisely, S. Kumar, S. Laha, S. Nanda, "Evolution of Wireless Data Services: IS-95 to cdma2000", *IEEE Communications Magazine*, Vol. 36, no. 9, Sep 1998, pp. 140-149

[Koh95] R. Kohno, R. Meidan, L.B. Milstein, "Spread Spectrum Access Methods for Wireless Communications", *IEEE Transactions on Communications*, Vol. 33, no. 1, Jan 1995, pp. 58-67

[Kur00] J. Kurzweil, *An Introduction to Digital Communications*, Wiley, 2000

[Lee88] E.A. Lee, D.G. Messerschmitt, *Digital Modulation*, Kluwer, Boston, 1988

[LeF89] B. LeFloch, R. Lassalle, D. Castelain, "Digital Sound Broadcasting to Mobile Receivers", *IEEE Transactions on Consumer Electronic*, Aug 1989

[Lin99] "*Wireless Communication, The Interactive Multimedia CD-ROM*", Editor J-P. Linnartz, Baltzer, Bussum, The Netherlands, 1999

[Lou98a] J. Louveaux, L. Vandendorpe, L. Cuvelier, F. Deryck, O. van de Wiel, "Capacity Sensitivity of Filter Bank Based High Bit Rate Transmission over Copper Wires to the MIMO Equaliser Rate", *Proceedings Int. Conf. on Communications*, ICC'98, Atlanta, GA, Jun 1998, pp. 1023-1027

[Lou98b] J. Louveaux, L. Vandendorpe, L. Cuvelier, T. Pollet, "Capacity Sensitivity of Filter Bank Based Multicarrier VDSL Transmission to Timing Errors", *Proceedings URSI Int. Symp. on Signals, Systems and Electronics*, ISSSE'98, Pisa, Italy, Oct 1998, pp. 235-240

[Mey98] H. Meyr, M. Moeneclaey, S.A. Fechtel, *Digital Communication Receivers: Synchronization, Channel Estimation and Signal Processing*, Wiley & Sons, New York, 1998

[Moe97] M. Moeneclaey , "The Effect of Synchronization Errors on the Performance of Orthogonal Frequency-Division Multiplexed (OFDM) Systems", *Proceedings COST 254 "Emerging techniques for Communication Terminals"*, Toulouse, France, Jul 97, pp. 41-45

[Moe99a] M. Moeneclaey, *Communicatietechniek*, graduate course, taught at Ghent University, Belgium

[Moe99b] M. Moeneclaey, *Mobiele Digitale Communicatie*, graduate course, taught at Ghent University, Belgium

[Moo94] P.H. Moose, "A Technique for Orthogonal Frequency Division Multiplexing Frequency Offset Correction", *IEEE Transactions on Communications*, Vol. 42, no 10, Oct 1994, pp. 2908-2914

[Mos96] S. Moshavi, "Multi-User Detection for DS-CDMA Communications", *IEEE Communications Magazine*, Vol. 34, no. 10, Oct 1996, pp. 124-136

[Nan00] S. Nanda, K. Balachandran, S. Kumar, "Adaptation Techniques in Wireless Packet Data Services", *IEEE Communications Magazine*, Vol. 38, no. 1, Jan 2000, pp. 54-64

[Oja98] T. Ojanper, R. Prasad, "An Overview of Air Interface Multiple Access for IMT-2000/UMTS", *IEEE Communications Magazine*, Vol. 36, no. 9, Sep 1998, pp. 82-95

[Pah95] K. Pahlavan, A.H. Levesque, *Wireless Information Networks*, Wiley, 1995

[Par96] S. Parkvall, E. Strm, B. Ottersten, "The Impact of Timing Errors on the Performance of Linear DS-CDMA Receivers", *IEEE Journal on Selected Areas on Communications*, Vol. 14, no. 8, Oct 1996, pp. 1660-1668

[Pel80] A. Peled, A. Ruiz, "Frequency Domain Data Transmission Using Reduced Computational Complexity Algorithms", *Proceedings IEEE Int. Conf. on Acoustics*, speech and Signal Processing (ICASSP'80), Denver, pp. 964-967, 1980

[Pol93] T. Pollet , M. Van Bladel, M. Moeneclaey, "BER Sensitivity of OFDM Systems to Carrier Frequency Offset and Wiener Phase Noise", *IEEE Transactions on Communications*, Vol. 43, no. 2/3/4, Feb/Mar/Apr 93, pp. 191-193

[Pol94] T. Pollet, P. Spruyt, M. Moeneclaey, "The BER Performance of OFDM Systems Using Non-Synchronised Sampling", *Proceedings Globecom 94*, San Francisco, Nov 1994, pp. 253-257

[Pol95a] T. Pollet, M. Moeneclaey, I. Jeanclaude, H. Sari, "Effect of Carrier Phase Jitter on Single-Carrier and Multi-Carrier QAM Systems", *Proceedings ICC 1995*, Seattle WA, Jun 95, Paper S29.4, pp. 1046-1050

[Pol95b] T. Pollet, M. Moeneclaey, "Synchronizability of OFDM Signals", *Proceedings Globecom 95*, Singapore, Nov 1995, pp. 2054-2058

[Pol96] T. Pollet, M. Moeneclaey, "The Effect of Carrier Frequency Offset on the Performance of Band-Limited Single Carrier and OFDM Signals", *Proceedings Globecom 96*, London, Nov 1996, pp. 719-723

[Pol97] T. Pollet, H. Steendam, M. Moeneclaey, "Performance Degradation of Multicarrier Systems by an Insufficient Guard Interval Duration", *Proceedings Int. Workshop on Copper Wire Access Systems "Bridging the Last Copper Drop" CWAS'97*, Budapest, Hungary, pp. 265-270, 1997

[Pol98] T. Pollet, M. Moeneclaey, I. Jeanclaude and H. Sari, "Comparison of single-carrier and multi-carrier QAM system performance in the presence of carrier phase jitter," *Wireless Personal Communications*, vol. 8, pp. 205-218, Sept. 1998

[Pro95] J.G. Proakis, *Digital Communications*, McGraw-Hill, New York, 1995

[Red95] S.M. Redl, M.K. Weber, M.W. Oliphant, *An Introduction to GSM*, Artech House, Boston, 1995

[Rei98] U. Reimers, "Digital Video Broadcasting", *IEEE Communications Magazine*, Vol. 36, no. 6, Jun 1998, pp. 104-110

[Rus95] M. Russel, G.L. Stber, "Terrestrial Digital Video Broadcasting for Mobile Reception Using OFDM", *Wireless Personal Communications*, Vol. 2, pp. 45-66, 1995

[Sal67] B.R. Saltzberg, "Performance of an Efficient Parallel Data Transmission System", *IEEE Transactions on Communications*, Vol. 15, no 12, Dec 1967, pp. 805-811

[Sal98] B.R. Saltzberg, "Comparison of Single-Carrier and Multitone Digital Modulation for ADSL Applications", *IEEE Communications Magazine*, Vol. 36, no. 11, Nov 1998, pp. 114-121

[San95] G. Santella, "Bit Error Rate Performances of M-QAM Orthogonal Multicarrier Modulation in Presence of Time-Selective Multipath Fading", *Proceedings ICC'95*, Seattle, WA, Jun 95, pp. 1683-1688

[Sar93] H. Sari, G. Karam, I. Jeanclaude, "Channel Equalisation and Carrier Synchronisation in OFDM Systems", *Proceedings 6th Tirrenia Int. Workshop*, Tirrenia (Pisa), Italy, pp. 191-202, 1993

[Sar95] H. Sari, G. Karam, I. Jeanclaude, "Transmission Techniques for Digital Terrestrial TV Broadcasting", *IEEE Communications Magazine*, Feb 95, pp. 100-109

[Sar96] H. Sari, Y. Lvy and G. Karam, "Orthogonal Frequency-Division Multiple Access for the Return Channel on CATV Networks," *Proceedings International Conference on Telecommunications ICT'96*, Istanbul, pp. 602-607, April 1996

[Sar99a] H. Sari, H. Steendam, M. Moeneclaey, "On the Uplink Capacity of Cellular CDMA and TDMA Over Nondispersive Channels", *Proceedings IEEE 1999 Vehicular Technology Conference VTC'99*, Houston, TX, May 16-20 1999, pp. 1638-1642

[Sar99b] H. Sari, M. Moeneclaey, H. Steendam, "On the Downlink Capacity of Cellular CDMA and TDMA over Nondispersive Channels", *Proceedings IEEE 1999 Vehicular Technology Conference VTC'99 Fall*, Amsterdam, The Netherlands, September 19-22 1999, pp. 1165-1169

[Sch97] T.M. Schmidl, D.C. Cox, "Robust Frequency and Timing Synchronisation for OFDM", *IEEE Transactions on Communications*, Vol. 45, no 12, Dec 1997, pp. 1613-1621

[Sim95] M.K. Simon, S.M. Hinedi, W.C. Lindsay, *Digital Communication Techniques - Signal Design and Detection*, Prentice Hall, 1995

[Snd95] S.D. Sandberg, M.A. Tzannes, "Overlapped Discrete Multitone Modulation for High Speed Copper Wire Communications", *IEEE Journal on Selected Areas on Communications*, Vol. 13, no 9, Sep 1995, pp. 1571-1585

[Sou90] E. Sousa, "The Effect of Clock and Carrier Frequency Offsets on the Performance of a Direct-Sequence Spread-Spectrum Multiple-Access Technique", *IEEE Journal on Selected Areas on Communications*, Vol. 8, no. 4, May 1990, pp. 580-587

[Ste96] H. Steendam, M. Moeneclaey, "Guard Time Optimization for OFDM Transmission over Fading Channels", *Proceedings IEEE Fourth Symposium on Communications and Vehicular Technology in the Benelux*, SCVT'96, Gent, Belgium, pp. 42-48, Oct. 1996

[Ste97a] H. Steendam, M. Moeneclaey, "Sensitivity of OFDM/CDMA to carrier phase jitter", *Proceedings 1st International Workshop on Multi-carrier Spread-spectrum*, MC-SS'97, Oberpfaffenhofen, Germany, Apr. 1997, pp. 145-152

[Ste97b] H. Steendam, M. Moeneclaey, H. Sari, "Degradations of OFDMA, OFDM and FDMA Caused by Carrier Phase Jitter", *Proceedings COST 254 "Emerging techniques for Communication Terminals"*, Toulouse, France, pp. 185-189, Jul 7-9 1997

[Ste98a] H. Steendam, M. Moeneclaey, "Pilot tone frame synchronization of OFDM signals for BDSL applications", *Proceedings Signal Processing Symposium - SPS 98*, Leuven, Belgium, March 26-27, 1998, pp. 187-190

[Ste98b] H. Steendam, M. Moeneclaey, H. Sari, "The Effect of Carrier Phase Jitter on the Performance of Orthogonal Frequency-Division Multiple Access Systems", *IEEE Transactions on Communications*, Vol. 46, No. 4, Apr 98, pp. 456-459

[Ste98c] H. Steendam, M. Moeneclaey, "Optimization of OFDM on Frequency-Selective Time-Selective Radio Channels", *Proceedings International Symposium on Signals, Systems and Electronics ISSSE 1998*, Sep 29-Oct 2, Pisa, Italy, 1998, pp. 398-404

[Ste98d] H. Steendam, M. Moeneclaey, "Sensitivity of OFDM and MC-CDMA to Carrier Phase Errors", *Proceedings 6th Symposium on Vehicular Technology and Communications 1998*, Oct 12-13, Brussels, Belgium (best paper award)

[Ste99a] H. Steendam, M. Moeneclaey, "The Effect of Carrier Phase Jitter on MC-CDMA Performance", *IEEE Transactions on Communications*, Vol. 47, No. 2, Feb 99, pp. 195-198

[Ste99b] H. Steendam, M. Moeneclaey, "MC-CDMA Performance in the Presence of Timing Errors", *Proceedings 2nd Conference on Telecommunications ConfTele'99*, Sesimbra, 15-16 April 1999, pp. 211-215

[Ste99c] H. Steendam, M. Moeneclaey, "The Effect of Synchronisation Errors on MC-CDMA Performance", *Proceedings International Conference on Communications ICC'99*, Vancouver, Canada, June 6-10, 1999, Paper S38.3, pp. 1510-1514

[Ste99d] H. Steendam, M. Moeneclaey, "The Sensitivity of MC-CDMA to Synchronisation Errors", *European Transactions on Telecommunications*, special issue on MC-SS, Jul-Aug 99, No. 4, pp. 429-436

[Ste99e] H. Steendam, M. Moeneclaey, "The Effect of Carrier Phase Errors on Downlink MC-CDMA and OCDMA", *Proceedings XXVIth General Assembly of the International Union of Radio Science URSI-GA'99*, Toronto, Canada, August 13-21 1999, Paper C2.04, pp. 207

[Ste99f] H. Steendam, M. Moeneclaey, "An Overview of MC-CDMA Synchronisation Sensitivity", *Proceedings 1999 Second International Workshop on Multi-Carrier Spread-Spectrum (MC-SS'99) & Related Topics*, Oberpfaffenhofen, Germany, Sep 99, pp. 261-270 (invited paper)

[Ste99g] H. Steendam, M. Moeneclaey, "Performance of a Flexible Form of MC-CDMA in a Cellular System", *Proceedings 1999 Second International Workshop on Multi-Carrier Spread-Spectrum (MC-SS'99) & Related Topics*, Oberpfaffenhofen, Germany, September 15-17 1999, pp. 45-52

[Ste99h] H. Steendam, M. Moeneclaey, "The Sensitivity of a Flexible Form of MC-CDMA to Synchronisation Errors", *Proceedings IEEE 1999 Vehicular Technology Conference VTC'99 Fall*, Amsterdam, The Netherlands, September 19-22 1999, pp. 2208-2212

[Ste99i] H. Steendam, M. Moeneclaey, "Analysis and Optimization of the Performance of OFDM on Frequency-Selective Time-Selective Fading Channels", *IEEE Transactions on Communications*, Vol. 47, No. 12, Dec 99, pp. 1811-1819

[Ste00] H. Steendam, M. Moeneclaey, "Sensitivity of Orthogonal Frequency-Division Multiplexed Systems to Carrier and Clock Synchronisation Errors", accepted for publication in *Signal Processing*, Vol. 80, no 7, 2000

[Stl92] R. Steele, *Mobile Radio Communications*, London, Pentech Press Publishers, 1992

[Tak98] H. Takanashi, R. van Nee, "Merged Physical Layer Specification for the 5-GHz Band", *IEEE P802.11-98/72-r1*, Mar 1998

[Tom96] L. Tomba and W.A. Krzymien, "Effect of Carrier Phase Noise and Frequency Offset on the Performance of Multicarrier CDMA Systems", *Proceedings ICC 1996*, Dallas TX, Jun 96, Paper S49.5, pp. 1513-1517

[Tom98] L. Tomba and W.A. Krzymien, "A Model for the Analysis of Timing Jitter in OFDM Systems", *Proceedings ICC 1998*, Atlanta GA, Jun 98, Paper S35.1, pp. 1227-1231

[Tuf98] F. Tufvesson, T. Maseng, "Optimization of Sub-Channel Bandwidth for Mobile OFDM Systems", *Proceedings Multiaccess, Mobility and Teletraffic - Advances in Wireless Networks (MMT'98)*, pp. 103-114, Kluwer Academic Publishers, 1998

[Van93] L. Vandendorpe, "Multitone Direct Sequence CDMA Systems in an Indoor Wireless Environment", *Proceedings IEEE First Symposium of Communication and Vehicular Technology in the Benelux SCVT'93*, Delft, The Netherlands, Oct. 1993, pp. 4.1-1 - 4.1-8

[Van99] L. Vandendorpe, M. Moeneclaey and M. Moonen, *Signal Processing for Digital Communications*, Post graduate course GSEC AT2, taught at the Catholic University of Louvain UCL, Belgium, 1999

[VBl98] M. Van Bladel, H. Steendam, T. Marongiu, M. Moeneclaey, "Some TDMA and OFDM/CDMA Receiver Structures for Communication Over the Return Path of the CATV Network", *Proceedings International Conference on Communications ICC'98*, Atlanta, Georgia USA, June 7-11, 1998, Paper S37.3, pp. 1013-1017

[vdB97] J. J. van de Beek, M. Sandell, P.O. Brjesson, "ML Estimation of Time and Frequency Offset in OFDM Systems", *IEEE Transactions on Signal Processing*, Vol. 45, no 7, Jul 1997, pp. 1800-1805

[vdB99] J.J. van de Beek, P. dling, S.K. Wilson, P.O. Brjesson, "Orthogonal Frequency Division Multiplexing (OFDM)", *URSI Review of Radio Science 1996-1999*, Oxford Publishers, pp. 177-206, 1999

[Ver98] S. Verdú, *Multiuser Detection*, Cambridge University Press, 1998

[vNe97] R. van Nee, "OFDM for High Speed Wireless Networks", *IEEE P802.11-97/123*, Nov 1997

[vNe00] R. van Nee, R. Prasad, *OFDM for Wireless Multimedia Communications*, Artech House, 2000

[War93] W.D. Warner, C. Leung, "OFDM/FM Frame Synchronisation for Mobile Radio Data Communications", *IEEE Transactions on Vehicular Techology*, Vol. 42, no 3, 1993, pp. 302-313

[Wei71] S.B. Weinstein, P.M. Ebert, "Data Transmission by Frequency-Division Multiplexing Using the Discrete Fourier Transform", *IEEE Transactions on Communications*, Vol. 19, no. 5, May. 1971, pp. 628-634

[Yee93] N. Yee, J-P. Linnartz, G. Fettweis, "Multicarrier CDMA in Wireless Radio Networks", *Proceedings IEEE PIMRC'93*, Yokohama, Japan, Sep. 1993, pp. 109-113

[Zog96] T.N. Zogakis, J.M. Cioffi, "The Effect of Timing Jitter on the Performance of a Discrete Multitone System", *IEEE Transactions on Communications*, Vol. 44, No. 7, Jul 96, pp. 799-808

[Zou95] W.Y. Zou, Y. Wu, "COFDM, an Overview", *IEEE Transactions on Broadcasting*, Vol. 41, no 1, pp. 1-8, 1995